Deliverable 15.1: Initial State-of-the-art of WP ConCorD

Work Package 15

EURAD (Deliverable n° 15.1) – Initial State-of-the-art of WP ConCorD
Dissemination level: Public
Date of issue of this report: 17/08/2022

Page 1

Document information

Project Acronym	**EURAD**
Project Title	**European Joint Programme on Radioactive Waste Management**
Project Type	**European Joint Programme (EJP)**
EC grant agreement No.	**847593**
Project starting / end date	**1st June 2019 – 30 May 2024**
Work Package No.	**15**
Work Package Title	**Container Corrosion under Disposal conditions**
Work Package Acronym	**ConCorD**
Deliverable No.	**15.1**
Deliverable Title	**Initial State-of-the-Art of WP ConCorD**
Lead Beneficiary	**GRS**
Contractual Delivery Date	**30/11/2021**
Actual Delivery Date	**17/08/2022**
Type	**Document**
Dissemination level	**Public**
Authors	**Abdesselam Abdelouas (SUBATECH), Ursula Alonso (CIEMAT), Rizlan Bernier-Latmani (EPFL), Cedric Bosch (EMSE), Andrea Cherkouk (HZDR), David Dobrev (UJV), Ana María Fernández (CIEMAT), Nicolas Finck (KIT-INE), Roberto Gaggiano (Ondraf/Niras), Vaclava Havlová (UJV), James Hesketh (JACOBS), Andrés Idiart (AMPHOS[21]), Kristel Mijnendonckx (SCK), Vanessa Montoya (UFZ), Andrés G. Muñoz (GRS), Cristiano Padovani (JACOBS), Arnau Pont (AMPHOS[21]), Pauliina Rajala (VTT), Olga Riba (AMPHOS[21]), Lola Sarrasin (SUBATECH), Sergey Sayenko (KIPT), Nicholas Smart (JACOBS), Nathalie Texier-Mandoki (Andra), Paul Wersin (University of Bern)**

To be cited as:

Abdelouas A., Alonso U., Bernier-Latmani R., Bosch C., Cherkouk A., Dobrev D., Fernández A.M., Finck N., Gaggiano R., Havlová V., Hesketh J., Idiart A., Mijnendonckx K., Montoya V., Muñoz A.G., Padovani, C., Pont A., Rajala P., Riba O., Sarrasin L., Sayenko S., Smart N., Texier-Mandoki N., Wersin P. (2022): Initial State-of-the-Art of WP ConCorD. Final version as of 17.08.2022 of deliverable D15.1 of the HORIZON 2020 project EURAD. EC Grant agreement no: 847593.

Disclaimer

All information in this document is provided "as is" and no guarantee or warranty is given that the information is fit for any particular purpose. The user, therefore, uses the information at its sole risk and liability. For the avoidance of all doubts, the European Commission or the individual Colleges of EURAD (and their participating members) has no liability in respect of this document, which is merely representing the authors' view.

EURAD (Deliverable n° 15.1) – Initial State-of-the-art of WP ConCorD
Dissemination level: Public
Date of issue of this report: **17/08/2022**

Page 2

Status of deliverable		
	By	Date
Delivered (Lead Beneficiary)	Andrés Muñoz	17/08/2022
Verified (WP Leader)	Nikitas Diomidis	17/08/2022
Reviewed (Reviewers)	Fraser King, Christina Lilja, Terhi Glas, Satoru Suzuki, Christiane Stephan-Scherb, Valérie Maillot, Peter Keech, Mehran Behazin, Jeff Binns, Birgitta Kalinowski	14/03/2022
Approved (PMO)	Michelle Cowley	16/09/2022
Submitted to EC (Coordinator)	Andra	20/09/2022

EURAD (Deliverable n° 15.1) – Initial State-of-the-art of WP ConCorD
Dissemination level: Public
Date of issue of this report: **17/08/2022**

Page 3

Executive Summary

This report provides a review of the current state of the knowledge on the corrosion behaviour of candidate container materials for the disposal of spent fuels (SF) and high-level radioactive waste (HLW). The influence of radiation, microbiological activity and of time dependent transformations of the physical, chemical and thermochemical properties of the bentonite barriers in contact with the metallic containers, e.g., temperature, saturation with geological waters, compaction, and chemical changes, are emphasized. The degradation mechanisms and the estimations of container durability derived from them are recognized as mature in the case of so-called traditional materials such as carbon steel and copper. On the other hand, a series of novel ceramic and metallic materials of potentially improved performance are being developed, but whose corrosion properties and mechanisms are still unexplored.

Therefore, reliable comprehensive corrosion mechanisms covering the different materials in predictable changing environmental conditions have still to be developed to improve the long-term safety prognoses. This review aims to constitute a basis guide, upon which research activities should be designed to yield a fruitful advance in covering the gaps still open in the elucidation of complex corrosion mechanisms, namely the corrosion behaviour of classical materials under perturbations of the environment and those still unknown of the new developed materials. The context is mainly referred to national programs being carried out in Europe, with some references to programs from non-European countries for the sake of completeness.

EURAD (Deliverable n° 15.1) – Initial State-of-the-art of WP ConCorD
Dissemination level: Public
Date of issue of this report: **17/08/2022**

Page 4

Table of contents

EURAD (Deliverable n° 15.1) – Initial State-of-the-art of WP ConCorD
Dissemination level: Public
Date of issue of this report: 17/08/2022

Page 5

EURAD (Deliverable n° 15.1) – Initial State-of-the-art of WP ConCorD
Dissemination level: Public
Date of issue of this report: 17/08/2022

Page 6

EURAD (Deliverable n° 15.1) – Initial State-of-the-art of WP ConCorD
Dissemination level: Public
Date of issue of this report: **17/08/2022**

Page 7

List of figures

EURAD (Deliverable n° 15.1) – Initial State-of-the-art of WP ConCorD
Dissemination level: Public
Date of issue of this report: **17/08/2022**

Page 8

EURAD (Deliverable n° 15.1) – Initial State-of-the-art of WP ConCorD
Dissemination level: Public
Date of issue of this report: **17/08/2022**

Page 9

List of Tables

EURAD (Deliverable n° 15.1) – Initial State-of-the-art of WP ConCorD
Dissemination level: Public
Date of issue of this report: **17/08/2022**

Page 10

Glossary

ABM	Alternative Buffer Material
ANSTO	Australian Nuclear Science and Technology Organisation
ARWA	Australian Radioactive Waste Agency
BCLT	Buffer Coupon Long-term Test
BFS	Blast Furnace Slag
C/S	CaO/SiO_2 ratio
CRH	Critical Relative Humidity
CRT	Canister Retrieval Test
C-S-H	Calcium Silicate Hydrates
CSIRO	Commonwealth Scientific and Industrial Research Organisation
DSR	Dissimilatory Sulphate Reduction
DSSC	Disposal System Safety Case
EBS	Engineered Barrier System
Ecorr	Corrosion Potential
EDZ	Excavation Disturbed Zone
Eh	Redox Potential
FEBEX	Full-scale Engineered Barriers Experiment
FEP	Features Events and Processes
GDF	Geological Disposal Facility
GDR	Geological Disposal Repository
GR	Green Rust
HE/E	*in situ* heater test (in PEBS project: Long-term Performance of Engineered Barrier Systems))
HHGW	High Heat Generating Waste
HIC	Hydrogen Induced Cracking
HLW	High Level Waste
HotBENT	High Temperature Effects on Bentonite Buffers
HSR	High-strength Rock
IAEA	International Atomic Energy Agency
ILW	Intermediate Level Waste
ITA	In Tunnel Axial
ITD	In Tunnel Deposition
IVD	In Vault Deposition

EURAD (Deliverable n° 15.1) – Initial State-of-the-art of WP ConCorD
Dissemination level: Public
Date of issue of this report: **17/08/2022**

Page 11

LET	Linear Energy Transfer
LHGW	Low Heat Generating Waste
LLW	Low Level Waste
LOT	Long Term Test of Buffer Material
LSSR	Lower Strength Sedimentary Rock
MBM	Mined Borehole Matrix
MIC	Microbiologically Influenced Corrosion
MOX	Mixed Oxide
MPC	Multi-Purpose Container
NRVB	Nirex Reference Vault Backfill
OPC	Ordinary Portland Cement
PA	Performance Assessment
PFA	Pulverised Fly Ash
RAWRA	Radioactive Waste Repository Authority (Czech Republic)
RH	Relative Humidity
SCC	Stress Corrosion Cracking
SNF	Spent Nuclear Fuel
SoTA	State-of-the-art
SRB	Sulphate Reducing Bacteria
TBT	Temperature Buffer Test
THMC	Thermal, Hydraulic, Mechanical, and Chemical
TOC	Total Organic Carbon
URL	Underground Research Laboratories
WMO	Waste Management Organisation

EURAD (Deliverable n° 15.1) – Initial State-of-the-art of WP ConCorD
Dissemination level: Public
Date of issue of this report: **17/08/2022**

Page 12

Introduction

The concept of a sealed container (or canister) for the disposal of high-level radioactive waste (HLW) and spent fuels (SF) is pursued basically in all deep geological repository programmes. The container constitutes the only barrier within the overall multi-barrier disposal system which provides a complete confinement of radionuclides. Therefore, the attention is frequently focused on the performance of the canister, specially concerning the length of the lapse of time during which the material stability and thus the barrier function can be guaranteed.

Preestablished lifetime requirements can vary significantly under the different national programmes. They are typically linked to the type of waste, the selected canister material(s) and disposal concept, and the characteristics of the near field and of geological environments. The failure of canisters is typically expected after the environmental induced degradation of the materials exceeds a permissible threshold, which depends i.a. on the mechanical stress. In such a case, the release of radionuclides in the nearfield cannot be excluded.

The source of stress during disposal can be residual, lithostatic and hydrostatic pressures, the swelling of buffer bentonites or rock displacements. The hydrostatic loads are essentially isotropic. The other types of canister loads, on the other hand, can be unevenly distributed, generating anisotropic stress fields and shear forces. The generated stresses in the canister wall, lid, and base, including the seal joint region, must remain under the failure limit for the expected lifetime of the canister by an adequate margin. This is typically demonstrated by structural assessments which consider the strength and fracture toughness of the canister material(s), the maximum conceivable size of manufacturing defects, and the evolving disposal environment.

The reduction of the wall thickness by environmentally induced corrosion is an important input data in the structural analysis for some canister concepts, as mentioned above. As the thickness reaches a critical value, stresses can lead to a plastic collapse. The intrinsic materials properties can also be altered by hydrogen uptake, neutron embrittlement or preferential leaching/dissolution, which often leads to a reduction of the fracture toughness and to a larger risk of mechanical damage.

An overview of the currently planned container concepts and their expected exposure conditions are shown in *Table 0-1*.

The required prediction of the degradation rate needs a precise knowledge of the corrosion mechanism under the environmental conditions created in the near-field environment of the canister after the sealing of the disposal area. This includes the long-term alteration of the physicochemical properties of the environment caused by chemical-geological activity, radiolysis, and microbial activity.

The aim of this report is to summarise the state of the art on the research targets of EURAD WP15 ConCorD. These are:

- to assess the corrosion mechanisms of traditional materials in complex scenarios where the corroding environment is under the influence of irradiation, microbial activity or temporal changes of the environmental chemistry (Chapter 1),

- to assess the potential of novel materials for improving the canister performance (Chapter 2), and

- to integrate experimental evidence on canister degradation in the improvement of prediction power of corrosion models used for performance assessments (Chapter 3).

EURAD (Deliverable n° 15.1) – Initial State-of-the-art of WP ConCorD
Dissemination level: Public
Date of issue of this report: 17/08/2022

Page 13

Table 0-1: Canister concepts and illustrative environmental conditions for various WMO repository designs

WMO	Canister concept	Estimated or target lifetime (yr)	Nominal buffer dry density (g/cm^3)	Max canister temperature (°C)	Time to full nearfield saturation (yr)	Maximum surface absorbed dose rate (Gy/hr)	Expected mechanical loads (MPa)
SKB	Copper-cast iron	>10^6	1.6	95	Few tens to a few thousand	0.2	15 50 (glacial)
Posiva	Copper-cast iron	>10^6	1.55	95	Few tens to a few thousand	0.3	14 50 (glacial)
Andra	Carbon steel	>500	No buffer	90		10	
Ondraf-Niras	Carbon steel	Several thousand	Cementitious buffer	100	5-10 up to a few thousand	25	8
Nagra	Carbon steel	10,000	>1.45	~120	A few centuries	0.2	22-29 max
SURAO	Carbon Steel	10,000	1.4	95	100	0.3	20
NWMO	Copper coated steel	>10^6	1.6	85	50-5,000 depending on host rock type	0.8	15 45 (glacial)
NUMO	Carbon steel	>1,000	1.6	100	<1,000 Host-rock dependent	0.006-0.011	11 (hard rock)

EURAD (Deliverable n° 1.1) - State-of-the-art Report ConCorD
Dissemination level: Public
Date of issue of this report: **xx/xx/**

Page 14

1. Environmental factors altering the corrosion process

1.1 Effects of radiation

1.1.1 Irradiation of buffer materials

The selection of bentonites as barrier material in nuclear waste repository concepts is accounted by their properties regarding the safety of the site. For instance, they constitute an efficient barrier against radionuclide migration. The physicochemical properties of the clay minerals present in bentonites as swelling, water retention, cation exchange capacity, or their solubility can however be altered by radiation. The radiation can also affect the clay structure causing its amorphization, undermining the long-term stability of these materials and thus the safety and integrity of the repository.

Most studies, however, report that radiation doses much higher than those expected in deep geological repositories should be necessary to alter the clay properties. Structural changes are observed for example only after clay amorphization. This is reached after large, cumulated doses under ionizing radiation. Ballistic damage, on the other hand, is more efficient by clay amorphization, but it is only in the case of barrier failure. Changes of the valency of structural iron, expressed as $Fe(II)/Fe_{tot}$, have been observed in several studies. This may modify the swelling behaviour and the surface reactivity (specific surface area and cation exchange capacity). As highlighted by Allard and Calas (2009), contradictory results arise from studies on the surface reactivity evolution with radiation. Some authors observed an increase of the specific surface area or the cation exchange capacity, while others observed the inverse effect or none of them under radiation. However, the increase of the cation exchange capacity was frequently observed.

A comprehensive review on the evolution of clay properties under radiation can be read in the works of Allard et al. (2012) and Dixon (2019).

1.1.1.1 Role of interlayer cations

Lainé et al. (2017) compared the behaviour of different types of clays under electron beam, analysing the influence of the location of excess negative charge layers (synthetic montmorillonite and saponite), and the amounts of iron (natural montmorillonite and beidellite). They showed that synthetic clays exhibit a similar behaviour under irradiation, which was monitored by the production of H_2. The yields of radiolytic H_2 are not controlled by the composition of the sheets and the location of excess negative charges. In natural clays, however, the presence of impurities such as iron has a strong impact on the behaviour under radiation, as Fe(III) acts as electron scavenger reducing the H_2 production.

Gu et al. (2001) observed different behaviours under electron beam of 200 keV depending on the clay composition: montmorillonite, saponite, nontronite. In particular, the amorphization dose, i.e., the dose at which a material loses its crystallinity, depends on the type of the clay (Figure 1-1a). The amorphization dose for montmorillonite is lower than that for saponite above 200°C. The amorphization dose for non-swelling clay nontronite is higher than those for montmorillonite and saponite, even at room temperature. These differences are attributed to the distinct interlayer cation substitutions. Thus, the interlayer cation seems to play an important role in the amorphization process. But it appears that it is not the only contributing factor, as Sorieul et al. (2008) did not observe significant differences in the amorphization dose (under 200 keV electron beam and 1 MeV Kr^+ radiation) under Ca-, Li-, Na- and K-montmorillonites (Figure 1-1b).

EURAD (Deliverable n° 15.1) – Initial State-of-the-art of WP ConCorD
Dissemination level: Public
Date of issue of this report: **17/08/2022**

Page 15
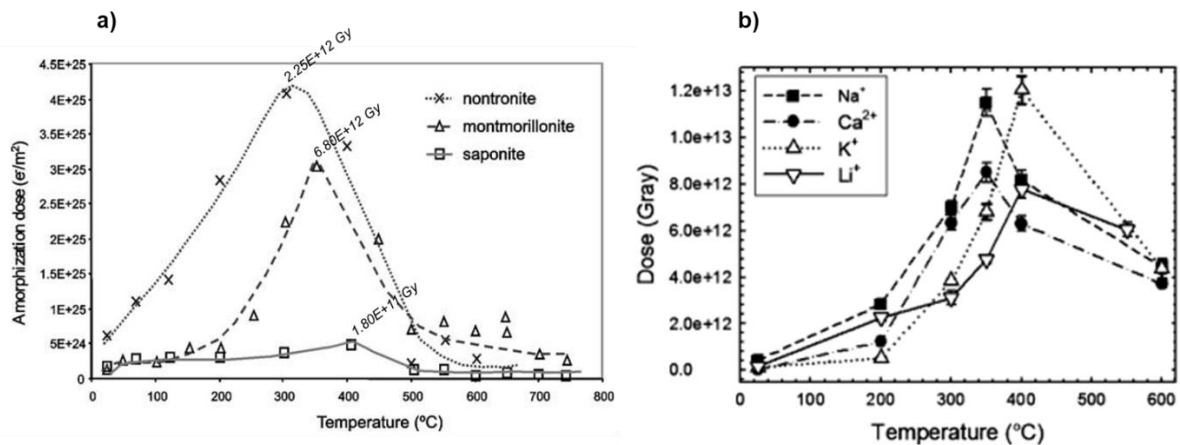
Figure 1-1: Temperature dependence of amorphization dose of clays irradiated by a 200 keV electron beam: a) montmorillonite, nontronite and saponite (Gu et al., 2011). Conversion factor of e m^{-2} to Gy is approx. 4.47×10^{11}, 1.81×10^{11} and 2.77×10^{11} for montmorillonite, nontronite and saponite respectively. b) Li$^+$-, Na$^+$, K$^+$ and Ca^{2+}-montmorillonites (Sorieul et al., 2008)

The composition and the distribution of accessory minerals may also influence the clay behaviour as their radiation stability is different from that of montmorillonite in smectites. They can dissolve locally under radiation changing the clay properties, e.g., inducing the formation of new phases (Dixon 2019) (Pusch et al. 1992) (Safi 2017).

1.1.1.2 Influence of temperature

In irradiated heated clays, two competing processes modify the clay properties and their mineralogy: the creation of defects by radiation and their thermal annealing. The amorphization dose of smectites increases with increasing temperatures up to 300-400 °C (Gu et al., 2001) (Sorieul et al., 2008) (Figure 1-1), which is directly linked to the healing effect of temperature. Beyond these temperatures, the amorphization dose decreases, implying another destabilizing process: the dehydroxylation. Irradiation also sinks the temperature at which dehydroxylation occurs: above 300-400 °C for irradiated clay against 700 °C for non-irradiated clays (Sorieul et al., 2008).

1.1.1.3 Influence of water and vapour hydration

The radiation stability of clays decreases with water content, it being very high in dry clays. This is due to the radiolysis of interlayer or pore water (Gu et al., 2001). The amount of water radiolysis products decreases with lesser water contents, thus increasing the clay stability.

Water in contact with bentonite is potential source of ions that may substitute the initial interlayer cations, thus affecting the behaviour of clays under radiation. This, indeed, requires that sufficient water content is available to allow water diffusing.

Lainé et al. (2017) studied the effects of radiation on clays as a function of the water content (expressed as relative humidity, RH). The evolution of the radiolytic yield indicated that the reactivity of synthetic swelling clay is controlled by the water amount. At low RH (<11%), water molecules are highly confined in the interlayer space, favouring the recombination of reactive species. Consequently, the H$_2$ yield G(H$_2$) strongly increases, being higher than that in bulk water. At higher RH, the confinement effect is

EURAD (Deliverable n° 15.1) – Initial State-of-the-art of WP ConCorD
Dissemination level: Public
Date of issue of this report: **17/08/2022**

Page 16

less pronounced, allowing the introduction of additional water molecules, and making the recombination of hydrogen less efficient. Above 74% RH, water molecules appear in the intergranular porosity, between the clay particles, and exhibit a bulk-water behaviour. Direct radiolysis of water takes place and $G(H_2)$ become constant at a value slightly higher than in bulk water.

The redox state of bentonite may change upon reaction with the species formed by water radiolysis. Radiation can modify the content of structural Fe(II) and Fe(III), which in turn exerts a considerable influence on the physical properties of the clay, as the cation exchange capacity, the layer charge, the swelling pressure, and the specific surface area. Holmboe et al. (2012) studied the redox behaviour of montmorillonite and the reactivity towards H_2O_2, one of the main oxidants produced by water radiolysis. Under anoxic conditions, the Fe(II)/Fe$_{tot}$ increases from ~3% to 25-30% after applying a gamma dose of 13 kGy (^{137}Cs source). A correlation between H_2O_2 decomposition rate and increasing Fe(II)/Fe$_{tot}$ ratio is shown, suggesting that the changes in the redox properties of the clay with irradiation arise from H_2O_2 decomposition.

Chikkamath et al. (2021) observed a decrease of the Fe(II)/Fe$_{tot}$ ratio in Fe(II)-montmorillonite with radiation (14% oxidation) for a dose of ~7 kGy. However, the Fe(II) is reverted to the initial oxidation state after a prolonged radiation exposure. For instance, after a dose of ~14 kGy the ratio is found to be similar as for that of the unirradiated sample. The dose at which this effect is observed is lower in the case of aerated samples than in samples saturated with inert Ar or N_2O. This difference is attributed to a change in concentration of solvated electrons e^-_{aq} under aerated and deaerated conditions. Otherwise, all samples exhibit quite similar behaviours.

Gournis et al. (2000), on the other hand, observed a partial reduction of structural Fe(III) (3%) in Na$^+$-montmorillonite at intermediate RH (~10 wt.% H_2O) after γ-irradiation at a dose rate of ~84 kGy/h, which was attributed to the diffusion of the reducing H radicals.

Concerning the impact of the gas phase, exposure of clays to steam at 200 °C, like to exposure to radiation alone, leads to changes in the cation exchange capacity and the sedimentation volume, due to changes in the charge distribution. Moreover, gaseous products resulting from radiation or corrosion may occupy voids, delaying or inhibiting water saturation, thus inducing a drying of the buffer adjacent to the hot canisters (Xie et al., 2012). Therefore, this effect may not be deleterious to the clay stability.

1.1.1.4   Influence of radiation source

According to the literature, the main influence of the radiation source is the efficiency to induce amorphization. Different radiation-induced damage processes are triggered by ionizing or heavy particles radiation. Heavy ions and recoil nuclei cause atomic displacements and collision cascades which can be considered as the origin of extended defects and mineral amorphization. Ionizing radiation creates mainly electronic point defects that are generally thermally unstable. In clays, ionizing radiations may produce electron-hole pairs, mostly located on oxygen atoms of the structure either associated to Si or to Al (Allard et al., 2012) (Jonsson, 2012). Hence, the dose to reach the clay amorphization is 3 to 4 orders of magnitude lower than that necessary under electron radiation.

1.1.1.5   Influence of the total dose and dose rate

Chikkamath et al. (2021) studied the effect of radiation on the redox behaviour of montmorillonite. They found that the irradiation of powdered samples of Fe(II)-clay at 0.6 and 12 kGy h^{-1} does not show any effect. These observations are probably because the irradiated clays were dry, thus minimizing the effect of water radiolysis and gas production.

EURAD (Deliverable n° 15.1) – Initial State-of-the-art of WP ConCorD
Dissemination level: Public
Date of issue of this report: 17/08/2022

Page 17

Studies show that very high doses are needed to induce changes in the clay. Negron et al. (2002) observed no changes of local atomic structure in montmorillonite exposed to a gamma radiation up to 2 MGy. Gamma radiation experiments performed with MX-80 bentonite in conditions of thermal gradient and water saturation did not show any mineralogical evolution over one year and with a total dose of ~3×10^7 Gy (Pusch et al., 1992). Gournis et al. (2000) reported that no detectable crystallographic modifications are observed for clay irradiated with 3×10^8 Gy. In fact, the structural modifications were reported for accumulated doses of 10^{11} - 10^{13} Gy of gamma radiation depending on the temperature. In the case of irradiation with heavy ions dosis ~$10^8 - 10^9$ Gy (corresponding to 0.1 - 0.2 dpa) are enough (Allard & Calas, 2009) (Dixon, 2019) (Gu et al., 2001) (Sorieul et al., 2008).

1.1.2 Effects of irradiation on the corrosion of carbon steel containers

It is well-known that the corrosion of carbon-steel, besides the formation of large amounts of corrosion products, induces the production of hydrogen gas. The corrosion rate depends on several factors, such as temperature, pH, water composition, atmosphere, and irradiation. The nature of the oxide phases formed on the surface can be changed by an increase in the corrosion potential (E_{corr}) due to water radiolysis products. Most of the studies concerning corrosion under irradiation found in the literature report on the formation of a passivating film constituted of magnetite and hematite. Some other phases such as lepidrocrocite and goethite are also reported. The corrosion rates often increase under radiation, which is ascribed to the presence of water radiolysis products. Several studies report that the corrosion rate, even after an initial increase, return to the same value as measured in unirradiated experiments (Nelson et al., 1983) (Smart et al., 2008). This can be explained in terms of the formation of a protective passive film. Generally, quite high doses rates in a kGy h^{-1} range are necessary to show corrosion enhancement under radiation.

Unless otherwise stated, all irradiation experiments referred below were carried out with a cobalt-60 gamma radiation source.

1.1.2.1 Effect of steel composition and microstructure

In their review about radiation effects on the corrosion of candidate container materials for the storage of HLW, Shoesmith & King (1999) compared results of corrosion experiments of several types of steel. They concluded that, except for low chromium and low molybdenum steels, the composition and microstructure of the steel do not seem to affect the corrosion rate under irradiation. The presence of impurities or welding induce localized corrosion (Ahn & Soo, 1995).

1.1.2.2 Effect of temperature

The temperature can play a major role by increasing the corrosion rate in aqueous media. Increases in temperature increases the rate of chemical and electrochemical reactions involved in the corrosion processes. Moreover, it modifies the rate of diffusion processes and the solubility of the corrosion products (Konovalova, 2021) (Kursten et al., 2003).
Gray (1987) observed an increase of the corrosion rate with the temperature when studying the corrosion of mild steel in salt brines under gamma radiation at 75 and 150 °C. These results, however, do not distinguish between the contributions of temperature and irradiation.

EURAD (Deliverable n° 15.1) – Initial State-of-the-art of WP ConCorD
Dissemination level: Public
Date of issue of this report: 17/08/2022

Page 18

Winsley et al. (2011) studied the corrosion of carbon steel in deaerated alkaline solution (pH ~13.4, $[O_2]$ < 10 ppm) under gamma radiation at a dose rate of 25 Gy h^{-1}. The initial corrosion rate at 80 °C is higher than at 25 °C but decreases more rapidly at 80 °C than at 25°C. The appearance of the oxide formed on the samples changes between 25 °C and 80 °C (magnetite). The irradiation, however, does not appear to modify the appearance or the composition of the formed corrosion products.

Daub et al. (2011; 2019) studied the effect of temperature (25 to 150 °C) on the corrosion of steel immersed in deaerated water with pH$_{25°C}$ ~7 or adjusted to 10.6 with LiOH ($[O_2]$ < 1000 ppm). They used a ^{60}Co gamma source with a dose rate of 6.2 kGy h^{-1} and samples irradiated for 20 or 66 hours (~12 - 41 kGy). They showed that, in comparison to irradiation, temperature has little influence on the corrosion potential and hence on the nature of the corrosion product formed. It may, however, determine the amount of corrosion products and the oxide layer thickness. These results are in line with the study by Čuba et al. (2011), who irradiated carbon steel plates immersed in deaerated deionized Millipore water or synthetic granitic water (pH of ~6.3 and ~6.9 respectively) at 25 °C, 50 °C and 70 °C. The dose rate was of 0.22 kGy h^{-1} and total dose ranging from 0 to 120 kGy. They also observed an increased quantity of dissolved iron in solution with the temperature, indicating a higher dissolution rate of iron.

1.1.2.3 Effect of water and vapour hydration

Upon exposition to radiation, the vapour or aqueous phase decomposes to a series of oxidizing and reducing species that can change the corrosion processes. The nature and concentration of the radiolytic species (radicals or molecular products) produced by irradiation depend on the environment. Beyond the iron ions, various inorganic ions present in groundwater such as carbonates, magnesium, calcium or chlorides can act as scavengers for radiolysis products. The water composition might therefore impact the corrosion behaviour of steel under irradiation. Marsh and Taylor (1988) for instance measured higher corrosion rate in seawater than in granitic water.

Smart et al. (2008) studied the anaerobic corrosion of carbon steel in two synthetic waters (modified Allard groundwater and bentonite equilibrated groundwater) and observed in both cases an increase of the corrosion rate with radiation: 30 times higher for the Allard water and 10 to 20 times for the bentonite water. Opposite to the Allard groundwater with a pH 8.8, the bentonite groundwater (pH 10.4) has a simpler composition but has a high concentration of chloride and sodium and also contains carbonates. The lower enhancement in the corrosion rate for the bentonite groundwater is attributed to its a higher ionic strength and initial pH.

Daub et al. (2011) studied the effect of gamma radiation (6.2 kGy h^{-1}, total doses of ~12 - 41 kGy) on the corrosion of carbon steel as a function of the pH of the water in which samples were immersed (pH 6 and 10.6). They observed that when the carbon steel samples were irradiated at 150 °C in either LiOH (pH$_{25°C}$ 10.6) solution or distilled water (pH$_{25°C}$ ~7), pH has no impact on the nature of the formed oxides, but does on its crystallinity. At mildly basic pH the layer formed is uniform and compact. This contrasts with that one formed at neutral pH which is is non-uniform and porous. This is attributed by the authors to influence of pH on the iron solubility which can alter the rates of the reactions forming the oxide, thereby affecting its crystallinity and overall protective ability.

Among the radiolytic species produced by water radiolysis, H_2O_2 plays a key role in the control of carbon steel corrosion under radiation. Daub et al. (2010) also compared the gamma radiation effect on corrosion with that of addition of H_2O_2. They demonstrated that H_2O_2 concentration can change the nature of the formed corrosion products. While irradiation transforms maghemite into magnetite, the reaction is reversed towards maghemite with $[H_2O_2]$<10^{-3} mol l^{-1}. At H_2O_2 concentrations higher than 10^{-3} mol l^{-1}, however, magnetite and maghemite transform to lepidocrocite. This study indicated that under the experimental conditions (i.e., room temperature and pH of 10.6), the corrosion rate of carbon steel in a γ-radiation environment can be predicted from the dependence of the corrosion potential on $[H_2O_2]$.

EURAD (Deliverable n° 15.1) – Initial State-of-the-art of WP ConCorD
Dissemination level: Public
Date of issue of this report: 17/08/2022

Page 19

Vanderborre et al. (2013) also pointed out the role of the hydrogen peroxide in the corrosion of carbon steel by showing similar results in the corrosion induced by the $^4He^{2+}$ water radiolysis (22 kGy) and by addition of H_2O_2 by comparable volumetric concentration (10^{-4} mol l^{-1}), among others the formation of lepidocrocite. An inhibition effect of H_2 in the corrosion process is also underlined, as well as a potential role of O_2 species.

Concerning the impact of the gas phase radiolysis on carbon steel, Brehm (1990) showed that, in an air/steam mixture, the irradiation effect is very limited on the corrosion of low-carbon steel at 150°C, but increases significantly the corrosion rate (factor of ~10) at 250 °C.

Lapuerta et al. (2006; 2008) studied the atmospheric iron corrosion under proton irradiation (3 MeV, 10 nA) as a function of the relative humidity (RH) values and under several gas phases (N_2 with O_2 or H_2O or both). Their results indicate that, in their experimental conditions the coupled action of H_2O and O_2 is necessary for the formation of an iron oxide layer, since no iron oxidation was observed in the absence of one of the species. Moreover, corrosion starts at lower RH values (<20%) under irradiation than without exposition (60%). A maximal corrosion rate was observed for a RH of 45% against 95% or higher without irradiation. A layer of water on the surface of the iron is necessary to induce atmospheric corrosion. It forms from RH of 40-60% on without radiation. Irradiation allows this layer to set at lower RH values in particular via the formation $H^+(H_2O)_n$ clusters.

1.1.2.4 Effect of the radiation source

The main effect of the radiation source is to change the radiolysis products. The production of the primary products relies on the type of radiation while their concentration depends on the Linear Energy Transfer (LET). This concept corresponds to the loss of energy by unit length in the irradiated medium and depends on the energy and type of radiation particles. High LET radiation (heavy ion radiation) have a high production of molecules and a low production of radicals while low LET radiation (ionizing radiation) have a tendency to produce more radicals (Mendoza, 2017).

1.1.2.5 Effect of the total dose and dose rate

There is some correlation between steel corrosion rates and the dose rate as visible in Table 1-1, which summarizes corrosion rates under irradiation found in the literature, although non-exhaustively. This effect is, however, limited in time and corrosion rates often evolve toward those of unirradiated steel coupons after a few months.

Gray (Gray 1987) observed that at 75 °C the corrosion potential and corrosion rate of mild steel in salt brines increases on increasing the dose rate. After three weeks of irradiation, the corrosion rate for a dose rate of 2.6 kGy h^{-1} is three times larger than that measured for a dose rate of 240 Gy h^{-1} (from 73 to 220 µm y^{-1}).

Marsh & Taylor (1988) observed a similar tendency on irradiating carbon steel in synthetic seawater at dose rates of 3, 35 and 1000-1500 Gy h^{-1} at 90 °C. The corrosion is accelerated when the radiation dose rate increases: at 35 Gy h^{-1} the measured corrosion rate is ~8 times higher than that for a non-irradiated sample and ~20 times greater for the highest dose rate applied. For a dose rate of 1000-1500 Gy h^{-1} and after a period of 100 days, a stabilization or even a decrease of the corrosion is observed. It is interesting to note that a negligible increase of the corrosion rate at a dose rate of 3 Gy h^{-1} was observed (Marsh a& Taylor 1988). A similar effect was pointed by Crusset et al. (2017) for 20 Gy h^{-1} dose rate irradiation in anoxic conditions.

EURAD (Deliverable n° 15.1) – Initial State-of-the-art of WP ConCorD
Dissemination level: Public
Date of issue of this report: 17/08/2022

Page 20

The variation of corrosion rate under irradiation with time was also reported by Smart et al. (2008) who compared the corrosion of carbon steel at dose rates of 11 and 300 Gy h^{-1} in anoxic Allard water at 30 °C and bentonite-equilibrated water at 50°C. In both media, the gamma radiation increases the anaerobic corrosion rate of steel. At 11 Gy h^{-1} the corrosion rate decreases after about 1000 h to finally reaches the same value than that for unirradiated conditions (roughly between 2000 and 4000 h, Figure 1-2 a). At 300 Gy h^{-1} the corrosion enhancement lasts longer and may even be continuous. Interestingly, the initial increase of corrosion rate seems to be less important at 300 Gy h^{-1} than at 11 Gy h^{-1}.
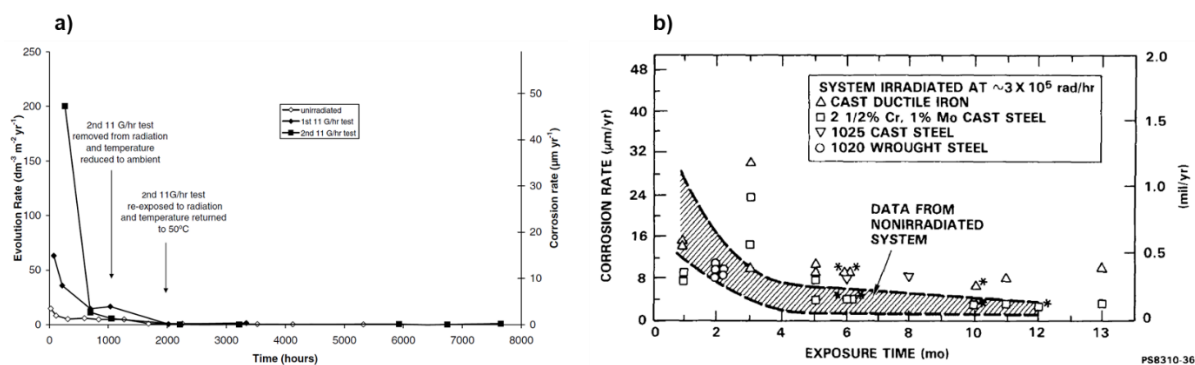
Figure 1-2: a) Hydrogen evolution and corrosion rates of carbon steel in anoxic bentonite-equilibrated water at 50°C at 0 and 11 Gy h^{-1} (Smart et al., 2008). b) Corrosion rates of iron-based alloys exposed to synthetic Hanford Grande Ronde basalt water at 250°C at 3×10^3 Gy h^{-1} (Nelson et al., 1983)

Westerman et al. (1983) studied the corrosion of ferrous materials at 150 °C in an anoxic brine. The corrosion rates observed at 1000 Gy h^{-1} were considerably higher than those obtained under non-irradiated conditions (by a factor of ~6). On the other hand, the corrosion rates determined at 150 ° C and 20 Gy h^{-1} showed an increase of the corrosion rate by factor of 1.5 - 2.0 after 1 month. But no significant increase over values measured under non-irradiated conditions was observed after 3 months of exposure. Similar results were observed at dose rates of 13000 Gy h^{-1} (Ahn & Soo, 1995) and 35000 Gy h^{-1} (Nelson et al., 1983) in basaltic water (Figure 1-2b).

1.1.2.6 Buffer-container system

There are only a few reports on buffer-container systems under irradiation. Pusch et al. (1992) studied MX-80 bentonite in conditions close to those found in a repository. They enclosed bentonite saturated in Allard water (low salinity) in contact with carbon steel plates in the presence of both a temperature and a radiation (^{60}Co source) gradient for 1 year. The temperature ranged from 130 °C in the clay area in contact with the carbon steel (strongest radiation: 3.97 kGy h^{-1}) to 90 °C at the opposite side in contact with stainless steel and where the irradiation dose was ten times lower (0.46 kGy h^{-1}). They replicated the experiment with no radiation source and extensively analysed the clay to determine if the bentonite properties were affected by the environmental conditions. The main conclusion is that the combined effect of gamma radiation and heating causes only insignificant modifications of the smectite properties.

The MX-80 bentonite is mainly composed of Na-montmorillonite and, as accessory minerals, of some amount of quartz, feldspars and low amounts of calcite and opal. For the two experiments, the structure of the clay remained almost intact after one year. The major mineralogical alterations were the disappearance of feldspars, the formation of calcium and magnesium-bearing sulphates in the hotter part of the samples, and a slight dissolution and transformation of a 10 Å thick sheet of minerals. A slight cementation of the clay associated to the precipitation of silicious compounds was also reported. As a

EURAD (Deliverable n° 15.1) – Initial State-of-the-art of WP ConCorD
Dissemination level: Public
Date of issue of this report: 17/08/2022

Page 21

consequence, the clay significantly strengthened in the part of the sample heated at 130°C. Physical properties such as hydraulic conductivity and rheological behaviour underwent only small changes indicating that cementation effects were not very important, and that the swelling capacity did not decrease significantly.

Extensive pitting corrosion is observed in steel plates after experiments with and without radiation (Pusch et al.,1992). Irradiation enhanced the corrosion. An average corrosion depth is of 80 µm was measured in the irradiated sample while 18 µm could be determined in the non-irradiated steel. The pitting depth was found up to 480 µm and 160 µm for the irradiated and non-irradiated system respectively. Iron was released from the steel and diffused into the clay by about 10 mm depth. This iron may have participated in the cementation of the clay and in the formation of new phases.

As in most of the studies on steel corrosion, radiation-enhanced corrosion has also been observed by Debruyn (Debruyn, 1988) who summarized results obtained on the corrosion of several candidate containers materials, including carbon steel and cast iron under clay repository conditions. In some of the tests, samples were in direct contact with the clay while others were in contact with interstitial clay water, humid clay atmosphere (up to 170°C) or Antwerpian groundwater. Some tests were performed under gamma radiation (^{60}Co) with dose rates of 1 kGy h^{-1} in inert or oxidizing atmosphere. Furthermore, they performed experiments on carbon steel in interstitial clay water and clay/clay water mixtures at 90°C for exposure times ranging from 50 to 1000 hours. After 40 days of irradiation the pH of the clay remained almost unchanged, but a slight acidification is observed in oxidic conditions. The production of H$_2$ with a yield close to the one calculated for the radiolysis of water was measured.

Concerning the steel corrosion mechanism, pitting was observed in both irradiated and non-irradiated samples with a similar penetration depth in both cases. A maximum corrosion rate of 150 µm y^{-1} was measured without radiation, whereas a value of 300 µm y^{-1} was determined under radiation in oxidic conditions.

In a more recent work, Liu et al. (2017) studied the corrosion of low carbon steel in bentonite containing 17 wt.% of Beishan groundwater (Na-Cl-SO$_4$ type) and irradiated with a cobalt-60 gamma source debiting 2.98 kGy h^{-1} for 1007 h (3 MGy). The same experiment was performed without radiation. Finally, samples were thermally aged at 90°C for 2880 hours. The corrosion products formed are mainly magnetite, hematite, and goethite with the formation of two new phases under irradiation: siderite and maghemite. The distribution of these corrosion products on the surface is not uniform and two corrosion layers were clearly observed on the samples, an inner and an outer layer, which is consistent with aerobic corrosion. Pitting was the main corrosion form observed in these experiments with deeper pits appearing in the irradiated sample. Irradiation was indeed shown to accelerate the corrosion rate of steel by ~33%, the corrosion rate being of 24 µm y^{-1} in the non-irradiated samples and of 32 µm y^{-1} in the irradiated samples.

1.1.3 Effect of irradiation on the corrosion of copper containers

The effect of irradiation on the corrosion behaviour of copper has recently been reviewed in Posiva (2021), from which the following text is taken.

1.1.3.1 Radiolysis effects on copper corrosion

Because of the general lack of oxidising species for copper in the repository, the generation of additional radiolytic oxidants is an important consideration. Figure 1-3 shows the enhancement factor for the rate of general corrosion for oxygen-free copper based on the results of seven different irradiation studies

EURAD (Deliverable n° 15.1) – Initial State-of-the-art of WP ConCorD
Dissemination level: Public
Date of issue of this report: 17/08/2022

Page 22

from various nuclear waste management programmes. Under saturated conditions (i.e., in bulk solution or in saturated buffer material), an enhancement in the corrosion rate is only observed for absorbed dose rates greater than 20 Gy/h (Figure 1-3(a)). At lower dose rates, the observed corrosion rate is typically lower in the presence of radiation. Neither the initial degree of aeration of the solutions nor the exposure period appear to have any significant impact on the enhancement factor. Alternatively, plotting the data in terms of the total dose (Figure 1-3(b)) suggests an increase in the degree of enhancement with increasing dose, with no apparent enhancement for absorbed doses <10 kGy. However, caution should be used in interpreting the data in Figure 1-3 as the various studies were not all conducted to the same total dose or for the same period of time. In addition, the absence of an observed enhancement in the corrosion rate may simply be a reflection of the sensitivity of the corrosion rate measurements, although the consistent observation for a decrease in the corrosion rate for irradiation at low dose rates or to low total doses does suggest the absence of any enhancement under these conditions.

EURAD (Deliverable n° 15.1) – Initial State-of-the-art of WP ConCorD
Dissemination level: Public
Date of issue of this report: 17/08/2022

Page 23

(a)

(b)
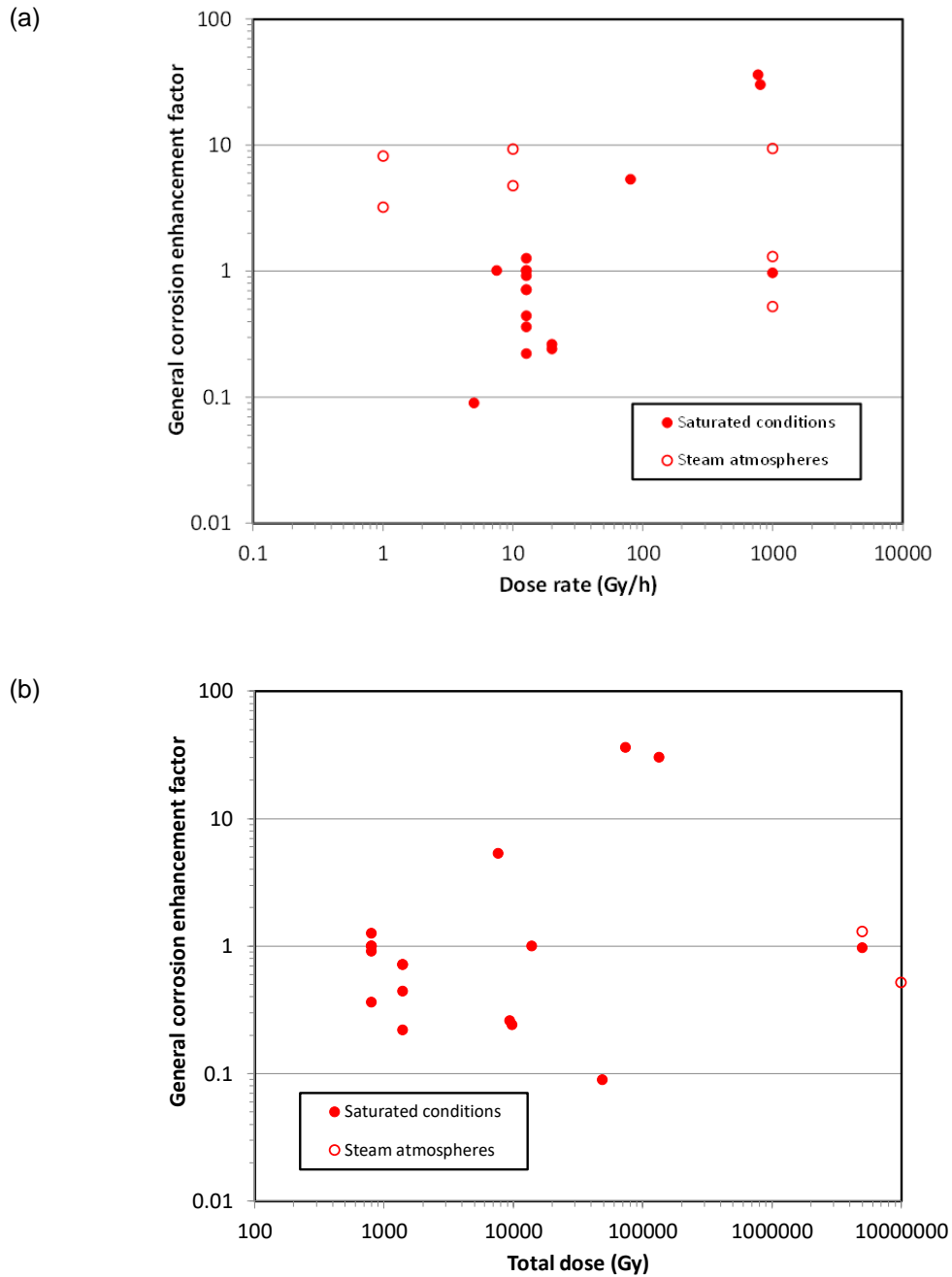
Figure 1-3: Effect of gamma irradiation on the enhancement of the rate of uniform corrosion of oxygen-free copper as a function of (a) dose rate and (b) total dose (King 2021). The enhancement factor is the ratio of the corrosion rate in the presence of radiation to that in the absence of radiation, as measured under similar environmental conditions and over a similar duration. An enhancement factor greater than one indicates that the corrosion rate is higher in the presence of irradiation.

EURAD (Deliverable n° 15.1) – Initial State-of-the-art of WP ConCorD
Dissemination level: Public
Date of issue of this report: **17/08/2022**

Page 24

Björkbacka and co-workers investigated the mechanism of the radiation-induced corrosion of oxygen-free, phosphorus-doped (OFP) copper in deaerated high-purity water (Björkbacka et al. 2012, 2013, 2015, 2016). Experiments were conducted at relatively high absorbed dose rates (80-770 Gy/h), but to total absorbed doses similar to those predicted for the a KBS-3 style canister for times up to 100 years (of the order of 100 kGy). Based on the early studies, Björkbacka et al. (2012, 2013) reported three unexplained observations:

- the total amount of corrosion (as both precipitated oxide and dissolved copper in solution) far exceeded that predicted based on a homogeneous radiolysis/surface kinetic model,
- the dissolved copper concentrations exceeded the solubility of either Cu_2O or CuO,
- and there was evidence for localised attack in the form of circular corrosion features (local depth of penetration of 0.8 μm).

Subsequent investigations have resolved these unexplained observations (Björkbacka et al. 2016, Soroka et a. 2021). Furthermore, even though the extent of corrosion was described by the authors as significant, the maximum predicted depth of penetration for repository-relevant total absorbed doses was only of the order of 1-2 μm.

Perhaps the most significant issue of those listed above, was the discrepancy between the observed extent of corrosion and the amount predicted on the basis of radiolysis modelling. For a time, this unexplained discrepancy led the investigators to suggest that an unknown process other than the radiolytic production of oxidants was responsible for the radiation-induced corrosion (Björkbacka et al. 2013, 2015, 2016). The initial modelling attempt was based on coupling a homogeneous radiolysis model to predict the time-dependent concentrations of various radiolysis products to a kinetic expression for the rate of corrosion as a function of oxidant concentration. The only two oxidants considered were H_2O_2 and hydroxyl radicals OH•, although the latter was considered to be the primary oxidant (Björkbacka et al. 2016). However, this modelling approach, which had proved successful in predicting the rate of oxidative dissolution of UO_2 (Ekeroth et al. 2006), could only account for a fraction (as little as one thousandth) of the observed corrosion. This lead the investigators to suggest that the presence of a semi-conducting oxide, which was found to enhance the extent of radiation-induced corrosion (Björkbacka et al. 2016), played a key role. It was suggested that irradiation of the oxide could lead to the formation of electron-hole pairs, which would lead to an increased potential difference between the (cathodic) oxide and (anodic) underlying copper. Alternatively, it was speculated that the yield (G-value) of OH• was much greater in the presence of the oxide than was assumed for the homogeneous radiolysis model. This increased yield of oxidants along with the large effective surface area of the oxide would result in a greater predicted degree of corrosion (Björkbacka et al. 2016).

Subsequnetly, however, Soroka et al. (2021) have resolved this discrepancy by modifying the radiolysis model. A series of experiments was performed in which copper coupons were exposed to H_2O_2-containing anoxic water and the oxide film thickness measured for different exposure conditions and durations. Corrosion was found to continue long after the added H_2O_2 had been completely consumed (either by electrochemical reduction to support corrosion or through heterogeneous decomposition to O_2 and H_2O), from which Soroka et al. (2021) concluded that O_2 rather than either H_2O_2 or OH• was the oxidant under irradiated conditions. A radiolysis model was developed that included the H_2O_2 decomposition reaction

EURAD (Deliverable n° 1.1) – Initial State-of-the-art of WP ConCorD
Dissemination level: Public
Date of issue of this report: **17/08/2022**

Page 25
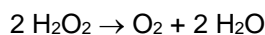
$$2 H_2O_2 \rightarrow O_2 + 2 H_2O \qquad\qquad (1.1\text{-}1)$$

as well as the subsequent reaction between O_2 and Cu. In this initial model, these two interfacial processes were treated as homogeneous reactions with rate constants characteristic of diffusion-controlled reactions. With these modifications, Soroka et al. (2021) were able to account for the oxide film thickness previously reported by Björkbacka et al. (2013). Thus, the apparent discrepancy between the observed and predicted corrosion was the result of an incomplete radiolysis model rather than an additional non-radiolytic process.

Björkbacka et al. (2016) also resolved another early unexplained observation related to the concentration of dissolved copper. Following irradiation, the amount of copper measured in solution was 30 times higher than that predicted based on the solubility of Cu_2O and three times higher than the solubility of CuO. However, the concentration of "dissolved" species decreased when the solution was filtered with a 20-nm pore filter suggesting that the solution contained nanoparticulate copper in addition to dissolved copper (Björkbacka et al. 2016). Bessho et al. (2015) have previously reported the formation of colloids during the irradiation-induced corrosion of copper.

A number of irradiation studies have been conducted in humid air because the period of highest radiation field will correspond with the early unsaturated phase in the repository. In an unsaturated system, the ratio of the surface area of copper (but also of other solids, such as bentonite) to the volume of the aqueous phase will be relatively high. The SA:V ratio will affect the relative influence of interfacial and homogenous processes. Björkbacka et al. (2017) found that the extent of corrosion was 7-9 times higher in humid air or humid argon (60% or 100% RH) in the presence of radiation (470-500 Gy/h, total absorbed dose 45-48 kGy) than in unirradiated systems. The similarity of the enhancement factor in air and Ar lead the authors to conclude that, although nitrate-containing corrosion products were observed in irradiated humid air, the radiolytically produced HNO_3 did not play a direct role in the increased corrosion. The extent of corrosion in these irradiated unsaturated systems (as measured by the mean film thickness) was higher than that in an equivalent experiment in bulk anoxic water. This was explained on the basis of the understanding at that time that the primary oxidant in irradiated systems is OH•. In a bulk water system, there is more opportunity for the more-stable, longer-lived H_2O_2 to scavenge the HO• radical prior to it reacting with the surface than there is in a thin-layer, high SA:V ratio unsaturated system. This explanation may have to be reconsidered now that molecular O_2 rather than the HO• radical is considered to be the primary oxidant (Soroka et al. 2021), although it is possible that the nature of the primary oxidant is different in saturated and unsaturated systems.

Björkbacka et al. (2017) had speculated that radiation-induced corrosion could render the surface more-reactive to other species present in the repository, but their own data show that this is not the case. After irradiation in humid air (60% RH) for a period of 96 h at 500 Gy/h (total dose 48 kGy), no additional corrosion occurred if the irradiated sample was then placed in anoxic water. Thus, irradiation does not "activate" the copper surface and make it more reactive.

Ibrahim et al. (2018) also studied the radiation-induced corrosion of copper in humid air (70-85% RH, 75°C). In the absence of radiation, the surface was covered by a thin water layer along with larger isolated water droplets. The surface under the thin water layer passivated due to the formation of a duplex Cu_2O/CuO layer, with thicker deposits under the droplets where the surface films appeared to remain porous and non-passivating. Irradiation at a dose rate characteristic of the canister (0.35 Gy/h) had relatively little impact. The oxide thickness under the thin water layer was the same as in the absence of radiation. Irradiation did increase the number and rate of secondary spreading of the

EURAD (Deliverable n° 1.1) – Initial State-of-the-art of WP ConCorD
Dissemination level: Public
Date of issue of this report: 17/08/2022

Page 26

condensed water droplets, but corrosion did not extend any deeper. Lateral spreading of the droplets was thought to result from the deliquescence of nitrate species formed from the radiolytically produced HNO_3, although no nitrate phases were found on the surface. In general, the rate of depth-wise penetration was relatively minor compared with the rate of lateral spreading of the droplets. As a consequence, irradiation resulted in superficial, rather than deeply penetrating, corrosion. After one year exposure to unirradiated conditions, the maximum thickness of the porous corrosion products in the droplet regions was 10 μm. No quantitative measure of the depth of penetration into the copper surface was given, but it would be expected to be a factor of 2-3 lower due to the difference in molar volumes of Cu and Cu_2O/CuO and due to the porosity of the corrosion products.

Irradiation has not been found to lead to the environmentally assisted cracking of copper. There was no evidence for the occurrence of stress corrosion cracking on various types of stressed samples exposed to irradiated environments at dose rates between 19 Gy/h and 4.9 kGy/h, for total doses up to 10 MGy, for exposure periods up to 5 years, and for temperatures up to 150°C (Johnson et al. 1996, Yunker 1990, Yunker and Glass 1987).

Lousada et al. (2016) have reported an increase in the hydrogen content of 99.98 wt.% copper following irradiation in anoxic pure water at a dose rate of 490 Gy/h and total doses of between 35 and 70 kGy. Figure 1-4 shows the dependence of the H content on total dose, as well as the amount of adsorbed H_2O. The lack of correlation between the two sets of data was used as evidence that the source of the absorbed H was not the dissociative adsorption of H_2O (Lousada et al. 2016).

EURAD (Deliverable n° 1.1) – Initial State-of-the-art of WP ConCorD
Dissemination level: Public
Date of issue of this report: 17/08/2022

Page 27
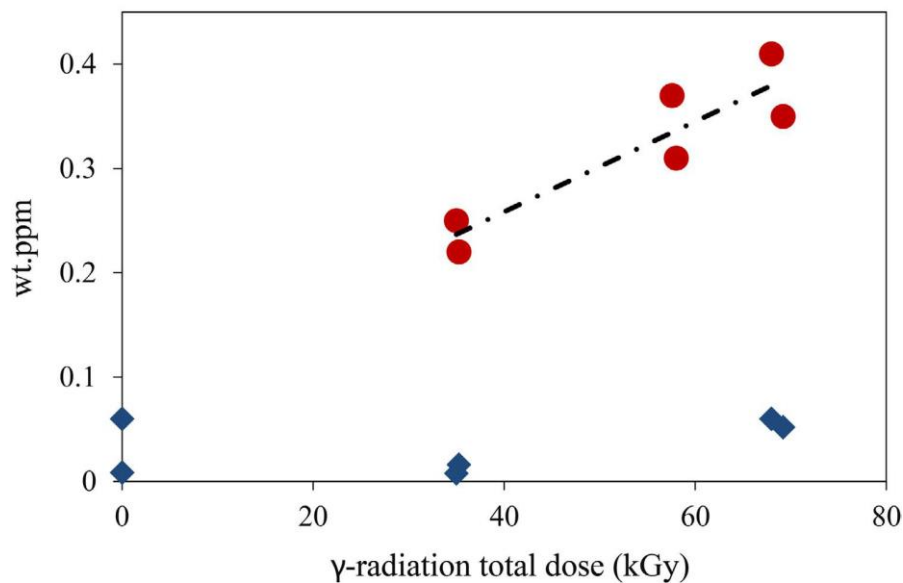
Figure 1-4: Effect of absorbed dose on the hydrogen content of pure copper following irradiation in anoxic water at a dose rate of 490 Gy/h (Lousada et al. 2016). The red circles indicate the H content and the blue diamonds represent the amount of adsorbed H_2O.

1.1.3.2 Effect of irradiation on material properties

The creation of radiation damage in materials, including copper (Li and Zinkle 2012), is generally associated with in-reactor exposure and high neutron flux. Radiation damage has been shown to affect the mechanical properties of copper alloys, including an increase in yield strength (radiation hardening), reduction in fracture toughness, an in-reactor creep (Li and Zinkle 2012). In contrast to these effects observed at high doses, the neutron- and γ-dose rates for the canister are considerably lower and radiation damage of the copper corrosion barrier has always been considered to be negligible (Guinan 2001, SKB 2010).

Nevertheless, SKB have recently performed additional analyses and experimental measurements (Padovani et al. 2019, SKB 2019, Yang et al. 2019). Using a different code and database, Yang et al. (2019) confirmed the earlier estimates of Guinan (2001) that the damage from neutron- and γ-irradiation over the lifetime of the canister will be between 10^{-7} displacements per atom (dpa) and 10^{-6} dpa. Any effects of radiation hardening are immeasurable below 10^{-4} dpa (Li and Zinkle 2012). In recent experiments, Padovani et al (2019) γ-irradiated 99.999% copper at a dose rate of 1 kGy/h to a total dose of 100 kGy. Irradiation did not cause any microstructural changes or changes to the population or nature of defects

EURAD (Deliverable n° 1.1) – Initial State-of-the-art of WP ConCorD
Dissemination level: Public
Date of issue of this report: 17/08/2022

Page 28

1.1.4 Summary

One of the first conclusions that can be drawn from the literature is that irradiation modifies the corrosion rate by altering the properties of clay and the corroding environment in contact with carbon steel. The clay structure can be severely disrupted leading to its amorphization. Steel corrosion, on the other hand increases under irradiation. Experiments clearly show that amorphization of clay can be excluded under the irradiation levels found in GDR. Severe irradiation conditions are needed to significantly alter the matrixes. For instance, clay was shown to become amorphous under ionizing radiation from a dose of 10^{11} Gy, which is several orders of magnitude larger than the expected value (Sorieul et al., 2008). The corrosion of steel is likely to be more influenced by lower radiation levels. But in general, radiation dose rates for which increased corrosion has been observed are much higher ($>10^3$ Gy h^{-1}) than the external dose rate estimated at the surface of the containers ($10^{-2} - 10^1$ Gy h^{-1}) (Padovani et al., 2017).

The corrosion of carbon steel involves the formation of a film of corrosion products which is often thicker under irradiation. The irradiation may change the chemical nature of the corroding environment, which in some cases can lead to the formation of less stable corrosion products, especially in complex environments such as those found in repository sites. Iron ions generated during corrosion migrate towards the clay and induce chemical and structural transformations that alter its physical and chemical properties. Non swelling Fe-rich phyllosilicates can be formed, modifying the retention capability for water and radionuclides. Radiation exerts indirectly some influence on the redox state and chemistry of the clay by radiolysis of structural water. Inasmuch as radiation processes depend on the water content, its influence is low if the relative humidity is not large enough. Corrosion and water radiolysis produce gaseous species (with oxidizing or acid species and large amounts of dihydrogen) that may fill the clay porosities, delaying or inhibiting its water saturation and ultimately causing a drying of the buffer adjacent to the hot canisters. They also might change the corrosion rate, increasing or decreasing it depending on the composition of the atmosphere (Crusset et al., 2017). Although the effects of water radiolysis have been studied in certain extent, little is known about the impact of the irradiated water vapor on the long-term evolution of the container-buffer system.

EURAD (Deliverable n° 1.1) – Initial State-of-the-art of WP ConCorD
Dissemination level: Public
Date of issue of this report: **17/08/2022**

Page 29

Experimental conditions			Corrosion rate (µm/y)							Reference
			0 Gy/h	10^{-1} Gy/h	1 Gy/h	10 Gy/h	10^2 Gy/h	10^3 Gy/h	10^4 Gy/h	
Granitic water	anoxic	90°C	0.1					3		(Marsh & Taylor, 1988)
Seawater	oxic	RT	6		~10	~50		~130		(Marsh & Taylor, 1988)
Brine A	oxic	RT	2 – 22			~2 – 22		60 – 175		(Westerman et al., 1983)
Brine A	oxic	RT	20 – 50		20 – 50	20 – 50				(Westerman et al., 1983)
Q-Brine	oxic	90°C	25 – 80		~20	~25 – 30		500 – 800		(Smailos et al., 1991)
Basaltic water	oxic	250°C	1 – 8						8 – 30	(Westerman, Pitman,& Nelson, 1982)
Air/Steam	oxic	150°C	0.05 – 0.1		0.08 – 0.2	0.09 – 0.15				(Brehm, 1990)
Air/Steam	oxic	250°C	0.03 – 0.6		3 – 5	7 – 10	7 – 10			(Brehm, 1990)
Brine	anoxic	75°C	~12				73	220		(Gray, 1987)
Basaltic water	oxic	250°C	5					11		(Nelson et al., 1983)
Allard water	anoxic	30°C	0,1			3	3			(Smart et al., 2008)
Bentonite-equilibrated water	anoxic	50°C	0.05			0.05 – 0.2	0,8			(Smart et al., 2008)
Cementous water	anoxic	25 or 80°C	~1	~1		~1				(Winsley et al., 2011)
Concentrated groundwater	oxic	150°C	25 – 107						11 – 44	(Ahn & Soo, 1995)
Bentonite saturated with beishan water	oxic	90°C	24					32		(Liu et al., 2017)
Clay or clay/clay water	oxic	90°C	150					300		(Debruyn, 1988)

Table 1-1: Corrosion rate (µm y^{-1}) under irradiation. Adapted from (Shoesmith & King, 1999).

EURAD (Deliverable n° 1.1) – Initial State-of-the-art of WP ConCorD
Dissemination level: Public
Date of issue of this report: **17/08/2022**

Page 30

1.2 Corrosion under environmental transients

1.2.1 Nature of environmental transients

The understanding of the evolution of the environment surrounding the canister in the repository over long periods of time is essential for a reliable analysis of the corrosion of canister materials.

There are two important aspects of the disposal environment impacting the corrosion behaviour of the canister (King & Padovani, 2011): i) the changes of the corrosive nature of the environment in the geological disposal repository (GDR), and ii) the type of canister material.

The evolution of the chemistry of the environment after the repository closure depends on the engineered barriers and the composition of groundwater. Other important factors include (King & Padovani, 2001):

(i)   the maximum canister surface temperature: typically, ~100°C (90°C is the maximum in the French concept, but higher temperatures are possible in other reference concepts)
(ii)   the engineered barriers: compacted bentonite, cement, or concrete
(iii)   the pore water in contact with the canister: this is likely to change its properties over time and, initially at least, differs from that of the ground water
(iv)   the amount of available O_2, limited in deep geological formations to that trapped after sealing of the GDR
(v)   the magnitude of the gamma (and neutron) radiation fields at the outer surface of the canister and the amounts of oxidising (and reducing) radiolysis products formed
(vi)   the time for the GDR to saturate with ground water following closure, typically a few decades or hundreds of years
(vii)   the rate of mass transport of reactants to, and of corrosion products from the canister, which is largely determined by the nature of the barriers
(viii) the possibility of microbial activity at, and away from, the canister surface.
(ix)   the magnitude of residual and applied stress
(x)   the permeability of the host rock and its transport capacity for any H_2 that may be produced by the anaerobic corrosion of the canister
(xi)   the mineral content of the rock; the oxidation of pyrite can lead to the formation of thiosulphate and other oxidised forms of sulphur that can be deleterious for some candidate canister materials

The corrosion of container materials has been extensively studied under constant conditions. Thus, the extrapolation of experimental results to the evolving chemical, mechanical, and redox conditions of the early post-closure period, needs to be verified and complemented. Conceptually, four phases are identified for the temperature-relative humidity (RH) and, for aerobic/anaerobic conditions, at the canister surface from the time of emplacement up to one million years (Landolt et al., 2009 for concept specific case of NAGRA design):

- Phase 1 – initial dry-out phase (oxic and dry conditions: first tens of years)
- Phase 2 – aerobic unsaturated phase (oxic and unsaturated conditions: first tens of years)
- Phase 3 – anaerobic unsaturated phase (anoxic unsaturated conditions: up to first hundred years)
- Phase 4 – long-term cool, anoxic phase (long term anoxic and fully saturated conditions).

EURAD (Deliverable n° 1.1) – Initial State-of-the-art of WP ConCorD
Dissemination level: Public
Date of issue of this report: 17/08/2022

Page 31

Figure 1-5 shows a schematic representation of the evolution of the temperature and relative humidity at the canister surface after the time of emplacement. The establishment of anoxic conditions after an initial oxidic period is a key consideration. The corrosion behaviour in steady-state conditions after the consumption of oxygen has been the focus of many studies (NFPRO Project, PEPs Project: https://cordis.europa.eu/project/id/249681/reporting/es, Arcos et al., 2005; 2008; Carlson et al., 2006). The role played by the 'dry' period preceding re-saturation (not corrosive or slight corrosive) and the transient period during re-saturation (potentially corrosive) should be also regarded. After facility closure, the saturation of the bentonite barrier during the thermal phase of the repository leads to swelling and the development of mechanical stresses on the container. Such transients can be further influenced by attempts at repository footprint optimisation (e.g., increased container heat production). Considering the time span of the processes we can presume that oxygen consumption < saturation < chemical transients < temperature.
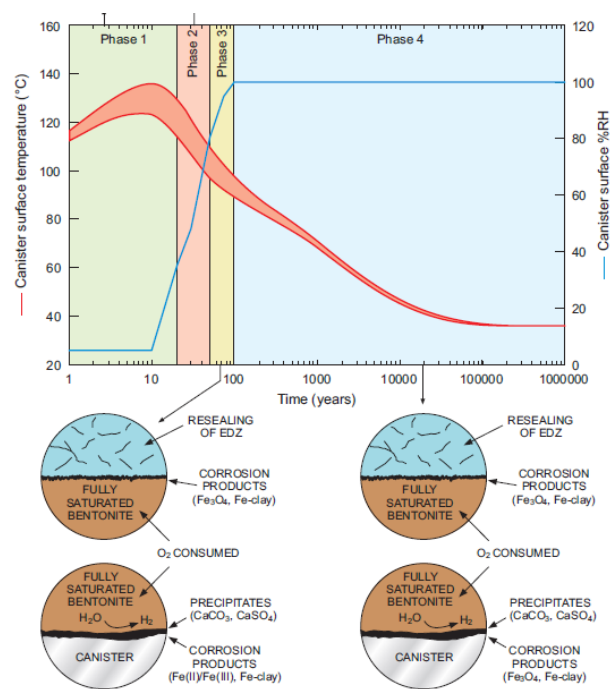
Figure 1-5: Evolution of temperature and relative humidity (RH) with time and the expected corrosion products and processes at the canister surface (lower diagrams) (Landolt et al., 2009).

1.2.2 Influence of transients on the corrosion process

The surface damage resulting from dry oxidation regarding oxygen entrapped upon closure is expected to be very limited. Typical corrosion products are Fe_3O_4 and Fe_2O_3 (Terlain et al., 2001). The oxygen will be consumed after certain time and the environment becomes anoxic. This modification of geochemical conditions influences the metallic corrosion as the reduction of higher oxides becomes the main cathodic reaction before water reduction start to dominate the cathodic process during the anaerobic phase for base materials (Johnson & King, 2008).

A series of studies on the effect of changing oxidic/anoxic conditions have been published. For example, the effect of fluctuating redox conditions on the corrosion mechanism has been investigated by Saheb et al. (2011) using archaeological artefacts. In that study, a nail, which was exposed to an aerated unsaturated soil for several hundred years was reburied and exposed to anoxic and saturated conditions. Goethite and smaller amounts of magnetite and maghemite formed under aerobic and

EURAD (Deliverable n° 1.1) – Initial State-of-the-art of WP ConCorD
Dissemination level: Public
Date of issue of this report: 17/08/2022

Page 32

unsaturated conditions, while ferrous carbonates were detected in the corrosion layer after subsequent exposure to anoxic and saturated conditions. Based on experimental findings and aided with geochemical modelling, authors concluded that phase transformation occurred rather than metallic corrosion progresses by direct formation of new phases. In the same study, an experiment was also conducted by applying the reverse sequence of changing conditions: a nail, which was exposed to anoxic and saturated conditions for several hundred years was immersed in an aerated carbonated solution for five weeks. Ferrous carbonate and iron oxides (magnetite, maghemite) formed as corrosion products upon exposure to anoxic water saturated conditions, and the subsequent exposure to aerated conditions resulted in the formation of an external goethite layer on the external part of the corrosion layer. In this last experiment (i.e., anoxic to oxidic transient), authors also concluded that the presence of the ferric phase resulted from the transformation of the corrosion layer.

El Hajj et al. (2013) investigated sequential aerobic and anaerobic microbiologically induced carbon steel corrosion experiments. They found that the corrosion rate under anaerobic conditions is lower when specimens experienced a prior phase of aerobic corrosion. This outcome was attributed to the nature of the formed corrosion products and their adherence to the steel surface. The transition aerobic-anaerobic conditions resulted in the formation of pyrrhotite as a single phase, while nanocrystalline mackinawite formed during direct anaerobic steel corrosion. The different results observed in this study were attributed to the stimulation of the activity of sulphate-reducing bacteria (SRB) and the hydrogen sulphide production upon transition from aerobic to anaerobic conditions.

Experiments performed at 85°C under *in situ* conditions showed that transient oxidic conditions can have substantial effects on steel corrosion. Fe^{2+}-bearing compounds in clay rock (e.g., pyrite) oxidise in the presence of oxygen (ingress due to loss of tightness), resulting in a decrease of pH of the porewater (Necib et al., 2016). These transient acidic conditions had, in turn, an impact on the corrosion rate, which were relatively important owing to the positioning of spatially decoupled anodic and cathodic areas (Schlegel et al., 2016). Galvanic coupling between areas exposed to different concentrations of O_2 in (sub)oxidic conditions can result in the formation of pits (Sherar et al., 2011; Refait et al., 2016). Areas more easily accessed by oxygen become cathodic while those less exposed may become anodic. The coupling is sustained by the precipitation of corrosion products and the driving force is the large difference in electrochemical potentials between O_2 reduction and Fe oxidation (Schlegel et al., 2018).

Besides, changing redox conditions due to e.g., the formation of oxidizing species upon water hydrolysis, geochemical conditions in a repository are also expected to evolve due to the metallic corrosion itself, which produces corrosion products and generates hydrogen. The accumulation of corrosion products at the steel/bentonite interface may influence the nature of the electrochemical reactions. For instance, the presence of magnetite at the steel-bentonite interface results in an increase of steel corrosion by acting as an external cathode coupled to the steel surface (Kojima et al., 1995; Taniguchi et al., 2003). It was shown that the observed increase in corrosion rates was caused by the reduction of Fe_3O_4 itself. Consequently, because magnetite dissolves itself, such corrosion product may not necessarily play any role on the long-term, but it may influence corrosion processes between its formation and its dissolution.

Only a few studies on Cu corrosion under transient conditions have been reported. Smith et al. (2006) have reported electrochemical experiments on the effect of pre-oxidation on the surface attack of Cu by sulphides in 0.1 mol/L NaCl under anoxic conditions. Cu was pre-oxidized to mimic the formation of corrosion products during the warm oxic period. Depending on the extent of pre-oxidation, the surface was covered either with a thin film made of Cu_2O or Cu_2O covered by $CuO/Cu(OH)_2$ for longer reaction times. Samples were subsequently immersed in a sulphide-containing solution (30 µmol L^{-1}) and the evolution of the corrosion potential (E_{corr}) was recorded. For all samples, E_{corr} stabilized at a value slightly more negative than observed in the absence of sulphide, then decreased to a value between -0.5 and -0.6 V (SCE) before a sudden decrease to the equilibrium potential for the Cu/Cu_2S redox reaction. The time needed during the first decrease in E_{corr} increased with the extent of pre-oxidation and probably reflects the penetration of SH^- (the predominant species) to the Cu metal surface. The second drop was comparable for all samples and indicates that the redox conditions are dominated by the Cu/Cu_2S redox

EURAD (Deliverable n° 1.1) – Initial State-of-the-art of WP ConCorD
Dissemination level: Public
Date of issue of this report: 17/08/2022

Page 33

couple. Overall, outcomes pointed out a beneficial effect of Cu pre-oxidation, indicating that deposits could impede the reaction of Cu with aqueous sulphide.

Smart et al. (2005b) used electrochemical techniques to investigate the galvanic corrosion of the copper-cast iron couple in artificial groundwaters while changing the oxygen content. The context was an unlikely event of outer copper canister being breached followed by water entering the annulus between the inner and the outer canister. In the presence of oxygen, copper was the cathode in the galvanic couple. In deareated conditions, potentials were considerably more negative than in aerated conditions: the potential of the copper in deaerated conditions was within the thermodynamic domain of stability of copper, while that of iron suggested that the hydrogen evolution by anaerobic corrosion of iron was thermodynamically possible. Accordingly, copper plating was observed on the surface of iron in the experience where conditions evolve from aerobic to anaerobic.

More recently, Senior et al. (2019) reported corrosion rates of copper in anoxic NaCl solutions at various temperatures by measuring the rate of hydrogen release. Copper exposed to 0.25 mol.kg^{-1} NaCl at 30°C or 50°C produced negligible amounts of H_2 below the detection limit. At 75°C, the H_2 release was in agreement with a corrosion rate of about 10 nm y^{-1}. When the temperature was returned to 50°C, the H_2 production immediately returned below the detection limit. Comparable findings were obtained for experiments performed in solutions containing up to 5 mol kg^{-1} NaCl. These results may suggest that the corrosion rate of copper in NaCl solutions up to 5 mol kg^{-1} is very low and decreases with temperature. Besides, changing redox conditions due to e.g., the formation of oxidizing species upon water hydrolysis, geochemical conditions in a repository are also expected to evolve due to the metallic corrosion itself, which produces corrosion products and generates hydrogen. The accumulation of corrosion products at the steel/bentonite interface may influence the nature of the electrochemical reactions. For instance, the presence of magnetite at the steel-bentonite interface results in an increase of steel corrosion by acting as an external cathode coupled to the steel surface (Kojima et al., 1995; Taniguchi et al., 2003). It was shown that the observed increase in corrosion rates was caused by the reduction of Fe_3O_4 itself. Consequently, because magnetite dissolves itself, such corrosion product may not necessarily play any role on the long-term, but it may influence corrosion processes between its formation and its dissolution.

More recently, Romaine et al. (2015) showed that the reactions are in fact more complex and highly dependent on the mineralogical composition of the used argillite. Coupling of a bare electrode under argillite (anode) with a pre-corroded electrode covered by a bilayer of corrosion products (magnetite/siderite) under argillite (cathode) resulted in the formation of heterogeneous layers of corrosion products. The heterogeneity of these layers resulted from the variation of the galvanic effect along the surface of the initially bare electrode due to the variation of the distance from the initially covered electrode. Such variation of galvanic effects may also be assimilated to transient conditions affecting corrosion processes.

In anoxic groundwaters, anaerobic steel corrosion generates hydrogen, which results in a decreasing of the E_h. However, with increasing reaction time, corrosion products will form a protective layer, which will result in a progressive lowering of the corrosion rate and thus of the hydrogen production (Smart et al., 2002b, Turnbull, 2009). The evolution of hydrogen is thus expected to decrease with time until reaching a lower constant value in the long-term (Smart et al., 2002b). Several studies reporting the effect of hydrogen on selected reactions have also been reported (Truche et al., 2009; 2010; 2013).

Under elevated temperature and calcite buffered conditions, pyrite can be reduced by hydrogen through a coupled dissolution-precipitation mechanism and involves the generation of H_2S (Truche et al., 2010; 2013). Similarly, aqueous sulphate can also be reduced by hydrogen (Truche et al., 2009), but this reaction is kinetically slow under expected disposal conditions. Experimental findings reported by El Mendili et al. (2015) indeed showed the formation of a continuous iron sulphide layer covering carbon steel contacting Callovo-Oxfordian argillite in experiments performed at 90°C. The origin of this layer was attributed to the presence at the corroding interface of H_2S formed by reduction of pyrite by hydrogen. Iron sulphide was likewise detected in experiments performed at 30°C, but the

EURAD (Deliverable n° 1.1) – Initial State-of-the-art of WP ConCorD
Dissemination level: Public
Date of issue of this report: 17/08/2022

Page 34

corrosion layer was thinner than in experiments performed at 90°C. At this lower temperature, the origin was attributed to the activation of sulphate reducing bacteria (absorption of hydrogen and release of hydrogen sulphide).

In the absence of argillite, Smart et al. (Smart et al., 2002a,b) reported experiments performed in the presence of a hydrogen overpressure. In their studies, they could not detect any significant effect of this parameter on the anaerobic corrosion of carbon steel and cast iron in artificial groundwaters.

Reported studies showed that evolving redox conditions at the steel/bentonite interface can have a substantial impact on canister corrosion by changing the corrosion rate and mechanism. Among them, the presence of oxygen plays an important role and involves an increase in corrosion rate. Similarly, the presence of hydrogen may have an impact on the geochemical conditions of the canister near-field, such as dissolution of selected minerals and formation of dissolved species, which in turn influence steel corrosion. The presence of hydrogen does not seem to modify directly the steel corrosion (e.g., no decrease in corrosion rate). Unfortunately, much less attention was devoted to the effect of fluctuating redox conditions on copper corrosion, but findings suggest that the presence of a thin oxide layer could impede the reaction of Cu with aqueous sulphide.

1.2.3   Transitional processes involving gas generation

The production of H_2 could be a general indicator of the predominant redox process. It can be taken as a tool for analysing the energetics of microbiological processes, because hydrogen produced during metal corrosion can participate in the microbial reactions. Further, hydrogen can be used by microbes as an electron donor, thus reducing the gas pressure and affecting the degree of metal corrosion (Smart et al., 2001).

King (2007), following Craig (1987) identified two of the most important H degradation mechanisms as

1. hydrogen stress cracking (or hydrogen-induced cracking), in which H accumulates under a stress gradient leading to internal crack formation, and

2. blister formation, due to H accumulation in internal voids, laminations, or inclusions.

In general, the susceptibility of C-steel to undergo these processes increases with material strength and concentration of absorbed hydrogen [H]. For these reasons, authors of the report JNC (2000) and Johnson & King (2003) argued that both the use of a low-strength steel container and the nature of the repository environment mitigate hydrogen-related degradation mechanisms.

Corrosion of iron metals of different compositions may also produce organic chemicals. Detailed experiments within the EU project CAST (Carbon-14 Source Term) about the corrosion of non-radiated and radiated carbon steels and carbides indicated the generation of CO_2, CO, and up to C5 volatile reduced hydrocarbons (Swanton et al., 2015)

In the context of other different experiments and investigation fields, it was observed that during corrosion of steels, CO_2, CO, H_2 and volatile reduced hydrocarbons (alkanes and alkenes: methane, ethane, ethene, propane, propene, butane, butene and pentene) were formed in the gas phase. Organic and inorganic carbon chemicals also form in the liquid phase (Wieland & Hummel, 2015). Inorganic carbon fraction corresponds to HCO_3^- and/or CO_3^{2-}, depending on pH. Oxidised hydrocarbons (alcohols and aldehydes, i.e., neutral species: methanol, ethanol, formaldehyde, etc.; and carboxylic acids, i.e., anionic species: formate, acetate, oxalate, etc.), were found in the organic fraction. In the context of the FEBEX project, formate, acetate and oxalate were only found in samples near the heater (Fernández et al., 2018). Studies about the evolution of gases in different in situ tests over time (e.g., FEBEX in situ

EURAD (Deliverable n° 1.1) – Initial State-of-the-art of WP ConCorD
Dissemination level: Public
Date of issue of this report: 17/08/2022

Page 35

test, FE-Experiment, HT-Experiment) were reported by Vinsot et al. (2014), Fernández (2019), Vogt et al. (2015), Giroud et al. (2019) and Tomonaga et al. (2019).

In the presence of organic matter, degradation/oxidation reactions may be produced abiotically or microbially mediated consuming the entrapped O_2. Although reactions may be thermodynamically spontaneous, they may require a microbial catalyst to proceed. Bacteria catalyse nearly all the important redox reactions driving the oxidant consuming processes. Organic matter (electron donor) is oxidized, whereas free oxygen, nitrate, sulphate and ferric ions (electron acceptors) are reduced. Thus, the redox potential is a supplementary indicator of which type of microbial population may dominate as conditions became reducing.

1.2.4 Redox transients

The redox conditions in the EBS constitute an important issue on the chemical framework controlling corrosion and the behaviour of the radionuclide transport in the near field (Giroud, 2014). A redox system may involve gases (O_2, N_2, H_2, CH_4, CO_2), dissolved components (NO_3^-, NH_4^+, CH_2O (TOC), Fe^{2+}, Mn^{2+}, SO_4^{2-}, HS^-, H^+), as well as solids ($FeOOH$, MnO_2, $FeCO_3$, $MnCO_3$) and components (Fe^{2+}, Mn^{2+}, NH_4^+) associated with the solids by ion exchange (Christensen et al., 2000). The most important species that undergo redox reactions contain carbon, iron, sulphur, and nitrogen. Thus, the knowledge of the kinetics and reactivity of the redox-active species involved is important for the determination of the redox conditions.

In the case of an SF/HLW repository (Figure 1-6), the redox conditions will be determined by the inventory of O_2 trapped during closure and by the radiolysis of the pore water, both depending on temperature. The different processes that a priori can have a larger influence on the short and long-term redox evolution of the repository are a) the metal corrosion, b) the organic matter degradation, and c) the microbial activity.

For a given evolution of the repository environment, material containers will be subject to corrosion under the following conditions (King, 2007):

1. aerobic, unsaturated vapour phase.
2. aerobic, saturated aqueous phase or an anaerobic, unsaturated vapour phase.
3. anaerobic, saturated aqueous phase.

The corrosion evolutionary path (CEP) defines the time-dependent corrosion behaviour of the canister and is closely tied to the evolution of environmental conditions. A useful indicator of this evolution of the corrosion behaviour is the time dependence of the corrosion potential (E_{CORR}) of the canister (Figure 1-7b). During the early aerobic phase, E_{CORR} is relatively noble (positive) because of the cathodic reduction of O_2. At longer times, E_{CORR} falls to a value determined by the relative rates of Fe dissolution and the reduction of H_2O, resulting in E_{CORR} values close to the H_2/H_2O equilibrium potential during the long-term anaerobic phase. Between these two periods, the value of E_{CORR} undergoes a transition, during which Fe(III) corrosion products formed during the aerobic phase are reductively dissolved to Fe(II) species (Johnson & King, 2008). Although H_2O is also an oxidant for some canister materials, the nature of the corrosion processes in anoxic conditions is typically less severe than in aerobic environments (Shoesmith, 2006). The redox potential of the repository (Eh) will be determined by the most dominant redox couple. In aerobic systems, the Eh will be determined by the O_2/H_2O couple, whereas equilibrium between Fe^{2+} and $Fe(OH)_3$ or involving pyrite may determine the redox potential under anaerobic conditions. Certainly, in systems where sulphide is present (either naturally in the ground water or produced by the action of sulphate-reducing bacteria (SRB)), the Eh of the repository will become reducing. The expected near-field redox conditions have been investigated in different EU Projects (NF-PRO, RECOSY) (Carlsson & Muurinen, 2008; Duro et al., 2014). Wersin et al. (2021)

EURAD (Deliverable n° 1.1) – Initial State-of-the-art of WP ConCorD
Dissemination level: Public
Date of issue of this report: 17/08/2022

Page 36

proposed a conceptual model of corrosion, the redox evolution and Fe-clay interaction processes in the ABM2 in situ test, and Hadi et al. (2019) in the FEBEX *in situ* test.
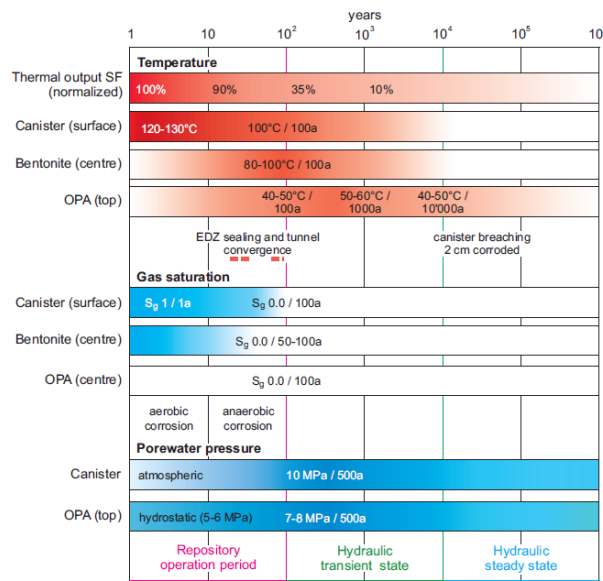
Figure 1-6: Overview of the expected evolution of the main processes in a HLW repository in Opalinus Clay (OPA) host rock based on a compilation of modelling reports and experimental data (Jenni et al., 2019; Leupin et al., 2016; Diomidis et al., 2016)
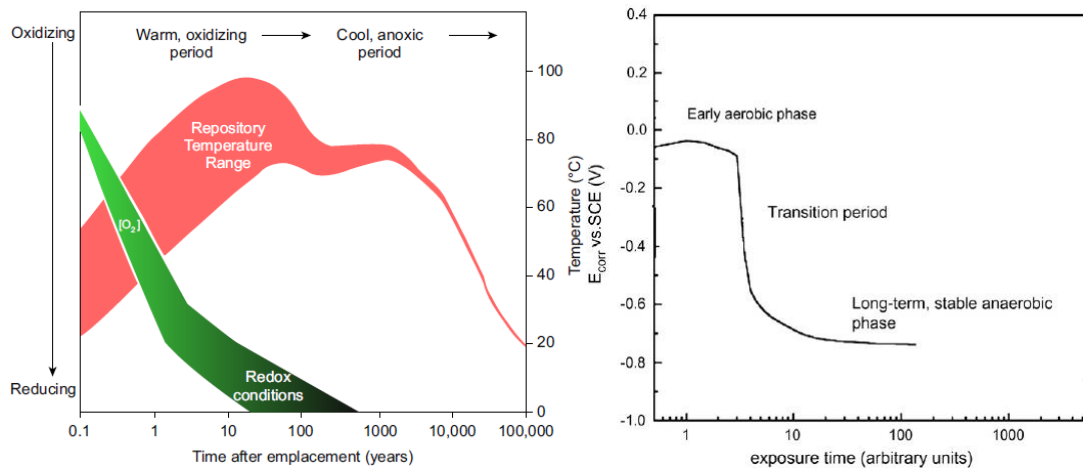
Figure 1-7: a) Schematic illustration of the evolution of the near-field environment for a repository located below the water table (King, 2017), b) Schematic representation of the evolution of the open circuit potential of carbon steel during the aerobic-anaerobic transition. Potentials are given with respect to the SCE, which is +242 mV versus the normal hydrogen electrode (NHE). (Diomidis & Johnson, 2014; King, 2008; Johnson & King, 2008)

EURAD (Deliverable n° 1.1) – Initial State-of-the-art of WP ConCorD
Dissemination level: Public
Date of issue of this report: 17/08/2022

Page 37

1.2.5 The oxygen consumption

The establishment of anoxic conditions after an initial oxidic period is a key consideration for evaluation of conditions for corrosion processes. Apart from the oxygen trapped in the pore spaces, the radiolysis of humid air or water also produces oxidising species, such as H_2O_2, resulting in an increase of the general corrosion rates of metals or to localised corrosion (Crusset et al., 2017). The effect of the radiolysis of water on corrosion, however, can be significantly attenuated in the absence of oxygen (Lapuerta et al., 2008).

Initially, (phase 1, Figure 1-5) oxygen can be consumed by corrosion of the canister and of the steel mesh stabilizing the tunnel wall (for the clay rock see Landolt et al., 2009), oxidation of Fe minerals in the bentonite (Wersin et al., 1994), (Puigdomenech et al., 2001), (Grandia et al., 2006), (Giroud et al., 2018), microbial activity in bentonite (Kotelnikova & Pedersen, 1998) (Giroud et al., 2018). Corrosion conditions in the phase 1 supports a uniform dry oxidation yielding trivalent iron oxide. Oxidation of sulphides in the backfill may contribute to oxygen consumption and would produce sulphate and thiosulphate (Landolt et al., 2009). All the oxygen is presumed to be consumed during the phase 2 (See Figure 1-5).

Wersin et al. (1994; 2007) proposed two ways for the $O_2(g)$ consumption in the buffer: (i) diffusion into surrounding rock, and (ii) reaction with mineral phases existing in the buffer and backfill materials. They predicted that anoxic conditions would be re-established in the buffer after a period ranging between 7 and 290 years (Wersin et al., 2007) depending on the value taken for the most uncertain parameter: the pyrite reactive surface area. Giroud et al. (2018) considered gas exchange with bentonite pore water and adsorption on mineral surfaces as the most important processes controlling O_2 in the drift of the FE experiment, which was fully consumed after only a few months. According to Grandia et al. (2006) aerobic conditions can prevail for more than 5,000 years in the absence of geochemical processes (consumption of O_2 in the buffer).

Other authors (Kotelnikova & Pedersen, 1998) determined the consumption of 5×10^{-10} mol l^{-1} by microorganisms in the range of 9 days to 4 years. Puigdoenech et al. (2001) also confirmed the short term of consumption and so as microbial involvement.

The Swedish research programme studied in more detail the consumption of O_2 trapped in the repository, reacting with rock minerals in tunnels and deposition holes. Malmstroem et al. (1995) studied the kinetics of dissolution of Fe(II)-bearing silicate minerals (biotite and chlorite) and presented a simple calculation of the time needed for oxygen consumption in fractured granite due to the oxidation of the Fe(II) contained in the silicates. Periods of time ranging from 50 to 300 years, depending on the type of mineral and on whether oxygen was considered to the depleted by direct consumption on the mineral surface or by oxidation of the Fe(II) previously released from the mineral.

Dry oxidation occurring during phase 1 is not considered a serious problem for canister safety (Landolt et al., 2009) (Johnson & King, 2008).

During phase 2, the environment is still aerated and the atmospheric corrosion takes place as the moisture starts to condense on the iron surface. Atmospheric corrosion is an electrochemical phenomenon and leads to a variety of corrosion products: in addition to Fe_3O_4 and Fe_2O_3, hydrated ferric species including different forms of FeOOH and green rust can be formed. Corrosion during phase 2 may be influenced by the deliquescence of salts and by the presence of particulates on the surface, in a process not necessarily uniform (Landolt et al., 2009). Droplets of water can form by deliquescence of individual salt crystals, or collections of crystals, with surrounding areas either dry or wetted by microdroplets or thin layers of moisture. If O_2 is still present in the bentonite at this time, the regions around the deliquesced droplets will tend to become cathodic because of the greater access of O_2 (Figure 1-7). The droplets themselves will tend to become O_2 depleted. Some degree of localised attack can be expected during this period (Diomidis & Johnson, 2014) (Johnson & King, 2008).

EURAD (Deliverable n° 1.1) – Initial State-of-the-art of WP ConCorD
Dissemination level: Public
Date of issue of this report: **17/08/2022**

Page 38

Concerning Cu corrosion, depending on the nature of the anions prevailing in the solution, insoluble Cu salts can precipitate upon the passive layer, sometimes being also capable of blocking the growth of pits at the Cu surface (Souto et al., 1990). Conversely, the formation of Cu salts favours a more extensive attack of Cu leading to pitting corrosion (Souto, 1992).

1.2.6 Saturation transients

The time-dependent degree of saturation of a repository let determine when and how corrosion may occur (King, 2013). At the initial stages (few tens to hundred years), the system will remain sufficiently dry to hinder aqueous corrosion. As the system cools and the RH increases, the surface of the canister turns wet and aqueous corrosion is possible.

The time for a complete saturation of a repository is estimated in the range of 100-1000 years (Johnson & King, 2008), although it may take tens of thousands of years in certain low permeability sedimentary host rocks. According to estimations using standard multi-phase flow process models, a complete re-saturation occurs in 3-4 years in a permeable, fully saturated host rock (Rutqvist & Tsang, 2008). Different *in situ* experiments, such as FEBEX test at Grimsel or the HE and FE Experiments at Mont Terri provide information about the saturation behaviour of the bentonite barrier (Villar et al., 2020).

The typical assumption applied to bentonite re-saturation is that ground water is available in the host rock. Due to the high chemical suction in partially saturated bentonite (SKB, 2006b), water is drawn in from the surrounding host rock into the bentonite. The rate at which re-saturation can occur will be controlled by the intrinsic permeability and water saturation state of the surrounding host rock.

The application of a thermal load on the inner (nominally 'dry') side of a bentonite buffer has a significant impact in terms of accelerating the generation and diffusion of water vapour. The water vapour migration is implicitly related to the water suction, and both vapour and liquid water are driven in proportion to the suction pressure. Therefore, water vapour mobilizes at the canister boundary and drive water away from the canister (Figure 1-8). Moving away from the heat source, some of this vapour returns to liquid state. The condensate migrates back towards the low-water saturation, high-suction inner surface, creating a local water circulation pattern.

However, if the availability of water from the host rock is low, or the heat source is relatively large, it is possible to dry large sections of the bentonite and to induce relatively high temperatures in the inner annulus. Intense desiccation can occur in the warmest part, causing a microstructural collapse. This leads to contraction of the stacks of ordered smectite lamellae, so that spontaneous expansion may be only partial when water finally enters. The affected part of the buffer may permanently lose some of its expandability and self-healing capacity, turning fine-fissured (Wilson et al., 2011).

These fluid processes would also lead to an accumulation chloride and sulphate salts near the hot canister surface (Figure 1-9a), whilst driving away dissolved silica. This induces the canister corrosion and a radial variation of clay density, resulting in changes of porosity (Figure 1-9b) (Couture, 1985).

The processes observed during the evolution of the environmental conditions in a GDR are summarized in Figure 1-10. Before saturation, localized corrosion is possible because surface salts wet (deliquesce) before the development of full saturation, leading to spatial separation of anodic and cathodic sites (King, 2013, 2016). Upon increasing RH, the wet surface of the canister extents, until covering uniformly the canister. The rate of supply of gaseous reactants (e.g., O_2) will be higher under unsaturated conditions, but the rate of removal of dissolved corrosion products will diminish, increasing the propensity for the formation of protective corrosion product films.

Aqueous corrosion requires an adsorbed water film on the metal surface able to sustain electrochemical reactions. At initial stages of repository, corrosion is expected to be very low, because of a relative humidity under Critical Relative Humidity (CRH). This is a threshold value, over which vapour can

EURAD (Deliverable n° 1.1) – Initial State-of-the-art of WP ConCorD
Dissemination level: Public
Date of issue of this report: 17/08/2022

Page 39

condense and form aqueous films on the metallic surface. In the case of a discontinuous adsorbed water film, localized corrosive attack of the canister surface may occur. Such adsorbed films form when the surface temperature of the canister decreases below 100°C and the relative humidity rises to about 60 % - 80%. However, an adsorbed water film can also form at relative humidity as low as 30% if particularly hygroscopic salts (such as $MgCl_2$ or $CaCl_2.xH_2O$) are deposited on the surface (King, 2008). Different studies have been performed about the corrosion of steel with time, as a function of RH, oxygen content and temperature, and how adsorption of water affects corrosion rates of different metals at different temperatures (Ben Lagha et al., 2007) (Dante & Kelly, 1993) (Lee & Staehle, 1997).

If the bentonite barrier is composed by compacted blocks and granular material, the blocks beneath the canister have a moisture content of 16 % while the granular material on top has a moisture content of about 5 % at the time of emplacement. Consequently, moisture initially flows from the partially saturated bentonite blocks beneath the canister into the less moist granular material. While the bentonite close to the canister will not swell, the redistribution of water to locations away from the surface could lead to development of a swelling pressure around the periphery of the tunnel.
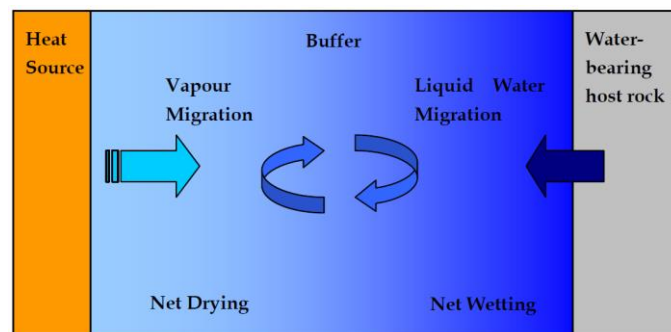
Figure 1-8: Schematic of the drying and re-saturation process of a clay buffer between a heat generating canister and the host rock (Wilson et al., 2011).
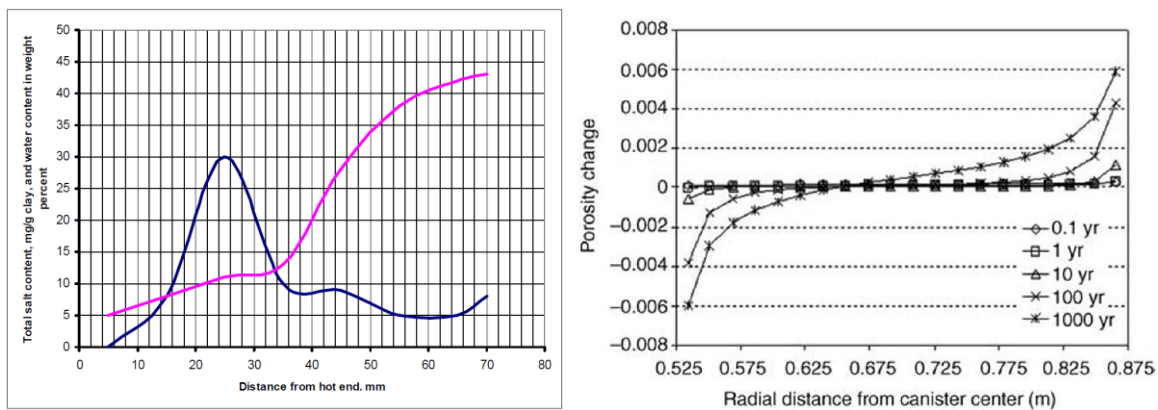
Figure 1-9: a) wetting of the clay from the cold end (steadily rising curve) and accumulation of salt at the wetting front (curve with peak) in a laboratory experiment (Pusch, 2008); b) calculated changes in the porosity of the buffer at various times during the thermal period in a KBS-3 repository (Arthur & Zhou, 2005). The canister-buffer boundary ('hot end') is located 0.525 m from the centre of the canister and the buffer-rock boundary ('cold end') is 0.875 m from the canister centre. Porosity variations reflect the cumulative effects of all mineral dissolution/precipitation reactions. A net reduction in porosity, for example, corresponds to a net increase in mineral volumes (mainly anhydrite in the present model).

EURAD (Deliverable n° 1.1) – Initial State-of-the-art of WP ConCorD
Dissemination level: Public
Date of issue of this report: **17/08/2022**

Page 40

Dry-out phase	Transition phase	Saturated phase
Redistribution of initial moisture content	Gradual saturation of bentonite	Complete saturation of bentonite
Poor thermal conduction	Improving thermal conduction	Good thermal conduction
No swelling of sealing materials	Development of swelling pressure	Swelling pressure fully developed
Possible tunnel convergence	Tunnel convergence diminishes as bentonite swells	Gradual equilibration of pore water with groundwater
Dissolution and re-precipitation of minerals	Dissolution of minerals	Corrosion in fully saturated bentonite
No deliquescence	Deliquescence of precipitated salts	H_2 generation once O_2 depleted
No corrosion	Corrosion due to formation of thin surface water film	O_2 completely consumed
No gas generation	H_2 generation possible once O_2 depleted	Onset of anoxic conditions
No O_2 consumption	O_2 consumption	No microbial activity in highly compacted bentonite
No microbial activity	No microbial activity in highly compacted bentonite	

Time ⟶

Figure 1-10: Evolution of Environmental Conditions in a Deep Geological Repository Characterized in Terms of the Stages of Saturation (King, 2005).

Dry conditions persist until cooling and an increasing level of saturation of bentonite causes the relative humidity to rise above the critical level for the formation of thin films of moisture on the metal surface. The resulting thin electrolyte layer can support aqueous corrosion and the formation of electrochemical corrosion cells. Wetting may be also facilitated by deliquescence of salts. Progressive saturation by water inflow (phase 2) will cause swelling of the bentonite starting from the periphery of the tunnel and gradually progressing towards the centre (Landolt et al., 2009).

Swelling of bentonite continues during phase 3. In the long-term anoxic phase 4, bentonite is completely saturated and all oxidized corrosion products formed at the canister surface and the support structures have been degraded. Over a period of a few hundred years, once complete saturation has been achieved, the groundwater pressure in the bentonite will slowly increase as the hydrostatic head is restored. Equilibration of the bentonite pore water with that in the surrounding host rock will take place over a longer period until pore-water chemistry reaches a steady state. In addition to the bentonite swelling pressure and the lithostatic pressures of about 15 – 22 MPa, the canister will be subject to a hydrostatic pressure of 4.5 - 8.5 MPa (Landolt et al., 2009; specific for NAGRA concept).

1.2.7 Thermal transients

In high-level waste (HLW) repositories, the engineered barriers are exposed to two separate sources of heat. One of them is the increase of ambient temperature with depth of the repository (temperature increases by 25-30 °C/km for dry rock formations, depending on geographical position). The second source is the heat release of nuclear wastes, due to the decay of radionuclides. The heat dissipates into the nearby engineered structures and the host formation.

The prediction of the temperature evolution within the bentonite barrier and the surrounding host rock depends on the reference concept for waste disposal of each Country. It is a critical factor, as it may alter the properties of the multi-barrier system by acceleration of the corrosion of the waste form and of metal components of the containment systems. Further, high temperatures may degrade the bentonite or cement used as backfill materials, as well as argillaceous host rocks (Finsterle et al., 2019) (King et al., 2017). Temperature variations may also create driving forces that affect the migration of radionuclides in the near field of the repository. Chemical thermodynamics, kinetics and diffusion processes are temperature dependent. Thus, the maximum allowable temperature needs to be determined by analysing the acceptable impact on barrier functions.

EURAD (Deliverable n° 1.1) – Initial State-of-the-art of WP ConCorD
Dissemination level: Public
Date of issue of this report: **17/08/2022**

Page 41

Metals in the passive state are protected by a thin, self-forming surface film. General corrosion rates of passive metals are extremely low, on the order of 0.01 μm/year. Localized corrosion processes, such as pitting and crevice corrosion, are risks to the durability of passive films, and temperature is a critical factor for the onset of localized corrosion (Payer et al., 2019).

The evolution of temperature is determined by thermal simulations (e.g., Finsterle et al., 2019). Heat generation from radioactive decay of the SF/HLW results in an initial period of elevated temperature (sometimes referred to as the 'thermal pulse'), followed by a period of slow cooling as the heat release of waste decays. The temperature evolution during the heat pulse has been extensively studied for various disposal systems using both laboratory and field experiments as well as numerical analyses (Payer et al., 2019). There have been several studies conducted to model the expected temperature profile for different conditions (Figure 1-11a). The maximum temperature that a container can withstand depends on each Country´s reference concept. For instance, Sweden specifies a maximum initial canister temperature of 70-80°C, France 90°C, United Kingdom up to 150°C. For proposed salt dome repositories, testing is carried out at temperatures up to 300°C. The curves for each country (Figure 1-11b) show that any viable container material needs to be able to maintain its structural, anti-corrosive, and shielding properties at temperatures far above 100°C, possibly even at the upper limit of 300°C.

Therefore, the concern that thermal ageing could produce sensitized microstructures that would be more susceptible to localized corrosion (and have compromised mechanical properties) does not seem to be significant for repository concepts under the temperatures mentioned above. Gordon (2002) stated that long-range ordering can occur only under temperatures still above 500 °C for Alloy 22 material (nominally 22% Cr, 13% Mo, 3% W, 3% Fe). This can potentially degrade the resistance to stress corrosion cracking (SCC) and hydrogen induced cracking (HIC). For UNS N06022, Rebak et al. (2000) showed that this occurs for temperatures over 427°C.
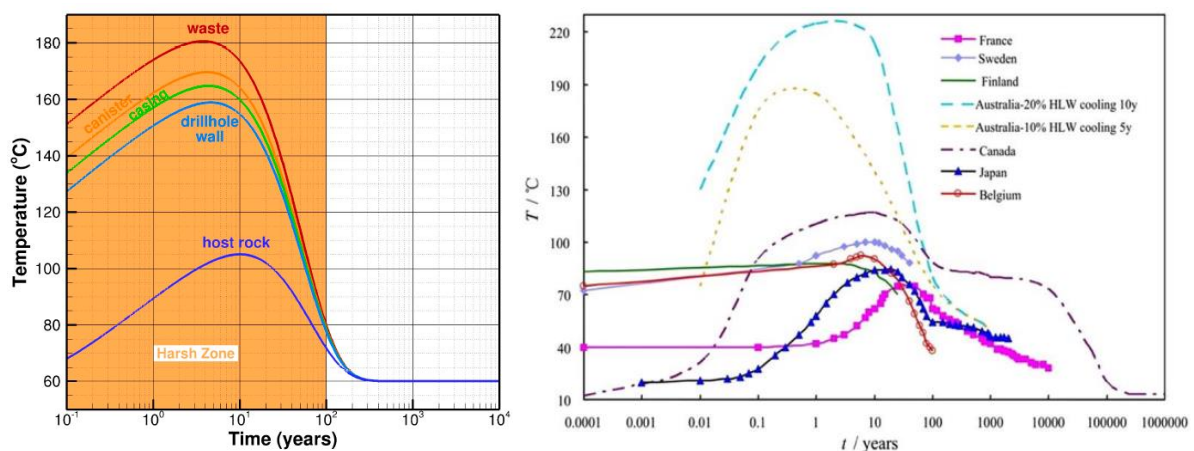
Figure 1-11: a) Temperature profile for HLW waste container inside a deep borehole over time (Payer et al., 2019); b) Temperature simulation near HLW containers for various countries (Zhang et al., 2019).

Large-scale, long-term heater tests for mined repositories in the saturated zone have been conducted in underground rock laboratories dedicated to nuclear waste research (HE-E Experiment: t>100°C, EB Experiment: isothermal, FEBEX in situ test: t_{max}=100°C, FE Experiment: t<120°C (see Villar et al., 2020). These studies reveal the importance of heat generation as it induces coupled thermal-hydrologic (TH) effects. Strong thermal perturbations also affect the geochemical conditions and corrosion products, as well as the geo-mechanical properties and stress state of the repository components, with complex feedback mechanisms to thermal and hydrologic processes (Nguyen et al., 2005) (Zheng et al., 2011) (Kumpalainen, 2016) (Gens et al., 2009) (Sánchez et al., 2012) (Finsterle et al., 2019). An important

EURAD (Deliverable n° 1.1) – Initial State-of-the-art of WP ConCorD
Dissemination level: Public
Date of issue of this report: 17/08/2022

Page 42

thermally induced effect in low permeability media is the pore water pressurization that occurs upon heating (Delage et al., 2010) (Mohajerani et al., 2012). Such strong THM couplings were clearly demonstrated from both *in situ* experiments and laboratory tests performed in the TIMODAZ Project.

Heat is transported from the canister surface to the buffer and the rock. After deposition, heat will be transported by a combination of radiation and conduction across gaps and by pure conduction across the bentonite that will be unsaturated. Some convection can be ignored because of the low permeability of the bentonite and the narrow gap geometries. After saturation of the bentonite barrier (completely swollen and all gaps and joints filled), the whole heat transport takes place by conduction though water-saturated bentonite. The transport of heat through the bentonite is independent of the bentonite heat capacity.

The heat transport can be quantified by the thermal conductivity, λ, which depends on density, water saturation and mineral composition (SKB, 2016).

The time dependence of the container surface temperature is reasonably well known. It depends on to some extent on the site-specific saturation behaviour, which affects the thermal conductivity of the buffer materials. In addition to the container surface temperature, the presence of temperature gradients through the buffer materials may impact the corrosion behaviour. For instance, due to spatial variations in reaction rates and solubility.

Heat conduction will establish temperature gradients between the relatively hot canister-buffer boundary and the relatively cool buffer-rock boundary. The temperature gradients will in turn generate concentration gradients among aqueous solutes due to the equilibrium and kinetic constraints on reactions involving buffer minerals and pore fluids. Diffusional mass transport of aqueous ions and neutral species responding to the thermally induced concentration gradients may cause secondary minerals to precipitate onto the surfaces of the primary clay minerals in the buffer. Should lead these complex and possibly coupled reactive transport processes to significant mineral mass transfer, then could be individual clay particles cemented in secondary solids. This is of concern because such cementation could alter the swelling pressure and other properties of the buffer irreversibly. This affects the primary performance function of this EBS component to provide a stable diffusional transport pathway between the canister and rock (Beattie & Williams, 2012).

According to Raikko et al. (2010), the thermal evolution (typical time history of temperature in the near field of canisters) occurs simultaneously with the swelling and reach its maximum after ca. 10 years. Then, it decays slowly, followed by a slow cooling towards natural temperature after 10,000-20,000 years. Temperature plays a decisive role within phase 1 – 3 in the environmental evolution of a GDR (Figure 1-5). However, it clearly spans over longer period time with slower changes than the other transient processes.

The humidity initially present in the bentonite will redistribute during phase 1 in the areas of lower temperature close to the bentonite–liner interface. Only dry oxidation can take place at the container surface, which has uniform access to oxygen. In the case of a carbon steel canister, a duplex corrosion layer is formed, consisting of an outer hematite film and a considerably thicker inner magnetite layer (Diomidis & Johnson, 2014). Several different growth laws have been proposed for the oxidation of iron and low-alloyed steel in air: parabolic (for thick films at high temperatures and durations), logarithmic (usually for thinner films at lower temperatures and durations), and combinations of both (Feron & Macdonald, 2006) (Lagha et al., 2007). Stoulil et al. (2019) have shown that the higher the temperature the more compact is the layer of corrosion products that slightly decelerates corrosion rate compared to the state at 40 °C.

Corrosion products are a complex mixture of different crystalline and amorphous phases of Fe oxides and hydroxides, mainly in the trivalent state. Due to evolving conditions (temperature, relative humidity, and oxygen concentration) during phase 2, many interrelated corrosion products and mechanisms can be present (Diomidis & Johnson, 2014).

EURAD (Deliverable n° 1.1) – Initial State-of-the-art of WP ConCorD
Dissemination level: Public
Date of issue of this report: 17/08/2022

Page 43

During phase 3, the temperature continues decreasing and thus the canister material equilibrates with bentonite porewater.

During phase 4, the temperature keeps decreasing until reaching the surrounding temperature. Depending on the temperature and pH of the surrounding environment, ferrous hydroxide may transform via the Schikorr reaction into magnetite, leading to the evolution of additional hydrogen (Diomidis & Johnson, 2014).

Most reported corrosion studies have been performed under defined and constant temperature. An increase of the corrosion rate with temperature is usually observed (e.g., Smart et al., 2002b). Only a few studies have been performed under fluctuating temperature conditions.

The effect of decreasing temperature in iron-bentonite interaction experiments was investigated by Pignatelli et al. (Pignatelli et al., 2013; 2014), with focus on the nature of formed corrosion products. In these experiments, Callovo-Oxfordian claystone was contacted with metallic iron (present both as coupon and as powder) in autoclaves and heated to 90°C for 6 months before the temperature was reduced by 10°C every month until reaching 40°C. The pH measured after cooling to 25°C did not change considerably. Unfortunately, neither the oxidation-reduction potential nor the value of iron corrosion rate have been reported. In all samples, the presence of magnetite, cronstedtite and greenalite were detected. These studies also indicated that cronstedtite may not be stable below 50°C. In all cases, the formation of these iron silicates was directly linked to the dissolution of silicates present in the argillite, the solubility being dependent on the temperature.

The effect of fluctuating temperature on steel corrosion under in situ conditions has been investigated by Schlegel et al. (2018). A series of carbon steel rods were inserted in a test chamber heated to 85°C and left to corrode for various reaction times. During the experiment, the heating system had a break down, resulting in a decrease of the temperature to 25°C. Some rods thus corroded at 85°C, then at 25°C and subsequently again at 85°C. Other rods were only corroded at 85°C, allowing to detect any effect of fluctuating temperature conditions. Samples reacted at 85°C were essentially covered by a thin layer of Fe silicates. Results were consistent with a low corrosion rate (~1 µm y^{-1}), hinting a surface protection by corrosion products. In contrast, coupons corroded at fluctuating temperature conditions presented areas of extensive corrosion, with depressions filled with corrosion products. Their results pointed out the absence of surface protection and at the occurrence of a spatial separation of anodic and cathodic reactions. A consequence of this separation was a local corrosion rate inside cavities significantly larger (~100 µm y^{-1}) than the average rate (<10 µm y^{-1}). Under fluctuating temperature conditions, carbonates, chloride, and sulphide phases were typical corrosion products, in addition to Fe silicates and magnetite. Schlegel et al. (Schlegel et al. 2018) concluded that the major impacts of low temperature transients would be the metal oxidation occurring more rapidly than the precipitation of corrosion products (Nesic et al., 2007), the development of microbial communities responsible for the formation of biofilms or Fe sulphides, and a partial loss of air tightness. In case of spatial separation of anodic and cathodic areas, a local larger surface damage is the consequence of a metal oxidation faster than corrosion products precipitation at low temperature. Upon subsequent temperature increase, the precipitation of corrosion products increases, slowing down the corrosion rate.

In the context of nuclear waste disposal, reported studies show that changes in temperature have a rather negative impact on metallic corrosion. Changes in temperature are not only altering the kinetic of metallic corrosion but also the solubility of mineral phases contacting the canister, which in turn modifies the composition of the contacting fluid.

1.2.8   Chemical (pore water) transients

The chemistry of the pore water is modified by bentonite/groundwater interactions over time, since bentonite is an ion-exchanger and contains impurity minerals (calcite, pyrite, halite, etc.) and organic

EURAD (Deliverable n° 1.1) – Initial State-of-the-art of WP ConCorD
Dissemination level: Public
Date of issue of this report: 17/08/2022

Page 44

matter, modifying the solution in contact with the canister material. The corrosion of the canister results from the contact of pore water with the canister surface.

The near field processes are complex, especially in the early, non-isothermal and unsaturated period, as thermal and hydraulic gradients influence the properties of the bentonite barrier and its performance. The bentonite pore water can be modified over time due to changes of the initial physicochemical conditions under different types of perturbations: a) interaction with granitic groundwater (saturation phase), b) desaturation phase due to heating, c) perturbations linked to the interactions between the bentonite and the engineered solid materials (concrete, iron, steel, organics, etc.), and d) interactions with different gases produced and consumed and in the system (CO_2, H_2, CH_4, etc.), due to mineral dissolution/precipitation, microbiological reactions and corrosion processes.

The impact of the different perturbations can be described in terms of: 1) modifications in the pore water chemistry and redox conditions, which may affect the smectite structural stability and speciation of dissolved ions, 2) mineralogical alteration: dissolution and redistribution of primary mineral phases and precipitation/neoformation of secondary minerals, 3) clay mineral stability and alteration of the clay mineral properties (especially cation exchange capacity, cation exchange population, crystallo-chemical structure, layer charge and swelling ability), and 4) modification of transport properties through modifications of porosity, permeability and tortuosity by cementation processes. The perturbation processes may change the physical, hydraulic and mechanical properties of the bentonite system (see Figure 1-19 in the next subsection).

The challenging scientific approach to tackle the problem of predicting the long-term clay barrier behaviour consists in analysing the results from experiments conducted in underground research laboratories (URL) in real scales and conditions (Tournassat et al., 2015). Most of the bentonite barrier experiments described in the literature have been carried out under laboratory conditions (e.g., Cuevas et al., 1997) (Fernández et al., 2010, and references therein) to study the chemical evolution of the pore water and the alterations of the bentonite barrier. There are only a few large experiments, as LOT, ABM, FEBEX and FE *in-situ* experiments (Karnland et al., 2009) (Svensson et al., 2011) (Villar et al., 2017) (Müller et al., 2017). Along years, a huge bunch of papers have reported results of geochemical and reactive transport modelling for the long-term analysis and near field evolution (Bradbury & Baeyens 2002) (Fernández et al., 2004) (Curti, 2011) (De Combarieu et al., 2007) (Savage et al., 2010) (Wersin et al., 2003; 2004) (Itälä, 2009) (Cervinka et al., 2018) (Jeni et al., 2019) (Zheng et al., 2015; 2020).

After repository closure, gradual saturation of the bentonite may lead to some redistribution of the water content, dry density, and salts during phase 1 (Figure 1-5). Precipitation of salts close to the canister surface may also occur, assisted by the desiccation of the bentonite (Landolt et al., 2009). Progressive saturation by water inflow causes re-dissolution of precipitated salts and the bentonite pore water equilibrates with the incoming water from the host rock. During the period 3, Fe(III)-rich corrosion products formed during the previous periods can reduce (Diomidis, 2014). Equilibration of the bentonite pore water with that in the surrounding host rock will continue until a steady state has been reached by approaching to phase 4 (Figure 1-5), few hundred years after closure. Steady state conditions for the chemical composition of the pore water, however, have not been achieved before 10.5 years of experiment in the EB experiment (Fernández, 2019), nor before 18 years in the FEBEX in situ test (Fernández et al., 2018), and during the ABM5 Experiment (Fernández et al., 2022). In different tests, it has been observed that the most important parameter for pore water chemistry is the bentonite composition, independently on ground water chemistry (deliverable D2.6 WP ACED) (Havlová et al., 2020). However, this is true if the infiltrating ground water is a diluted granitic pore water. Modifications in the pore water chemistry and in the cation exchange composition of the bentonites have been observed in the ABM5 experiment after the interaction of a saline granitic groundwater with Na- and Ca-bentonites during 4.4 years (Figure 1-12), indicating the influence of the type of the infiltrating water and the type of bentonite (main cation at exchange sites) on the evolution of the pore water chemistry of the bentonite barrier (Fernández et al., 2022).

EURAD (Deliverable n° 1.1) – Initial State-of-the-art of WP ConCorD
Dissemination level: Public
Date of issue of this report: 17/08/2022

Page 45
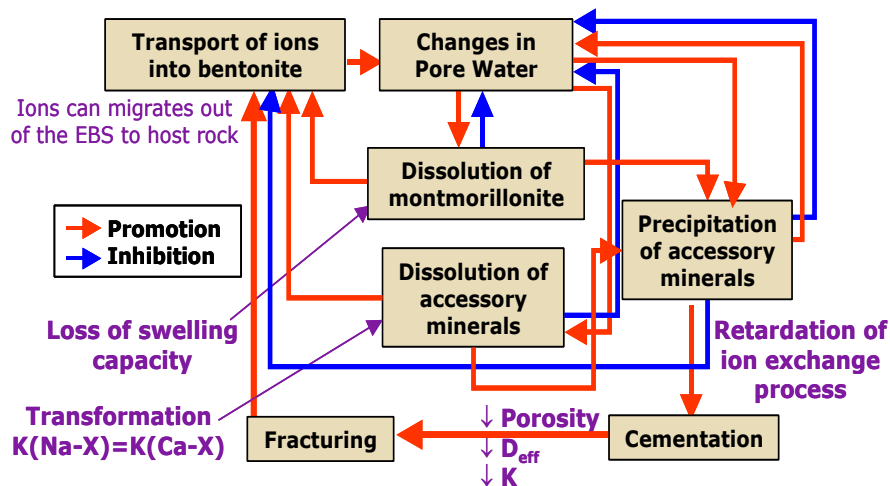
Figure 1-12 : Water-bentonite interaction processes and possible buffer alterations after (Takase, 2004).

The nature of corrosion products is a function of the redox conditions, solution composition, temperature, water saturation and the reaction kinetics (see Fernández & Alonso, 2021). Indeed, the durability of canister materials are particularly influenced by the presence of chloride, sulphate, carbonates and sulphides (Table 1-2), as well as by dissolved gases generated and consumed (Figure 1-13, Figure 1-14, Figure 1-15, Figure 1-16). In addition, pH is also a critical parameter, not only for the iron speciation. Carbon steel corrodes actively in compacted bentonite backfill since the pH of bentonite pore water (pH 7–8) is not alkaline enough to induce passivity. Thus, C-steel canisters are expected to corrode uniformly with some degree of surface roughening but with little tendency for localised corrosion. Chloride and sulphates increase the corrosion of metals. Sulphur and thiosulphate species are aggressive towards canister materials. Carbonates can induce passivity of active materials, such as copper or C-steel, and can inhibit the localized corrosion of passive materials, such as stainless steel and Ni-based alloys. Cations can also influence the corrosion behaviour. For instance, the hydrolysis of Mg leads to acidification of brine inclusions and species such as Ca and Mg can be incorporated into corrosion product layers (King, 2020). Precipitation of GR-Cl (green rusts), other chloride salts and Cl-bearing Fe(III) oxyhydroxide (akaganeite) were observed after dismantling the FEBEX *in-situ* test. Due to the high contents of chlorides in the pore water at the Heater #2 contact (Fernández et al., 2018) (Wersin & Kober, 2017), corrosion processes are favoured close to this place (see Figure 1-19 of the next subsection). pH variations due to the thermo-hydraulic gradients are observed in the bentonite barrier. Itälä (Itälä, 2009) evaluated the evolution of the chemistry of the MX-80 bentonite chemistry by geochemical modelling over 10 years of saturation and heating (up to 130°C). He observed that pH decreases with evolving saturation. Cervinka et al. (2018) evaluated the influence of the Ca-Mg-bentonite chemistry in contact with granitic groundwater on the GDR barrier performance on a simplified time axis (0 ths., 1 ths., 10 ths., 100 ths. and 1 mil. years) after the thermal phase (under ambient temperature). They found that the concentration of chloride in bentonite pore water decreased, reducing its aggressivity and increasing the pH. Several modelling studies describe the pH evolution of typical nearfield porewaters for a range of disposal concepts (Atkinson et al., 1988) (Arcos et al., 2008) (Small & Thompson, 2010).

EURAD (Deliverable n° 1.1) – Initial State-of-the-art of WP ConCorD
Dissemination level: Public
Date of issue of this report: **17/08/2022**

Page 46

Parameter	Carbon steel	Copper	Stainless steels	Titanium alloys	Nickel alloys
Host rock	High sulphide mineral content	High sulphide mineral content	High sulphide mineral content	None	High sulphide mineral content
Redox conditions	Permanently aerobic	Permanently aerobic	None	None	None
Temperature	>200°C	>150°C	<100°C (in absence of cementitious backfill)	>200°C	>150°C
Gamma radiation	>1–10 Gy h^{-1}	>1–10 Gy h^{-1}	>1–10 Gy h^{-1}	>1000 Gy h^{-1}	>1–10 Gy h^{-1}
Backfill material and near field mass transport	None	No backfill	Requires the use of a cementitious backfill to ensure adequate corrosion performance	Cementitious backfill	None
Chloride concentration	>400 mg L^{-1} with cementitious backfill	No upper limit, lower limit 0·01–0·1 mol L^{-1}	Dependent on nature of backfill and alloy	Alloy dependent	Alloy dependent
Other ground water species	None	($[SO_4^{2-}]+[HCO_3^-]$)/$[Cl^-]$>0·1–1·0, ammonium ions	None	Fluoride	None (sensitivity to Pb)
Sulphur species	Uncertain	Uncertain	Thiosulphate, sulphide	None	H$_2$S, elemental S
Microbial activity	Microbial activity at the canister surface	Microbial activity at the canister surface	Microbial activity at the canister surface	None	Minimal
Residual stress and external load	None	None	Dependent on nature of backfill and alloy	Dynamic loading	None
GDF saturation time	None	None	None	None	None

*Critical conditions are shown in bold font, and marginal conditions are shown in regular font. Critical conditions are those for which the durability of candidate canister materials may be questionable or not recommended. Marginal conditions are those in which the durability of a candidate canister material may prove to be acceptable but for which a more detailed analysis is warranted.

Table 1-2: Summary of critical and marginal conditions for durability of candidate HLW/SF canister materials (King, 2009).

Landolt et al. (2009) stated that the formation of steel corrosion products and the redistribution of soluble salts cannot influence the performance of bentonite. But anaerobic corrosion does, e.g., by production and migration of hydrogen gas. The interaction of corrosion products with bentonite was described by De Combarieu et al. (2007), Hunter et al. (2007), Samper et al. (2008), Wersin et al. (2008). Simultaneous development of canister- buffer chemistry/mineralogy is being solved within EURAD WP ACED Task 2.
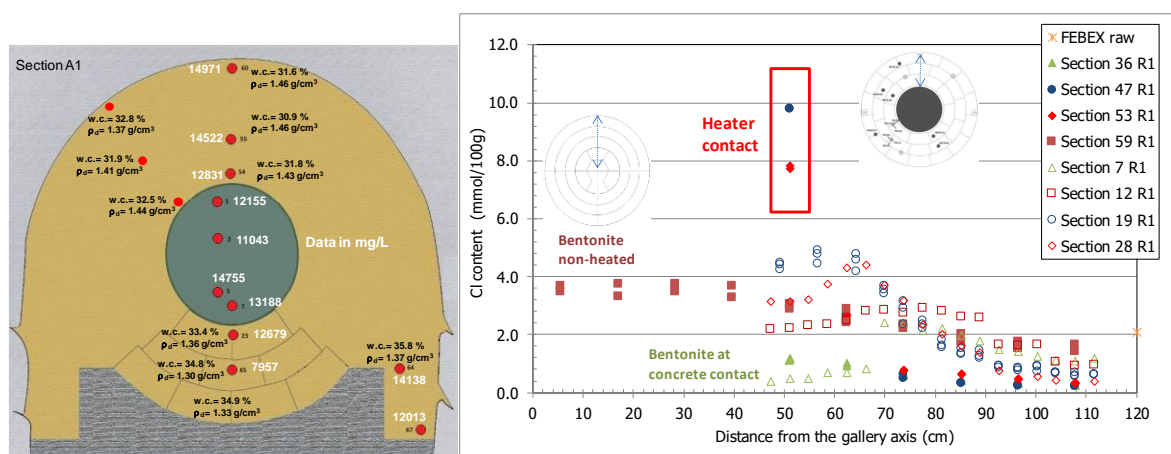
Figure 1-13: Distribution of chloride concentration in the bentonite pore water from large-scale in situ experiments: a) EB Experiment at Mont Terri, data in white color (Fernández, 2019), b) FEBEX in situ test (Fernández et al., 2018): comparison of chloride content data after dismantling of Heater #1 (5 years of experiment, open symbols) and Heater #2 (18 years of experiment, filled symbols).

EURAD (Deliverable n° 1.1) – Initial State-of-the-art of WP ConCorD
Dissemination level: Public
Date of issue of this report: 17/08/2022

Page 47
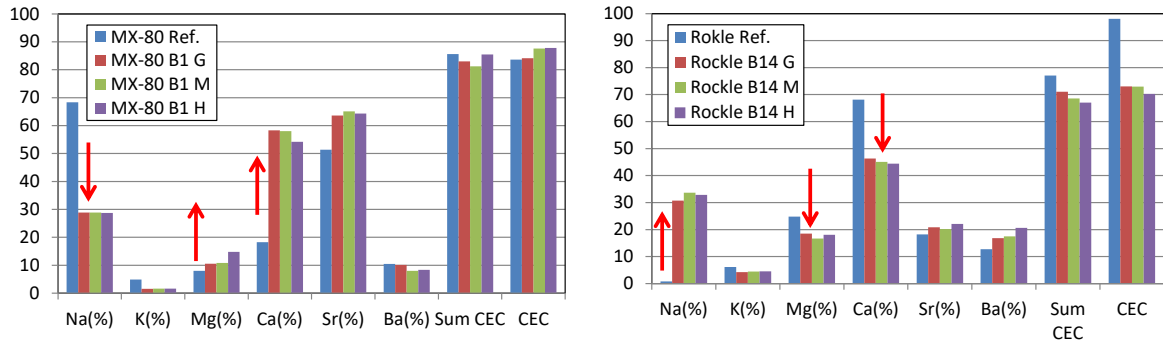
Figure 1-14: Distribution of the cation exchange population in percentage (Y-axis) after dismantling of the ABM5 experiment for sodium (MX-80) and calcium (Rokle) bentonites. Sr and Ba percentage is multiplied by 100 and 1000, respectively (Fernández el al., 2022).
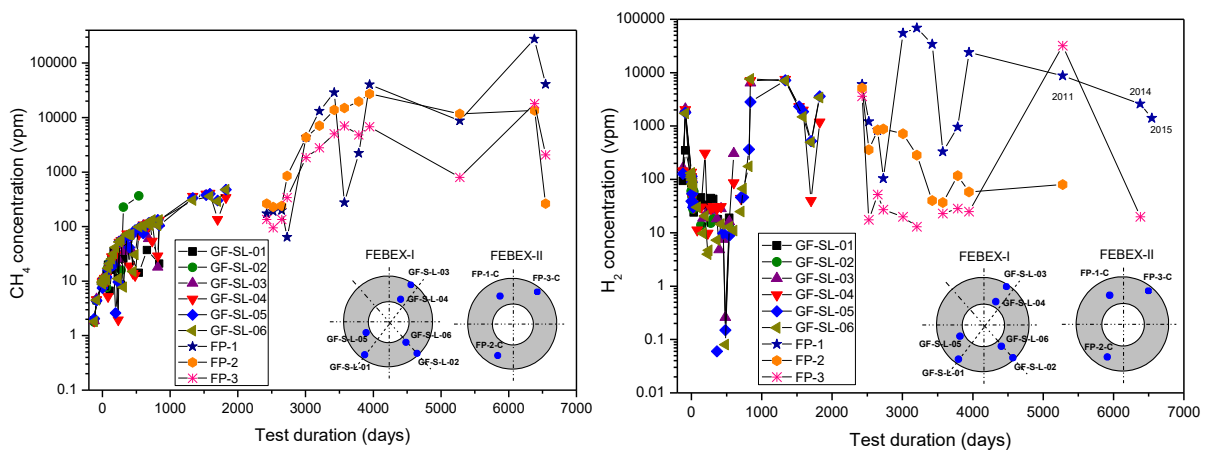
Figure 1-15: Methane and hydrogen evolution inside the bentonite barrier during the FEBEX in situ test (Fernández et al., 2019).
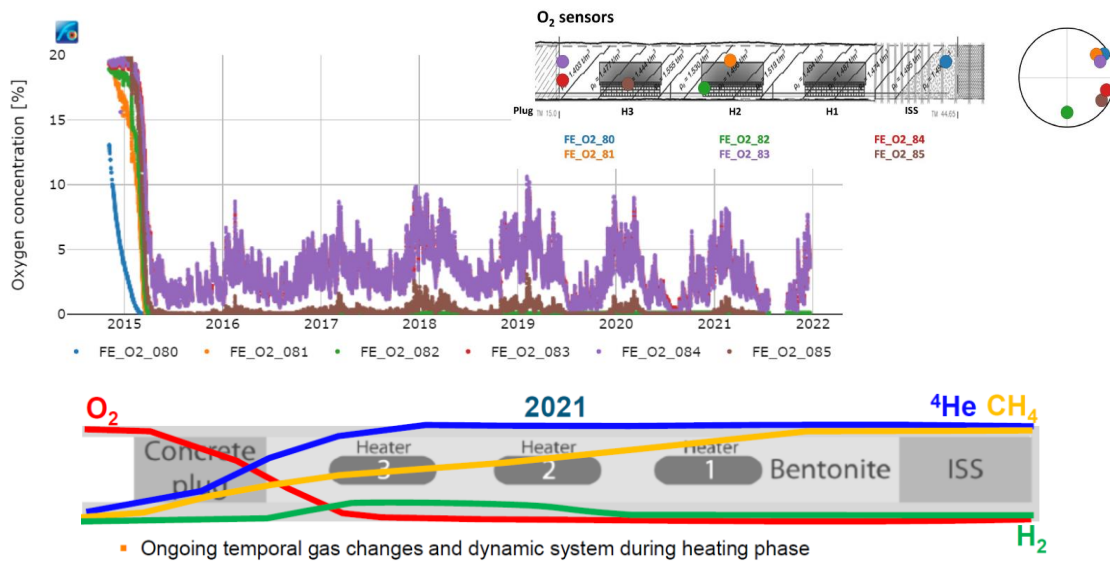
Figure 1-16: Gas evolution during the FE in situ test (NAGRA, 2022).

EURAD (Deliverable n° 1.1) – Initial State-of-the-art of WP ConCorD
Dissemination level: Public
Date of issue of this report: **17/08/2022**

Page 48

King (2007b) modelled the anodic corrosion of copper in the presence of sulphide. The anodic reaction involves the formation of a Cu_2S film. This film is only partially protective and dissolution continues via a two-step process involving an adsorbed intermediate species. At more positive potentials, the reaction becomes limited by transport of HS-. The cathodic reaction involves the reduction of HS- with the evolution of H_2. Under repository conditions in the presence of compacted bentonite, the overall corrosion rate is limited by the supply of HS- to the canister surface.

In the case of waste disposal concepts in clay formations as host rock, concrete structures are needed for supporting galleries. In this context, the pore water pH will evolve as the alkaline mineral phases are leached out over time (see Deissmann et al., 2021) (De Windt et al., 2020). There will be an interface between cement-based materials and metal supporting structures. Highly alkaline pH values during the thermal phase keep the carbon steel canister passivated, thus limiting the corrosion.

The stability of the passivation layer depends on the conditions of the surrounding geochemical environment. Cement ageing processes (especially leaching and carbonation) can influence the corrosion processes and the depassivation of the steel (dissolution of the protective layer) by a) pH decrease due to carbonation, b) ingress of aggressive species such as chloride. The protective oxide film is believed to be stable as long as the pH remains higher than a threshold value (~9 < pH < ~11.5). The most stable corrosion products in highly alkaline conditions (pH >11), is magnetite and goethite under anoxic and oxidic conditions, respectively. Depending on kinetics, temperature, and local composition, the formation of stable iron oxides/hydroxides can be inhibited, resulting in the formation of different intermediate metastable phases such as amorphous oxide/hydroxide phases, hydroxy-chloride phases and green rust GR1(Cl-). Iron released by steel corrosion diffuses into the cement leading to the formation of various solids and/or to its incorporation in existing phases (Fe-containing cement minerals, such as Fe-ettringite, Fe-monosulphate, Fe-hemicarbonate, Fe-monocarbonate, Al-Fe hydrotalcite, hydrogarnet, etc.).

Volume variations due to corrosion products may lead to stress and (local) alteration of the pore structure at the interface, changing the microstructural properties of the concrete. However, a decrease of pH caused by active corrosion implies a chemical degradation of concrete. Thus, the available pore space might be smaller or larger depending on carbonation or calcium leaching.

1.2.9   Mechanical transients

Canisters are exposed to residual and applied stresses and, hence, the possibility of environmentally assisted cracking (Shoesmith, 2006). The magnitude of the applied stress (~ 20-50 MPa) depends on the repository design and the host rock formation. The external load will comprise the swelling pressure of the backfill (if used), the hydrostatic pressure, and the lithostatic load (the later only for non-self-supporting rock, such as salt domes and sedimentary deposits).

The pressure on the canister depends on (Hasal et al., 2019):

1) hydrostatic water pressure in the rock, which is transferred to the canister through almost fully saturated bentonite,
2) swelling pressure of bentonite (saturation), even including saturation (Raikko et al., 2010),
3) the increase of temperature of bentonite and surrounding rocks,
4) degradation of the canister and influence of corrosion products on the bentonite (potential influence of corrosion products, having larger volumes then the ancestors),
5) increase in pore pressure due to gas release,
6) chemical changes of materials, namely bentonite, and,
7) borehole deformation (Raikko et al., 2010).

EURAD (Deliverable n° 1.1) – Initial State-of-the-art of WP ConCorD
Dissemination level: Public
Date of issue of this report: 17/08/2022

Page 49

The mechanical load on the canister develops with continuing saturation of the bentonite. It depends on bentonite dry density (Figure 1-17), temperature (Figure 1-18) and the bentonite pore water composition. Stress increases with decreasing temperature altogether with gradual bentonite saturation (Figure 1-5). After the bentonite barrier is completely saturated, the total pressure is constituted by the sum of the bentonite swelling pressure and water pressure. While the water pressure is isostatic, the bentonite density variations in combination with imperfections in the deposition hole/gallery can impose an asymmetric pressure on the outer surface of the canister, which is considered to be permanent, and may yield an over-stress affecting the canister integrity (Jonsson et el, 2018) (Posiva SKB Report 04). Corrosion-allowance materials, such as carbon steel, corrode uniformly and are less susceptible to localised corrosion and environmentally assisted cracking. Corrosion resistant materials, such as stainless steels, Ti- and Ni-based alloys, tend to be more susceptible to localised attack in the form of pitting or crevice corrosion. The corrosion behaviour of the canister is determined primarily by the environmental conditions of the near field.

In the last years, considerable research has been carried out to evaluate the behaviour of compacted clay-based buffer material in the frame of coupled thermo-hydromechanical (THM) processes at nuclear waste repositories (Villar et al., 2020). An important issue is the total time for saturation of the bentonite, the changes in dry density and porosity of the bentonite barrier, and the pressure withstood by the canisters (pore water pressure, gas pressure, etc.). The time-dependent degree of saturation of the repository is an important factor in determining when, and in what form, corrosion can occur (King, 2006). The process of hydration depends on the hydraulic permeability and thermal conductivity of the bentonite and the host rock, the salinity, and temperature (Figure 1.18, Figure 1.19). In addition, hydration triggers swelling of inter layers space in clay particles and transforms the material from an initial heterogeneous to a homogeneous one, changing the local volume constraint conditions. The changes of macroscopic volume due to clay-water interactions is associated with the evolution of the microstructure and its interaction with the macrostructure, being described by dual porosity models and water retention behaviour. The changes in pore size distribution domains in terms of micro- to macro-porosity fractions are highly sensitive to the physicochemical processes involved in the applied loading paths, especially in the frame of couple THM processes at nuclear waste repositories (Schanz, 2016).
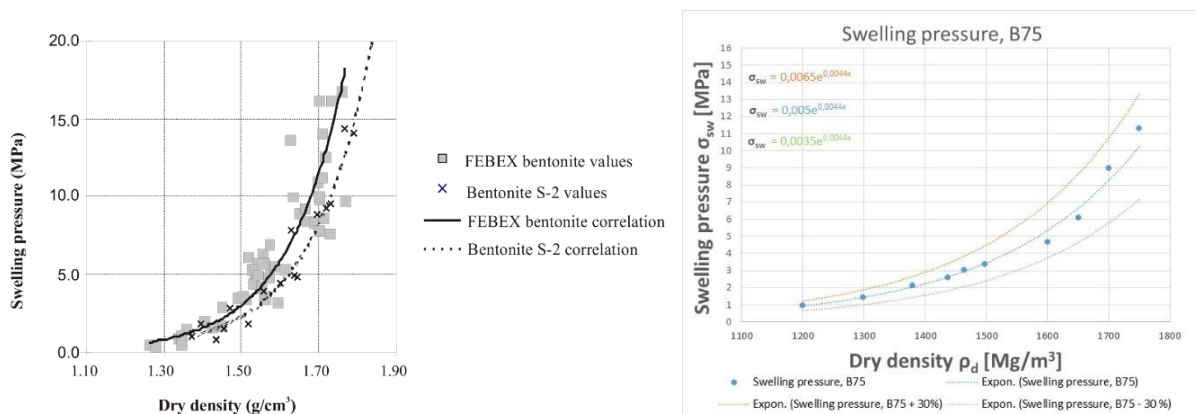
Figure 1-17: Dependence of the swelling pressure on dry density for FEBEX bentonite (left) (Gens, 2016) and CZ Ca-Mg bentonite (right) (Hasal et al., 2019).

EURAD (Deliverable n° 1.1) – Initial State-of-the-art of WP ConCorD
Dissemination level: Public
Date of issue of this report: 17/08/2022

Page 50
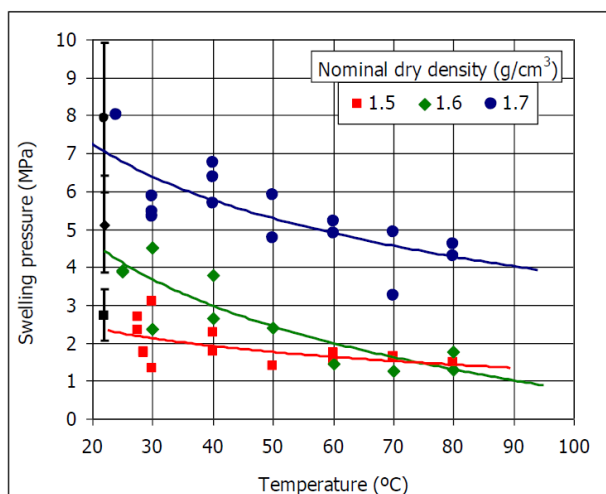
Figure 1-18: Swelling pressure dependence on temperature for FEBEX bentonite blocks at different dry densities (Villar and Gómez-Espina, 2009).
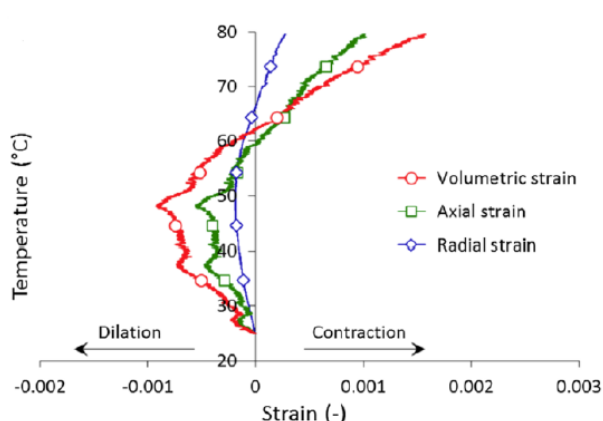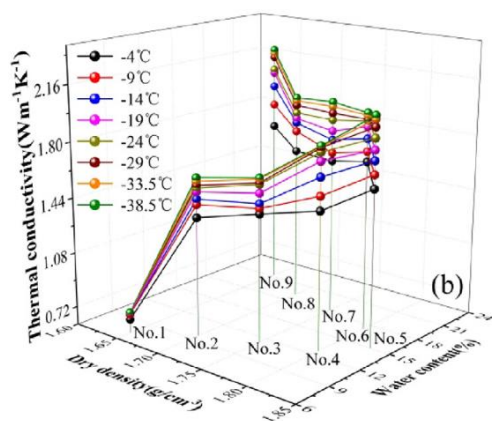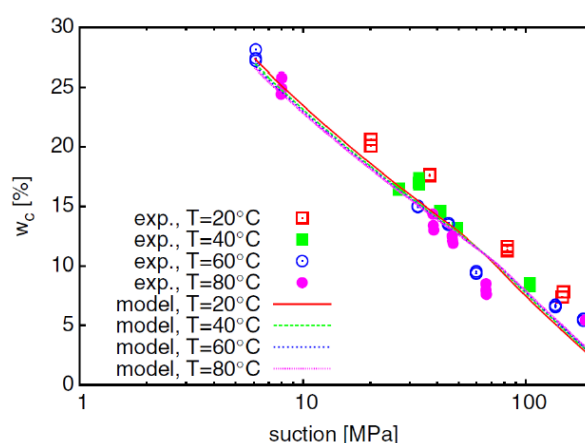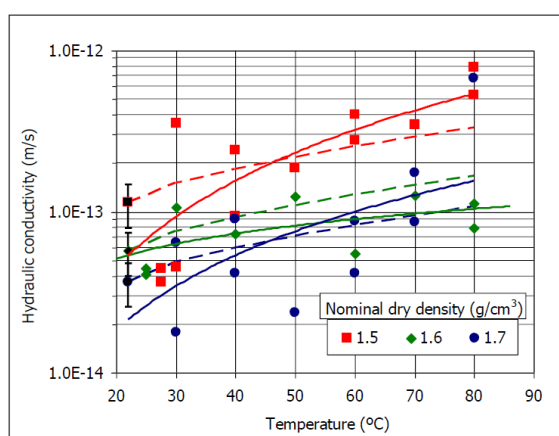
Figure 1-19: Variations of hydraulic conductivity (Villar & Gómez-Espina, 2009), water retention curve (Tang & Cui, 2007), thermal conductivity (Xu et al, 2019;2020) and strain (Belmokhtar et al., 2017) with temperature.

EURAD (Deliverable n° 1.1) – Initial State-of-the-art of WP ConCorD
Dissemination level: Public
Date of issue of this report: **17/08/2022**

Page 51
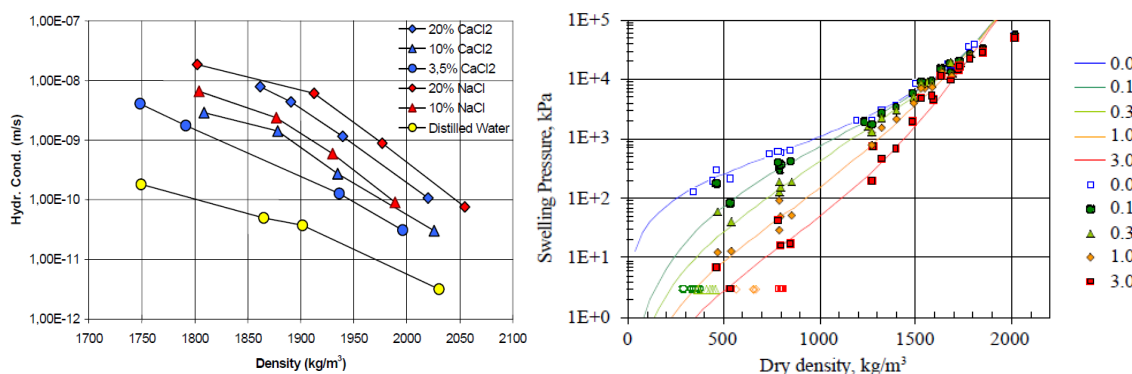
Figure 1-20: a) Effect of pore fluid salinity on hydraulic conductivity of Friedland clay (Push & Jonhs, 2006), b) swelling pressure versus clay dry density for different concentrations in a NaCl solution (in mol l⁻¹) in equilibrium with the Na-montmorillonite (SKB, 2006).

1.2.10 Microbial transients

Canister materials are susceptible to undergo microbiologically influenced corrosion (MIC). The key to the MIC of HLW/SF canisters is the extent and location of microbial activity. In principle, nuclear waste repositories are inhospitable environments for microbes (King, 2009). The combined effects of high temperature, radiation fields, pore water salinity, redox condition, the lack of space in the compacted bentonite barrier, the low water activity and the lack of organic nutrients and terminal electron acceptors reduce the microbial activity (Figure 1-21). A recurring topic in microbiology is the source of carbon and energy available for microbial growth. Microbes require sources of nutrients and energy to support the metabolic processes. Energy is provided by redox reactions involving the oxidation of organic matter, H_2, or other reduced species and the reduction of terminal electron acceptors (TEA), such as O_2, NO_3^-, Fe(III), SO_4^{2-} and CO_2. On the assumption that there is no microbial activity in the buffer, MIC can only occur if remotely produced metabolic by-products, such as sulphide produced under anaerobic conditions by sulphate reducing bacteria, can reach the canister surface. Microbes can also be beneficial, by consuming the initially trapped O_2 and H_2 generated during corrosion (decreasing the pressure in the system), or by forming protective biofilms.

Different studies on compacted bentonites have shown that the microorganisms stop their activity at: a_w < 0.96, swelling pressures > 2 MPa, pore size < 0.2 μm, dry density $\geq$ 1.6 g/cm³ or pore water salinity > 100 g l⁻¹ NaCl (Stroes-Gascoyne et al., 2010;2011) (Masurat el al., 2010). However, this issue is still a matter of discussion. The presence of microbes and microbial activity has been demonstrated in different laboratory and *in situ* tests. For example, FEBEX bentonite contains dormant bacterial spores which can grow under certain appropriate conditions (i.e., sufficient nutrients, decreased bulk density of buffer, temperature, sufficiently high water-activity, etc.). Activity of microorganisms was observed in different experiments (Figure 1-22). After 18 years of the FEBEX *in situ* test, the main conclusions were: a) very few or no cultivable cells from the sections around and adjacent to the heater, with temperatures between 84 and 99 °C and dry densities between 1.6 and 1.7 g/cm³; b) significantly higher number of cultivable cells on different media: SRB, NRB and IRB (Figure 1-23), are found in the sections where temperatures were lower (20-30°C), the dry density slightly lower (1.4-1.5 g/cm³), and the water content higher (>20%). However, cultivation techniques implied bacterial viability, but not if they were actually active at the sample location. The genus *Desulfosporosinus* was found in many of the cultures. This genus included spore-forming, mesophilic sulphide-producing bacteria with the ability to grow with molecular hydrogen as source of energy. The detection of a large diversity of spore-forming genera was

EURAD (Deliverable n° 1.1) – Initial State-of-the-art of WP ConCorD
Dissemination level: Public
Date of issue of this report: 17/08/2022

Page 52

expected because spores will survive for a long time in dry clay until water saturation is reached. When water is available, spores can germinate to active bacteria. In the ABM1 experiment the microbial growth was scarce due to the extreme incubation temperatures (90-130°C) (Svensson et al., 2017).
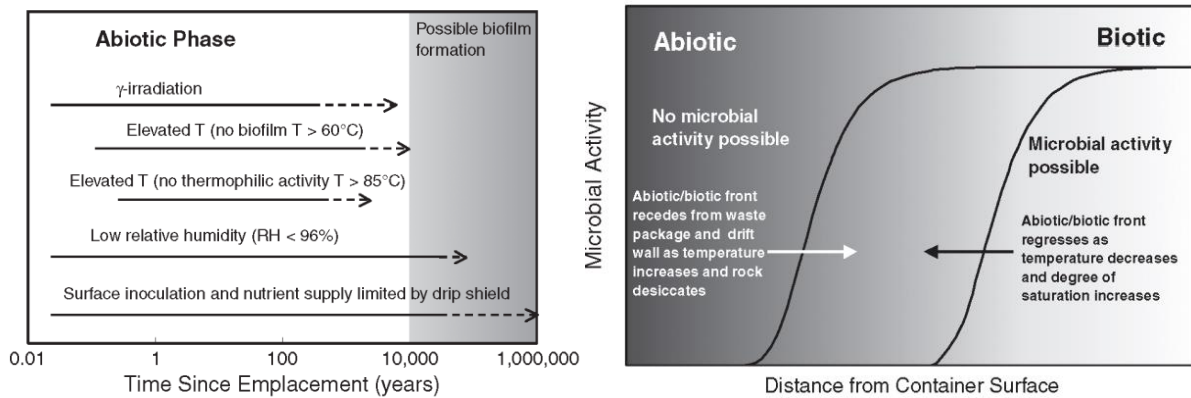
Figure 1-21: a) Factors that prevent or limit microbial activity at the surface of waste packages in the repository environment (King 2009); b) Schematic illustration of the initial recession of the abiotic zone during the thermal pulse in a repository and the subsequent regression as the temperature decreases and the RH increases in the tunnel and rock wall (Lloyd et al., 2004).
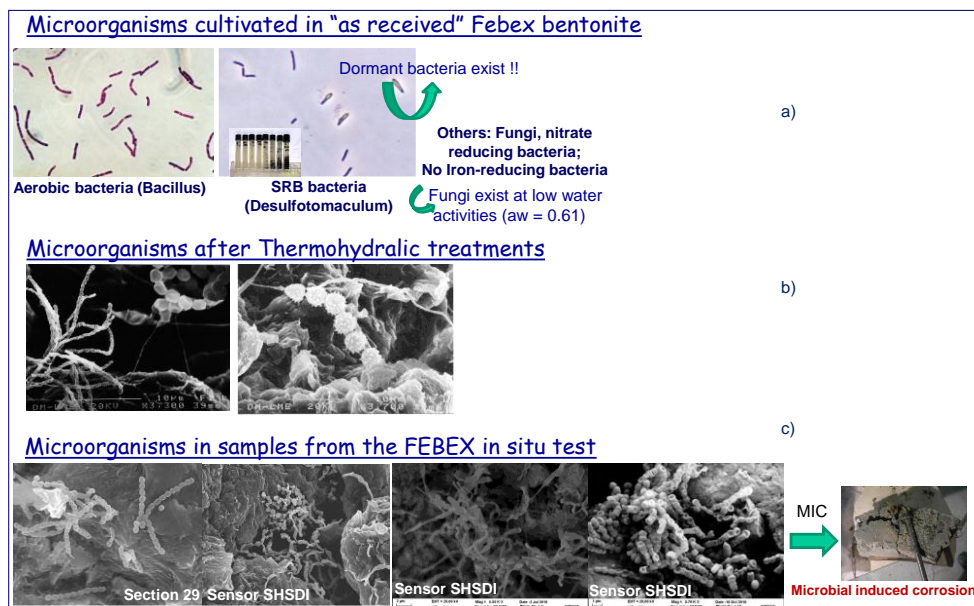
Figure 1-22: Microorganisms observed in the FEBEX bentonite: a) cultivated in as received bentonite, b) observed after thermohydraulic treatments (Fernández & Villar, 2010), and c) observed in samples from the first dismantling of the FEBEX in situ test (Huertas et al., 2006).

EURAD (Deliverable n° 1.1) – Initial State-of-the-art of WP ConCorD
Dissemination level: Public
Date of issue of this report: 17/08/2022

Page 53
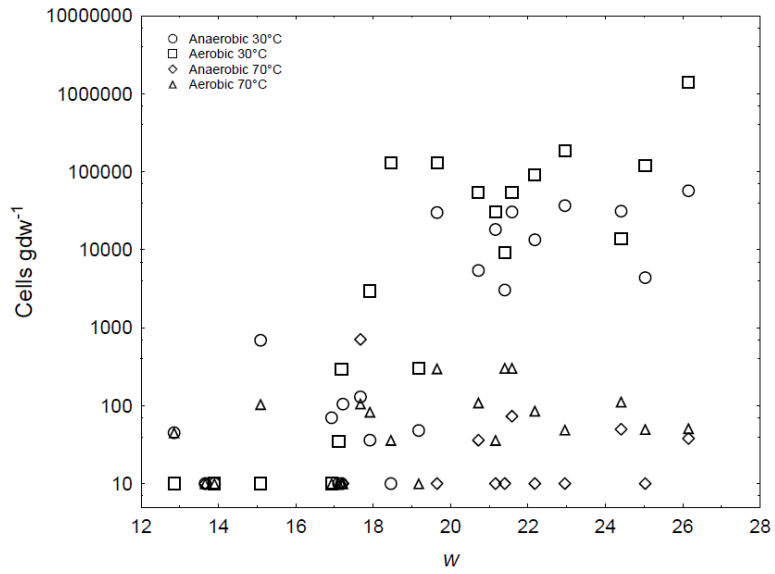
Figure 1-23: Numbers of aerobic and anaerobic cells cultivated by BGR at 30°C and 70°C versus gravimetric water content (w) (Bengtsson et al., 2017).

EURAD (Deliverable n° 1.1) – Initial State-of-the-art of WP ConCorD
Dissemination level: Public
Date of issue of this report: 17/08/2022

Page 54

1.3 Microbial effects

1.3.1 Microbial corrosion in the context of nuclear waste disposal

The impact of microorganisms on the rate of corrosion is well established but a lot remains to be clarified with respect to the mechanism of corrosion and how to control it. In the literature, microbially-influenced corrosion (MIC), the process by which microorganisms impact the corrosion of a metal, directly or indirectly, is proposed to be categorised in two broad groups: chemical MIC (CMIC) that relies on corrosive chemical by-products of microbial metabolism and electrical MIC (EMIC) that entails the transfer of electrons from the metal to the bacterium (directly or indirectly) (Venzlaff et al., 2013) (Enning & Garrelfs, 2014) (Figure 1-23). The latter is presumed to require biofilm formation (Jia et al., 2019) (Little et al., 2020), which, for nuclear waste, is only relevant in the absence of a bentonite backfill.

In the context of nuclear waste disposal, the major concern is the corrosion of the waste canisters, whether made of steel or copper. Here, we are exclusively concerned with anoxic corrosion and will not discuss MIC under oxidic conditions. Anoxic corrosion will take place regardless of microbial activity, with an anodic and a cathodic half-reaction (Feron & Crusset, 2014):

Anodic reaction: $M^0 \leftrightarrow M^{2+} + 2e^-$ (M= Fe or Cu)   (1.1)

Cathodic reaction: $2H_2O + 2e^- \leftrightarrow H_2 + 2OH^-$ (1.2)

The mechanism by which microbial activity accelerates this process was long attributed to cathodic depolarization theory, by which microbial activity can consume H_2 and thus accelerate the process but this theory has been already invalidated (Costello, 1974).

The major form of CMIC is through the production of corrosive by-products of microbial metabolism. A diversity of metabolisms has been identified in metal-corroding biofilms, including sulphate-reducing bacteria (SRB), sulphide-oxidizing bacteria, manganese-oxidizing bacteria, iron-oxidizing bacteria, iron-reducing bacteria as well as microorganisms producing acidic compounds (Amendola, 2022). However, it is unclear how oxidative processes, typically requiring either oxygen or nitrate as an electron acceptor could be extant in a high-level waste repository, as neither of these compounds is expected to be available. Reductive metabolisms, such as sulphate reduction, iron reduction, acetogenesis, and methanogenesis, on the other hand, are expected in the repository if the appropriate electron donor (e.g., H_2) and acceptor (i.e., sulphate, ferric iron, and CO_2) are available.

Amongst those, SRB are considered the most relevant for MIC because through dissimilatory sulphate reduction (DSR), they utilize sulphate as an electron acceptor and produce the corrosive compound, sulphide (H_2S) or bisulphide (HS^-), depending on the pH value of the environment. Methane is not corrosive but could facilitate MIC through EMIC (Mand et al., 2016). Acetogens produce acetate that is acidic and that can fuel sulphate reduction and they likely also corrode via EMIC (Mand et al., 2016). Here, we will focus on SRB as they are the major players in CMIC.

DSR stoichiometry depends on the electron donor that is available (either H_2 or organic carbon) (eq. 1.3 and 1.4):

$4 H_2 + SO_4^{2-} + 2 H^+ \leftrightarrow H_2S + 4 H_2O$ (1.3)

$2 CH_2O + SO_4^{2-} + 2H^+ \leftrightarrow H_2S + 2 CO_2 + 2 H_2O$ (1.4)

EURAD (Deliverable n° 1.1) – Initial State-of-the-art of WP ConCorD
Dissemination level: Public
Date of issue of this report: 17/08/2022

Page 55

Sulphide reacts chemically with zerovalent Fe (Fe^0) to produce mackinawite and H_2 (eq. 1.5).

$$Fe^0 + H_2S \rightarrow FeS + H_2 \qquad (1.5)$$

The overall reactions (with H_2 or organic carbon as the electron donor) become (eq. 1.6 and 1.7):

$$3 H_2 + SO_4^{2-} + Fe^0 + 2 H^+ \rightarrow FeS + 4 H_2O \qquad (1.6)$$

$$2 CH_2O + SO_4^{2-} + Fe^0 + 2 H^+ \rightarrow FeS + 2 CO_2 + H_2 + 2 H_2O \qquad (1.7)$$
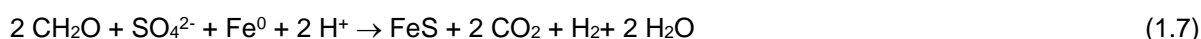
Thus, sulphide-driven CMIC generates a layer of FeS that ultimately covers the surface of metallic iron, resulting in the formation of a film of FeS that serves as a protective layer (a passivation layer), precluding the diffusion of Fe^{2+} from the metal anode (Enning & Garrelfs, 2014). Thus, in the absence of other processes, the rate of sulphide-dependent CMIC is expected to decelerate over time. However, if the FeS film is interrupted, the corrosion rate will increase (Lv & Du, 2018). CMIC can take place in the absence of a biofilm as long as there exists a diffusion path for H_2S (or HS^-) to the metal surface.

EMIC depends on the transfer of electrons from metallic iron to SRB (or other microorganisms). Thus, iron serves as the electron donor for DSR (eq. 1.8) and the ferrous iron generated precipitates with sulphide as mackinawite (eq. 1.9) or for instance, with carbonate as siderite (eq. 1.10) due to the production of CO_2 in heterotrophic sulphate reduction (eq. 1.4):

$$4 Fe^0 + SO_4^{2-} + 10 H^+ \rightarrow 4 Fe^{2+} + H_2S + 4 H_2O \qquad (1.8)$$

$$Fe^{2+} + H_2S \leftrightarrow FeS + 2 H^+ \qquad (1.9)$$

$$Fe^{2+} + CO_3^{2-} \leftrightarrow FeCO_3 \qquad (1.10)$$

However, because of the stoichiometry of the reaction, there is a single sulphide produced per four ferrous ions produced, which means that the production of mackinawite will be threefold lower than that of siderite (eq. 1.11):

$$4 Fe^0 + SO_4^{2-} + 3 CO_3^{2-} + 8H^+ \rightarrow 3 FeCO_3 + FeS + 4 H_2O \qquad (1.11)$$
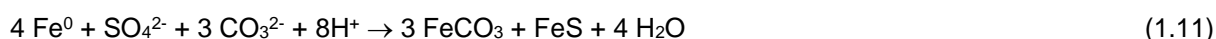
The different mineral products detected during EMIC and CMIC can be leveraged to decipher which of the two mechanisms takes place, or even the relative contribution of each MIC mechanism in the presence of carbonate (Enning et al., 2012).

While the formation of FeS is thought to passivate the corrosion of metallic iron in the CMIC scenario, this is not the case of EMIC. Indeed, the conductivity of the FeS crust allows the extraction of electrons from metallic iron and their transport through the iron sulphide. Thus, the lack of direct contact between cell and iron is not an impediment to continued EMIC. As a result, the rate of EMIC is considerably faster than that of CMIC and so is the extent of the corrosion.

SRB can carry out both forms of MIC (Figure 1-24), depending on the species considered. EMIC strains such as *Desulfovibrio ferrophilus* (Chatterjee et al., 2021) or *Desulfopila corrodens* (Beese-Vasbender et al., 2015) are currently a minority. This is likely due to the use of organic carbon in the isolation of most SRB. In order to capture EMIC-specific SRB, it is necessary to consider a lithotrophic medium that

EURAD (Deliverable n° 1.1) – Initial State-of-the-art of WP ConCorD
Dissemination level: Public
Date of issue of this report: **17/08/2022**

Page 56

requires metallic Fe to be the only electron donor and thus favours EMIC-SRB. The mechanism of electron transfer from the metal surface to the bacterium remains matter of discussion (Liang et al., 2021). Sulphate-reducing bacteria are the most relevant organisms for CMIC, but other sulphide-producing microorganisms such as thiosulphate- or sulphite-reducing bacteria or sulphate-reducing archaea are also important. Furthermore, other organisms are likely to be capable of carrying out EMIC via the abstraction of electrons from the iron metal surface, such as nitrate-reducing bacteria and methanogenic archaea. There is increasing evidence of microbially-mediated electron transfer from mineral surfaces and this phenomenon of electrochemistry is likely to be underestimated to date.

A. EMIC (eq. 1.11)
B. Reaction of H_2S with Fe^0
C. Dissimilatory sulphate reduction
D. Sulphide stress crack (SSC) due to the enhanced diffusion of H_2 into metallic iron
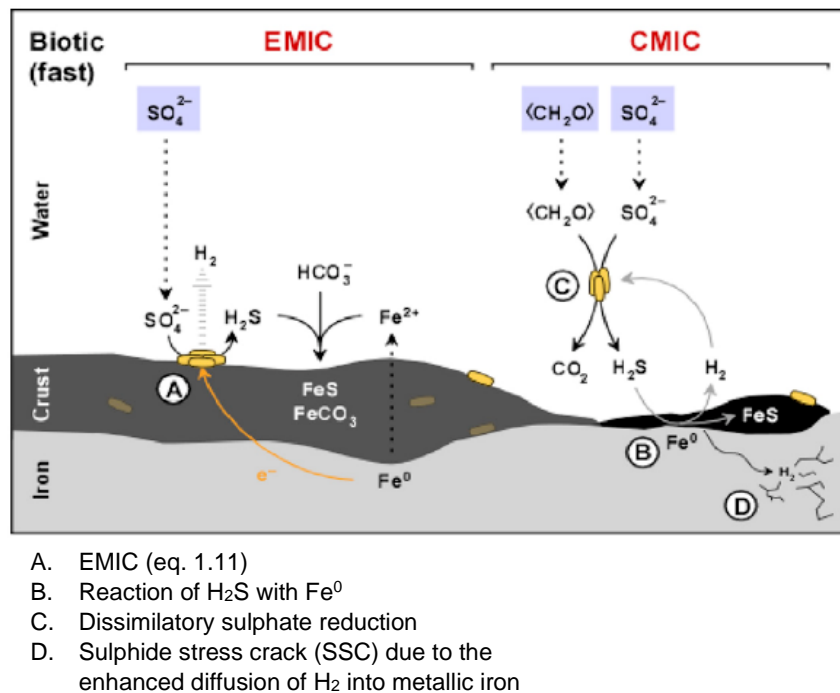
Figure 1-24: Microbially influenced corrosion pathways modified from (Enning & Garrelfs, 2014).

In the context of nuclear waste disposal, particularly those concepts that require a bentonite backfill in direct contact with the waste canister, it is unlikely that biofilms will develop on canister surfaces. Thus, the main mechanism of concern is the formation of corrosive by-products of microbial metabolic activity (CMIC). If information about biofilm formation on metal surfaces were to emerge, naturally, EMIC would become an important consideration.

A number of studies have considered the corrosion of steel by exposing steel coupons to a solution representative of repository conditions (Shrestha et al., 2021) (Diler et al., 2021) (Rajala et al., 2015).

The study by Shrestha et al. (2021) relying on the exposure of metal coupons to a solution of synthetic bentonite porewater (sterilized) that was inoculated with groundwater from the Josef Underground Research Center. Pitting corrosion, and the formation of mackinawite and magnetite, was observed on the steel only in the biotic sample while the abiotic sample exhibited a uniform layer of magnetite. The biofilm that formed on the surface of the steel coupon included SRB but also nitrate-reducing organisms such as *Pseudomonas, Methyloversatilis* and *Acidovorax*, which is consistent with the presence of 10 mM nitrate in the water. Probably, a combination of CMIC and EMIC occurred here due to the absence of a solid phase and the formation of a biofilm. This type of study is only relevant for the French concept that calls for a technological gap filled with resaturation water between the carbon steel microtunnel casing and canister overpack (Diler et al., 2021).

EURAD (Deliverable n° 1.1) – Initial State-of-the-art of WP ConCorD
Dissemination level: Public
Date of issue of this report: **17/08/2022**

Page 57

Similarly, Rajala et al. (2015) evaluated the corrosion of carbon steel in the presence of Olkiluoto groundwater (at RT and at 6ºC) and found that after 3 and 8 months, pitting corrosion occurs and a biofilm developed at the surface of the coupons. Betaproteobacteria appeared to thrive in the presence of carbon steel perhaps through the utilization of H_2 as an electron donor (as they are known hydrogenotrophic bacteria). Additionally, iron oxidizers and reducers were observed, suggesting iron cycling. The electron acceptor for iron oxidation was not identified in this anoxic environment and it is presumed that H_2 drove iron reduction. SRB were also observed in the biofilm and some genera (e.g., *Desulfopila*) were presumed to use elemental iron as an electron donor for sulphate reduction. A similar study was conducted with copper and confirmed the ability of SRB to accelerate copper corrosion as well (Carpen et al., 2018).

Also relevant to the French concept, an experiment (IC) (Necib et al., 2017) was performed at the Mont Terri Underground Laboratory. It consisted of test chambers placed within a core of Opalinus clay confined in stainless steel screens and introduced into a borehole within the same rock formation. The test chamber contained four steel electrodes, electrically insulated from each other with alumina, and mounted on a central tubing. Thus, the electrodes were close (~1 mm) to the Opalinus clay. A synthetic solution representative of Opalinus clay porewater was injected into the test chamber. The water flow rate was manually set to ensure circulation between the metallic electrodes and the Opalinus clay core. Electrochemical measurement on the electrodes allowed an estimation of the corrosion rate. After a total period of 7 years, the equipment was dismantled, and the iron was characterized. Inspection of the metal surface/Opalinus clay interface revealed several layers of corrosion products. Various iron-bearing minerals such as magnetite, goethite, lepidocrocite, akageneite, chukanovite, and siderite were observed. Fe sulphide at various oxidation states as well as elemental sulphur, were also observed and the original surface had been replaced by iron sulphide, likely pointing to MIC.

However, for the bentonite-backfilled repository environment, CMIC in the clay buffer is the more relevant question. A study by Grousset et al. (2020), investigated the sulfur isotopic fractionation during the exposure of steel embedded in Toarcian Argillite to a sulphate-rich water inoculated with a SRB isolate and an iron-reducing bacterium. The novelty of the study was the use of Nano-SIMS to spatially delineate the S isotope signature. Mackinawite was detected at the surface of the steel coupon, but it was not possible to conclusively determine whether its formation resulted from microbial processes due to the poor constraints on the isotopic signature of the sulphate source.

One study probed the corrosion of steel by exposing coupons to a solution representative of the Callovo-Oxfordian (Cox) rock formation in contact with cement-bentonite with or without uncompacted representative solid phases (Cox or Cox+cement/bentonite) and with or without Cox-derived microbial amendments (Diler et al., 2021). A strong corrosion was observed in the systems in which microorganisms were amended in comparison to the control systems that were left unamended (but not sterile). However, in the presence of a cement-bentonite mix, the extent of corrosion decreased considerably for 47 days. In addition, the embedding of the Cox clay rock in the cement/bentonite mix, further decreased the extent of corrosion. These results are in line with expectations, as alkaline conditions are inhibitory to sulphate reduction. The microbial community was dominated by Firmicutes, including sulphate reducing bacteria (SRB) in the incubations with cement-bentonite and Cox as well as the incubation with Cox alone.

Another experiment (IC-A) carried out at the Mont Terri rock laboratory, was designed to measure the *in-situ* rate of iron corrosion. Metal coupons (carbon steel of various types) embedded in bentonite were deployed in a borehole by using stainless steel modules. The modules included holes and a sintered stainless-steel filter to allow for the exchange of pore-water with the host rock. The bentonite (MX-80) varied in its formulation (compacted or granular) and in its dry density. At time intervals, modules were retrieved, and the corrosion was evaluated along with the microbial community within the bentonite. This is an ongoing experiment. Findings do not point to any detectable microbial impact on corrosion (Smart et al., 2017). However, it was also suggested that sulphate-reducing bacteria did not grow within the

EURAD (Deliverable n° 1.1) – Initial State-of-the-art of WP ConCorD
Dissemination level: Public
Date of issue of this report: 17/08/2022

Page 58

bentonite due to the persistence of O_2 (Burzan, 2021). Thus, this would suggest that longer deployment times are needed to reach conditions representative for a repository, i.e., to allow the consumption of O_2 and the potential growth of SRB. Another scenario is that bentonite is fully saturated at the point in time at which O_2 is depleted, precluding SRB growth. The latter scenario would ensure the inhibition of SRB growth during saturation, providing an excellent protection against MIC. This experiment presents strong evidence that the borehole water microbial community did not colonize the bentonite significantly but that the bentonite microbial community grew initially and persisted.

The evidence presented above indicates the absence of CMIC in the bentonite backfill. However, the question remains as to whether the experiments conducted so far were carried out long enough to show that SRB do not grow within bentonite after depletion of the adsorbed O_2. In order to put to rest the question of whether the inhibition of SRB growth would persist in the absence of O_2, experiments should be conducted with bentonite from which O_2 was stripped. The bentonite, embedded with carbon steel coupons, would receive H_2 as an electron donor and steel corrosion should be monitored over time.

1.3.2 Impact of irradiation on microbial viability in the context of nuclear waste disposal

Microorganisms can cope with ionizing radiation to some extent. This depends on the type of microorganism. In the context of the safe long-term storage of high-level radioactive waste the impact of the ionizing radiation on the microbial community structure, viability and activity is of concern because it affects the possible microbial processes. The expected radiation doses depend on various factors such as the disposal concept. This latter includes the dose rate radionuclide inventory, the distance from the source, the engineered barriers, especially the container material, the half-life of radionuclides and daughters (Černá & Bartak, 2019). In the case of the Swedish KBS-3 HLW repository concept, a maximum dose outside the container of less than 500 mGy h^{-1} was calculated. The dose is dominated by Cs-137 (Svensk Kärnbränslehantering AB, 2006). The gamma and neutron radiation are expected to be significant during approximately 1,000 years post deposition (Svensk Kärnbränslehantering AB, 2006). Lundgren (2004) calculated an average dose rate outside the copper container of 100-150 mGy h^{-1} (Lundgren, 2004). On the other hand, the latest Canadian and Belgian HLW concepts predict a maximum surface dose rate of 1 Gy h^{-1} and 25 Gy h^{-1}, respectively. Therefore, a low ionizing radiation is expected for a longer period.

Radiation, independent from its source, affects biomolecules like nucleic acids, proteins and lipids directly or indirectly (Jung et al., 2017). The ionizing particles can directly damage DNA. The indirect effect considers the impact of secondary reactive species produced by ionizing radiation. The indirect effect concerns the aqueous solution chemistry of water radiolysis products, which produces reactive oxygen species (ROS) - hydroxyl radical ($^{\bullet}OH$), ionized water (H_2O^+), hydrogen radical ($H^{\bullet}$) and hydrated electrons (e^-) followed by secondary ROS products superoxide ($O_2^{\bullet-}$) and hydrogen peroxide (H_2O_2) formed within one picosecond (10^{-12} s) after irradiation (Daly, 2009) (Jung et al., 2017).

The microbial radiation resistance includes a combination of diverse defense mechanisms. One of them is the DNA repair system. This includes unique DNA repair signaling components, constitutively activated or expressed DNA repair machineries, or harbor of the polyploidy chromosome set (Jung et al., 2017). Another mechanism is the enzymatic antioxidant system with a higher activity or expression of ROS-related proteins. And finally, the non-enzymatic antioxidant system which comprises high intracellular concentration of inorganic solutes, high Mn/Fe ratios and pigments (Jung et al., 2017).

Microbial radiation sensitivity also depends on other factors (van Gerwen et al., 1999) (Shuryak et al, 2017). One factor is the type of ionizing radiation as an acute ionizing radiation (AIR) or chronic ionizing radiation (CIR) (Shuryak et al., 2017). Other factors are cell concentrations, physiological and genetic features as well as the ability to apply defense mechanisms (Jung et al., 2017) (Shuryak et al., 2017). It was also demonstrated that certain resistant microbial cells can protect radiosensitive cell types

EURAD (Deliverable n° 1.1) – Initial State-of-the-art of WP ConCorD
Dissemination level: Public
Date of issue of this report: 17/08/2022

Page 59

(Shuryak et al., 2017). In addition, the vegetative state of the microbial cell has an influence on the microbial radiation sensitivity, because spores have many times higher radiation tolerance than vegetative cells (van Gerwen et al., 1999).

The radiation resistance of a microorganism is commonly measured by the decimal reduction dose (D10). This is defined as the radiation dose (kGy) required to reduce the number of that microorganism by one log (reducing 90% of the total number) (van Gerwen et al., 1999). This unit is often used to compare the species radiation sensitivities. The average D10 dose for most vegetative microorganisms was calculated to be 0.420 kGy, although it varies significantly between species and even strains (van Gerwen et al., 1999). Organisms with high radiation resistance were discovered within the three domains of life (Bacteria, Archaea, and Eucarya) (Jung et al., 2017). The most popular representative within the domain Bacteria is Deinococcus radiodurans, which was formerly named Micrococcus radiodurans and can survive high doses of gamma radiation (~ 17,000 Gy) (Daly, 2009). Studies on D. radiodurans revealed that in the non-enzymatic antioxidant defense system, high cellular content of manganous ions play a major role (Daly, 2009) (Sharma et al., 2017). Another example of a radiotolerant bacterium is Kinecoccus radiotolerans, which was isolated from a high-level radioactive waste cell at the Savannah River Site in Aiken, South Carolina. This indicated high levels of resistance to gamma-radiation and desiccation (Philipps et al., 2002). The domain Archaea includes microorganisms from extreme environments such as hydrothermal or highly saline. For example, the extremophile Thermococcus gammatolerans was isolated from an enrichment of hydrothermal chimney samples collected at the Guaymas Basin that were submitted to gamma-irradiation at a dose of 30 kGy (Jolivet at al., 2003). Halophilic archaea from the genus Halobacterium are highly resistant to desiccation, high vacuum and 60Co gamma irradiation (Kottemann et al., 2005). The Halobacterium sp. is able to repair extensive double strand DNA breaks (DSBs) in its genomic DNA within hours of damage induction. The gamma resistance depends on the growth stage with cultures in earlier stages exhibiting the highest resistance (Kottemann et al., 2005). Furthermore, membrane pigments, specifically bacterioruberin, offered protection of Halobacterium sp. against cellular damages induced by high doses of gamma irradiation (5 kGy) (Kottemann et al., 2005).

Within the domain Eucarya, a radiation resistant intraspecies of the filamentous fungus Alternaria alternata appears. Several strains originating from the highly radiation-polluted reactor of the Chernobyl (Ukraine) Nuclear Power Plant possess high radiation resistance. Genomic investigations showed that these strains are genetically adapted to this high radiation habitat by means of selection, thus providing a natural source of genetically homogeneous fungal lineages (Mironenko et al., 2000). Melanized fungi as e.g., Cryptococcus neoformans belong as well to the radiation-resistant fungi. It was even postulated that the melanin could employ γ-radiation as an energy source by converting electromagnetic energy into chemical energy and that this might enhance the growth of melanized fungi (Dadachova and Casadevall, 2008).

Taken together, organisms with high radiation resistance were discovered within all three domains of life (Bacteria, Archaea, and Eucarya) and the extreme ionizing radiation resistance originates in most cases from a combination of DNA repair systems and enzymatic as well as non-enzymatic antioxidant processes (Jung et al., 2017). In addition, tolerance to radiation might be a common phenomenon among extremophiles microorganisms (including thermophiles and halophiles), which must have evolved mechanisms to survive extreme environmental conditions such as desiccation. Furthermore, most of the organisms described above were detected in radioactive contaminated areas. Survival data from pure culture studies may not be fully applicable to relatively nutrient limited environment of proposed HLW, where different species of the community will be competing, and where radiation is highly probably not the only selective stress (Černá and Bartak, 2019).

Gamma irradiation is also a common method to sterilize rocks, soils and sediments, which is necessary to distinguish between biotic and abiotic processes in laboratory experiments (Otte et al., 2018). Such studies give us additional information about how natural microbial ecosystem reacts to the presence of radiation. The effects of ionizing radiation exposure on soil biota were studied by exposing soil microcosms to weekly bursts of 60Co gamma radiation over six weeks (three levels of exposure (0.1

EURAD (Deliverable n° 1.1) – Initial State-of-the-art of WP ConCorD
Dissemination level: Public
Date of issue of this report: 17/08/2022

Page 60

kGy/hr/wk [low], 1 kGy/hr/wk [medium] and 3 kGy/hr/wk [high]). The results showed that the bacterial diversity decreased. The diversity of fungi and algae, however, increased unexpectedly and the functional gene diversity of algae, bacteria, fungi and total biota increased as well. In addition, large overall changes in community composition were observed after radiation exposure and several potential novel radiation-tolerant groups as Deinococcus-Thermus, phyla Chloroflexi (bacteria), Chytridiomycota(fungi) and Nanoarcheota (archaea) (Ogwu et al., 2018).

Brown and colleagues (2015) studied the effect of ionizing radiation (8 weeks, 0.5 or 30 Gy h^{-1}) on microbial communities in sediment systems. Results indicates that biogeochemical processes are likely not restricted by dose rates in such environments, and electron-accepting processes may even be stimulated by radiation. The effect of gamma radiation on the viability of a soil microbial community under conditions similar to those in the Mars surface was investigated by Cheptsov et al. (2018). Doses of gamma radiation of 100 kGy under –50°C and 1 Torr were applied. In this case, the irradiation did not result in the death of the microbial community. On the contrary, the number of living cells, metabolic activity, and functional diversity remained high. But of course, it is always a matter of radiation dose. Most soil bacteria are eliminated by 20 kGy. A dose higher than 70 kGy, however, may be required to kill certain radio-resistant bacteria (McNamara et al., 2003). Furthermore, it was also mentioned that γ-irradiation may not be an appropriate method for all experiments as it can influence soil chemical properties, in particular soil nitrate and ammonium levels (McNamara et al., 2003). To sum up, low doses of radiation influence biogeochemical processes, microbial diversity and activity in natural rock, soil or sediment environments but these will not be completely restricted. However, a radiation dose higher than 70 kGy will effectively eliminate the bacterial presence in various soil materials. A high dose for a relatively short period represents only one aspect of radiation resistance. However, nuclear waste storage in a deep geological repository is associated with chronic low-dose irradiation. Many microorganisms can grow under chronic gamma ionizing radiation dose rates of 13-126 Gy h^{-1}, but this does not mean that they can cope with acute ionizing radiation (Shuryak et al., 2017). Bacteria and fungi that exist in extremely radioactive waste and contaminated sites (e.g., Hanford, Chernobyl, Fukushima) have to cope with chronic ionizing radiation. The diversity of bacterial communities exposed to radioactive contamination in Chernobyl soils was examined by a combination of culture-independent and culture-dependent approaches (Chapon et al., 2012). Both highly and weakly contaminated soils contained highly diverse bacterial communities, suggesting that long-term exposure to radionuclides does not lead to the extinction of bacterial diversity (Chapon et al., 2012). Subsequent analysis based on NGS revealed profound changes in community composition at the phylum and OTUs levels and higher diversity in the trench soils as compared to the outside and identified specific phylotypes affiliated to the phyla Crenarchaeota, Acidobacteria, AD3, Chloroflexi, Proteobacteria, Verrucomicrobia and WPS-2, which were unique for the trench soils (Theodorakopoulos et al., 2017).

In the multi-barrier concept, the barrier material, which is at the interface with the container, plays an important role regarding the radiation effects on the mineralogy and its barrier performance as well as the microbial communities. Bentonite is a suitable barrier material for clay and crystalline host rocks. Chemical and mineralogical analyses and physical testing of bentonite MX-80 after heating up to 130°C and with and without gamma radiation showed only insignificant alteration in the smectite content and physical properties (Pusch et al., 1992). The radiation sensitivity of naturally occurring microorganisms in bentonite and the sensitivity of *Bacillus subtilis* spores and *Acinetobacter radioresistense* in a buffer matrix was studied by Stroes-Gascoyne and colleagues (1995). The D10 values at dose rate 100 Gy min^{-1} was between 0.65 and 1.68 kGy in these experiments.

Within the EU-project Microbiology in Nuclear waste Disposal (MIND) the deliverables D1.2 and D1.3 reported the effects of radiation and microbial degradation of organic polymers and bitumen in low and intermedium level wastes. The effect of Gamma radiation and pressure on the indigenous microbial community in bentonite type BaM (Keramost, Czech Republic) enriched with granitic porewater VITA from Josef Undeground Research Center (Czech Republic), a natural source of anaerobic sulfate-reducing bacteria, was studied. Microorganisms that adapted and survived under harsh conditions underwent further selection caused by the Gamma radiation. Notably, application of 19,656 Gy absorbed

EURAD (Deliverable n° 1.1) – Initial State-of-the-art of WP ConCorD
Dissemination level: Public
Date of issue of this report: 17/08/2022

Page 61

dose at the constant dose rate 13 Gy h^{-1} did not eliminate completely bacteria in bentonite suspension. A decline of the total microbial biomass was observed, but not of species richness. Minor changes in the microbial community structure (Černá et al., 2015) were also noted. The results imply that some of the naturally present bacteria in bentonite are radiation resistant. However, the evolution of microbial communities under long-term low-level as well as high-level irradiation still needs to be investigated by long-term experiments under repository conditions including the effect of irradiation and compaction of bentonite.

1.3.3   Inhibition of microbial activity and growth by bentonite

Natural and commercial uncompacted bentonites harbor a diverse microbial community, including sulfate-reducing bacteria (SRB) (Matschiavelli et al., 2019) (Lopez-Fernandez et al., 2015) (Masurat et al., 2010). The number of culturable cells (SRB and others) differs among different types of bentonites. For SRB, this number was correlated with the initial water content of the bentonite (Haynes et al., 2018) (Vachon et al., 2021). Cultivation-based approaches are biased to the species that can be cultivated and fail to detect viable but non-culturable species. Nevertheless, the indigenous bentonite microbial community is shown to be able to survive extreme conditions such as high pressures, high temperatures and high levels of gamma irradiation (Masurat et al., 2010) (Haynes et al., 2018) (Masurat et al., 2010). The number of culturable SRB depending on the treatment and the type of bentonite. Wyoming bentonite harbors the least amount of culturable SRB (Haynes et al., 2018).

The highly compacted bentonite buffer in a geological waste repository is expected to play an important role in precluding microbial activity due to its high swelling pressure and low water activity (Stroes-Gascoyne et al., 2010) (Pedersen et al., 2000). Microbial activity may be limited when the water activity remains below 0.96 (Pedersen et al., 2000). Desiccation results in membrane disruption, denaturation of proteins and enzymes and DNA damage. However, many bacteria have developed mechanisms to mitigate stress induced by desiccation by increasing production of exopolysaccharides, changing composition of the membrane, improving the stability of proteins, reducing oxidative stress, and repairing DNA damage (Esbelin et al., 2018) (Greffe & Michiels, 2020). There seems to be a large overlap between responses to desiccation and radiation (see also part 1.2.2). For example, mechanisms that govern tolerance to desiccation are believed to be responsible for the high levels of radiation resistance in Deinococcus radiodurans (D10 = 16 kGy), the model organisms for radiation resistance (Daly et al., 2007).

The high swelling pressure generated at high bentonite densities imposes space limitations, which interfere directly and indirectly microbial growth and activity. Direct effects occur if the pore spaces are too small to enable the presence of microbial cells. Pore throats with a diameter > 0.2 μm are essential to sustain microbial activity in subsurface environments (Rebata-Landa & Santamarina, 2006) (Fredrickson et al., 1997). A decrease of pore space results in diffusion-limited nutrient transport. As microorganisms themselves become immobile in such conditions, access to nutrients is restricted and microbial growth is inhibited (Kiczka et al., 2021). The decreasing rate of water inflow when the bentonite reaches its saturation state further limits transport. Full saturation of the bentonite, however, may take several years, and microbial growth was observed during the saturation phase. Nevertheless, no growth of sulfate-reducing bacteria was observed during this phase, putatively due to the persistence of O_2 (perhaps as an adsorbed species) in the bentonite (Burzan et al., 2022).

Both water activity and swelling pressure depend on the dry density of the bentonite (Stroes-Gascoyne et al., 2007) (Villar & Lloret, 2008). Water activity in bentonite decreases as the density increases as response to interactions with solutes and adsorption of water to mineral surfaces (Stroes-Gascoyne et al., 2007). On the other hand, swelling pressure increases with increasing dry density (Kaufhold et al., 2015). As long as the bentonite buffer maintains a uniform dry density ≥ 1600 kg m^{-3}, microbial activity is expected to be inhibited (Stroes-Gascoyne, 2010) (Stroes-Gascoyne et al., 2011). However, the

EURAD (Deliverable n° 1.1) – Initial State-of-the-art of WP ConCorD
Dissemination level: Public
Date of issue of this report: 17/08/2022

Page 62

fundamental determinants of the threshold bentonite dry density at which microbial activity is inhibited remain unknown. It remains unclear why different boundaries are observed between different bentonites (Pedersen et al., 2000) (Stroes-Gascoyne, 2010) (Bengtsson & Pedersen, 2017). Furthermore, the high density not necessarily eliminates the viable microbial population in bentonite and upon expansion of compacted bentonite into a void, the resulting reduction in dry density stimulated or restored microbial cultivability (Stroes-Gascoyne et al., 2011). Microbial viability at interfaces is comparatively much higher than that in bulk clay material as interfacial regions provide a more favorable environment with increased access to nutrients and water (Pedersen, 2010) (Stroes-Gascoyne et al., 2002) (Jalique et al., 2016). Long-term persistence of microorganisms has also been observed in laboratory and in-situ experiments (Burzan, 2021) (Jalique et al., 2016) (A. Bengtsson et al., 2017). Cultured species are often known as spore-forming bacteria, which could facilitate their long-term persistence (Haynes et al., 2018) (Vachon et al., 2021) (Jalique et al., 2016). Sporulation enables microorganisms to withstand unfavorable and potentially lethal environmental conditions but are metabolically inactive until conditions become more favorable for vegetative growth. The triggers that control endospore formation are still unclear (Hutchison et al., 2014).

Bentonite is considered a limited nutrient environment with very low amounts of available organic carbon, mainly composed of plant-derived waxes and highly aromatic carbon with low contributions from small molecules (Marshall et al., 2015). Based on the molecular-level analysis of the organic matter, it is believed to be recalcitrant for microbial reproduction. However, recent analysis showed the presence (in bentonite) of alkanes, toluene, and other aromatic compounds, which are known as potential energy sources for microbial metabolism. The amount of these more easily accessible electron donors, however, is not known (Matschiavelli et al., 2019) (Pedersen, 2017). A recent study showed that dissolved organic material from different types of bentonites is able to sustain a sulfate-reducing microbial community (Maanoja et al., 2020) (Maanoja et al., 2021). Another possible mechanism to fuel sulfate reduction is autotrophic growth with H_2 as an electron donor and CO_2 as a carbon source (Muyzer & Stams, 2008). In turn, heterotrophic microorganisms can use the organic carbon generated by autotrophic hydrogen-oxidizing SRB. Hydrogen can originate from radiolysis of water and the anoxic corrosion of steel but also from microbial metabolism such as fermentation processes (Bagnoud et al., 2016) (Smart et al., 2001). Hydrogen has been shown to fuel sulfate reduction in bentonite microcosm experiments (Matschiavelli et al., 2019). However, H_2 consumption within bentonite as a function of dry density remains inconclusive.

Based on this literature review, it is tempting to design experiments that capture repository conditions to assess the potential for microbially influenced corrosion of canisters. Such experiments would consider either pre-compacted bentonite or bentonite at a target dry density and physically, chemically, and biologically relevant conditions. However, such experiments preclude the real-time monitoring of processes and require appropriate controls that detangle the role of microorganisms. Furthermore, the timeline is an important parameter as transient processes are expected that could impact the overall conclusion. Bringing together all these conditions in a meaningful way is a considerable challenge.

EURAD (Deliverable n° 1.1) – Initial State-of-the-art of WP ConCorD
Dissemination level: Public
Date of issue of this report: 17/08/2022

Page 63

2. Novel technological concepts for nuclear waste disposal canisters

2.1 Context

The waste container is an essential part of the multibarrier systems designed for deep geological disposal. IAEA lists several characteristics that should be considered when the integrity of the waste canister is considered during its whole lifespan (IAEA 2006). From the material engineering point of view, the long-term integrity of the waste container under environmental conditions should be emphasized. This means that requirements for corrosion and mechanical properties are considered.

There are many different nuclear waste disposal canister concepts proposed for adoption worldwide, their configuration depending mainly on the type of waste to be disposed, the surrounding geological structure, and the material solution adopted to minimise the risk of canister integrity breakdown due to environmental damage (Holdsworth, 2014). Copper (i.e., Sweden and Finland) and carbon steels (i.e. Belgium, France, Switzerland, Czech Republic, Slovakia, and Hungary) are the container materials that have been traditionally considered for the disposal of SF/HLW in countries with advanced disposal programs. The feasibility of containers made from these materials has been demonstrated and the required manufacturing technology is available and mature. The container concepts also vary according to the type of waste to be stored namely spent fuel (SF) assemblies or vitrified high level waste (VHLW) cylinders.

After emplacement in a deep underground repository, canisters will be exposed to the repository environment and its evolution in time. Assuming the nuclear waste repository remains undisturbed (i.e., there are no earthquakes or related phenomena), the only mechanism by which radionuclides could reach the biosphere is by the dissolution of the waste in the groundwater, followed by migration of the radioactive solution to the surface. Consequently, one of the major factors in selecting a container solution for ultimate disposal in an underground repository is its resistance to leaching by groundwater that may eventually penetrate the repository environment. Following disposal, resistance to irradiation damage and other environmental damage processes is therefore important (Holdsworth, 2013).

While steels provide a strong solution for this application, corrosion under anoxic conditions yields hydrogen gas which moves away from the canister surface by mass transport processes through both the engineered barriers of the repository and the geological barrier. In a closed system, such as a closed geological disposal facility, the gas can accumulate to the point of creating pressure zones. In order to provide alternative solutions to the use of steels for containers and thus limit the production of hydrogen in the long term, alternative materials to non-alloy steels have been studied in recent years in different countries. One of the difficulties lies in achieving equivalent or better properties than steels to meet the requirements for the concerned components.

In addition to this, the container material is required to have and to maintain its structural integrity under the expected repository conditions for a certain required time. For this reason, alternative materials for nuclear waste containers should guarantee sufficient resistance to localised corrosion (e.g., stress corrosion cracking of welds). In this context the choice of the material and of the production route for the canister are very important. Chemical compatibility with all other components, including waste, must also be part of the formulation/manufacturing requirements. Recent developments (e.g., copper coatings) considered in Canada and investigated in Switzerland (Holdsworth 2018), France and Japan have demonstrated that container optimisation is indeed possible. Further alternative and novel container materials are also in focus (e.g., steels with more controlled composition, Cu-based alloys and composites, ceramics, Zr alloys) (Hodsworth, 2013) (Baroux, 2016)

EURAD (Deliverable n° 1.1) – Initial State-of-the-art of WP ConCorD
Dissemination level: Public
Date of issue of this report: 17/08/2022

Page 64

The current state of the art for these different alternative solutions is given in the following sections:

- Ceramic materials (mainly alumina based and silicon carbide solutions) and ceramic coatings;
- Alternative metals and metallic coatings.

2.2 Ceramic Materials and Coatings

2.2.1 Ceramic containers (Alumina, SiC)

The minimisation or complete avoidance of canister surface hydrogen generation is one of the reasons for the evaluation of alternative solutions such as that provided by bulk ceramic containers or ceramic coatings (Landolt, 2009).

The use of ceramics for nuclear waste disposal containers was first seriously considered in the 1970s (Mattson, 1980) (Bienek, 1984) and has continued to be an option (Holdsworth, 2013) (Baroux, 2016) (Adams, 2000) (Wötting, 2007) (Kerber, 2013) albeit apparently without a high level of commitment since the early 2000s. There seems to be insufficient motivation to invest in the research which would be necessary to overcome known difficulties when feasible metallic solutions have already been recognised (Holdsworth, 2013). The reluctance of ceramic components manufacturers to invest without external support is almost certainly due in part to insufficient customer demand in the near future for large ceramic pieces. Nevertheless, there have been significant developments relating to the consideration of ceramics as a candidate nuclear waste disposal canister material.

While ceramics are an attractive option in terms of their high corrosion resistance and lack of gas (e.g. H_2) formation when installed for a long time, their mechanical strength and toughness characteristics are low. Although the existing press and sintering furnace capacities around the world limit the size of the canister sections that can be manufactured, such limitations can be overcome with adequate investment. However, the main manufacturing challenges to be overcome through systematic development included: i) efficient handling of very large lumps in the green state just after shaping (before sintering), and ii) achieving adequate density (porosity levels) with section thicknesses ≥ 50 mm. Moreover, achieving effective sealing of thick ceramics will never be possible without significant research and development. With no demand for large diameter ceramic pressure vessels from any other industrial sector, funding for such R&D can only come from the nuclear waste disposal community. Recently, there have been significant changes related to the consideration of ceramics as a candidate material for containers for nuclear waste disposal (Holdsworth, 2013), and they have been comprehensively analysed (Holdsworth, 2014). Potential ceramics candidates for overpack nuclear waste disposal canister applications are alumina (Al_2O_3), pure or in combination with silicon oxide (SiO_2) (Baroux 2016) (Mattson,1980) silicon carbide (SiC) (Wötting, 2007) (Kerber, 2013), silicon nitride (Si_3N_4), partially stabilised zirconia (PSZ), and titania (TiO_2), because of their chemical stability, reasonable mechanical properties, and ready availability (Willfinger, 1994). At present, the main attention is paid to the alumina (Al_2O_3) and the silicon carbide (SiC) solution. The state of the art for these two candidate materials is described below.

2.2.1.1 Alumina solutions

The development of alumina or alumina-silica canister ceramic has been the subject of several studies.

EURAD (Deliverable n° 1.1) – Initial State-of-the-art of WP ConCorD
Dissemination level: Public
Date of issue of this report: 17/08/2022

Page 65

SKB (Sweden)

A first patent by Larker (1977) presents a concept of a ceramic-metal capsule (Figure 2-1). In this concept, the waste (in the form of spent fuel or vitrified waste) is placed in the alumina capsule, consisting of an open container and a cover fitting the open end of the container. These two parts are produced from ceramic powder material (alumina), which is then compacted by hot isostatic pressing (1,300°C - 1,400°C 0.5 kbar to 2 kbar). The capsule is then enclosed in a gas-tight metal casing and joined by means of hot isostatic pressing (at the same pressure and temperature conditions as described for the compaction of the container and the cover fitting) in order to obtain a homogeneous monolithic body. The developed capsule allows waste to be stored in a single cavity or multiple separate ones. A thermal insulating material can be placed between the waste and the body of the ceramic container in order to limit the temperature in the vicinity of the waste during the closure phase of the capsule. In order to mechanically reinforce the sealing area, a ceramic insert is placed in the lid of the container.
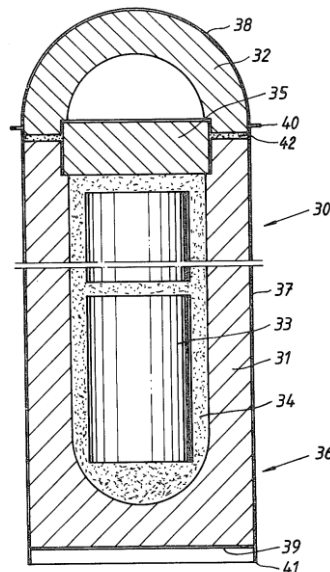
Figure 2-1: Scheme of a capsule (30) containing a number of nuclear waste cylinders arranged for connection of the cover and the hollow cylinder by isostatic hot pressing. In this scheme the main elements are: 31) the cylindrical ceramic container, 32) the dome-shaped cover, 33) the vitrified waste glass cylinders, 34) powdered or grain-formed material embedding the waste, 35) a support plate, 36) a gas-tight sheet metal casing consisting of 37) a sheet metal cylinder, 38) a sheet metal cover and 39) a sheet metal bottom. Other elements are 40-41) the welds and 42) ceramic powder layer which is bound together with the container during sintering (Larker, 1977).

Lawrence Livermore National Laboratory (USA)

In the early 1990s, the Lawrence Livermore National Laboratory was commissioned to study alternative solutions to metal containers for the geological disposal of radioactive waste at Yucca Mountain (Wilfinger, 1994). Two exploratory paths were chosen:

- solid ceramic containers
- composite containers: metal structure for mechanical strength and ceramic coating/liner for chemical inertia

The specifications state that these cylindrical containers (5.50 m high and 1.80 m in diameter) have no transport function and will be placed "nose to nose" in horizontal tunnels dug into the rock. They must allow for the storage of spent fuel assemblies or vitrified waste and be identifiable and retrievable for 50

EURAD (Deliverable n° 1.1) – Initial State-of-the-art of WP ConCorD
Dissemination level: Public
Date of issue of this report: 17/08/2022

Page 66

years, leakproof for 300 to 1,000 years. The closure system of these containers must be feasible remotely in a radiation hot cell without thermal damage to the waste package. On the basis of these specifications, different selection criteria were identified for the materials and associated manufacturing processes:

- Good tensile strength and impact resistance of the material
- High toughness material
- Dense material with no open pores or cracks
- Joint or weld areas must have the same properties as the body material
- Good chemical resistance of the material in the storage environment
- Sufficient thermal conductivity to remove heat from the waste
- Use of conventional processes requiring only minor adaptations

For the last two criteria, the difficulty of manufacturing large ceramic parts is highlighted. Cost is not the primary criterion but must be taken into account. The authors point out that these developments of large objects will require development time.

The various existing materials and processes applicable to the nuclear waste container are (Holdsworth, 2013;2018):

- **Alumina (Al_2O_3)**: one of the best candidates for the manufacture of ceramic containers. It is a refractory polycrystalline ceramic, chemically inert and with good mechanical strength. Its properties are known, and large parts are produced industrially. Seals are made by brazing, diffusion bonding or glass phase sealing
- **Zirconia (ZrO_2)**: it is more mechanically resistant than alumina but more expensive and less chemically resistant. Its more refractory nature makes it difficult to manufacture large non-porous parts
- **Alumina-Zirconia composites**:
  - ○ ZTA (zirconia toughened alumina): the addition of zirconia increases the mechanical properties of the material
  - ○ ATZ (alumina containing tetragonal zirconia): the addition of alumina reduces the hydrothermal ageing of the zirconia

These composites are interesting because of their higher mechanical properties than alumina and lower manufacturing costs than zirconia

- **Silicon carbide (SiC)**: a light, tough, refractory material that is chemically resistant in acid and basic environments. Tubes with diameters of 0.5 m and 3 m are produced industrially but are porous (≈ 15% porosity). Some SiC structures are made by reaction bonding. On the other hand, residual silicon can corrode in geological environments and open up porosity
- **Silicate materials**: interest in commercial stoichiometric phases: silica (SiO_2), mullite ($3Al_2O_3$-SiO_2), forsterite ($2MgO$-SiO_2) and cordierite ($2MgO$-$2Al_2O_3$-$5SiO_2$). All these compounds have a more or less high level of glassy phase which facilitates the densification, but which has the consequence of reducing the chemical resistance of the compound
- **spinel phases**: magnesium aluminate $MgAl_2O_4$ has properties close to alumina but without phase transition during thermal spraying processes. It is a good candidate for the production of coatings (industrial process)
- **Titanium oxide (TiO_2)**: a less refractory material than alumina, it sinters at lower temperatures but is more expensive. It is chemically inert except under very alkaline pH conditions and is soluble in H_2SO_4. It is proposed as a sealing aid for alumina containers. This route has been explored by SKB. The addition of TiO_2 causes significant thermal gradients that cause cracks in the material

EURAD (Deliverable n° 1.1) – Initial State-of-the-art of WP ConCorD
Dissemination level: Public
Date of issue of this report: 17/08/2022

Page 67

- **Graphite**: large pieces of crystalline graphite in an amorphous carbon matrix exist but are porous, having a theoretical density of 80% to 92%. Vapor deposition of SiC can fill the porosity but this process is time consuming and expensive

BNL/Nucon (USA)

In the late 1990s, the company Nucon developed containers for the transport and storage of nuclear waste in the USA (Rockhvarger, 1998; 1999; 2000). These containers, based on the Russian doll system, are composed of a multi-layer system ensuring radiological, mechanical, and corrosive protection of the encapsulated waste both during transport and for geological disposal of the waste. The different liners used are:

- a first ceramic container that encloses the waste. This first structure acts as a thermal, chemical, and radioactive protection,
- a second ceramic liner acts as a mechanical and corrosion barrier and,
- the space between these two ceramic bodies is filled with a graphite or metal powder which acts as a radiation shield.

Two concepts have been proposed depending on the size of the waste to be encapsulated (Rockhvarger, 2000).

The developed processes concern the watertight sealing of ceramic containers made of $MgAl_2O_4$ using the microwave process. The sealing is carried out using a ceramic paste of the same composition as the parts to be joined. This paste is doped in order to promote the absorption of microwaves by the material (hydrogenation of the powder).

The switch to compounds doped with ceramic fibres is envisaged. In addition to the mechanical reinforcement of the container, the addition of ceramic fibers can favour the thermal treatment of the material (e.g. SiC, which has an high permittivity value and it is preferentially heated during microwave heat treatment) or increase the radiological properties of the container (addition of boron nitride).

Andra (France)

The first part of the work (2007-2009) focused on the development and characterisation of alumino-silicate ceramics with leaching resistance and mechanical properties superior to conventional silicate ceramics (Baroux, 2016):

- the development of a ceramic with an alumina-rich composition that meets the required physical and chemical properties. After chemical characterization using pure water Soxhlet tests at 100°C and column tests in Callovian-Oxfordian deep groundwater at temperatures between 50 and 90°C were performed, it was concluded that the chemical durability of the examined ceramic was suitable for purpose, an effective thickness reduction of ~3- 4mm over a period of 1000 years.
- the design (shape and thickness) of a container for high activity nuclear wastes adapted to the ceramic material
- the development of casting, drying and sintering processes adapted to these thick ceramic parts.

These developments have made it possible to demonstrate the feasibility of the body and lid of an ½ scale, 4 cm thick container (Figure 2-2). This constitutes a real advance compared to the current state of the art in industry.

EURAD (Deliverable n° 1.1) – Initial State-of-the-art of WP ConCorD
Dissemination level: Public
Date of issue of this report: **17/08/2022**

Page 68

Figure 2-2: Andra half-scale model of Al2O₃/SiO₂ VHLW canister (Baroux, 2013) (a) complete model, (b) lid.

The technological roadblock on these new silico-alumina containers remains the closure of such a system. Current studies focus on the development of a sealing technology adapted to the application, with constraints associated with the vitrified waste and the watertightness of the HA waste disposal container (Kalfayan, 2019). In order to preserve the containment properties of the glass matrix of the waste (maximum temperature 450°C), the sealing process will have to meet two major constraints:

- a maximum surface temperature of the ceramic container of 600-700°C
- a heating technology localised to the closure area.

One of the ways identified to assemble ceramic parts is to use the interaction of ceramic materials and microwaves to locally heat the joining area until the material melts, in order to achieve a tight weld. A lot of work is currently being developed for the sintering of ceramic materials, in particular for alumina (Clark, 1996) (Zymelka, 2013) (Zhang, 2003). These works led to a better understanding of these wave/material interactions. This process can now be considered for the welding of ceramic specimens with an alumino-silicate composition. The work carried out since 2014 made it possible:

- to improve the quality of the ceramic/glass sealing interface via a two-stage enamelling process: first firing in a conventional furnace, then sealing the enamelled parts by microwave heat treatment. The process can then be industrialized with this pre-firing, which can be carried out by the porcelain manufacturer supplying the ceramic container,
- to confirm that the selected and tested glasses have processing temperatures compatible with the constraints imposed by the presence of the primary package,
- to confirm the feasibility of sealing by microwave heating (no influence of the microwave frequency on the process, the sizing of a furnace will not be limited by the wave-material interaction),
- to make a clear improvement in the quality of the joints for heating under minimal load, and
- to verify the viability of the process: a study was carried out with an industrial manufacturer of microwave ovens. An industrial prototype was proposed, taking into account the size of the full-scale container and the localized heating constraint.

With a view to going further and designing and testing a first prototype to reinforce the proof of concept, the following avenues are being considered:

- to produce a prototype furnace for testing the annular shapes of test bodies and the localised heating of these parts,
- to understand the resistance of the ceramic to the thermal gradients resulting from localised heating, and

EURAD (Deliverable n° 1.1) – Initial State-of-the-art of WP ConCorD
Dissemination level: Public
Date of issue of this report: **17/08/2022**

Page 69

- to optimise the compositions of sealing glasses to reinforce their mechanical and leaching resistance (example: glass-ceramics).

2.2.1.2 SiC Concept

It has previously been shown that silicon carbide (SiC) is a viable option for container fabrication (Holdsworth, 2013) (Knorr, 2008). Until recently, it was only feasible to manufacture large pieces out of SiSiC (silicon impregnated silicon carbide) and RSiC (recrystallised silicon carbide). However, now there was a possibility to make larger pieces from conventional SSiC (sintered silicon carbide), Figure 2-3 (Kerber, 2013) and even high strength grades of SSiC (Wötting, 2007).
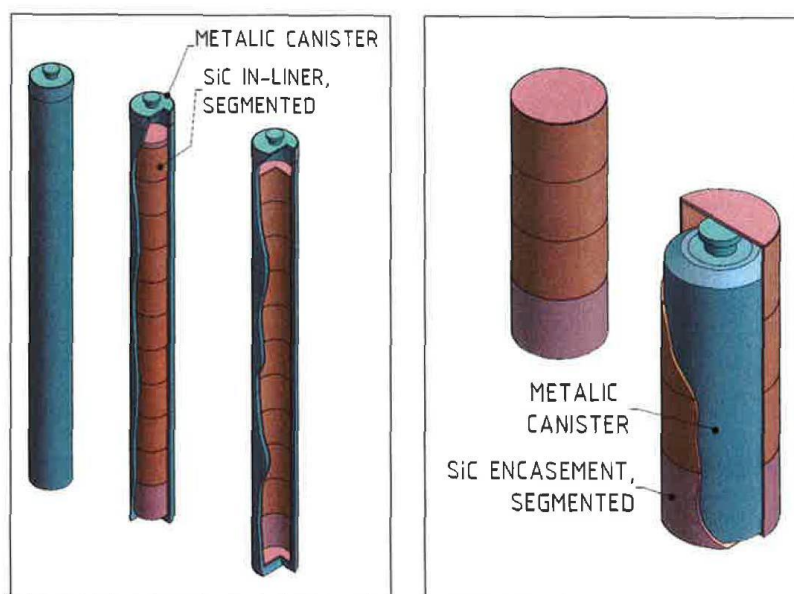
Figure 2-3: Proposed SSiC encasement solutions for (a) SF rod disposal, with diameter 430 mm and height 4980 mm, and (b) VHLW disposal, with diameter 465mm and height 1,390mm (Kerber, 2013).

The study of SiC behaviour (as material for SF/HLW containers) under aggressive conditions is highly relevant. Nowadays the world's leading R&D centers make corrosion resistance tests of SiC and SiC with various alloying additions under conditions simulating the various environmental conditions.

In 2018 two companies "General Atomics" and "Westinghouse Electric" conducted corrosion tests of modern fuel pipes made of SiC/SiC composites (under conditions of normal operation of water-cooled reactors) (Deck, 2018). The composition of the liquid in the autoclave during the tests corresponded to different types of coolants; the tests were carried out for 3 months. Obtained results indicate that SiC has a high corrosion resistance; the authors calculated the dissolution rate of 1 µm per year, which is approximately 1% of the total thickness of the fuel cladding.

The positive effect of Cr on the corrosion resistance of SiC ceramics (Lobach, 2020) was experimentally shown under conditions simulating the inner environment of VVER-1000 reactor. It is shown that doping of SiC with Cr decreases the dissolution rate of SiC(Cr) compared to SiC without additives, due to the formation of corrosion-resistant products (Cr_2O_3), which significantly affect the ability of SiO_2 films to passivate the surface of the samples. Also it should be noted that the authors in (Lobach, 2018) showed

EURAD (Deliverable n° 1.1) – Initial State-of-the-art of WP ConCorD
Dissemination level: Public
Date of issue of this report: **17/08/2022**

Page 70

the effect of Cr additives on the mechanical properties of SiC. Found that doping of SiC with 0,5 %wt Cr leads to an increase in fracture toughness (K1c) by (25 – 50)% (from 4,2 to 6,2 MPa·m1/2) while maintaining a high level of hardness with a value of 28,0 GPa.

The results of scientific research indicate that SiC-based ceramics have high corrosion resistance in hydrothermal conditions and are promising for use as a material of the fuel claddings. Despite the fact that the described lixiviation tests of SiC were carried out under severe conditions (t = 350°C, P = 16,8 MPa), there is a need to study the mechanisms of corrosion processes in the system (SiC - compound - SiC) under the conditions simulating geological disposal (t = 90°C), because the interconnection of SiC segments is an important and actual task, taking into account the conditions (corrosion and radiation exposure) of their usage. There are two most promising directions in the world for interconnecting SiC segments:

- the first one is Laser joining method (Knorr, 2008), which is based on a combination of pure oxidic braze filler (trademark: CERALINK ®) and laser beam. The filler inside the joining zone is melted locally by using a laser beam. CERALINK ® shows an ideal wetting of ceramic surface and high oxidization resistance. The ceramic joint surface does not need pre-treatments (no metallization). This paper indicates that obtained joints are gas-tight, have high mechanical strength and have no cracks. Joining surfaces do not require preliminary treatment, and,
- the second direction is soldering based on various materials (for example, glass-ceramic). So, in work (Le, 2020) the joining scheme of SiC/SiC composites is given, where the material Y_2O_3-Al_2O_3-SiO_2 (YAS) was used. Authors consider that a reliable glass-ceramic joining with strong joints is obtained. Shear strength tests showed an increase in the strength of the joining with increasing soldering temperature; maximum strength reached 51,7 MPa at a soldering temperature of 1400°C.

2.2.2 Ceramic Coatings

The main requirement of a ceramic coating applied to a carbon steel (or cast iron) nuclear waste disposal canister is the prevention over a period of ≥ 10000 years of access of bentonite and/or clay pore waters to the substrate via cracking or leaching (Holdsworth, 2018). Ceramic coating solutions for SF/HLW disposal canisters appear to be less mature than metallic coatings. The main issues to be addressed are related to the inherent brittleness of ceramics, the mismatch of thermal expansion coefficient with the underlying steel, the requirement for relatively large thickness and very low porosity. Nevertheless, yttria-stabilised zirconia or graded multilayer coatings of alumina and titania appear to be promising options that would require additional development before their feasibility can be better assessed. Irrespective of the selected ceramic coating material, methods for covering the lid-to-canister weld and for coating repair would also have to be developed.

Physical Vapour Deposited (PVD) coatings have good corrosion protection compared to coatings that are deposited by traditional spraying. Despite the smaller thickness of the PVD coatings, they have much lower porosity than the coatings deposited by spraying. Also, a serious advantage of the PVD methods over the methods of electrochemical deposition is the environmental friendliness of the process.

Titanium oxide-based coatings

The most studied class of high-hard coatings formed by the PVD methods (magnetron sputtering and cathodic arc evaporation) are titanium nitrides and carbides. Problems in the synthesis of various metals oxides by vacuum arc method were discussed in the review (Tay, 2006). Earlier KIPT's specialists have

EURAD (Deliverable n° 1.1) – Initial State-of-the-art of WP ConCorD
Dissemination level: Public
Date of issue of this report: **17/08/2022**

Page 71

developed vacuum-arc nanostructured TiO_2-based coatings (structure - anatase) with controlled bactericidal activity for orthopedic implants (Belous, 2013). The influence of the negative bias potential of the substrate was investigated by the authors (Belous, 2018). It is shown that titanium coatings deposited in an oxygen medium under pressure of 0,03 Pa represent a dispersed system of oxides, composition of which depends on the magnitude of the bias potential on the substrate. Results of electrochemical measurements show that the current density characterizing the dissolution of steel coated with titanium nitrides and oxynitrides thickness of ~ 6 μm is 0,5...1 order lower than for uncoated one in the range of corrosion potentials -0,5...0 V. With the increase in the coating thickness to 12 μm the samples corrode much slower, which correlates with a decrease of the coating porosity, where the density of the corrosive current decreased by 2,5…3 orders of the magnitude. The highest corrosion resistance is observed in the samples with coatings thickness of ~12 μm deposited from the oxygen and nitrogen mixture at an oxygen pressure $P_{O2} = 3{\times}10^{-2}$ Pa. These coatings provide high corrosion resistance of steel close to the of a pure titanium nitride coating in a 3 % aqueous solution of NaCl (Belous, 2018). The anodized and thermally oxidized Ti samples with TiO_2 coatings showed relatively high corrosion resistance in 4M HCl and 4M H_2SO_4 solutions at 100±5°C and the passive current density values of the thermally oxidized samples were five orders of magnitude lower under the electrochemical testing condition compared with that of the anodized titanium sample (Minhas, 2021). The protection against corrosion provided by the conversion layer combined with TiO_2 coating on stainless steel in pure water and saline solution was quite good (Bamoulid, 2008). According to the corrosion test results, it was shown that TiO_2 films deposited on $MgCa_2Zn_1Gd_3$ effectively protect this alloy from corrosion in Ringer's solution at 37°C (Kania, 2021). While it is difficult to relate these qualitative electrochemical corrosion data to long-term storage performance, It can be assumed that titanium oxide coatings deposited by PVD methods are promising for corrosion protection of the low carbon steel containers. Additional studies are needed on the mechanisms of long-term corrosion processes in the TiO_2 coating-steel substrate system under conditions simulating a geological disposal (t = 90°C).

Chromium nitride coatings

Chromium nitride (CrN) has been proven to be one of the most successfully and extensively used PVD coatings in industry due to its high hardness, excellent wear resistance and remarkable stability against corrosion (Milošev, 1997). The CrN coating deposited on AISI 304 stainless steel possesses high corrosion resistance in 0,5M H_2SO_4 solution and 0,5M NaCl solution (Milošev, 1993). The CrN film with gradient structure design showed a lower coefficient of friction (COF) and wear rate than a single CrN layer under high load and frequency conditions, indicating a good potential to improve the anti-wear and anti-corrosion abilities of pump valve pipes and hydraulic and power transmission systems in marine environments (Cen, 2018). The demand for high quality coatings in the recent years has led to intensive research in further evolution of chromium-based coating family (Cedeno-Vente, 2021). K.Daub et al, (Daub, 2015) provided comparative analysis on corrosion resistance of 2–4 μm-thick CrN-, TiAlN- and AlCrN-coated Zry-4 alloy. It was shown that CrN coating demonstrates better overall performance in both aqueous and steam environments. CrN coatings on the Stellite™ (Cobalt based alloy) samples showed excellent wear and corrosion resistance in high temperature and high-pressure water with γ-rays of 100 Gy/h by ^{60}Co source irradiation during testing (Kawana, 1996). The Co elution rate from stellite decreased drastically with film thickness, and it can decrease about 4 orders of magnitude in CrN coatings thickness of 7 μm. This is the only publication known to us where the effect of γ-radiation on the corrosion resistance of coatings was studied. Chromium nitride coatings are promising for corrosion protection of the carbon steel, but additional studies are needed on the long-term corrosion processes in the simulating a geological disposal (t = 90°C).

EURAD (Deliverable n° 1.1) – Initial State-of-the-art of WP ConCorD
Dissemination level: Public
Date of issue of this report: 17/08/2022

Page 72

2.3   Metallic Materials and Coatings

2.3.1   Metallic containers

The concepts for deep geological disposal in Finland, Sweden, Canada, Korea and Switzerland, propose copper as outer barrier material for containers. Also, several other metallic materials have been investigated as candidates for containers, such as carbon steel, stainless steels, nickel and titanium alloys. Several extensive review reports and articles have been made comparing the metallic candidate materials (King et al., 2016) (Padovani *et al.*, 2017). In these reports, the key properties of candidate materials are extensively presented as well as their engineering aspects together with the interactions with certain geological environments. This chapter aims to summarise the main aspects of scientific interest in these material candidates and give background for the motivation behind studies on corrosion of new materials and material grades.

The requirement on waste containers were discussed previously in Section 2.1. In order to achieve the long-term integrity, the metallic waste container material should have sufficient resistance towards:

- general corrosion,
- pitting corrosion,
- hydrogen-induced cracking (HIC) and
- stress corrosion cracking (SCC).

The materials planned to be used in the final disposal may be subject to these corrosion phenomena and it is recognized that their susceptibilities towards the different corrosion modes vary between materials and environments. The corrosion phenomena listed above do not necessarily occur simultaneously, but merely become relevant during the different phases of the final disposal. In deep geological repositories, the chemical environment in the initial phase is usually oxidizing and the temperature is elevated (up to ca. 100°C). The entrapped oxygen is consumed in various chemical and biological reactions in the confined space and the environment will eventually change to anoxic. The temperature decreases along with the decreasing activity of the waste, eventually reaching the same level as the ambient temperature of host bedrock.

The mechanical properties required from the waste canister include:

- Tensile strength
- Ductility
- Compressive strength
- Creep resistance
- Resistance to mechanical impact
- Grain size
- Weldability
- Machinability

Tensile strength, ductility, compressive strength, creep resistance and thermal resistance are properties that are required during the disposal phase. Sufficient tensile strength and ductility are required against external stresses that may be applied on the waste canister (e.g., movement of the bedrock). Sufficient compressive strength is required against external isostatic pressure yielding e.g., from the swelling bentonite. During the initial oxidic phase, metallic materials may be exposed to creep due to the elevated temperature and load from the swelling bentonite, isostatic pressure of the groundwater or residual stresses (e.g., in welds).

Properties that are required prior to the disposal phase include resistance to mechanical impact, grain size, weldability, and machinability. The waste canister should withstand a mechanical impact without

EURAD (Deliverable n° 1.1) – Initial State-of-the-art of WP ConCorD
Dissemination level: Public
Date of issue of this report: **17/08/2022**

Page 73

fracturing if the canister is accidentally dropped etc. during handling. The material should have a certain grain size for enabling non-destructive testing with e.g., ultrasound method (Raiko and Salo, 1999). Weldability and machinability are required for proper sealing of the canister and to produce the desired surface finish, respectively.

Influence of host rock properties on material requirements

The surrounding host rock at planned repository sites sets limitations for canister materials. Canister failure can be driven by for example groundwater, microorganisms or mechanical factors linked to host rock. In addition, temperature allowance of canisters differs between the host rock types.

The properties of the host rock to be considered in selection of canister materials are presented in Table 2-1. by Ojovan, Lee & Kalmykov (2019). For example, under Fennoscandian and Canadian granitic bedrock conditions the groundwater contains substantial chloride concentrations (Johnson et al., 1994), thus making the use of stainless steel non-viable. For clay conditions where water conductivity is low, carbon steel or stainless steel can be an option.

Host rock	Rock characteristics	Radionuclide transport mechanisms	Heat conductivity	Country
Crystalline (Granite)	Fractured, groundwater flow in open fractures	Advection and some diffusion	medium	Canada, China, Finland, Russia, Sweden, United Kingdom
Salt bedded, dome	No open fractures, no groundwater	No transport	High	Germany, United States (WIPP)
Volcanic tuffs and lavas	Fractures and pores, unsaturated	Percolating water	medium	United States (YMP), United Kingdom (Longlands Farm)
Clays and mudrocks	No open fractures, stagnant pore water	Diffusion	low	Belgium, China, Hungary, France, Russia, Switzerland

Table 2-1: Properties of host rock to be considered for the selection of canister materials: adapted from (Ojovan et al., 2019).

Low alloyed steels

Steels are among the most studied material options for copper as canister material. Conventional carbon steels have several benefits as it is widely available for reasonable price and easy to machine (Landolt et al., 2009). This enables constructions with relatively thick walls that result in good mechanical strength and radiation shielding. Compared to copper, the corrosion resistance of carbon steel is low, although in anaerobic phase the corrosion rate of steel is also very low. The SCC risk for low alloyed steels exists in carbonate-bicarbonate environments that may be the case in phases of cooling down of canister. However, SCC could occur not only at neutral pH but also in highly alkaline environments. Carbon steel overpack is considered for example in the French concept (Crusset et al., 2017).

Lead

Lead is studied to some extent as candidate material for canisters in waste programs of Argentina, Brazil and Russia, although the technical feasibility is still unclear (Xiong et al., 2021). The superior radiation shielding ability and low cost of lead is an asset. However, uncertainties lie in the corrosion behaviour,

EURAD (Deliverable n° 1.1) – Initial State-of-the-art of WP ConCorD
Dissemination level: Public
Date of issue of this report: 17/08/2022

Page 74

mechanical strength, and especially environmental aspects of using lead. Therefore, it is not considered as potential candidate, at least in the near future.

Stainless steels

Stainless steels are passive materials of which the corrosion resistance is based on the thin passive film formed on the surface of metal (Landolt et al., 2009). They exhibit very low uniform corrosion rates andthe most emphasis must be put on the risks of localized corrosion. It is known that stainless steel is susceptible for localized corrosion in chloride containing solutions. Additionally, the self-healing properties of protective passive film on stainless steel works as designed only in oxidic conditions.

Titanium

Titanium alloys are also passive alloys that are extremely corrosion resistant in waste disposal environments (Braithwaite et al., 1980). The uniform corrosion is practically negligible due to the inertness of titanium oxide passive layer. The alloys are immune to pitting at most aqueous environments (Landolt *et al.*, 2009). The corrosion related challenge of titanium alloys is the crevice corrosion risk in oxidic phase that was considered as critical failure mechanisms in early stages of studies and the need for further research in this area is recognized (Padovani *et al.*, 2017). However, it is also stated that the risk of crevice corrosion of titanium alloys can be avoided by using alloys with Pd or Ru (Schutz, 1996) (Landolt et al., 2009). Hydrogen induced cracking (HIC) has been considered also as potential risk for titanium alloys under anoxic conditions. The absorption of hydrogen is shown to be linked to corrosion at residual impurities in grain boundaries.

Nickel alloys

There are six major groups of Ni alloys, each characterised by the principal alloying elements: Ni-Cu, Ni-Mo, Ni-Cr, Ni-Cr-Mo, Ni-Fe-Cr, and Ni-Fe-Cr-Mo alloys. All of the alloys selected in the various international HLW/SF programmes belong to either the Ni-Cr-Mo group (i.e., Alloys 625 and 22, Hastelloy C-4, and C-276) or the Ni-Fe-Cr-Mo group (Alloy 825), primarily because of their resistance to corrosion under both oxidising (due to the presence of Cr) and reducing (due to the presence of Mo) conditions. Furthermore, Mo (and W in Alloy 22 and Hastelloy C-276) provides improved resistance to localised corrosion. Silicon can improve the corrosion performance under high-temperature oxidising conditions through the formation of protective Si-O films. Manganese is added as a deoxidant, but it can increase the susceptibility to localised corrosion because of the tendency for film breakdown to occur at MnS inclusions (King, 2014).

Copper

It is emphasized that term *copper* refers to group of grades and alloys that need to be specified, since the properties of material are dependent on these dopants and possible impurities present in the microstructure. In container materials, typically copper grades with purity of ≥99.3% (w/w) are concerned (Hall *et al.*, 2021). Almost all research to the date has been focused on the OFP-copper, which is oxygen-free copper with phosphorous addition and further described later in this chapter.

The copper material selected in KBS-3 concept is specified so that it has to fulfil standard EN 1976:1988 (UNS C10100) for the grades Cu-OFE or Cu-OF1 with additional requirements for concentrations for critical elements/impurities (Andersson *et al.*, 2004). The requirements for critical elements are as follows: 0<5 ppm, P 30–70 ppm, H<0.6 ppm and S<8 ppm (Andersson et al., 2004). The EN standard has lower limit for phosphorous content and thereby also the name "OFE+P" has been used for the selected alloy.

EURAD (Deliverable n° 1.1) – Initial State-of-the-art of WP ConCorD
Dissemination level: Public
Date of issue of this report: **17/08/2022**

Page 75

The benefits of copper are its superior corrosion resistance and good mechanical properties. Downside especially for highly pure copper grades being high cost.

2.3.2 Coatings

Titanium, chromium, and copper are well known materials for corrosion protection (Ahmad, 2006). Good protective properties of Cr coatings were demonstrated under normal operation conditions: autoclave tests in PWR and BWR simulated medium (Wei, 2019) (Brachet, 2015). The use of copper as an exterior container corrosion barrier has been considered for many years by many national research programs in nuclear waste management, including those in Sweden and Finland, and by Canada's Nuclear Waste Management Organization (NWMO) (Keech, 2014). In the Canadian program, NWMO, the copper coating methods are still under development and the exact composition and property requirements of the copper are not yet established.

Candidate titanium coating solutions for application to carbon steel nuclear waste disposal canisters are immune to microbially induced corrosion. Open questions for the use of titanium, chromium, and copper as protective coatings on steel substrates: the required thickness to exclude through porosity, the effect of through defects and irradiation on corrosion resistance.

Nickel alloys are widely used in industry as corrosion barriers and specific alloys, such as C22 proposed as waste package material for Yucca Mountain, can provide extremely low corrosion rates. Also, coating with Ni-based alloys is well developed and numerous options exist. However, even though nickel alloys tend to be resistant to microbially induced corrosion, they are not immune and MIC can be enhancement factor for general corrosion (King, 2020). Consequently, inherent uncertainties associated with MIC rates and mechanisms would be eliminated completely by adopting a different material which is known to be immune to MIC.

Titanium alloys are known to be immune to MIC (King, 2020). They also exhibit extremely low general corrosion rates, high resistance to corrosion under irradiation, and certain alloys are also immune to localized forms of corrosion (Hua, 2005). Titanium coatings deposited by PVD methods were studied mainly by electrochemistry methods (Zhou, 2012). Titanium coatings possess better corrosion resistance in both corrosive media (0.5 N NaCl and 0.5 N Na_2SO_4 + 0.1 N H_2SO_4) than uncoated steel (Zhujmg, 1991). Hydrogen absorption as a result of anaerobic general corrosion under disposal conditions will occur. However, such processes are generally predictable and long canister lifetimes can be expected with confidence. No corrosion resistance study of titanium, copper and chromium PVD coatings on the carbon steel under specific nuclear waste repository environment conditions has been published to date.

The concept of manufacturing a dual-shell container with a copper coating for corrosion protection directly on the steel structure was raised to avoid the drawbacks related to classical manufacturing approaches including machining/forging (Lee, 2011) (Keech, 2014) (Legoux, 2014). It also exists the possibility of creep and stress corrosion cracking of the copper shell in case of gap between the outer copper corrosion barrier and the steel insert with conventional dual-shell container (King, 2017). The benefits are as follows: no issues with tolerance of fabrication of copper part; the copper layer is produced directly on the steel part without any gap between layers; welding joint could be covered by copper after welding steel cover. Several processes of deposition are available.

The method reviewed here is the cold gas dynamic spray, which satisfies the requirements of dual-shell container concept: able to produce thick layer of copper on steel surfaces, guarantee low level of copper oxidation during treatment, able to deposit copper coating on localized surface, able to be applied in radioactive environment. The principles of cold spray are described in the following references (Alkhimov, 2012) (Sova, 2013).

EURAD (Deliverable n° 1.1) – Initial State-of-the-art of WP ConCorD
Dissemination level: Public
Date of issue of this report: **17/08/2022**

Page 76

While the corrosion behaviour of solid copper in waste repository conditions is well known and guarantees a very long-life containment (King, 2010) (King, 2017), some further development work is required on copper cold spray coating materials both on the process itself and the materials obtained.

From a general point of view, the quality of coatings (density, absence of porosity) contributes to increase both the mechanical and resistance to corrosion properties. This quality is strongly dependant on the cold spray coating (CSC) process parameters.

One of the first parameters of CSC is the nozzle displacement, in particular the influence of nozzle traverse speed and distance between deposited tracks. It was shown that cold spraying copper-silicon carbide powder at low nozzle traverse speed leads to formation of thick tracks with quasi-triangular cross-section (Matts, 2019). Consequently, the particle impact angle on the sides of spraying track increases. Thus, the particle deformation at impact on the track periphery becomes insufficient and local porosity value rises. Increase of nozzle traverse speed allows increasing coating density and mechanical properties due to amelioration of particle deformation conditions. In this work, compressive tests revealed significant anisotropy of mechanical properties of copper-silicon carbide cold spray deposits. In particular, compressive strength measured in vertical direction (perpendicular to the substrate) was significantly higher than one measured in horizontal plane (parallel to substrate). This anisotropy could be explained by the orientation of particle deformation pattern during impact.

Carrier gas velocity and its nature have also a significant effect on copper cold spray coating quality (Jakupi, 2015). The grain size and number of coincident site lattice grain boundaries increased, and plastic strain decreased, with carrier gas velocity. Post-annealing treatment (4h at 400°C) improved the quality of the coatings by increasing texture and coincidence site-lattices, but also increased the number of physical voids, especially when a low temperature cold spray carrier gas was used. Tensile testing showed a better adherent coating to the steel substrate when He carrier gas is used contrarily to N_2 gas.

Mechanical performances of bonded thick copper coatings on steel have been assessed by H. Boyle et. al. (2015) and validated the "proof of concept" of the CSC process. They showed the mechanical performance of the annealed cold spray coatings were comparable or exceeded that of the reference wrought copper and are suitable for the container design with adhesion strengths exceeding 45 MPa. In general, cold spray is used for production of metal deposits. However, possibility of deposition of metal-ceramic composite coatings by spraying of different mixtures of metal and ceramic powders was also studied (Yin, 2017) (Sudharshan Phani, 2007) (Ogawa, 2008) (Lee, 2017) (Fernandez, 2018) (Koivuluoto, 2010). In this case the adhesion of the metal to the substrate as well as primary matrix formation is ensured by the plastic deformation of metal particles, whereas the ceramic particles stick to the surface by mechanical anchoring mechanism and form hard inclusions in softer metal binder (Koivuluoto, 2010) (Triantou, 2015) (Wang, 2014). Previous studies showed that addition of ceramic powder to the metal ones increases the coating adhesion and density, ameliorates its mechanical properties and corrosion resistance in comparison of the cold spray deposits of the same but pure metal without ceramic inclusions (Yin, 2017) (Sudharshan Phani, 2007) (Ogawa, 2008) (Lee, 2017) (Fernandez, 2018) (Koivuluoto, 2010) (Triantou, 2015) (Wang, 2014). Several studies also revealed increased performance in wear resistance behaviour. For example, in the work of Triantou et al. (2015) devoted to comparison of pure copper and copper-alumina cold spray deposits the authors found that wear resistance of composite deposits is higher due to the presence of alumina in copper matrix. In addition, the hardness, the density and the corrosion resistance were also improved.

No corrosion resistance study of CSC under specific nuclear waste repository environment conditions has been published to date. The environment selected for corrosion studies are NaCl solutions under anoxic or, on the contrary oxygenated conditions to simulate the long- and short-term redox conditions (Keech, 2014) (Lee, 2011), and more or less acidic environments to quickly screen corrosion resistance between wrought copper and cold spray copper coating (Lee, 2011). The corrosion behaviour of Cu cold spray coatings and wrought Cu in 3 mol l^{-1} NaCl under both sets of conditions are similar (Keech, 2014). No evidence was observed to suggest the particle boundaries in the cold sprayed coating were preferential corrosion sites. In more concentrated NaCl solution and acidic 10% HCl solution, the

EURAD (Deliverable n° 1.1) – Initial State-of-the-art of WP ConCorD
Dissemination level: Public
Date of issue of this report: 17/08/2022

Page 77

corrosion rate was a little higher in the CSC coppers than the commercial wrought coppers. The authors indicated however that to further clarify these findings, more experiments, such as a field test for the CSC copper would be beneficial.

EURAD (Deliverable n° 1.1) – Initial State-of-the-art of WP ConCorD
Dissemination level: Public
Date of issue of this report: **17/08/2022**

Page 78

2.4 Discussions and outlook

The literature review provided an overview of current concepts and planned innovations for storage containers. Each solution has advantages and disadvantages.

	Material	Advantage	Disadvantage
Metal	OFP-Cu	Excellent corrosion behaviour	High price
	Other Cu-grades	Price (compared to OFP-Cu), availability	Not yet as widely studied in repository conditions if compared to Cu-OFP
	Carbon Steel	Low price, mechanical integrity, weldability	Corrosion in bentonite-based or cementitious backfill hydrogen formation on corrosion, higher general corrosion rates compared to other passive alloys
	Stainless steels	General corrosion resistance, availability	Tendency for localized corrosion in certain environments
	Titanium alloys	Corrosion performance in aggressive brine solutions	High price, tendency for localized corrosion in certain environments
	Nickel alloys	General corrosion resistance, availability, (improved pitting corrosion resistance compared to stainless steels)	Tendency for localized corrosion in certain environments
	Lead	Low price, corrosion resistance, available	Toxic to environment
Ceramics	Alumina	Chemically inert with good mechanical properties	Feasibility of large ceramic pieces
	Silicon Carbide	Chemically resistant for SSiC. Feasibility of large pieces	SSiC vulnerable to leaching. High temperature for sealing processes
	Silicate materials	Commercial phases, low porosity due to glassy phases	Glassy phases can reduce lixiviation properties, mechanical properties
	Titanium Oxide	Less refractory than alumina, lower temperature sintering	Expansive, chemically inert except under very alkaline pH
Coatings	TiO_2 coatings	High hard coating, bactericidal activity	Ceramic coatings must be without defects
	CrN coatings	High hardness, excellent wear resistance, chemically resistant	
	Cu coatings	Cu corrosion well known, less expensive than Cu container	Risk of galvanic corrosion in case of defects
	Ti and Ni alloys	Corrosion performance	Long term prediction is difficult, microbial induced corrosion cannot be excluded

Table 2-2: Summary of advantages and disadvantages of candidate materials for containers.

EURAD (Deliverable n° 1.1) – Initial State-of-the-art of WP ConCorD
Dissemination level: Public
Date of issue of this report: 17/08/2022

Page 79

The development and qualification of new materials for storage containers still requires extensive development/studies. The diversity of the solutions envisaged leads to a great variability of the tests to be carried out (mechanical for ceramics, quality of the coating for anti-corrosion coating solutions...) Task 2 of the ConCorD programme aims to complete the data on the most promising/advanced solutions, in particular:

Ceramics solutions

Alumina-silica-based ceramics and silicon carbide (SiC) are the most promising solutions. The production of large-scale pieces needs more developments with industrial partners and will not be covered in the ConCorD program.

With regard to the Silicon Carbide solution, the addition of chromium seems to improve the corrosion properties. In ConCorD, KIPT proposes to study ceramic composites based on SiC doped with Cr in various proportions. The first part of the KIPT contribution will be dedicated to the optimization of the sintering process of the Cr-doped SiC ceramics, the manufacturing and the preparation of a pilot batch of samples for corrosion tests.

The sealing process is also a technological issue for ceramic canisters. As far as silicon carbide is concerned, the necessary temperature seems still high and this point will not be studied yet. For alumina-silica-based materials, microwave heating seems to be promising in particular with especially for microwave-responsive sealing materials. This technology is proven on a laboratory scale with sealing glasses. The development of specific furnaces is not addressed in this programme and needs industrial partnership. However, IRCER and EMSE propose to optimise the composition of sealing glasses using core-shell technology in order to increase the coupling of the material with microwaves but also to reinforce the mechanical properties of the seal. The assemblies produced will be the subject of mechanical characterisations.

Alternative copper grades

As mentioned at the beginning of this chapter, almost all research related to copper, the most potential material in most countries' programs, focuses on the studies of OFP-copper. However, as the final concepts are still being modified with several open engineering aspects and taking into account the availability and costs of the systems, other copper grades should be further investigated as candidate alloys.

Potential alternative copper grades could include DLP, XLP or HCP copper. The advantage of using these grades would be lower price, better availability (more suppliers), and use of recycled material. Many of the proposed alternative copper alloys have been widely used in other industrial applications. However, the repository conditions differ greatly from that of traditional industrial applications. There is a clear knowledge gap in how these materials behave under repository conditions within the whole repository timeframe, for example under anoxic atmosphere, or in the chemical environment generated in contact with buffer materials or induced by biological functions.

With copper, the question of durability is not simple and not related only to the alloy composition but also to the microstructure of copper. The microstructure and important engineering aspects are also highly dependent on the heat treatments, mainly annealing, age hardening and stress relieving. The last one is done to eliminate residual stresses. These engineering concerns naturally depend on the concept, so that certain mechanical properties, e.g., creep related, are emphasized in certain designs, e.g., in concepts where a dual canister system is used rather than a coating (Hall et al., 2021).

EURAD (Deliverable n° 1.1) – Initial State-of-the-art of WP ConCorD
Dissemination level: Public
Date of issue of this report: 17/08/2022

Page 80

The alternative alloys need to meet the standards set for canister materials. For copper these include:

- **Weldability** – oxygen content must be kept low
- **Tensile strength** – Sulphur that is not dissolved concentrates on grain boundaries and affect strength properties
- **Ductility** – Hydrogen embrittlement risk occur with copper, so maximum hydrogen content is stated. Sulphur in grain boundaries will also decrease ductility.
- **Creep ductility** – Phosphorous content of 30-70 ppm reduces the influence of sulphur impurities, increases creep ductility. It also increases recrystallization temperature and has minor influence on the weldability too.
- **Grain size** - less than 360 um to allow use of NDT methods

	Cu-OFP	Cu-XLP	Cu-DLP	Cu-HCP
		UNS 103000	UNS C12000	UNS C10300
		CW020A	EN CW023A	EN CW021A
Description	Very pure, oxygen-free copper	Low phosphorus content	Deoxidized, oxygen-free copper, low residual P content	Deoxidized, oxygen-free copper, low residual P content.
Composition	Cu (min. 99.99 wt.%) Bi (max. 0.0005 wt.%) Pb (max. 0.005 wt.%) O (max. 0.001 wt.%)	Cu (min. 99.95 wt.%) P (0.001-0.005 wt.%)	Cu (min. 99.90 wt.%), P (0.005-0.013 wt.%), Bi (max. 0.0005 wt.%) Pb (max. 0.005 wt.%)	Cu (min. 99.95 wt.%) P (0.002-0.007 wt.%)
Typical use	Current canister material in national concept	Telecommunication cables, Terminals, Clad products, Busbars, Electrical conductors	Architecture, roofing, components of electrical engineering, cladding band, wire, heat exchangers, transistors, air conditioners, air-, hydraulic and oil-pipes	Telecommunication cables, terminals, clad products, busbars, base plates for power modules, electrical conductors, pressure vessels

Table 2-3: Properties of proposed novel copper alloys (Aurubis, 2022).

.

Coatings

Nickel alloys, titanium alloys and ceramics have been assessed as coating materials for SF/HLW disposal canisters, especially for cases where microbial activity in the nearfield, and thus the risk of microbially induced corrosion, cannot be excluded. All three types of materials exhibit very low corrosion rates and can, in principle, lead to canisters with very long lifetimes. At the same time, long-term corrosion data and archaeological analogues do not exist for any of them, which makes long-term predictions difficult.

TiO_2 and CrN ceramic coating solutions obtained by physical vapour deposition (PVD) methods are proposed by KIPT. This contribution is based on well-developed in KIPT PVD process and the laboratory facilities for the deposition of protective coatings at industrial scale and rate. KIPT's works are dedicated

EURAD (Deliverable n° 1.1) – Initial State-of-the-art of WP ConCorD
Dissemination level: Public
Date of issue of this report: **17/08/2022**

Page 81

to the enhancement of the process for obtaining ceramic (TiO$_2$, CrN) coatings on steel substrates by PVD method and the preparation of a batch of samples for corrosion tests.

Process for manufacturing metallic (Ti, Cu) coatings on various steel substrates by physical vapour deposition (PVD) method are proposed by KIPT. PVD process are well-known at KIPT, only some work mode optimization of the coating manufacturing process will be made taking into account the chemical composition of the metallic substrates considered as the container material. The main focus will be on manufacturing of the test (Ti, Cu) coating samples and study of their behaviour under corrosion conditions.

New copper/alumina composite coatings provided by cold spray technology will also being investigating (EMSE). The metallic/ceramic composite will allow the use of nitrogen as carrier gas and lead to decreased porosity and improved adhesion (based on recent research on Cu/SiC coatings). After optimisation of the cold spray technology parameters for Cu/Al$_2$O$_3$ compositions, corrosion studies will be performed in repository conditions. The results will be compared to those of wrought Cu alloys (VTT) as well as electrodeposited and cold spray copper coatings. This work will also focus on the effects of synergy between deformation (by creep for instance) and corrosion of coatings, particularly in the vicinity of porosity defects. These mechanisms can lead to the phenomenon of stress corrosion.

EURAD (Deliverable n° 1.1) – Initial State-of-the-art of WP ConCorD
Dissemination level: Public
Date of issue of this report: **17/08/2022**

Page 82

3. Prediction tools for assessment of long-time barrier integrity

3.1 Integrity: process-level models for corrosion processes

In radioactive waste disposal, the main aims of modelling corrosion processes of canisters designed to contain radioactive wastes (particularly high-level waste and spent nuclear fuels) are to:

i) at a very high level, predict the durability of the disposal canister (and the uncertainties associated with durability estimates), to provide a key input into performance assessments (PAs), and

ii) consolidate and demonstrate scientific understanding of the processes involved in the evolution of the disposal container and, more broadly, engineered barrier system (EBS), to underpin the treatment of container durability PAs, which are typically very simple, even if the results of the models are not used directly in PAs in any calculations of risk. A diverse range of approaches have been taken in the field to modelling corrosion processes, mechanisms and underpinning experimental results. These have been reviewed by King (King F., 2014), in the context of spent fuel/HLW disposal containers. Reviews focusing on corrosion, and the associated gas generation processes, of materials relevant to the disposal of intermediate level waste, including of metallic materials present in some wastes, are also available in (Hoch, Smart, Wilson, & Reddy, 2010) and (Smart & Hoch, 2010).

3.2 Generic corrosion modelling approaches

3.2.1 General corrosion

3.2.1.1 Empirical extrapolation

One of the simplest ways of modelling the effects of general corrosion on container lifetime is to assume that the general corrosion rate measured in laboratory experiments, typically over a period of less than 20 years, can be extrapolated to long-term corrosion rates that pertain to radioactive waste disposal (i.e., 10^3 to 10^6 years, depending on the national safety requirements). In order to be able to make this extrapolation, it is necessary to assume that the environmental conditions remain stable over the period of interest and that there are no step changes in the mechanism of corrosion. In stable geological conditions, this is a reasonable assumption to make, and the corrosion evolutionary path, can be assumed to evolve smoothly. It is possible to create empirical fits to laboratory corrosion rate data to enable extrapolations to the long-term. Such fitted curves can also be used as the basis for comparing model predictions, based on fundamental scientific understanding, to real-life data. It is frequently seen that the corrosion rate falls gradually over time and so this approach has an in-built conservatism. It is useful to consider the possible use of archaeological analogues to validate such an approach.

EURAD (Deliverable n° 1.1) – Initial State-of-the-art of WP ConCorD
Dissemination level: Public
Date of issue of this report: 17/08/2022

Page 83

3.2.1.2 Mass balance and mass transport considerations

In oxygenated conditions, the extent of corrosion of a metal such as iron by reduction of oxygen is determined by the amount of residual oxygen available within the GDF after closure. A simple mass balance calculation then determines the maximum amount of metal loss that can occur due to oxygen reduction. Once all the oxygen has been consumed, in the case of ferrous materials, the corrosion mechanism reverts to anaerobic corrosion in which the cathodic reaction is the reduction of water, which is always present in excess in a GDF, so the corrosion rate is not determined by the total available mass of the cathodic reactant.

In situations where the corrosion rate is determined by the rate of supply of the corrodent, modelling of the corrosion rate can be related to such factors as the rate of mass transport of the corrodent through the surrounding matrix. This approach is particularly relevant to consideration of the corrosion rate of copper in bentonite, in which it is generally agreed that the corrosion rate is determined by the rate of mass transport of sulphide, which is produced by the action of SRBs on sulphate in the groundwater, through the surrounding bentonite matrix to the surface of the copper.

3.2.1.3 Reactive transport modelling

Corrosion, or charge transfer at a metal-solution interface, involves the following processes:

- Transport of reactants to, and products from, the surface
- Reactions in the bulk aqueous environment
- Charge-transfer reactions at the metal surface

Of these, the reactions in the bulk aqueous environment can be modelled using a range of commercially available software systems (e.g., PhreeqcRM, Geochemist's Workbench), that have been designed specifically to perform equilibrium and kinetic reaction calculations for reactive transport simulators. The basic function of PhreeqcRM is to take species concentrations from the numerical grid blocks of a transport simulation, run geochemical reactions, and return updated species concentrations to the transport simulator. This approach has been used for example to model the transport of iron released by anaerobic corrosion into the surrounding bentonite matrix (Hunter, Bate, Heath, & Hoch, 2007) and it can also be coupled to flow modelling in a geological environment (e.g. (Joyce, et al., 2015)).

3.2.2 Localised corrosion

3.2.2.1 Pitting factors

In radioactive waste disposal 'pitting factors' (typically derived empirically) express the between the average loss of thickness of a surface by corrosion to the maximum loss of thickness on the same surface. Hence a pitting factor of 1 would describe a surface that exhibited a perfectly uniform loss of thickness across the whole surface. Pitting factors can be used to describe surfaces that exhibit true corrosion pits, or those that exhibit uneven/patchy general corrosion. Using pitting factors evaluated on the basis of comparatively short empirical observations is typically considered somewhat conservative, as it assumes that regions that exhibit a greater loss of thickness will continue to do so indefinitely at a rate proportional to that of the average material loss. The latter hypothesis is contrary to what typically observed in long-term field observations, in which pitting factors tend to decrease substantially over time (i.e., the ratio between the maximum pit depth and the depth of general corrosion typically tends to

EURAD (Deliverable n° 1.1) – Initial State-of-the-art of WP ConCorD
Dissemination level: Public
Date of issue of this report: **17/08/2022**

Page 84

decrease with the depth of general corrosion, and thus with time). An authoritative analysis of this effect for buried steel pipeline is available in (Romanoff M. , 1957). Pitting factors can be measured in environments representative of a GDF over the short-term from specimens that have undergone in-situ or laboratory testing. Pitting factors based on corrosion occurring on timescales closer to those anticipated for a GDF have been estimated using archaeological analogues. However, due to the potential differences between the typical exposure conditions and material properties of archaeological analogues compared to those anticipated for a GDF, the directly applicability of knowledge and data associated with these materials is subjected to a substantial degree of uncertainty (King & Kolar, 2018; King F., 2014).

3.2.2.2 Empirical roughening factor

Empirical surface roughening factors are analogous to pitting factors in that they basically aim to provide a topographical model of a corroded surface that is not necessarily based on mechanistic understanding. Surface roughening factors assume that a corrosion process will produce a surface with a given surface roughness profile that deviates from the mean line of the surface within a predefined constraint (e.g., 100 μm). This approach is less conservative than use of an empirical pitting factor as the predicted deviation between surface low and high points does not increase with increasing loss of thickness and is taken as a time-independent constant. This approach is not suitable for true corrosion pitting of passive materials and is better suited for dealing with uneven corrosion of non-passive materials (e.g., copper) (King, Lilja, Pedersen, Pitkänen, & Vähänen, 2010).

3.2.2.3 Empirical localised corrosion growth rate

In a similar manner to that used for extrapolating general corrosion rates to the long-term, it is possible to measure pit depths experimentally as a function of time and develop an empirical pit growth rate curve, which can then be fitted and used to develop empirical models of pit growth rates, in a similar manner to that used in References (Romanoff M., 1957) and (Taylor, Smart, & Porter, 2002), in the form:

$$P = kt^n \qquad (3.1)$$

where P is the maximum pit depth, t is time, and n and k are constants.

3.2.2.4 Electrochemical prediction

A mechanistic approach for estimating whether localised corrosion could occur or not based on electrochemical considerations is by comparison of the free corrosion potential with the critical potential for localised corrosion[1]. The advantage to this approach is that, if the transient conditions within the repository are well characterised, the corrosion potential and critical potential can be measured and

---

[1] Typically, this potential is defined as the pitting potential E_P or the repassivation potential E_{RP} and can be measured at a free surface or within a crevice (in which localised corrosion will onset at a lower potential).

EURAD (Deliverable n° 1.1) – Initial State-of-the-art of WP ConCorD
Dissemination level: Public
Date of issue of this report: 17/08/2022

Page 85

predicted with reasonable accuracy over comparatively long-time scales. When using this approach, the critical potential for localised corrosion can be taken as the pitting/crevice potential, or the pitting/crevice repassivation potential, in the electrochemical conditions of interest (e.g., chemistry of the environment, temperature and redox potential).

The disadvantage to this approach is that it does not enable the prediction of localised corrosion rates, or depth of penetration over time, just whether its occurrence is feasible or not. Measurements of the critical potential for corrosion to occur are influenced by numerous factors (including measurement technique, material properties, microstructure, environment and statistical factors), so it may be necessary to have a large database of measurements to give a high degree of confidence in the critical potential selected.

3.2.3 Modelling chemistry within sites of localised corrosion

A number of authors have applied mass transport and electrochemical models to predict the chemistry within cracks and crevices (e.g. (Turnbull, 1982), (Sharland, 1987) (Turnbull, 2001) (Gunasegaram, Ventaraman, & Cole, 2014)). These models are well established, but they are best suited to aiding understanding of the fundamental processes occurring within sites of localised corrosion rather than making reliable predictions of growth rates. The difficulty with these approaches is defining and justifying the size of the coupled cathode. The cathode area/anode area ratio usually determines the rate of depthwise growth.

3.2.4 Statistical approaches

Statistical approaches are often applied to analyse (a) experimental results from pitting corrosion studies, or (b) inspection results to estimate in service corrosion rates. In the context of these approaches, it has been usual to consider "extreme" corrosion events, so that extreme value analysis has been widely applied. Conventional statistical models, such as extreme value statistics (EVS), or deterministic models with statistically variable input parameters, have been typically applied or proposed. For example, this approach has been applied previously (Taylor, Smart, & Porter, 2002) in the context of the corrosion of carbon steel intermediate level radioactive waste containers in a disposal facility.

Extreme value analysis is a well-established method for extrapolating corrosion or inspection data from small test coupons or inspection sites to the large surface areas of real structures. The analysis is based on the work of Gumbel (Gumbel, 1958). Early applications of the technique to the analysis of corrosion data were described by Aziz (Aziz, 1956) and Eldredge (Eldredge, 1957), and there are numerous other examples in the literature (e.g. (Sato, 1976)). The technique is recommended in ASTM standards on pitting corrosion (ASTM, Standard Guide for Examination and Evaluation of Pitting Corrosion, 2005), (ASTM, 2010) and its application has been reviewed by Kowaka (Kowaka, 1994), Laycock (Laycock, Cottis, & Scarf, 1990), Turnbull (Turnbull, 1993) and Shibata (Shibata, 1996). The review papers provide a detailed discussion of the method.

Extreme value statistics is an approach that can be used to estimate the maximum pit that could form over a period of time by fitting a sample of observed pit depths to an extreme value distribution (e.g., a Gumbel distribution) and extrapolating over the duration of exposure of the container.

Due to the lack of a mechanistic basis, this approach tends to be very conservative, as it enables the prediction of large pit sizes that would normally be bounded by physicochemical constraints.

Another statistical approach that has been applied, is probabilistic assessment of pitting corrosion of copper canisters, based on consideration of the breakdown and repassivation potentials for the pitting

EURAD (Deliverable n° 1.1) – Initial State-of-the-art of WP ConCorD
Dissemination level: Public
Date of issue of this report: 17/08/2022

Page 86

of copper, and the predicted evolution of the environment (Briggs et al., 2020). This approach has been combined with machine learning techniques.

3.2.5 Thermodynamic modelling of environmental chemistry

3.2.5.1 Pourbaix diagrams

Pourbaix (Pourbaix, 1974) developed an approach to understanding aqueous corrosion on the basis of purely thermodynamic considerations. Specifically, he introduced E pH stability diagrams, which indicate what phases are stable as a function of the potential and pH. The potential and pH were chosen as independent variables because they play a key role in corrosion, and because they make it possible to construct stability diagrams (semi) analytically.

Since then, advances in modelling the thermodynamics of electrolytes, and of concentrated solutions at higher temperatures, have made it possible to improve the accuracy of the stability diagrams, but also to perform a range of thermodynamic analyses that go well beyond E pH stability diagrams.

The main objective of studying the thermodynamics of corrosion is to predict the conditions under which a given metal may react with a given environment, leading to the formation of dissolved ions or solid reaction products. Thermodynamics can predict the properties of a system in equilibrium, or, if equilibrium has not been achieved, the direction in which the system will move towards equilibrium. Thermodynamics cannot predict how rapidly the system will approach equilibrium (i.e., it cannot predict the rate of corrosion).

3.2.5.2 Reactive transport modelling

The use of reactive transport models, such as those described in Section 3.3.1, provides a mechanistic basis for estimating the maximum amount of corrosion that can occur in a disposal canister. In the case of copper containers, this type of treatment focused on reaction of copper with sulphide, this species being the key corrodent for the material. Approaches of this type need to take into account both sources (e.g., sulphate reduction by microbiological processes) and sinks (e.g. reaction of sulphide with Fe-bearing phases) of the species of interest, and of transport-related factors. As with standard mass-transport approaches, this can either assume that any corrosive species that reach the container surface will react instantaneously (transport control) resulting in a zero-concentration boundary condition at the interface, or that corrosive species are not fully consumed at the interface leading to a gradual accumulation over time (activation control).

Reactive transport models are typically complex and take account of several physicochemical processes. Depending on their complexity, models of this type can take a long time to construct, run and validate and may require as input a substantial amount of good-quality data. However, once they have been developed, they can be used to estimate a wide range of relevant information (e.g., corrosion potential, pH and chemical speciation) that can be used to support long-term predications of corrosion behaviour (King & Kolar, 2018; King F., 2014).

EURAD (Deliverable n° 1.1) – Initial State-of-the-art of WP ConCorD
Dissemination level: Public
Date of issue of this report: **17/08/2022**

Page 87

3.2.6 Artificial intelligence techniques

3.2.6.1 Neural networks

One of the new artificial intelligence techniques that has been applied to the analysis of corrosion data is artificial neural networks (ANNs). These are an artificial intelligence technique that is increasingly being used for the analysis of complex sets of data. The technique is based on the concept of setting up a series of artificial neurons in a 'layered structure' that are analogous to the networks of neurons in biological organisms' brains, using software engineering techniques. The network can then be 'trained' by providing a set of data with known features, so that when the network is presented with a new set of data it can be used to identify patterns in the data.
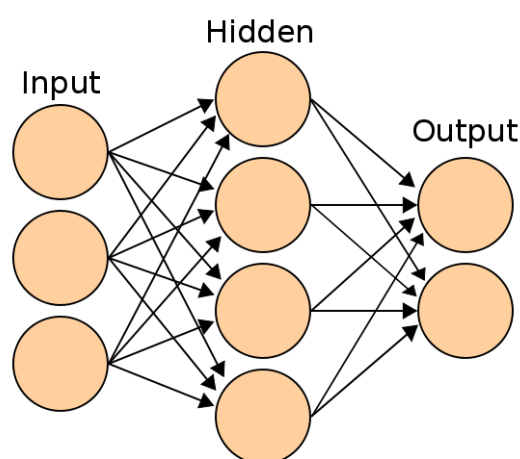
Figure 3-1: Schematic idealised structure of an Artificial Neural network (ANN), showing the input and output layers of neurons and the weighted connections with the inner hidden layers[2]

The training step involves applying weights to the connections between the neurons with the network. ANNs can usefully be used when it is not possible to address a problem with conventional 'rule-based' programming techniques, or there are several variables controlling the behaviour of the system in a non-linear fashion. They are a means of analysing large amounts of data to produce an empirical 'model' of a system, based on experimental data, rather than being a means of developing a model based on scientific principles. There are a number of recent examples of the application of ANNs for dealing with corrosion issues in the literature, such as modelling the relationship between material composition and corrosion behaviour (Simanjuntak, et al., 2015), high temperature corrosion (Osgerby & Fry, 2007) (Kumari, Das, & Srivastava, 2016) (Khadom, 2016), stainless steel corrosion in aqueous environments (Jiménez-Come, Turias, Ruiz-Aguilar & Trujillo, 2015) (Jiménez-Come, Turias, & Ruiz-Aguilar, 2016) (Mareci, Suditu, Trincă, & Curteanu, 2016) (Jiménez-Come, Turias, Ruiz-Aguilar , & Trujillo, 2015) also contains a review of the literature on the use of neural networks to analyse experimental and field corrosion data), analysis of stress corrosion cracking data (Shi, Wang, & D.D. Macdonald, 2015) and electrochemical noise analysis (Hou, Aldrich, Lepkova, Machuca, & Kinsella, 2016). One potential criticism (Gunasegaram, Ventaraman, & Cole, 2014), (Cottis, 2010) of the use of ANNs is that the 'black box' approach does not lead to any fundamental advance in physical understanding of the processes and mechanisms involved but nevertheless ANNs do have potential advantages for processing multi-

---

[2] C. Burnett, from https://commons.wikimedia.org/w/index.php?curid=1496812

EURAD (Deliverable n° 1.1) – Initial State-of-the-art of WP ConCorD
Dissemination level: Public
Date of issue of this report: **17/08/2022**

Page 88

variate data. For this approach to work, it is desirable to have a large data set for the training step and to use some data to test that learning has been successfully achieved. There appear to be a number of aspects of the application of neural networks to corrosion studies that require further development to enable full confidence, but they remain an area of promise to handle data analysis problems that are intractable using more conventional methods.

There are several possible situations where ANNs might be considered for application to the analysis of data obtained in relation to corrosion studies of waste container materials, such as:

- Analysis of experimental data obtained to map out the regions of stability and environmental conditions, for example those conditions which give rise to localised corrosion, or unacceptably high general corrosion rates.
- Analysis of data from sensors from monitoring various aspects of spent fuel disposal during in situ experiments, for example, environmental sensors to monitor fluctuations in environmental parameters, corrosion parameters (e.g., electrochemical noise parameters from corrosion probes installed in the storage environment (Mabbutt, Picton, Shaw, & Black, 2012)).
- Prediction of time to failure as a function of multiple variables (e.g. pH, [Cl], [dissolved O_2], T, applied stress, contamination levels, etc.), based on analysis of a set of data produced by carrying out an experimental matrix, for example using electrochemical techniques, such as polarisation measurements in representative environments (e.g. simulated groundwaters with various contaminant levels).

In order to be able to apply ANNs to analysing experimental corrosion data, it would be necessary to generate sufficient data to train the network and this may require a programme of experimental research to be carried out, for example to:

- Measure breakdown or pitting potentials for materials of interest in a range of potential disposal environments, including normal and fault conditions, using electrochemical techniques (e.g. potentiodynamic polarisation measurements).
- Measure electrochemical noise for materials of interest in a range of potential disposal environments, including normal and fault conditions. The trained network could then be used to process data obtained from on-line sensors systems, for example to detect the onset of localised corrosion.
- Carry out a matrix of experiments to map out the conditions that lead to corrosion under disposal conditions as a function of key variables, such as aqueous chemistry, temperature, surface contamination levels, radiation levels.

The software for creating and operating neural networks is available commercially. More recently, data mining techniques on 'big data' sets, using neural networks and other AI techniques, have been applied to determine empirical correlations between corrosion performance and key metallurgical factors, such as alloy composition and microstructural features, and environmental factors (e.g. as proposed by Li and co-workers (Li, et al., 2015)).

EURAD (Deliverable n° 1.1) – Initial State-of-the-art of WP ConCorD
Dissemination level: Public
Date of issue of this report: 17/08/2022

Page 89

3.3 Copper canister corrosion

Among the models presented in Section 3.2 for quantifying uniform copper corrosion in spent nuclear fuel canisters located in deep geological repositories, the Copper Corrosion Model (CCM) (King et al. 2005, King et al. 2008) has been the most complete approach to the phenomenon. The model accounts for electrochemical processes at the container surface together with reactive transport and heat transfer in the near field, which provide a continuous description of the corroding environment. The equations are solved in a 1D domain using finite difference methods. The first version included the 10 most relevant species when focusing on chloride and oxygen transport-controlled corrosion (Figure 3-2). The model has been progressively updated (King et al., 2010) and extended to long-term anoxic corrosion due to sulphide with the Copper Sulphide Model (CSM) (King, 2008, King & Kolár, 2019).

Next, several relevant issues for a proper estimation of corrosion in spent fuel copper containers are presented. Some of them have been already widely addressed by the CCM and CSM models, such as microbial sulphide production or the interaction of sulphide with Fe-bearing mineral phases, but some others still need to be further analysed and modelled. In this sense, alternative transport models in compacted bentonite have been reviewed, along with the impact of two-phase flow on sulphide fluxes at the nearfield at the early transient stage during groundwater intrusion into the repository. Finally, the last sub-section is fully devoted to irradiation-induced corrosion, which might be relevant in the short-term for dose rates over 100 Gy h^{-1} according to King (King et al., 2010).
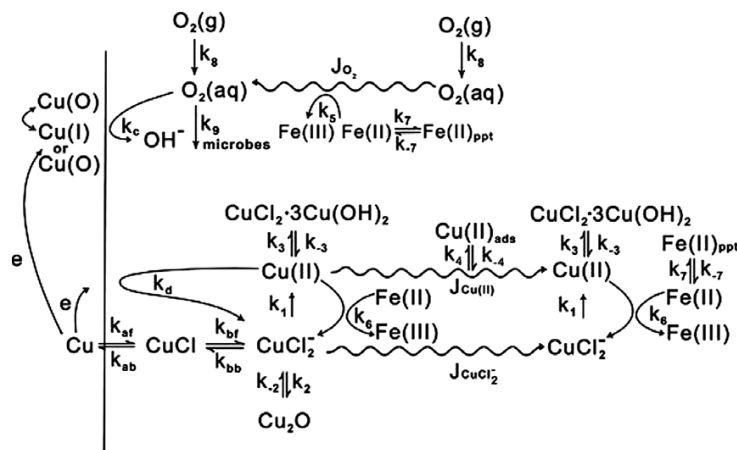
Figure 3-2: Schematic representation of the uniform corrosion sequence of copper in O_2 saturated bentonite containing saline groundwater. The letters j and k refer to diffusive fluxes and rate constants for various processes, respectively (King et al., 2008).

3.3.1 Reactive transport models in compacted bentonite

The diffusion coefficient of dissolved species in compacted bentonite is known to strongly influence corrosion due to the limited mass transport rate of corroding agents from the near field to the metal surface. According to Wersin et al. (Wersin et al., 1994), values of pore diffusivity have an uncertainty of a factor of 10 (Brandberg & Skagius, 1991). In the CCM (King et al., 2008), Fickian diffusion is considered with an effective diffusivity that is directly proportional to empirical values of tortuosity and effective porosity of the medium. The latter assumes that a relevant fraction of available porosity corresponds to dead-end storage pores (King & Kolár, 2019). In the case of sulphide, diffusivity has been estimated experimentally (King et al., 2010).

EURAD (Deliverable n° 1.1) – Initial State-of-the-art of WP ConCorD
Dissemination level: Public
Date of issue of this report: 17/08/2022

Page 90

The definition of effective porosity and the assumptions regarding different types of porosity have led to several mechanistic and empirical approaches for describing diffusion of ions through compacted bentonite. In (Idiart & Coene, 2019), all these models were tested for quantifying the diffusion of the radionuclide ^{36}Cl- across the bentonite backfill in the SFL repository (Sweden). The multi-porosity model (Appelo, 2013) considered three porosity types: free, electrical double layer (EDL), and interlayer, which was assumed to be inaccessible to anions due to its structural negative charge. The size of the EDL porosity was coupled with the porewater ionic strength, for which this model was prone to be more computationally demanding than the alternatives. In this sense, Wersin et al. (Wersin et al., 2014b) simplified the formulation by deriving an empirical expression for the effective diffusion coefficient as a function of bentonite dry density and ionic strength and considering that the interlayer porosity was also devoid of anions.

Van Loon et al. (Van Loon et al., 2007) proposed an empirical approach which related the available porosity to the ionic strength of the external solution for the range between 0.01 and 1mM before applying Archie's law for the effective diffusion coefficient. On the other hand, Ochs and Talerico (Ochs & Talerico, 2004) proposed a table of values of available porosity, effective diffusivity, and distribution coefficient for 38 different elements and oxidation states.

Finally, the Donnan equilibrium model (Birgersson & Karnland, 2009) assumed a single interlayer porosity with net positive charge to compensate the structural negative charge of the smectite sheets. Consequently, a concentration jump appears at the clay-water interface, thus leading to limited transport of anions through the bentonite (anion exclusion) as observed in the results obtained by Idiart and Coene (2019). This hypothesis posed a new uncertainty for the calculation of chloride and sulphide fluxes in the oxic and anoxic corrosion of copper canisters, respectively. In this sense, the CSM model was recently extended with a dual porosity transport model accounting for Donnan equilibrium (King & Kolár, 2019), leading to higher corrosion rates. Idiart et al. (2019) and Pękala et al. (2019a) also applied dual continuum approaches to assess copper corrosion in the canister of a KBS-3V repository due to the presence of sulphide. While the former implemented a model in the reactive transport modelling framework iCP (Nardi et al. 2014), an interface coupling Comsol Multiphysics (COMSOL, 2020) and PhreeqC (Parkhurst and Appelo, 2013), the latter adapted PFLOTRAN to include dual porosity according to the approach proposed by Gimmi and Alt-Epping (2018) (see below). It was found that it had a relatively small effect on the results as compared to the traditional modelling approach, only observing a slightly reduced mackinawite precipitation and increased sulphide fluxes reaching the canister. However, this model did not account for the barriers outside the bentonite buffer, where significant sulphide generation is expected to take place. In both cases, it was concluded that further research was needed for a proper understanding of the impact of considering Donnan equilibrium on the transport of sulphide through compacted bentonite.

In terms of numerical tools for a complete electrochemical description of corrosion, Gimmi and Alt-Epping (2018) derived a Nernst-Planck equation accounting for immobile charge and Donnan equilibrium, which allowed a coupled transport simulation of all components while preserving the different diffusivities depending on their charge and the concentrations in the electrolyte. Note, however, that in that work there is no analysis of corrosion processes, and the scope is restricted to bentonite.

3.3.2   Modelling of sulphide fluxes in the early transient stage (2 phase flow)

Sulphide is considered the main corroding agent for copper canisters during the long anoxic phase in a nuclear waste repository. Its fluxes depend on different sources distributed in the host rock, the backfill and the buffer. On one hand, sulphate-bearing waters and sulphate reducing bacteria (SRB) are the main contributor to the sulphide generation, whereas the formation of iron sulphide phases (mainly mackinawite) though the dissolution of Fe-bearing minerals is expected to be the main sink.

According to the models developed as part of the work in Wersin et al. (2014a) with FASTREACT (FrAmework for Stochastic REACtive Transport, Trinchero et al., 2014) and PFLOTRAN (Hammond et al., 2014), the concentration levels foreseen in a repository are too low for significant corrosion to occur.

EURAD (Deliverable n° 1.1) – Initial State-of-the-art of WP ConCorD
Dissemination level: Public
Date of issue of this report: 17/08/2022

Page 91

Severe damage of the copper coating was only predicted in a few extreme cases that applied multiple conservative assumptions. Similar outcomes were obtained by Cloet et al. (2017), Wersin et al. (2017), Pękala et al. (2019b), Pękala et al. (2020) and the CSM (King et al., 2011). However, these models did not consider a hypothetical early transient stage, during which higher sulphide concentrations may reach the container surface. This scenario, although restricted by the low microbial activity in the buffer materials due to its low porosity, would be possible in the case of relevant sulphide sources together with limited iron availability.

In this sense, Wersin et al. (2014a) analysed the maximum sulphide fluxes that could reach the buffer and the canister assuming that the reduction of sulphates takes place at the backfill/rock interface and no precipitation of iron sulphides, although the early transient phase was not specifically considered in this study. First, the evolution of the gypsum inventory at the backfill and the corresponding sulphate fluxes were calculated with a 1D diffusion-reaction model implemented in PhreeqC (Parkhurst and Appelo, 2013) for both saline and brackish groundwaters in Olkiluoto (Finland). Then, the maximum sulphide flux was derived analytically as a balance between diffusion to the buffer and flow transport to the host rock. It was found that 5-11% of the generated sulphide reached the canister surface, which is enough to induce corrosion failure. However, it was also stated that the complete reduction of sulphate to sulphide was totally unrealistic as ferrous minerals would indeed capture a significant part of the sulphate inventory (see Section 4.2.4).

Besides the geochemistry, the thermal and hydrological conditions in the repository need also to be assessed, which can significantly affect both diffusive and advective transport of sulphide. For example, Briggs et al. (2017) developed a 3D model with COMSOL Multiphysics of sulphide diffusion within the Canadian repository concept (NWMO) and concluded that the isothermal assumption was not realistic as changes in the saturation profile around the canister during the initial thermal transient might have a strong influence on the transport of sulphides until the systems reaches the cool and anoxic state. In this sense, the effect of two-phase flow during the early water intrusion in the repository should be analysed. Significant vapor and liquid fluxes are expected due to the high temperatures at the container surface and the heat dissipation in the near-field. This, together with the motion of trapped gas bubbles, might lead to less regular sulphide fluxes in the short-term than those predicted by Wersin et al. (2014a) or by the CSM model (King and Kolár, 2019), which only consider transport under the stable saturated conditions expected during the long-term anoxic period. A key concern that arises for this is the potential for gaseous H_2S to be transported during the unsaturated period. H_2S is corrosive to copper in dry atmospheres, even at comparatively low concentrations (>3 ppb) and becomes increasingly more corrosive at higher temperature and higher relative humidity. H_2S is also corrosive to carbon steel and under certain conditions can lead to localised corrosion and environmentally assisted cracking.

3.3.3 Modelling of microbial sulphide production

In the early non-saturated phase of the repository, oxygen consumption by aerobic microbes, which is expected to limit corrosion, was already implemented in the first version of the CCM model with a rate constant derived from in situ tests (King et al., 2008). This protective effect is removed when the system turns anoxic and microbial reduction of sulphate becomes dominant. In this sense, this model was updated by King et al. (2010) with 15 processes, including microbial sulphide production, and a mass balance for each organic agent (CCM-MIC), so the microbial population could be tracked in space and time. According to King and Kolar (2006), who used the model to predict the microbial population in a Canadian repository, the presence of microbes in the near-field was minimal and the sulphide concentrations reaching the canister were predicted to be small due to mackinawite precipitation in the buffer and backfill. Moreover, the elevated temperatures and lack of water foreseen for the initial transient described in Section 4.2.2 were expected to suppress most of the microbial activity.

The definition of the kinetic rate constant for microbial sulphate reduction was addressed by the joint SKB-Posiva Integrated Sulphide Project. Bengtsson et al. (2017) quantified this parameter ($6.1 \ 10^{-11} \ s^{-1}$) after monitoring radioactively labelled sulphate in an experimental setup consisting of

EURAD (Deliverable n° 1.1) – Initial State-of-the-art of WP ConCorD
Dissemination level: Public
Date of issue of this report: 17/08/2022

Page 92

copper test plates buried in compacted bentonite with groundwater containing SRB (Pedersen, 2010). Results showed no SRB activity for bentonite wet densities of 1900 kg/m3 and above, whereas iron sulphide precipitates were observed on the plate surface when reducing the compactness to 1750 kg/m3. The maximum sulphate reduction rate determined in MX-80 bentonite was $8.2 \cdot 10^{-7}$ mol s^{-1} m^{-3} in bentonite porewater. The experimentally measured kinetic rate constant was used to feed a transport model using finite differences as a next step towards the quantification of the amount of sulfide reaching the surface of the test plates.

The CSM model has been recently extended by King et al. (2021) with two different pathways for microbial sulphate reduction: organotrophic (dissolved organic carbon as electron donor) and chemotrophic (H$_2$ as electron donor). It has also been applied to the KBS-3 concept for the disposal of spent nuclear fuel, leading to the precipitation as mackinawite of 98.5% of the microbially generated sulphide due to the dominance of siderite over organic matter in the buffer and the backfill. As a result, only 3 μm of copper would be corroded after one million years. However, this outcome might be less beneficial in repositories with higher amounts of organic material and lower gypsum and reactive Fe(II) contents, since the system would become sulphate limited and a smaller fraction of the microbially produced sulphide would precipitate before reaching the canister.

The most recent 3D reactive transport sulphide model developed for the KBS-3 repository in Olkiluoto, Finland (Posiva 2021) also considers organic carbon and H2 as pathways for microbial sulphate reduction, which is represented with a kinetic Monod model. The selected maximum sulphate-reducing bacteria (SRB) activity rate constants were defined as 5×10^{-5} and 10^{-4} mol sulphide/(Lwater, respectively, based on experimental and field studies from the literature. The simulations showed corrosion depths below 1 mm averaged over the whole copper canister surface after one million years. The maximum cell-resolved depths, however, were higher, in the range of one to a few millimeters.

3.3.4   Modelling the interaction of sulphide with Fe-bearing mineral phases

In the SR-Site safety assessment, it was assumed that pyrite dissolution could lead to the corrosion of the canister (SKB, 2010). The extent of corrosion was estimated according to mass-balance and mass-transport, leading to a maximum depth of canister corrosion of 0.1 mm and 0.9 mm for MX-80 and Ibeco-RWC bentonites, respectively. However, when the limited solubility of pyrite and the low diffusivity of sulphide were considered, it was found that only the pyrite within 2 cm of the canister surface contributed to corrosion after one million years, resulting in 1 μm of corrosion for the reference values of solubility and diffusivity (SKB 2010). Simulations using the CSM (King et al., 2011) predicted long-term corrosion rates of the order of <1 nm/year, of the same order of magnitude as those predicted for the SR-Site safety assessment (SKB, 2010), with the contribution of pyrite dissolution being less than 5% of the total extent.

Similarly, Marty et al. (2010) used the reactive-transport code KIRMAT to predict the alteration of bentonite for the French nuclear waste programme. In this case, as well as in the model developed with CRUNCH by Bildstein et al. (2006), the rate constant for the anaerobic dissolution of pyrite was taken to be that of the oxidative dissolution. In a later extension of the CSM (King and Kolár, 2019), the rate constant for the anaerobic dissolution of pyrite was excluded from the model after a review of its properties by King (2013) due to its extremely low solubility. Instead, the CSM provided a wider description of the interaction between sulphide and ferrous minerals, especially the precipitation of FeS leading to reduced sulphide fluxes. In this sense, four Fe(II) solid phases were included in the reaction scheme: biotite (K(Mg$_{0.6-1.8}$Fe(II)$_{2.4-1.2}$)(Si$_3$Al)O$_{10}$(OH,F)$_2$), which is initially present in the backfill and rock layers, and which undergoes temperature-dependent dissolution releasing Fe(II), pyrite (FeS$_2$), which is expected to be fully oxidized during the aerobic phase, iron carbonate (FeCO$_3$), which is initially present in both the buffer and backfill materials, and which precipitates reversibly in the presence of excess Fe(II), and finally mackinawite (FeS), which precipitates if the dissolved Fe(II) and HS$^-$ concentrations exceed the value of the solubility product. With all these considerations, and assuming

EURAD (Deliverable n° 1.1) – Initial State-of-the-art of WP ConCorD
Dissemination level: Public
Date of issue of this report: 17/08/2022

Page 93

the expected conditions in a KBS-3 repository, the long-term corrosion extent was predicted to be less than 10 µm after one million years.

An alternative hydrogeochemical model using PhreeqC (Parkhurst and Appelo, 2013) was presented by Wersin et al. (2014a). A similar outcome was obtained, including copper corrosion limited to 1-1.7% of the total inventory, and sulphide fluxes controlled by mackinawite precipitation.

In the 3D reactive transport model used for the recent safety case of the spent fuel repository in Olkiluoto, Finland (Posiva 2021), the main sources of iron reacting with sulphide are ferric (oxyhydr)oxides present in the buffer and backfill as accessory minerals. The reaction of sulphide with Fe(III) follows a complex redox reaction scheme leading to oxidized sulfur species (elemental sulfur, polysulphides) and Fe(II). The latter reaction products further react with sulphide to form iron sulphide (mackinawite).

3.3.5 Modelling irradiation-induced corrosion

The radiation from a spent fuel canister could affect the chemical conditions in the near field. The ionizing radiation will produce both molecular and radical oxidants and reductants through radiolysis. The concentrations of the different species formed during radiolysis depend on the type of radiation, the dose rate, the composition of the aqueous solution, and the material of fabrication and wall thickness of the canister (King, 2010). In the gamma-irradiated system, the reducing electron and hydrogen radicals (e- and H·), formed with yields higher than oxidizing species, rapidly react with both H_2O_2 and O_2, decreasing the concentrations of the corroding species (Soroka et al., 2021).

Apart of the extended amount of experimental work, a few numerical simulations which include the effect of water radiolysis on the iron and copper corrosion have also been performed in literature (Soroka et al., 2021; Wada et al., 2016). Soroka et al. (2021) performed numerical simulations using MAKSIMA-CHEMIST and considered the full set of chemical reactions describing the radiation chemistry of water together with a reaction of Cu oxidized by O2. The simulations showed that the amount of molecular oxygen produced directly via γ-radiolysis of water and via catalytic decomposition of radiolytically produced H2O2 on the oxide surface could account for the amount of corrosion observed in the experiment. Wada et al. (2016) performed radiolysis calculations with the radiolysis code SIMFONY and determined the temporal evolution of the generated O2, H2 and H2O2 by gamma radiation (no comparison with experimental data was included). Recently, the complete set of kinetic reactions dealing with recombination of water radiolysis species have been modelled in Comsol Multiphysics in the context of spent fuel corrosion (Riba, 2020).

EURAD (Deliverable n° 1.1) – Initial State-of-the-art of WP ConCorD
Dissemination level: Public
Date of issue of this report: 17/08/2022

Page 94

3.4   Steel canister corrosion

3.4.1   Modelling of steel canister corrosion

The available models of the interaction between bentonite / steel is also available in the deliverable 2.5 of the ACED work package of EURAD.

Modelling studies on iron canister corrosion in contact with different geotechnical barriers (i.e. bentonite, cement) or pure clay minerals (i.e. montmorillonite) performed in the last 15 years (Savage, 2012) have been mainly simulated by mechanistic reactive transport models in porous media, including more or less simplifications (Montes-H et al., 2005; Bildstein et al., 2006; Wilson et al. (2006a, 2006b); Hunter et al., 2007; Wersin et al., 2008; Samper et al., 2008, 2016; Pena et al. 2008, Savage et al., 2010; Marty et al., 2010; Lu et al., 2011, Bildstein et al. 2012; Mon et al. 2017, Chaparro et al. 2021). Most of the works mentioned are related to long term simulations (> 10 000 years) predict that magnetite is the principal steel corrosion product in contact with bentonite, along with significant alteration of the clay minerals to a mixture of non-swelling silicates, such as chlorite, berthierine or cronstedtite and zeolites (Ngo et al., 2014; Wilson et al. 2015). Although, some authors have focused on the principal reaction products (i.e., magnetite) considering sorption of Fe on clay surfaces (Hunter et al., 2007; Samper et al., 2008; Lu et al., 2011), others have tried to model the growth of iron-bearing aluminosilicates (Wersin et al., 2008; Savage et al., 2010; Marty et al., 2010). On the other hand, Peña et al. (2008) modeled the attenuation of the corrosion of carbon steel canisters due to the influence of diffusive transport through the corrosion product and compared it with data from Smart el al. (2006) that studied the corrosion rate of steel in bentonite under a wide range of conditions.

In the first modelling works, mineral dissolution-precipitation were originally treated as equilibrium reactions (e.g., Montes-H et al., 2005; Bildstein et al., 2006), but a posterior, some of these processes have been treated kinetically (Savage et al., 2010; Lu et al., 2011). As later discussed by Lichtner and Carey (2006), the uncertainties associated with kinetic data do not justify that equilibrium assumptions are considered. Processes of aqueous speciation, cation exchange and clay edge protolysis have also been included (Hunter et al., 2007; Wersin et al., 2008; Savage et al., 2010). Although some modelling studies (Wersin et al., 2008) have shown that the zone undergoing mineral transformation in a repository may remain spatially limited (a few centimetres) for very long times, early works did not address changing physical properties of the bentonite with time (either increased hydraulic conductivity or clogging by corrosion products), nor the kinetics of clay transformation (Savage et al., 2010).

Most of the works mentioned above are described and summarized in the review of Savage (2012). More recent reviews (Bildstein and Claret, 2015, Claret et al. 2018, Bildstein et al. 2019) have provided new insights and information on model development. For example Bildstein and Claret, (2015) indicated not only the dissolved / precipitated solids expected or considered in the system, but also the modifications of mineral properties (especially related to the exchange capacity, the interlayer cation content, and the swelling ability of clay minerals) and transport properties through modifications in porosity, permeability and tortuosity. Claret et al. (2018) presented a review focused on recent improvements and perspectives for reactive transport modeling showing a detailed description of the main modelling approaches, assumptions and simplifications used in the most recent reactive transport model focused at the scale of the disposal cell. Bildstein et al. (2019) reviewed both, reactive transport at the lab scale and at the scale of the disposal cell.

Some key issues for modelling of iron-bentonite interactions arising from these studies are:

•   One of the most sensitive parameters is the corrosion rate;

•   The most abundant corrosion product predicted by the models in the long-term is magnetite, sometimes with Fe-carbonates (siderite) and Fe-silicates (greenalite), sometimes incorporating Al (berthierine, cronstedtite);

EURAD (Deliverable n° 1.1) – Initial State-of-the-art of WP ConCorD
Dissemination level: Public
Date of issue of this report: 17/08/2022

Page 95

- The choice of Fe solubility-limiting solids at the corroding steel surface is important, since this defines the concentration of iron at the canister boundary and hence, the concentration gradient of Fe across the bentonite. Some authors have chosen to use solids with very low solubilities, such as magnetite or pyrite (e.g. Bildstein et al., 2006; Wersin et al., 2008), but there is mineralogical evidence that more soluble, poorly crystalline iron oxyhydroxide may be more relevant (Milodowski et al., 2009).

- The transformation of clay minerals into Fe-chlorite, and the timing, very much depend on whether it is included as a secondary mineral (in which case it is the most stable phase and precipitates from the beginning of the simulation or it results from a ripening process

- Numerical studies often differ on the precise nature of the main secondary minerals;

- There is strong evidence that the physical properties of compacted bentonite in contact with steel degrade over very short timescales. For example, samples of bentonite from corrosion experiments Carlson et al., (2008) show increased hydraulic conductivity after only 3 years of reaction.

- Primary minerals in clay are often destabilized in favor of Fe-phyllosilicates or zeolites if they are allowed to precipitate;

- Detailed mineralogical investigations of compacted bentonite from steel corrosion experiments show greatest penetration of Fe into the bentonite matrix along hairline microfractures that radiate outwards from the corroding metal. Milodowski et al. (2009) consider that: "The early formed fractures may have represented potentially important pathways for gas and solute transport during the experiments. The irreversible shrinkage of the bentonite, as a result of interaction with Fe released from corroding iron or steel may therefore be significant in evaluating the long-term behaviour of the bentonite seal and the transport of gas and solutes around corroding waste canisters emplaced in bentonite backfill.

- The extent of the perturbation is always predicted to be limited to a few centimetres, up to 20 centimetres into the clay barrier

- Porosity clogging is considered in some simulations under different assumptions.

- Complete inhibition of the corrosion process has never been observed, even if a dense corrosion product layer is often identified; and the ubiquity of magnetite in simulation results as the dominant corrosion product in the long-term is questioned by many experimental results and archaeological analogues.

Hydrogen, generated as part of the anaerobic corrosion of steel, has been ignored in simulations carried out thus far, except as a monitor of the overall corrosion rate of the steel. Some experimental studies suggest that hydrogen may act as a catalyst for the chemical reduction of aqueous sulphate (e.g. Truche et al., 2009). Very recently, Leupin et al. (2021) have indicated by two-phase flow modelling that the consumption of water by the corrosion outpaces the diffusion of water through the bentonite, leading to shrinkage micro-fractures in bentonite that act as preferential pathways for corrosion products.

Another approach to iron corrosion modelling was presented by Bataillon et al. (2010). They developed the Diffusion Poisson Coupled Model (DPCM) as a tool to investigate the corrosion processes at the surface of the carbon steel canisters. The numerical scheme was implemented in the simulation code CALIPSO. This code was recently coupled with a geochemistry-transport code, Kirmat (Gerard et al. 1998). This makes it possible to give a realistic representation of both the corrosion behaviour of iron as well as the alteration of clay base material. More recently, another model (Marion, 2014, Mohamed-Said, 2017) has also been developed to predict the evolution of the corrosion rate of carbon steel under a protective deposit.

EURAD (Deliverable n° 1.1) – Initial State-of-the-art of WP ConCorD
Dissemination level: Public
Date of issue of this report: 17/08/2022

Page 96

This model was proposed to describe the oxidation of iron in anaerobic neutral or slightly alkaline conditions. These chemical conditions correspond to those expected in the French HLW disposal concept. The model allows assessing the evolution of the carbon steel corrosion rate (reduction by oxide layer formation), the chemical species release and the characteristic time of these processes. The model assumes that the solution is in contact with a dense disordered spinel-like oxide layer which covers the iron. Two interfaces bound the oxide layer: (1) The inner interface which corresponds to the metal/oxide layer; and (2) The outer interface which corresponds to the oxide layer/solution interface. The metal (an electronic conductor) could be charged either by accumulation or depletion of electrons. The solution (ionic conductor) could be charged either by accumulation of cations or anions. The oxide layer is a mixed electronic and ionic conductor. The outer and the inner interfaces could move with time. The model considers the electrostatic and kinetic effects and accounts for moving boundaries. The electrostatic module gives the potential profile in the solution-oxide layer–metal system. The kinetics module gives the concentration profiles; one per each charge carrier. The moving boundaries module gives the locations of the two interfaces which bound the oxide layer. These three modules are coupled because each module involves the solution of the others. Bataillon et al. (2010) tested the DPCM in a simplified situation where the locations of the outer and the inner interfaces are fixed and after that with moving boundaries. These data could be used to estimate the lifetime of the carbon steel overpack and the pressure rise resulting from hydrogen release. The convergence of the scheme was studied by Chainais-Hillairet et al. (2015) for the two-species model on a fixed domain. Chainais-Hillairet and Gallouët (2016) presented an updated version of the model of Bataillon et al. (2012) by studying the pseudo-stationary state for a corrosion model. The approach implemented in the CALIPSO code has the potential to be coupled with multicomponent reactive-transport models to study the interactions at the interface steel/iron-bentonite under typical HLW-EBS conditions and the effects of corrosion products on the bentonite.

Table 3-1 provides a comparison of the main assumptions and results obtained in the previously explained modelling exercises at the disposal scale and below is given more detail of each work.

Bildstein et al. (2006) modelled the interactions of a carbon steel canister with the MX-80 bentonite and a clay formation with a 1D purely diffusive model under full saturation conditions. The model accounts for a 7 cm thick stainless steel canister, an 80 cm thick MX-80 bentonite-based EBS, and a 10 m long geological barrier of clay host rock. The reaction-transport code CRUNCH was used to investigate the iron-clay interactions at 50 ºC over 10000 years. A constant corrosion rate of 4.3 µm/y was considered. They considered the following corrosion products: iron oxides and hydroxides, iron carbonates, and iron-rich smectite and Fe-phyllosilicates. Their simulations showed that most of iron released during corrosion processes was partly immobilized by the precipitation of iron oxides (mainly magnetite) and small amounts of siderite. In the bentonite or the argillite in contact with the container, the primary clay minerals are destabilized and iron-rich serpentine-like minerals precipitate as observed in the experiments (cronstedtite and berthierine). These minerals show low cation exchange and swelling capacities (Montes-H et al., 2005).

King (2007) described a conceptual model for corrosion of a carbon steel (C-steel) used fuel container in a deep geological repository in sedimentary rock. The model takes into account various corrosion processes that might affect the container in the repository environment. Some processes, such as uniform corrosion and localized (pitting) attack, are specifically included in the conceptual model for the calculation of the used fuel container lifetime. Other processes, such as hydrogen-related effects, stress corrosion cracking, microbiologically influenced corrosion, preferential weld corrosion, and dry air oxidation are excluded from the conceptual model. This is based on the assumptions that either the environment will not support these processes or that these corrosion processes can be avoided by proper container design and fabrication procedures. The validity of these assumptions would still need to be demonstrated in the future through more-detailed engineering assessment, mathematical modelling, and experimental studies. The extent of uniform corrosion should be assessed through a combination of (i) mass-balance arguments in the case of aerobic conditions, (ii) empirical corrosion rate data for the anaerobic phase, and (iii) a mechanistic mixed-potential model to provide support and

EURAD (Deliverable n° 1.1) – Initial State-of-the-art of WP ConCorD
Dissemination level: Public
Date of issue of this report: 17/08/2022

Page 97

justification for the calculations of the rate of wall loss. This combination of empirical calculations and mechanistic modelling provides a justifiable, robust prediction of the long-term uniform corrosion behaviour of a C-steel used fuel container. Similarly, the effect of localized corrosion on the lifetime of C-steel containers should be assessed through a combination of empirical data and mechanistic modelling. Empirical data can be used to estimate the time-dependence of the degree of localization, whereas mechanistic modelling is used to justify these long-term predictions. Preliminary C-steel corrosion assessments suggest that, based on a combination of uniform and pitting corrosion, the range of wall penetrations will be 9-34 mm after 10,000 years and 34-175 mm after 100,000 years. It is expected that a steel container would still have sufficient remaining wall thickness and mechanical strength to avoid container failure or through-wall penetration for a period of more than 10,000 years after it is placed in a repository in sedimentary rock. This analysis suggests, therefore, that C-steel containers can provide containment of used fuel for substantial periods of time in a deep geological repository in sedimentary rock.

Wersin et al. (2008) studied the impact of iron components released from the canister corrosion on the bentonite buffer (MX-80) for the KBS-3H concept at the Olkiluoto site in Finland. They performed 1D diffusion reactive transport model simulations with CrunchFlow. They accounted for iron corrosion, cation exchange, protonation/deprotonation, Fe(II) surface complexation and thermodynamic and kinetic mineral dissolution/precipitation. They concluded that the extent of the bentonite zone transformed to non-swelling material is likely to remain spatially limited (a few centimetres) for very long times.

Samper et al. (2008) presented a 1-D and 2-D axisymmetric water flow and multicomponent reactive solute transport models to simulate canister corrosion, the interactions of corrosion products with bentonite and the long-term hydrochemical evolution of porewater composition in the near field of a repository in fractured granite. Numerical simulations were performed at a constant temperature of 25 ºC for 0.3 Ma. Coupled hydrogeochemical calculations of interactions of corrosion products with bentonite have been performed with CORE2D V4. They found that: (1) Magnetite is the main corrosion product; (2) Fe diffusion from canister into bentonite leads to magnetite precipitation in the buffer; (3) Siderite precipitation is small due to the limited carbonate availability; (4) Corrosion causes an increase of pH in the bentonite; (5) Proton surface complexation is the main pH buffering mechanism. Other mechanisms such as Fe^{2+} exchange and calcite and iron minerals dissolution/precipitation are much less effective; and (6) Magnetite precipitation causes a reduction of porosity in bentonite. The largest changes in porosity occur at the canister–bentonite interface. Corrosion products have a larger volume than carbon-steel, but not large enough to clog bentonite pores. Lu et al. (2011) presented an updated version of the model of Samper et al. (2008), which considers 3 types of sorption sites in the bentonite, kinetically-controlled canister corrosion and magnetite precipitation, and the competition of dissolved Ni^{2+} for sorbing sites. Simulations were carried out with CORE2D V4 at a constant temperature of 25 ºC for a time horizon of 0.3 Ma. Model results show that: (1) Accounting for kinetically-controlled canister corrosion leads to a significant reduction in the corrosion rate; (2) The uncertainties in the surface complexation model play a minor role in the time evolution of the computed pH in the bentonite and the granite. The computed concentrations of dissolved and sorbed Fe, on the other hand, are very sensitive to changes in the surface complexation model; (3) The apparent Kd of Fe is 10 times larger for the triple-site sorption model; (4) The concentration of dissolved Fe computed with kinetic magnetite precipitation is smaller than that obtained at local equilibrium; and (5) The competition of Ni^{2+} for sorption sites affects significantly the chemical evolution of the bentonite porewater. The pH in the bentonite porewater decreases compared to the value computed without Ni transport because the sorption of Ni^{2+} releases protons. The sorption of Ni^{2+} leads to a smaller concentration of sorbed Fe and a larger concentration of dissolved Fe in the bentonite water for $t < 10^5$ years.

Savage et al. (2010) reported a model of the iron-bentonite interactions based on natural analogues. They claimed that the sequence of the alteration of the clay by Fe-rich fluids may proceed via an Ostwald step sequence. They modeled iron corrosion and the alteration of the MX-80 bentonite by incorporating processes of nucleation, growth, precursor cannibalisation, and Ostwald ripening (Steefel and Van

EURAD (Deliverable n° 1.1) – Initial State-of-the-art of WP ConCorD
Dissemination level: Public
Date of issue of this report: 17/08/2022

Page 98

Cappellen, 1990) to address the issues of the slow growth of bentonite alteration products by modifying the computer code QPAC. They modeled iron corrosion (corrosion rate of ~2 µm/year) and the alteration of MX-80 bentonite in a typical EBS environment. Their model neglected protonation-deprotonation reactions at clay edge sites and cation exchange reactions. They considered two model cases; one with fixed reactive surface areas for secondary minerals; and one with time-dependent variation of the surface areas of secondary mineral. Simulations with fixed mineral surface areas showed that berthierine dominates the solid product assemblage, with siderite replacing it at simulation times greater than 10.000 years. The simulations with time-dependent mineral surface areas show the following sequence: magnetite-cronstedtite-berthierine-chlorite. The evolution of the secondary minerals is somewhat different to that predicted by the fixed surface area model. Near to the corroding canister, at first magnetite is the dominant Fe-bearing mineral; this is followed by cronstedtite, which dominates between ~0.04 years and 500 years. Berthierine is again present throughout, but in reduced quantities compared with the fixed surface area model; after 500 years cronstedtite dissolves away and berthierine is the dominant Fe-bearing mineral. Eventually, after about 5.000 years, chlorite grows in, using the berthierine surface growth sites rather than nucleating directly. Further into the clay, there is much less Fe-based mineral precipitation than in the fixed surface area case, with only small amounts of berthierine present.

Marty et al. (2010) modeled the long-term alteration of the engineered bentonite barrier in an underground radioactive waste repository. Their study focused on the feedback effects of geochemical reactions on the transport parameters of compacted MX-80 bentonite. The system was modelled in reducing conditions by using the KIRMAT code. The model considers a 1 m thick buffer of MX-80 bentonite which is in contact on one side with a geological fluid (Callovo-Oxfordian groundwater at 25 ºC) diffusing into the engineered barrier. Their calculations assumed a constant temperature of 100 ºC to estimate the maximum thermal effect on the mineralogy of the engineered barrier. The model was run for 105 years. By considering the temperature and the long-term evolution of the system, the mineralogical transformations were considered as being more important than the surface complexation and cation exchange reactions. As a consequence, these reactions were neglected in the model. After 100000 years of simulated mass transport-reaction, the model predicted mineralogical modifications of the EBS in contact with the geological interacting fluid and with Fe^{2+} ions provided by the corrosion of the steel overpacks. According to the degree of smectite transformations the mineralogical modifications of the MX-80 bentonite until 100000 years showed three distinct zones: (1) The first zone results from the mass transport of the groundwater through MX-80 bentonite. The resulting alteration front corresponds to a strong illitization of the montmorillonite together with the precipitation of quartz, saponite and vermiculite; (2) In the middle of the EBS, the volume of montmorillonite remains constant. The saponitization and the illitization processes can be distinguished in lower proportions as minor phase; and (3) The third alteration front is constituted by significant precipitations of Fe(II)Al-chlorite, Fe(II)-saponite and magnetite in contact with the steel overpack. The precipitation of these phases decreases significantly the porosity of the EBS. Marty et al. (2010) concluded that only the outer parts of the simulated system are significantly affected. The dissolution of the montmorillonite contained in the MX-80 bentonite is mainly observed in the zone influenced by the groundwater mass transport and partly in a zone adjacent to the container.

Ngo et al. (2014) presented a coupled transport-reaction model for the long-term interactions of iron, bentonite and Callovo-Oxfordian (COX) claystone which extended the work of Marty et al. (2010) by investigating the influence of the reactive surface area of the primary minerals on the bentonite and the COX claystone and the diffusion coefficient on the evolution of the iron-bentonite system.

Wilson et al. (2015) presented three fully-coupled reactive transport models of a steel-bentonite interface to provide new insights into the nature of steel-bentonite interactions, especially the potential for the alteration of the montmorillonite component of bentonite to iron-rich clay minerals. The conceptual model comprises a 1D cross section through a cylindrical bentonite/sand buffer (70 cm thick) that surrounds a steel overpack and inner waste package with a combined diameter of 82 cm. The temperature was set at a constant value of 70 ºC. In the simulations, which were undertaken using the multi-purpose

EURAD (Deliverable n° 1.1) – Initial State-of-the-art of WP ConCorD
Dissemination level: Public
Date of issue of this report: 17/08/2022

Page 99

modelling code QPAC, the following processes were included: steel corrosion, mineral dissolution, mineral precipitation, cation exchange, diffusion and porosity evolution (Archie's Law). The three models simulated were: (1) steel corrosion reaction applied on a boundary directly in contact with bentonite at a fixed rate; (2) steel corrosion reaction applied on a boundary directly in contact with bentonite at a diffusion-limited rate; and (3) a corrosion cell representation with a fixed steel corrosion rate. In models 1 and 3 steel corrosion was assumed to occur at a fixed rate of 1 µm/y while in Model 2, the corrosion reaction was assumed to be diffusion limited. The extent and nature of the alteration predicted by the models was found to be sensitive to model conceptualisation. The corrosion cell assumption leads to steel corrosion products including magnetite and siderite and the alteration of primary minerals to berthierine. In contrast, the boundary corrosion assumption with a fixed steel corrosion rate leads to quicker alteration to iron-rich clay minerals. If the diffusion-limited corrosion rate assumption is made, the steel corrosion rate varies over time as the bentonite porewater composition evolves, and the spatial extent of alteration is much more limited (mm scale).

Samper et al. (2016) presented a non-isothermal reactive transport model for the long-term (1 Ma) interactions of the corrosion products and compacted bentonite in a HLW repository in granite. Simulations were carried out with the multicomponent reactive transport code CORE2D V4. Canister corrosion causes an increase in the pH and the concentration of dissolved Fe^{2+} of the bentonite porewater. Iron precipitates as magnetite and siderite and sorbs via cation exchange and surface complexation on weak sites. The largest pH in the bentonite is almost 9.5 at $2 \cdot 10^5$ years. Several fronts are observed in the concentration of dissolved Fe^{2+}, pH and Eh which are related to sorption and mineral dissolution/precipitation fronts. Magnetite is the main corrosion product and its precipitation reduces significantly the porosity of the bentonite barrier near the canister and could even clog the pores. The thickness of the bentonite zone affected by the decrease of porosity increases with time and is equal to 7 cm at t = 1 Ma. A detailed sensitivity analysis has been performed to changes in model parameters and conceptual model assumptions.

Mon et al. (2017) presented a non-isothermal multicomponent reactive transport model of the long-term (1Ma) interactions of the compacted bentonite with the corrosion products of a carbon-steel canister and the concrete liner of the engineered barrier of a HLW repository in clay. Simulations were carried out with CORE2D V4. Model results show that: (1) Magnetite is the main corrosion product and its precipitation reduces significantly the porosity of the bentonite near the canister; (2) The degradation of the concrete liner leads to the precipitation of secondary minerals and the reduction of the porosity of the bentonite and the clay formation at their interfaces with the concrete liner. The reduction of the porosity becomes especially relevant at t=10^4 years; (3) The zones affected by pore clogging at the canister-bentonite and concrete-clay interfaces at 1 Ma are approximately equal to 1 and 3.3 cm thick, respectively; (4) The hyper-alkaline front (pH > 8.5) spreads 2.5 cm into the clay formation after 1 Ma. Sensitivity runs were performed to analyse the uncertainties in cation exchange selectivities and evaluate the relevance of surface complexation reactions, kinetic smectite dissolution, and Mg-saponite precipitation.

Chaparro et al. (2021) used, a 1D radial reactive transport model in order to better understand the processes occurring during the long-term iron-bentonite interaction. The numerical model accounts for diffusion, aqueous complexation reactions, mineral dissolution/precipitation and cation exchange at a constant temperature of 25 °C under anoxic conditions. Our results suggest that Fe is sorbed at the montmorillonite surface via cation exchange in the short-term, and it is consumed by formation of the secondary phases in the long-term. The numerical model predicts precipitation of nontronite, magnetite and greenalite as corrosion products. Calcite precipitates due to cation exchange in the short-term and due to montmorillonite dissolution in the long-term. Results further reveal a significant increase in pH in the long-term, while dissolution/precipitation reactions result in limited variations of the porosity. A sensitivity analysis has also been performed to test the effect of selected parameters, such as corrosion rate, diffusion coefficient and composition of the bentonite porewater, on the corrosion processes.

EURAD (Deliverable n° 1.1) – Initial State-of-the-art of WP ConCorD
Dissemination level: Public
Date of issue of this report: 17/08/2022

Page 100

3.4.2 Modelling gas generation due to corrosion

One of the main concerns about the anaerobic corrosion of ferrous materials in a repository, is the production of hydrogen, due to its potential implications for damage to the structure of the EBS and the possible transport of gaseous radionuclides to the biosphere. A model known as SMOGG (Simple Model for Gas Generation) has been developed, with the aim of predicting the amount of gas that may arise due to both corrosion and radiolysis, under various conditions. Literature reviews and assessments of the corrosion rate data for steel and Zircaloy (Smart & Hoch, 2010), and reactive metals (Magnox, uranium and aluminium, (Hoch, Smart, Wilson, & Reddy, 2010)]) have been prepared to identify corrosion data that should be applied in the SMOGG model to predict the amount of gas produced by anaerobic corrosion.

EURAD (Deliverable n° 1.1) – Initial State-of-the-art of WP ConCorD
Dissemination level: Public
Date of issue of this report: 17/08/2022

Page 101

Table 3-1: Comparison of steel corrosion modelling for deep geological disposal.

Reference	Type of interface	T (ºC)	Simulation time (years)	Corrosion rate	Assumptions	Main corrosion product	Main secondary minerals	Maximal perturbation extent	Relevant results
Bildstein et al. (2006)	Fe-MX80 bentonite	50	10.000	Constant (4,3 µm/y)	1D diffusive model Porosity feedback effec	Magnetite	Cronstedtite Berthierine	5 cm	Porosity clogging after 5.000 years
Wersin et al. (2008)	Fe-MX80 bentonite	100	500.000	Constant (1 µm/y)	1D model (Test case D0) Porosity update Clay reactions are considered Use of cation exchange and surface complexation	Magnetite	Cronstedtite Berthierine	Few cm	The interaction of Fe with bentonite remains spatially limited for very long times mainly because of Fe clay re-precipitation and diffusional limitation
Samper et al. (2008)	Fe-FEBEX bentonite	25	300.000	Constant (0.2 µm/y)	1D and 2D model No reactivity for clay minerals Use of cation exchange and surface complexation	Magnetite	Siderite Goethite	7 cm	Bentonite porosity decreases due to magnetite precipitation (no clogging) Proton surface complexation is highly effective in buffering pH in bentonite
Savage et al. (2010)	Fe-MX80 bentonite	-	1.000.000	Constant (~2 µm/y)	Time-dependent variation of reactive surface areas for the Fe-bearing minerals The sequence of the alteration of the clay by Fe-rich fluids may proceed via an Ostwald step sequence	Sequence of precipitation: magnetite-cronstedtite-berthierine-chlorite	Cronstedtite Berthierine	-	The secondary minerals evolution is different to that predicted by the fixed surface area model
Marty et al. (2010)	Fe-MX80 bentonite	100	100.000	Non-constant (decreases from 5 to 0.2 µm/y)	Porosity update Clay reactions are considered	Magnetite	Fe-chlorite Fe-saponite	15 cm	Porosity clogging after 100.000 years
Lu et al. (2011)	Fe-FEBEX bentonite	25	300.000	Constant (0.1 µm/y) and non-constant (max. of 0.7 µm/y)	1D model Use of cation exchange and 3 types of sorption sites in the bentonite Kinetically-controlled canister corrosion and magnetite precipitation	Magnetite		-	Accounting for kinetically-controlled canister corrosion leads to a significant reduction in the corrosion rate The concentration of dissolved Fe computed with kinetic magnetite precipitation is smaller than that obtained at equilibrium
Ngo e al. (2014)	Fe-MX80 bentonite	100	10.000	Non-constant (decreases from 5 to 0.2 µm/y)	Similar to Marty et al. (2010) Porosity update Clay reactions are considered	Magnetite	Greenalite Fe-saponite Fe-chlorite Berthierine	10 cm	The large surface area of the primary clay minerals provides a significant decrease in porosity in the zone in contact with the steel overpack, which in turn limited the diffusion of the

EURAD (Deliverable n° 1.1) – Initial State-of-the-art of WP ConCorD
Dissemination level: Public
Date of issue of this report: 17/08/2022

Page 102

Reference	Type of interface	T (°C)	Simulation time (years)	Corrosion rate	Assumptions	Main corrosion product	Main secondary minerals	Maximal perturbation extent	Relevant results
					With and without accounting for the influence of the reactive surface areas of the primary minerals				aqueous corrosion products toward the bentonite barrier. This induced an important porosity reduction and intense mineralogical transformation in the bentonite zone close to the bentonite/steel overpack interface.
Wilson et al. (2015)	Fe-bentonite	70	100.000	Constant (1 μm/y) and non-constant (diffusion limited)	Model 1: fixed steel corrosion rate Model 2: diffusion-limited corrosion rate Model 3: corrosion cell approach	M1 and M2: - M3: Magnetite Siderite	M1: Berthierine Fe-saponite Greenalite M2 and M3: Berthierine	2 cm	The extent and nature of the alteration predicted by the models is sensitive to model conceptualisation
Samper et al. (2016)	Fe-FEBEX bentonite	Non-isothermal	1.000.000	Constant (2 μm/y) and non-constant corrosion rate (T and chemical conditions dependence)	1D model Use of cation exchange and 3 types of sorption sites in the bentonite Kinetically-controlled canister corrosion and magnetite precipitation Smectite dissolution is considered	Magnetite	Analcime Cronstedtite	7 cm	Magnetite precipitation reduces significantly the porosity of the bentonite near the canister (7 cm thickness of the zone of reduced porosity at 1 Ma) The thickness ranges from less than 5 cm for a corrosion rate of 5 μm/year to nearly 12 cm for a rate of 0.5 mm/year. The thickness increases significantly when the corrosion rate dependence on the chemical conditions is considered and decreases 3 cm when smectite dissolution and analcime precipitation are taken into account
Mon et al. (2017)	Fe-Febex bentonite	Non-isothermal	1.000.000	Constant corrosion rate (2 μm/y)	1D model Use of cation exchange and 3 types of sorption sites in the bentonite. Smectite dissolution is considered	Magnetite	Gypsum Sepiolite	1 cm	Pore clogging at the canister-bentonite interface Narrow alteration zones Limited smectite dissolution after 1 Ma

EURAD (Deliverable n° 1.1) – Initial State-of-the-art of WP ConCorD
Dissemination level: Public
Date of issue of this report: 17/08/2022

Page 103

3.5   Integration of corrosion phenomena in performance assessments

According to the NRC in the U.S. the definition of a performance assessment[3] is:

In the context of disposal of radioactive waste, a performance assessment is a 'quantitative evaluation of potential releases of radioactivity from a disposal facility into the environment, and assessment of the resultant radiological doses'.

There are two main aspects of the PA where corrosion needs to be taken into account. The first is related to radionuclide release into groundwater and the second is concerned with radionuclide release in the gaseous phase. Both forms of release have the potential to affect, directly or indirectly, the transport of radionuclides to the biosphere and hence increase the radiological risk to future human populations in proximity to the disposal facility. Specifically, in many disposal concepts and associated evolution scenarios, the corrosion of the disposal canisters containing the radioactive waste is expected to be a key factor in determining the durability of the disposal canisters and hence the timescales over which any residual radioactivity might be released in the 'near-field'. Conversely, the accumulation of gas at elevated pressure in a disposal facility, for example hydrogen generated by the anaerobic corrosion of iron-based materials, may threaten the integrity of any buffer and backfill materials used in the EBS and thus affect radionuclide transport pathways.

Currently, 36 countries operate nuclear power plants. Those with well-developed radioactive waste disposal programmes are listed in Table 3-1*,* together with their respective Waste Management Organisations (WMOs) responsible for developing and underpinning the technical and scientific basis for radioactive waste disposal programmes.

Table 3-3 shows the remaining countries operating nuclear power plants and their respective WMO. The waste disposal programmes in these countries are less well developed – these countries are not known to have yet developed performance assessments (and, more broadly, safety cases) for geological disposal concepts focusing on deep disposal. The majority of countries operating nuclear reactors have not yet progressed to the point of preparing full performance assessments for geological disposal facilities.

Internationally, there is no standardized prescriptive approach to including corrosion information in quantitative PAs, although general guidance regarding the preparation of safety assessments for a complete disposal system has been published by IAEA (IAEA, 2012). The details of every safety case and performance assessment will be specific to each individual concept and set of environmental conditions. The aim of this section is thus to provide a high-level overview of how different countries and their respective WMOs incorporate corrosion behaviour into their PAs. One of the aims of the ConCorD programme is to use the results obtained in the planned experimental and modelling activities to refine how corrosion processes of the disposal containers are dealt with in PAs. This will be considered in the current SoTA document when it is updated at the end of the project. In the following discussion, we highlight where we expect the specific activities within the ConCorD project to lead to enhanced PA capabilities relating to the treatment of corrosion as a result of the ConCorD programme.

---

[3]   https://www.nrc.gov/about-nrc/regulatory/performance-assessment.html

EURAD (Deliverable n° 1.1) – Initial State-of-the-art of WP ConCorD
Dissemination level: Public
Date of issue of this report: **17/08/2022**

Page 104

Country	Waste Management Organisation /	Regulator
Sweden	SKB*	SKI
Finland	Posiva	STUK
France	Andra*	ASN
Switzerland	Nagra*	ENSI
Canada	NWMO*	CNSC
UK	NWS (previously RWM)*	ONR EA NRW NI EA
Japan	NUMO*	NRA Japan
Korea	Kigam	NSSC
Germany	DBE / GRS*	BfS
Czech Republic	Surao* / RAWRA /	SÚJB
Belgium	Ondraf-Niras*	FANC
Spain	ENRESA /	CSN
Taiwan	Taipower	Atomic Energy Council
Ukraine	KIPT*	MEPNS
Australia	ARWA	NRWMF
U.S.	US DoE	NRC

*Table 3-2: Countries currently operating nuclear reactors and their respective WMOs and who are known to have previously prepared performance assessments for their chosen repository designs and those planning to prepare new performance assessments in the short-term. Members of the ConCorD project are indicated by *.*

EURAD (Deliverable n° 1.1) – Initial State-of-the-art of WP ConCorD
Dissemination level: Public
Date of issue of this report: **17/08/2022**

Page 105

Country	Waste Management Organisation
Argentina	National Atomic Energy Commission (CNEA)
Armenia	None – under direct government control
Belarus	None - under direct government control
Brazil	National Nuclear Energy Commission, CNEN
Bulgaria	Nuclear regulatory authority
China	Beijing Research Institute of Uranium Geology (BRIUG)
Hungary	PURAM
India	Department of Atomic Energy
Iran	Iran Radioactive Waste Management Company (IRWA)
Lithuania	RATA, State Enterprise Ignalina NPP
Mexico	National Institute of Nuclear Research (NINR)
Netherlands	Central Organization for Radioactive Waste (COVRA)
Pakistan	Pakistan Atomic Energy Commission
Romania	ANDRAD, Nuclear and Radioactive Waste Agency
Russia	ROSATOM
Slovakia	Slovak Nuclear and Decommissioning Company (JAVYS)
Slovenia	ARAO
South Africa	National Radioactive Waste Disposal Institute of South Africa, NRWDI
UAE	Emirates Nuclear Energy Corporation
Netherlands	Central Organization for Radioactive Waste (COVRA)

Table 3-3: Countries currently operating nuclear reactors and their respective WMOs. These organisations are not known to have prepared performance assessments although all plan to develop a deep disposal facility in the long-term.

Based on the disposal concepts that are currently considered prominent candidates for the implementation of geological disposal, the consideration of corrosion in PAs can broadly be divided into those concepts where a copper-based waste container is used, including copper-coated steel containers, and those using an iron-based container, predominantly carbon steel but with some concepts considering the use of stainless steel. The subsequent discussion deals with the treatment of

EURAD (Deliverable n° 1.1) – Initial State-of-the-art of WP ConCorD
Dissemination level: Public
Date of issue of this report: 17/08/2022

Page 106

corrosion in PAs for these two categories of materials and summary tables are used to compare and to contrast the different approaches taken in different countries.

Any repository design will experience an evolution in conditions over time and this can be summarised in a generic diagram such as that shown in Figure 1-7a. The details will vary between specific concepts and disposal locations, but in general the initial conditions will be warm, oxidising and relatively dry, with potentially elevated (gamma) external radiation dose rates, depending on the thickness of the canister wall. As the exposure time increases, resaturation of the facility with groundwater will occur, making the system humid and eventually fully saturated. At the same time the temperature, dose rate and oxygen concentration will fall, the latter over much shorter timescales than the former two. Eventually the conditions will become fully saturated, cooler and with lower redox potential (and dose rates). The detailed chemistry of the environment and the corresponding microbiological ecosystem will evolve during this time. The aim of the treatment of corrosion processes in a PA is to reflect these phenomena as far as is possible in a pragmatic way. It is generally recognised that it is not possible to produce a detailed unified model for all aspects of corrosion processes that could be incorporated into a PA. Rather it is necessary to make some reasonable simplifying assumptions, based on the mechanistic understanding gained from experimental investigations and detailed mechanistic models, as described in the previous section.

3.6 Performance assessments for copper-based canister corrosion

3.6.1 Introduction

Oxygen-free copper has been considered as the canister material in several European and international waste management programmes, Key countries of interest include Sweden (SKB, 2010a), Finland (Posiva, 2007), Switzerland (Johnson & King, 2003), the United Kingdom*** (RWM, 2016), Canada (NWMO 2016). The furthest developed disposal concept in Europe is the KBS-3 concept which utilises a ~50 mm thick barrier layer of phosphorus-doped oxygen free copper (SKB, 2010a). It is worth noting explicitly that performance assessments typically indicate expected depths of corrosion substantially less than that container wall thickness. However, the assumed wall thickness is currently conceived to both sustain the canister under its own weight (including during manufacture) and to ensure sufficient resistance to the risk of creep rupture. An alternative copper canister design comprises a copper coating, a few mm thick, applied to a carbon steel substrate as is considered in the Canadian (NWMO, 2016) and Swiss concepts (Johnson & King, 2003). For coated designs the corrosion allowance is considerably less than for the thicker copper canister designs, consequently for coated containers a greater certainty regarding the prevailing corrosion mechanisms is required. Currently electrodeposition and cold spraying are being considered as possible coating methodologies.

Copper canisters used to dispose of SNF and HLW are designed to be emplaced within a bentonite buffer. Unless specific environmental conditions were present in the groundwater (e.g., high carbonate and/or sulphate content, and low chloride content), copper would not be expected to passivate in a repository environment and much of its lifetime can be predicted based on a general corrosion occurring with moderate uniformity. For a particular corrosion process (e.g., oxic corrosion, anoxic sulphide-driven corrosion, microbiologically influenced corrosion, pitting) the loss of material is either bounded by a maximum loss of material that is distributed over an area or is ascribed a rate of loss of thickness that is applicable over a particular phase in the repository lifetime. (e.g., early aerobic post-closure conditions, long-term anaerobic conditions) (RWM, 2016; Scully & Edwards, 2013).

Early in the repository lifetime and for a comparatively short-lived period (previously estimated at decades (Johnson & King, 2003) but more recently estimated as shorter based on the results of full-scale field testing experiments (Huertas, et al., 2005)), the corrosion of copper is governed by the concentration of oxidants within proximity to the canister, including trapped O_2, radiolysis products and

EURAD (Deliverable n° 1.1) – Initial State-of-the-art of WP ConCorD
Dissemination level: Public
Date of issue of this report: 17/08/2022

Page 107

Cu(II) species produced by the oxidation of Cu(I) corrosion products. Over time, these species are consumed and not replaced (or not replaced at the same rate), leading to a reduction in the oxidising power of the environment and a change in the dominant corrosion mechanisms that are predicted to prevail over the long-term lifetime of the repository. In this phase, the corrosion of copper is expected to be governed by the flux of sulphide to the copper surface from outside the near field. This process is expected to be kinetically limited by the low solubility and slow diffusion of sulphide through compacted bentonite (Scully & Edwards, 2013). In the absence of other degradation processes, which are not expected to occur, provided the swelling pressure of the buffer is maintained, copper canisters are predicted to last more than 10^5 years (RWM, 2016) (Johnson & King, 2003) and potentially over 10^6 years (Keech, Behazin, Binns, & Briggs, 2020).

The main types of corrosion affecting copper-based canisters, and which need to be considered in any performance assessment, are as follows:

- Corrosion under unsaturated conditions
- General corrosion
- Localised corrosion
- Microbiologically influenced corrosion
- Radiation assisted corrosion
- Environmentally assisted cracking

3.6.2 Corrosion in unsaturated conditions

Corrosion of the copper overpack during the unsaturated phase (including any corrosion before emplacement in the buffer and within the buffer before groundwater resaturation occurs) has been evaluated for a KBS-3 repository environment. Based on empirical evidence from the literature, corrosion rates are expected to be negligible (Posiva, 2013; SKB, 2010a). In these conditions it is assumed that the elevated surface temperature of 50 °C will ensure that the relative humidity close to the canister surface is lower than the critical relative humidity required to cause corrosion, generally considered to be around 50-70% RH (SKB, 2010a). In dry air, the corrosion rate of copper increases with temperature and is predicted to be of the order of 10s of nm/y at temperatures between 50 -150 °C (SKB, 2010b; Roy & Sircar, 1981; Pinnel, Tompkins, & Heath, 1979). These values are consistent with measurements made at the underground Äspö Hard Rock Laboratory in Sweden, which indicated corrosion rates <0.1 μm^{-1} at 75 °C (Taxén, 2003). Consequently, the atmospheric corrosion of copper canisters awaiting disposal is pessimistically bounded by assuming the corrosion will not exceed 1 µm and will produce a copper oxide surface film (SKB, 2010a).

3.6.3 General corrosion

For copper canisters emplaced within clay buffer materials, after closure of the repository oxygen is assumed to be present within the void space in both the buffer and backfill materials. A pessimistic assumption is that all the oxygen present in the buffer material reaches the canister surface and is consumed uniformly by corrosion (Keech, Behazin, Binns, & Briggs, 2020) (SKB, 2010b). A more realistic assumption, applied to the Swedish KBS 3 repository design, is that oxygen will also diffuse towards the oxygen-free rock and away from the canister, hence only around 50% may reach the canister surface, which equates to an expected corrosion loss of approximately 17 µm and bounded at 36 µm. The backfill is estimated to contain a greater amount of trapped oxygen than the buffer owing to its greater total volume, however, it is assumed that a smaller fraction of the oxygen trapped in the backfill would reach the canister. This fraction has been estimated for the KBS 3 design by considering the ratio of the canister diameter in relation to that of the deposition hole, with the assumption that the oxygen is consumed as it diffuses downwards by reaction with only the canister lid and the top 10% of the canister height. Under these assumptions a further corrosion loss of approximately 106 µm is

EURAD (Deliverable n° 1.1) – Initial State-of-the-art of WP ConCorD
Dissemination level: Public
Date of issue of this report: 17/08/2022

Page 108

anticipated, which gives a total expected loss of 123 μm (SKB, 2010b). In the Swiss program, the amount of copper corrosion arising from trapped O_2, assuming all the trapped O_2 reacts with the canister to form Cu(I), was estimated at around 70 μm (Johnson & King, 2003). No credit is taken for the consumption of oxygen by reaction with steel rock supports, microbial activity or oxidation of Fe(II), making the approach conservative.

Once oxygen has been consumed, sulphide will be the primary oxidant remaining in the repository. There is an initial stock of sulphide that is present as minerals (e.g., pyrite) within the buffer and backfill that dissolve and diffuse toward the canister surface during hydration of the borehole. The corrosion of copper by sulphide can lead to the formation of copper sulphide [e.g., Equation (3.2) and (3.3)], although other reactions are also possible). Sulphide is also produced by microbial activity and is discussed separately in greater detail in Section 3.3.6. The contribution of the sulphide present as pyrite in the buffer can be pessimistically bounded by a mass balance estimate as demonstrated for residual oxygen. The contribution of the dissolution of pyrite and the diffusional transport of sulphide from the pyrite to the canister surface has been considered as a source of corrosion in the KBS 3 repository design (SKB, 2010b), however, an allowance is not currently made for it owing to the low solubility of sulphide in the buffer.

$$2\ Cu(s) + HS^- + OH^- \rightarrow Cu_2S(s) + H_2O + e^- \qquad \text{anodic process} \qquad (3.2)$$

$$2\ H_2O + e^- \rightarrow H_2 + OH^- \qquad \text{cathodic process} \qquad (3.3)$$

In process models underpinning performance assessments, the corrosion rate due to the diffusion of corrosive species towards the canister surface is typically treated using the assumption that they react immediately upon contact with the canister surface, and that any future reaction rate is unhindered by the formation of corrosion products. In the case of the copper/bentonite system, this assumption is justified by the slow rate of transport of sulphide in compacted bentonite in relation to the inherent reaction rate of copper with sulphide. In these conditions the corrosion reaction is treated as being transport-limited and the rate of corrosion is proportional to the flux of species reaching/leaving the surface (SKB, 2010b). It has been demonstrated that for copper corroding due to reaction with HS^-, the shift for kinetic limitation to transport limitation occurs at HS^- fluxes greater than 2×10^{-12} mol/cm^2, which is considerably greater than the anticipated long-term sulphide fluxes through an intact bentonite buffer (~10^{-14} mol/cm^2) (King, Chen, Qin, Shoesmith, & Lilja, 2017). The lack of impact of corrosion product formation on the subsequent corrosion rate is supported by experimental observations that copper sulphide corrosion product layers are porous and non-protective in the pH range and sulphide concentration anticipated within a bentonite buffer (King, Chen, Qin, Shoesmith, & Lilja, 2017) (Keech, Behazin, Binns, & Briggs, 2020). The mass transport approach can be applied as well to deal with the concentrations of any oxygen that is trapped in the buffer and backfill materials, although in conventional disposal scenarios (GDF tunnels sealed effectively) the treatment based on mass balance is considered both cautious and sufficient. On the other hand, whilst this approach is still conservative (as the consumption of oxygen by other sources is also not considered), this approach could be used to treat the corrosion of disposal canisters in relevant scenarios, including either deliberately or inadvertently unsealed tunnels during the GDF operational period (i.e. whilst operations in other tunnels are still taking place) or access of glacial-melt water (see below) (King, Watson, Wilson, & Mackenzie, 2011).

Corrosion of copper by sulphide transport in groundwater is evaluated by mass transport limitation. The equilibrium concentration of sulphide in the groundwater is determined by the source (i.e., sulphate reduction by microbial activity) and sink (i.e., oxidation and precipitation with metals) terms (SKB, 2010b). Mass transport modelling has been used to evaluate the effect of buffer erosion on the sulphide transport from flowing groundwater, supplied from a rock fracture to the canister surface for a KBS-3 repository (SKB, 2010b). For an intact buffer and a sulphide concentration of the order of 0.01 mM, corrosion rates lower than 0.001 μm year^{-1} have been predicted for all conditions modelled, with vastly

EURAD (Deliverable n° 1.1) – Initial State-of-the-art of WP ConCorD
Dissemination level: Public
Date of issue of this report: 17/08/2022

Page 109

lower corrosion rates predicted for most cases. For a partially eroded buffer, predicted corrosion rates are much higher, and under the most pessimistic combinations of flow rate and sulphide combination (≥0.161 m/s and 0.12 mM) failure of a canister (taken as 47 mm of corrosion or greater) could occur within 10^5 years (SKB, 2010b). However, for a more realistic sulphide concentration (0.01 mM), failure is only predicted to occur after around 850,000 years, even at a high flow rate of 0.251 m/s (SKB, 2010b). Likewise, similar hydrogeology models are used to evaluate oxygen transport from glacial melt water. This can be done by assuming an upper limit of oxygen concentration (1.5 mM) in the groundwater that is supplied to the canister surface from rock fracture intersecting a deposition hole over fixed exposure period of 1,000 years, resulting in a corrosion loss of less than 6 mm (SKB, 2010b). In the Swiss disposal system, the corrosion loss based on the diffusion of HS^- to the container surface has been estimated as 80 μm over 10^6 years. This is based on reactive transport modelling of sulphide in bentonite (Cloet et al. 2017).

3.6.4 Localised corrosion

Pitting of copper canisters is only considered viable during the aerobic early post closure phase, while conditions are oxidising, but water chemistry is still quite dilute as the groundwater will have not yet reached the disposal container (or buffering by the initial porewater still occurs) (RWM, 2016). Based on short-term laboratory testing in simulated GDF conditions and in situ corrosion testing in disposal programmes considering the use of the material, copper has been shown to exhibit non-uniform general corrosion rather than formation of discrete 'classical' pits that are characterised by a small, fixed anode spatially separated from a supporting cathode. Consequently, the relative non-uniformity in the extent of corrosion across the surface is anticipated to reduce over time (RWM, 2016). Therefore, predictions of pit depths based on the assumption of a fixed anode that corrodes at a greater rate than the mean corrosion rate are unrealistically pessimistic (e.g., empirical pitting factor and extreme value statistical analysis).

Another form of localised corrosion that has been evaluated in some disposal programmes, for example the Canadian disposal concept, is under-deposit corrosion (Scully & Edwards, 2013). The specific mechanism of concern is a form of crevice corrosion that proceeds underneath a precipitated surface film. The film would act as a selective ion exchange membrane and enable the development of a locally aggressive solution chemistry, forming a permanent anodic region. Such a mechanism would preclude the use of a surface roughening factor to account for local attack in favor of the more conservative pitting factor (Scully & Edwards, 2013). Localized corrosion including under deposit corrosion has been considered by ascribing a 0.1 mm corrosion allowance to this mechanism, on the assumption that anodic and cathodic sites will not remain permanently fixed but will change with time within the overall anodic region (under the deposit) (Scully & Edwards, 2013) (Keech, Behazin, Binns, & Briggs, 2020). The assumption is underpinned by measurements of the surface profiles produced from corrosion of copper underneath precipitated films in simulated Canadian repository conditions. The results showed a depth of attack of around 50 μm, following 18 months exposure under conditions that were conservative, with respect to oxygen concentration, in comparison to those anticipated during the aerobic phase of deep geological disposal (Scully & Edwards, 2013) (King, Litke, & Ryan, 1992).

- Empirical pitting factor

Pitting factors for buried copper and copper alloys have been found to vary between 0-25 but exhibit a tendency to decrease with time. The longest exposure durations used to determine pitting factors are those of bronze-age artifacts (~3,000 years) reported by (Bresle & Arrhenius, 1983) and gave pitting factors between 2-5. These values are broadly consistent with measurements made of buried lightening conductor plates, which exhibited pitting factors of between 0-5 following exposures between 50-80 years (Hallberg, Engvall, & Wadston, 1984). Hence, for buried copper canisters, a pessimistic pitting factor of 5 may be assumed (SKB, 2010a). A pitting factor of 5 was applied to give a conservative

EURAD (Deliverable n° 1.1) – Initial State-of-the-art of WP ConCorD
Dissemination level: Public
Date of issue of this report: 17/08/2022

Page 110

estimation of the maximum depth of penetration of a copper canister in a Swiss repository due to sulphide flux (Johnson & King, 2003). However, the use of a pitting factor for copper is, in general, considered to be overly conservative when applied to GDF performance assessment. This is due to a shift to less oxidising conditions (i.e., decreasing concentrations of O_2 and Cu(II)), and the progression of general corrosion into the surface, both of which act against the separation of anodes and cathodes (SKB, 2010a). Consequently, it is anticipated that a measured pitting factor would decrease with increasing time of exposure, consistent with archaeological observations.

- Empirical amount of surface roughening

Roughening of ±50 μm has been applied for copper corrosion due to initially entrapped oxygen (SKB, 2010b; SKB, 2010a), based on observations by (Litke, Ryan, & King, 1992) (Brennenstuhl, McBride, Ramamurthy, & Davidson, 2002). Similarly, in the Canadian system, a corrosion allowance of 100 μm has been assigned to address surface roughening during conditions where the oxygen level is still relatively high (Keech, Behazin, Binns, & Briggs, 2020) (Scully & Edwards, 2013) and is based on arguments supporting the of switching anodic and cathodic regions (Kwong, 2011).

- Extreme-value statistical analysis

Pitting data generated by (Bresle & Arrhenius, 1983; Hallberg, Engvall, & Wadston, 1984; Romanoff M. , 1989) was analysed by (King & Kolar, 2000) and (King & LeNeveu, 1991) and fitted to an extreme-value distribution (Equation 3.4). Application of this data to a copper canister in the KBS-3 type repository environment led to the prediction of a 10^{-6} chance of a pit exceeding 7.5 mm after 10^6 years and a 10^{-6} chance of a pit exceeding 5 mm after just 10 years (SKB, 2010a).

$$F(x) = \exp\left[-\exp(-ax + b)\right]$$
(3.4)

An underpinning observation that indicates that long-term prediction of pit depths making use of extreme value statistical analysis (and empirical pitting factors) may not be particularly meaningful is that copper will not passivate under anticipated repository conditions, as passivation is required to cause pitting (King & Lilja, 2014). In the early oxidic period where pitting is more feasible, the presence of Cl^- ions tends to promote general active corrosion at near-neutral pH, with passivation occurring more readily in more alkaline solutions with a lower salinity (Briggs, Lilja, & King, 2020) (Qin, et al., 2017). Whereas, in the long-term, corrosion proceeds via the formation of copper sulphide, which has been shown to form porous non-protective films under anticipated repository conditions in Canada, Sweden and Finland (King, Chen, Qin, Shoesmith, & Lilja, 2017).

- Comparison of corrosion potential to critical potential for localised corrosion

For copper in neutral conditions, when the oxygen concentration is sufficiently low that hydrogen evolution is the dominant cathodic reaction, the anodic overpotential required to cause pitting is estimated as being approximately 600 mV based on the potential at which copper oxide formation occurs. Pitting of a copper oxide film is expected to occur more readily with increasing chloride concentration, and less favourably with increasing HCO_3^- concentration, due to their destabilising and stabilising influence on passivity, respectively (Drogowska, Brossard, & Ménard, 1992). When sulphide is present, the pitting potential of the protective sulphide film was shown to shift in the negative direction with increasing HS^- concentration (de Chialvo, Slavarezza, Vasquez, & Arvia, 1985). For copper, in the presence of 0.01M HS^- an anodic overpotential of around 200 mV is assumed necessary to induce pitting corrosion based on corrosion potentials reported in (Escobar, Silva, Silva, & Ubal, 1999). Whilst pitting of copper oxides and sulphides has been shown to be possible under certain conditions, the

EURAD (Deliverable n° 1.1) – Initial State-of-the-art of WP ConCorD
Dissemination level: Public
Date of issue of this report: 17/08/2022

Page 111

potentials at which such pitting occurs are hundreds of mV more positive than anticipated in repository environments (King, Lilja, Pedersen, Pitkänen, & Vähänen, 2010).

3.6.5 Radiation assisted corrosion

Radiation assisted corrosion is considered separately for the saturated and unsaturated environment as the prevalent corrosion mechanisms in each case are quite different. In unsaturated conditions, the major corrosion mechanism considered in safety case assessment is that caused by radiolytically produced nitric acid that arises from irradiation of the humid air trapped within the buffer. Once saturation is complete, radiolysis of the anoxic porewater leads to the production of oxidants, primarily H_2O_2, which in high enough concentrations can influence the corrosion rate and shift the corrosion potential in the positive direction (King & Behazin, 2021).

- Mass balance of radiolytically produced oxidants

In the unsaturated phase, the influence of radiolytically generated oxidants on the corrosion of copper canisters within a bentonite buffer has been estimated by calculating the radiolytic yield within a given volume around the canister (liquid or gas phase) and assuming the oxidants produced will react with the canister surface to give a bounding value (SKB, 2010b).

This approach is adopted to take account of the formation of nitric acid from gamma irradiation of the humid air present in the canister-buffer gap during the buffer saturation phase. The total amount of nitric acid generated is calculated from the G value for NHO_3 generation, the total absorbed gamma dose and the irradiated volume (e.g., 1 cm gap around canister) (SKB, 2010b).

Radiolysis of water is considered to form hydrogen and oxidants that will react with the canister material causing corrosion. It is assumed that there exists a volume around the canister in which all radiolytically generated oxidants will reach the canister surface (e.g., 5 mm gap around canister) and that there is a fixed stoichiometric ratio between the moles of oxidant produced and the moles of metal that are corroded uniformly from the surface of the canister (SKB, 2010b). Overall, the effect of radiolysis on the corrosion of copper in the Swedish system (KBS-3 type repository), after taking into account the aforementioned contributions, is around 7nm (SKB, 2010a).

A similar approach has been adopted to bound the extent of corrosion that may be experienced by copper due to radiolysis of water in the KBS-3 concept. If it is assumed that all the radiolytically produced oxidants within 5 mm of the canister can reach the surface, and it is also assumed that Cu is oxidized as efficiently as dissolved Fe(II), then approximately 14 µm of corrosion would be expected.

- Reasoned argument for exclusion

Intact canisters provide shielding against alpha and beta radiation with only gamma and neutrons penetrating through the walls to cause radiolysis of the porewater and groundwater. Due to the shielding afforded by the canister, the surface radiation dose is greatly attenuated, for the thinner walled Canadian design the surface dose rate is approximately 1 Gy hr^{-1} (Keech, Behazin, Binns, & Briggs, 2020), whereas, for the thicker KBS-3 containers the average surface dose is around 0.055 Gy hr^{-1}. At these dose rates, it is anticipated that there will be no corrosion enhancement rates (Pusch, Karnland, Lajudie, & Decarreau, 1992; Posiva, 2013). This perspective is supported by the work reported on in the review article by (King & Behazin, 2021), who compared the general corrosion enhancement by gamma radiation at dose rates from 0-20 Gy hr^{-1} and total absorbed doses from 1,000 to 50,000 Gy. At dose rates relevant to repository conditions (<10 Gy hr^{-1}) there was either no effect, or an inhibiting effect of radiation. At dose rates >10 Gy hr^{-1} there is no consensus within the literature, with some studies showing an enhancement in corrosion and others showing an inhibition of corrosion, when compared to uninhibited rates. These studies also showed that for all dose rates considered there was no consistent effect of increasing cumulative radiation dose.

EURAD (Deliverable n° 1.1) – Initial State-of-the-art of WP ConCorD
Dissemination level: Public
Date of issue of this report: 17/08/2022

Page 112

Of the papers considered by (King & Behazin, 2021) the only studies that demonstrated an increase in corrosion rate due to gamma radiation were conducted at dose rates considerably greater than those anticipated at a copper canister surface during emplacement within a GDF. Moreover, (King & Behazin, 2021) draw attention to the mechanistic impacts of radiation dose rate on the corrosion potential, which supports the suggestion that radiation dose rate is a critical factor in determining the influence of gamma radiation on corrosion rate of emplaced canisters. Consequently, laboratory studies at dose rates far in excess of 10's Gy hr^{-1} are not expected to accurately simulate the corrosive conditions encountered within a GDF repository.

3.6.6 Microbiologically influenced corrosion

- Reasoned argument for exclusion

It has been shown that microbial activity is suppressed in highly compacted bentonite above a certain density due to the low water activity (≤0.96) (Scully & Edwards, 2013), the high swelling pressure and the lack of physical space. In the Swedish SR-Site safety case, microbiologically activity leading to sulphide production via sulphate reduction is not considered within the intact bentonite buffer whose dry density exceeds 1,800 kg/m^3 (SKB, 2010a). In the Finnish safety case for the disposal of spent fuel at Olkiluoto, a bentonite dry density greater than ~1650 kg/m^3 is considered the upper threshold for microbial activity (Posiva, 2013). Consequently, microbial corrosion is generally not considered feasible within the bentonite buffer provided it remains compact and retains its density. Microbial activity is instead considered away from the near field (e.g., in the backfill) (Johnson & King, 2003), (Scully & Edwards, 2013), (SKB, 2010a) and (Posiva, 2013).

- Mass transport

Corrosion of copper by microbiologically generated sulphide outside of the near-field in a KBS-3 repository environment is pessimistically bounded by the supply of nutrients for microbes (SKB, 2010a). The amounts of nutrients available have been estimated in several ways. The backfill contains an abundance of organic matter, but it would be unrealistic to assume the whole stock is available for dissolution and could be used to produce sulphide that could reach the canister surface within the lifetime of the repository. Bounding calculations based on 1D diffusion of sulphide formed at the same location as the organic matter predict that only a fraction of the sulphide that could be produced would reach the canister surface within 10^6 years. A bounding corrosion loss from sulphide in the backfill is obtained by 1D diffusion modelling using pessimistic values for diffusivity and sulphide concentration (10^{-4} M) and applying the assumption that sulphur transported from the backfill is consumed by corrosion of the top 10% of the canister uniformly and gives a depth of penetration of 2 mm (SKB, 2010b). In the Canadian system a corrosion allowance for to microbial activity of 1 mm is considered sufficient provided the buffer remains intact (Scully & Edwards, 2013) (Wolfaardt & Korber, 2012).

The contribution of H$_2$, generated via anaerobic corrosion of rock bolts and other iron components, to the formation of sulphide via acetogenesis and sulphate reduction has also been considered and bounded for specific repository conditions based on the amounts of steel present (SKB, 2011) if a conservative mass balance approach is adopted that assumes that all of the sulphide produced by acetogenesis reacts with the canister, then an upper bound corrosion loss of 300 μm is obtained (SKB, 2010b).

- Empirical rates of sulphide formation

Another method to estimate bounding the rates of sulphide production has been considered based on experimental studies performed in conditions that are more favorable for microbial activity than expected in a repository environment. The rates of copper sulphide production were measured in bentonite at

EURAD (Deliverable n° 1.1) – Initial State-of-the-art of WP ConCorD
Dissemination level: Public
Date of issue of this report: 17/08/2022

Page 113

different densities that was supplemented with lactate to act as a source of organic carbon and nutrient (Masurat, Eriksson, & Pedersen, 2010). The experimentally determined rates of sulphide production were converted into an equivalent corrosion rate and the wall thickness loss after 10^6 years was extrapolated linearly to give a pessimistic estimation of thickness loss of about 3 mm (SKB, 2010b).

3.6.7 Environmental-assisted cracking

- Reasoned argument for nonsusceptibility

A combination of stress, aggressive ions and oxidising conditions are required for SCC of copper to occur. Even in the early oxic period where temperatures are elevated it is unlikely that sufficient concentrations of aggressive ions would be available within the KBS-3 type repository. There are no mechanistic arguments known that can justify the assumption that cracking of copper could be sustained long-term in the anaerobic phase of the repository environment (SKB, 2010b) (King, Lilja, Pedersen, Pitkänen, & Vähänen, 2010), (Posiva, 2013).

This argument has been further underpinned by experimentally validated mixed-potential modelling of the anticipated E_{corr} of copper, evaluated over a repository lifetime based on the interfacial chemistry as predicted by reactive transport modelling. Modelling of E_{corr} and the surface pH demonstrated that a CuO_2/CuO surface film is not thermodynamically stable, which is a requirement for the SCC of copper (Maak & King, 2006) beyond the initial aerobic period (Posiva, 2013).

In the Canadian concept, SCC is not considered to be likely during the steady state conditions encountered during deep geological disposal. Specifically, the interfacial pH and corrosion potential are expected to be far from the range in which SCC is a feasible corrosion mechanism, given the lack of aggressive species. Certain species, such as ammonia, nitrate ions, acetate and sulphides are known to promote SCC of copper, however, the concentrations in groundwater are below the threshold levels for which they have been shown to promote SCC. It has been acknowledged, that activities such as mining could lead to an increase of such species, however, the increase in SCC susceptibility is somewhat offset by the presence of Cl⁻, which reduces the risk of SCC by promoting general corrosion (Kwong, 2011).

The risk of gradual embrittlement of copper by long term anoxic exposure to HS⁻ at concentrations of around 10^{-4} mol, has been highlighted as a risk to copper canisters (Scully & Edwards, 2013). However, it has also been argued that HS⁻ transport in bentonite is sufficiently slow that corrosion by sulphide could be transport-limited, resulting in surface or crack tip concentrations approaching zero, assuming that Cu(I) will sequester sulphide by precipitation of CuS_2 (Jacobs & Edwards, 2000). It was similarly concluded that for the KBS-3 concept, the possibility of SCC in copper, even at high sulphide fluxes is not anticipated and even if copper were susceptible to SCC in the presence of sulphide, the sulphide fluxes in the repository environment are not at the level that would be possible to induce SCC (SKB, Supplimentary information on canister intgrity issues - TR 19 15, 2019).

3.6.8 Mechanical degradation and combined corrosion-mechanical effects

There are a number of modes of mechanical degradation that could potentially affect the integrity of waste containers, specifically fracture, plastic deformation and creep. It is also possible that there could be detrimental interactions between mechanical factors and corrosion processes. These issues have been discussed in detail by King et al. (2016). Fracture processes can be sub-divided into brittle fracture, characterised by cleavage or intergranular failure, and ductile fracture, resulting in the typical 'cup and cone' dimpled fracture surface. Brittle fracture is normally caused by some form of embrittlement

EURAD (Deliverable n° 1.1) – Initial State-of-the-art of WP ConCorD
Dissemination level: Public
Date of issue of this report: 17/08/2022

Page 114

process, such as radiation embrittlement, solute segregation within the metal or hydrogen embrittlement. Plastic deformation can occur when a metal is overloaded past its yield strength, eventually leading to ductile failure if the load is sufficiently high. This form of failure is avoided in container design by choosing wall thicknesses that are appropriate to the expected loads. If the load tolerance is exceeded deformation of the container may occur.

Creep involves the slow deformation of a material under the influence of an applied static load below the yield stress. In the case of copper, this problem is ameliorated by the use of oxygen-free, phosphorus doped copper, which has a higher creep resistance.

It is possible that some forms of corrosion may have an effect on the mechanical performance of the container, and vice versa. This includes environmentally assisted cracking, which is considered in the previous section, where the mechanical factors affect the corrosion susceptibility, and conversely corrosion processes such as general corrosion will cause wall thinning, leading to a loss of wall strength and load-bearing capacity, and hence an increased risk of wall deformation or buckling. These interactions have been examined in detail by King (King, 2016) and they are summarised in the diagram shown below. Other corrosion phenomena of note in this context are hydrogen-induced degradation of mechanical properties, since hydrogen may be generated by the anaerobic corrosion of iron, or may be present in the geological environment, and expansive corrosion due to the formation of a corrosion product with a larger volume than the original metal. The latter effect has been examined experimentally by Smart et al. (Smart, 2003) and by comparison to analogues, such as archaeological artefacts (Smart, 2004, 2006).

EURAD (Deliverable n° 1.1) – Initial State-of-the-art of WP ConCorD
Dissemination level: Public
Date of issue of this report: 17/08/2022
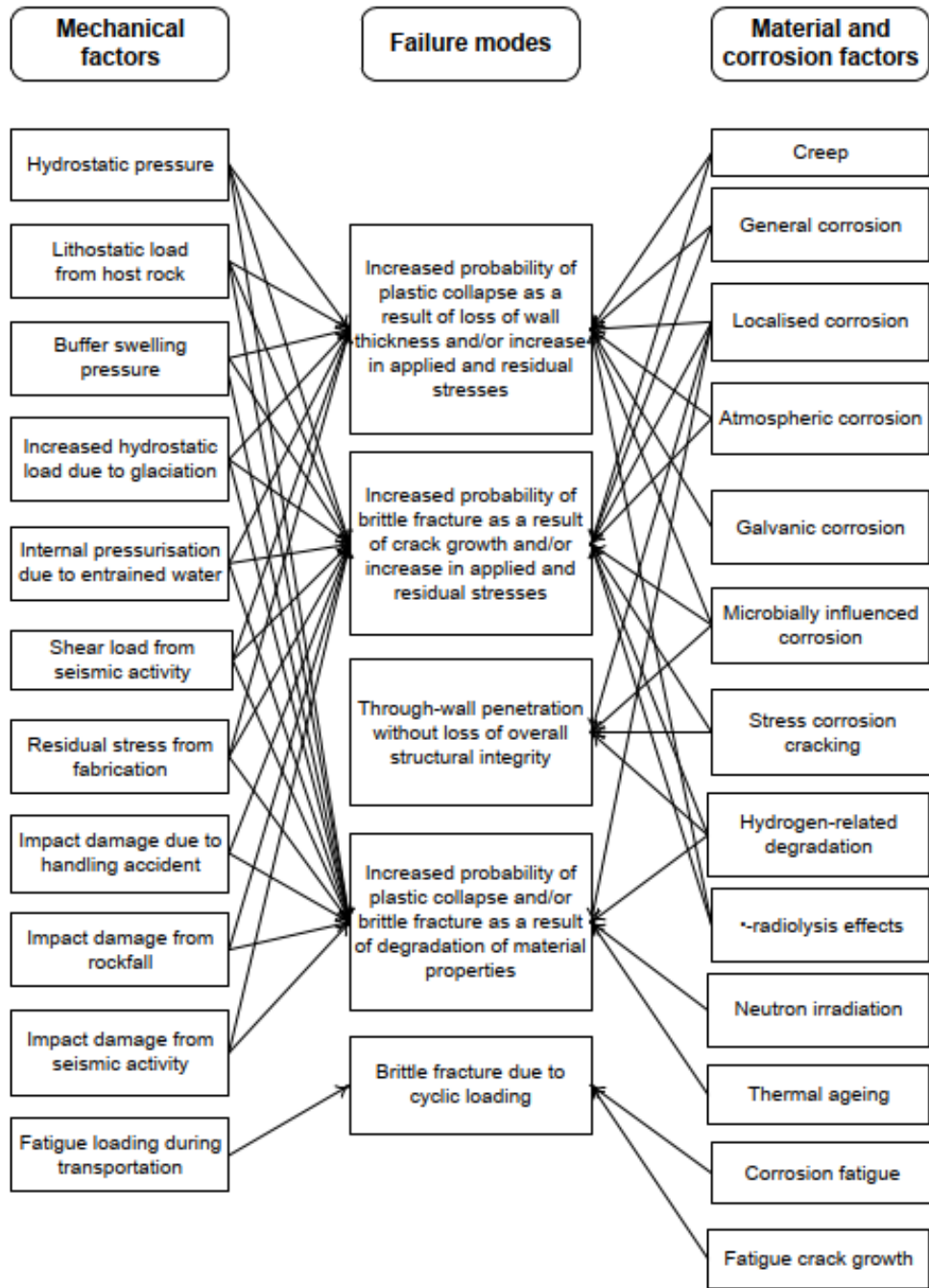
Page 115

Figure 3-3. Schematic illustration of the mechanical and material-related factors leading to container failure and their relationship to various failure modes (from King et al, 2016)

EURAD (Deliverable n° 1.1) – Initial State-of-the-art of WP ConCorD
Dissemination level: Public
Date of issue of this report: **17/08/2022**

Page 116

3.6.9   In-situ testing of copper spent fuel canisters

In situ testing has been performed to validate the key assumptions that underpin the estimated corrosion rate of copper canisters exposed to a repository environment. Two very relevant studies are the Prototype Repository Experiment (Svemar, Johannesson, Grahm, & Svensson, 2016) and the MiniCan experiment (Smart, et al., 2011).

In the Prototype Repository Experiment, conditions were designed to simulate those expected in a KBS-3 type repository- as per the Swedish/Finnish concept. This involved emplacement of six full-sized dual-shell copper canisters within vertical deposition tunnels whilst in contact with bentonite disks. Canisters were heated to simulate radiogenic heating and were instrumented with a range of sensors to closely monitor the environmental conditions (e.g., temperature, oxygen concentration, relative humidity and pressure). Testing was consistent with assumptions regarding the early-post closure period and demonstrated a shift to anaerobic conditions and a very low level of corrosion of two retrieved canisters following 7 years' exposure. Microbial activity was not observed in the bentonite buffer, which is expected for the specified acceptable saturated buffer density range of $1,950 - 2,050$ kg/m^3 (SKB, 2010c), although a small amount was observed in the backfill.

The MiniCan Experiment was also designed to the conditions anticipated within a KBS-3 repository concept, but testing was performed on five small-scale canisters. A key focus of the study was to evaluate the impact of a small through wall defect in the copper canister on the corrosion of the iron insert and its influence on canister integrity. The canisters were emplaced within boreholes at a depth of 450 m and flushed with anaerobic groundwater. After close to 5 years of exposure, whilst emplaced in a bentonite buffer, one of the canisters was removed for analysis. Analysis of the copper canister and iron insert showed evidence of widespread microbial activity that resulted in complete dissolution of the iron weight loss coupon (equivalent to a corrosion rate in excess of 500 μm year^{-1}). Despite the high level of microbial activity, the corrosion rate of copper coupons within the vicinity was just 0.15 μm year^{-1} (Smart, et al., 2011; RWM, 2016) (Johansson, et al., 2017).

3.6.10   Prediction of canister lifetimes and implications for PA

At present, the most comprehensive predictions of canister lifetime have been performed for the KBS-3 concept and estimates have been made for the maximum corrosion loss that may be caused by each mechanism over a period of 10^6 years. In the absence of erosion/corrosion scenarios that are considered separately, no single process gives an estimated corrosion loss of greater than a few mm, with the greatest loss estimated to arise from sulphide flux caused by microbiological reduction of sulphate in buffer on the assumption that all the organic material in the backfill is available to support this process. If the estimated contribution from each process is aggregated by addition, the sum is expected to be an overestimate of the true expected corrosion loss, as it takes no account of statistical variation, However, even when this is done, the total loss estimated over 10^6 years is less than 5 mm (SKB, 2010b).

For scenarios involving erosion of the buffer by groundwater flow, the maximum predicted corrosion rates are greater than for any other mechanism considered. However, extremely high rates of corrosion are only estimated when the least favourable conditions are assumed (i.e., maximum flow rate and maximum sulphide concentration). When a statistical analysis is performed that considered the range of possible flow rates and the range of possible sulphide concentrations the likelihood of a canister failing within 10^6 years can be estimated based on the number of canisters being stored. Application of this methodology estimates that between 0 and 2 canisters would fail within 10^6 once uncertainties are taken in to account (SKB, 2010b).

For the Canadian system, a corrosion allowance of 1.27 mm over 10^6 years was described by (Kwong, 2011) and was based on several assumption that have since been shown to be highly conservative (Keech, Behazin, Binns, & Briggs, 2020). In particular, the corrosion allowance is dominated by sulphide corrosion due to an assumed sulphide concentration of 3 ppm (Kwong, 2011), which has subsequently

EURAD (Deliverable n° 1.1) – Initial State-of-the-art of WP ConCorD
Dissemination level: Public
Date of issue of this report: 17/08/2022

Page 117

been shown to be considerably higher than what is expected in Canadian deep subsurface water (Keech, Behazin, Binns, & Briggs, 2020).

Table 3-4 *summarises* the approaches taken for dealing with the corrosion of copper in performance assessments by various WMOs, according to the various possible corrosion mechanisms for copper. It should be noted that the planned experimental work should provide information that can be used to support the assessment of radiation-induced corrosion effects and microbial corrosion.

Confidence in the predictions of longevity of containers can be increased by reference to results from (i) in situ corrosion experiments (see Section 3.6.9), where the environmental conditions are close to those expected in the real repository, with the exception of the external radiation dose rates, and the temperature, and (ii) comparison with natural and archaeological analogues (IAEA, 1989, 2005). Natural analogues include geological deposits, for example of native copper deposits (Milodowski, 2000, 2002), which have been found to exist for millions of years, and archaeological artefacts, such as a bronze cannon (King, 1995) and an iron-copper helmet (Smart, 2004). They have been applied to support the development of performance assessments for waste repositories (e.g., for Yucca Mountain, Simmons, 2004).

Mode of corrosion	Canada	Finland	Sweden	Switzerland	United Kingdom
Oxidic general corrosion	**Mass balance within corrosion allowance**				
Radiolysis-induced corrosion	**Excluded or Mass Balance within Corrosion allowance**				
Sulphide-induced anaerobic corrosion	**Mass transport controlled – key factor driving corrosion allowance**				
MIC before buffer saturation		**Exclude by reasoned argument**			
SCC	**Exclude by reasoned argument**				
Pitting	**Fixed corrosion allowance to account for surface roughening**		**Fixed corrosion allowance to account for surface roughening**		

Table 3-4: Comparison of approaches currently taken to account for different types of corrosion in performance assessments for <u>copper</u> canisters by international waste management organisations (blank cells reflect an absence of information within the public domain).

EURAD (Deliverable n° 1.1) – Initial State-of-the-art of WP ConCorD
Dissemination level: Public
Date of issue of this report: **17/08/2022**

Page 118

3.7   Performance assessments for iron-based alloy canister corrosion

3.7.1   Introduction

Carbon steel has been proposed as a canister material for SNF and HLW in several national disposal concepts including the UK (RWM, 2016), Belgium (Kursten B., 2017), France (Andra, 2005), Japan (JNC, 2000) and Switzerland (Patel, et al., 2012). Different WMOs specify different alloys for the canister material but in general, low strength, low carbon alloys are favored. Carbon steel is a desirable canister material as its corrosion mechanisms are well characterized and predictable, based on decades of research, which enables canisters to be designed with suitable corrosion allowances (RWM, 2016). Moreover, due to the extensive use of carbon steel as an engineering material it can be readily sourced and fabricated, and it is considerably cheaper than many alternative canister materials such as copper, nickel alloys, titanium etc.

Carbon steel has been considered for use with both bentonite and cementitious buffers as well as crushed rock (RWM, 2016). The high pH environment afforded by a cementitious buffer material supports the formation of a stable passivating magnetite film, which reduces the corrosion rate. However, under repository conditions, anaerobic corrosion of steel (even when passivated) leads to the formation of hydrogen gas, which has the potential to destabilize the surrounding buffer material. There is also concern that the interaction of ferrous ions released by corrosion could adversely alter the characteristics of the surrounding bentonite buffer.

Steel canisters for the disposal of SNF and HLW emplaced within a bentonite buffer have a regulatory lifetime requirement of 1,000 years, with the expectation that 10,000 year lifetimes may be readily achieved (Nagra, 2002) and this is the design lifetime. Similarly, complete containment provided by the Belgian Supercontainer concept is expected to endure for at least 5,000 years (for conditions defined within the design reference scenario) although, considerably longer lifetimes are anticipated if long-term corrosion behaviour is governed by the uniform anaerobic corrosion rate (Weetjens, Marivoet, & Govaerts, 2012). In the Czech concept, the double walled steel canister comprising an inner stainless steel layer surrounded by an outer carbon steel layer is designed to last for a minimum of 10,000 years (Popsikova, et al., 2017), whereas the Japanese concept, which also has an inner stainless steel container surrounded by an outer carbon steel layer (termed an overpack) focuses on a 1,000 year lifetime specification, but it is expected to last considerably longer (NUMO, 2021).

3.7.2   Atmospheric corrosion

The atmospheric corrosion behaviour of steel canisters in air is dependent on the relative humidity; below ~60% RH, the corrosion rate can be considered to be extremely slow (Nagra, 2002). The presence of hygroscopic salt deposits (e.g., NaCl and $CaCl_2$) at the canister surface can influence the relative humidity at which corrosion can occur, depending on the chemical composition of the contaminating salt (Shindleholtz, Risteen, & Kelly, 2014). However, due to the elevated temperature within the buffer close to the container surface, the canister is expected to remain dry even when the outer layers of bentonite begin to saturate (Nagra, 2002). Consequently, in the initial dry period, which is estimated to persist for a few decades, the extent of corrosion is expected to be less than 100 μm (Nagra, 2002) and has been accounted for in an Opalinus clay repository by applying a corrosion allowance of <1 mm (Johnson & King, 2008). This value is in broad agreement with atmospheric corrosion rates reported in (RWM, 2016), which shows that the atmospheric corrosion of embedded iron in subterranean environments is of the order of a few of μm yr^{-1}. It is anticipated that the atmospheric corrosion of iron will generally form iron (hydr)oxides and this is not expected to directly undermine the integrity of the containers significantly in environments of limited corrosivity. However, there is uncertainty regarding the impact that the formation of a layer of rust could have on the corrosion performance a steel container during the long-term post-closure phase (RWM, 2016).

EURAD (Deliverable n° 1.1) – Initial State-of-the-art of WP ConCorD
Dissemination level: Public
Date of issue of this report: 17/08/2022

Page 119

3.7.3 General corrosion

Following depletion of oxygen within the repository and a shift to more reducing conditions, the long-term corrosion of emplaced steel canisters is expected to occur as uniform general corrosion under anoxic conditions. In this environment a corrosion rate of ~1 μm yr^{-1} is anticipated for corrosion occurring in a bentonite buffer (Smart, Blackwood, & Werme, 2001). These rates are within the range reported for natural analogues, which exhibit corrosion rates as low as 0.1 μm yr^{-1} for conditions that are not aerated (Miller, Alexander, Chapman, McKinley, & Smellie, 1994). For the Czech concept, uniform anoxic corrosion of the outer carbon steel canister when emplaced in Czech bentonite is assumed to occur at a rate of 5 μm yr^{-1}, based on average corrosion rates determined by mass loss over a 4-month period. However, use of these rates to make lifetime predictions is known to be conservative, as in the same study, comparison of the total corrosion loss of specimens after 2 and 4 months' exposure, implied that the instantaneous corrosion rate after 2 months had reduced to less than 1 μm yr^{-1} (Popsikova, et al., 2017).

For concepts involving a cementitious buffer, such as the Belgian Supercontainer concept, the high pH (>13) cement porewater, that is anticipated to form upon hydration of the buffer, ensures that the steel will passivate by forming a stable magnetite surface film. The passive corrosion rate under these conditions can fall below 0.1 μm yr^{-1} (Weetjens, Marivoet, & Govaerts, 2012).

In the Japanese disposal concept, the corrosion rate of carbon steel in a bentonite buffer is considered in a range of rock types and groundwater chemistries of varying chloride and carbonate concentration. Based on laboratory testing it was found that corrosion rates dropped after 1 year of exposure and remained linear for several years at rates less than 2 μm yr^{-1}. Based on these observations, an anaerobic general corrosion rate of 2 mm over the 1,000 years design life can be assumed. However, due to the possibility of uneven corrosion, a 6 mm corrosion allowance is applied, based on an assumed pitting factor of 3 (NUMO, 2021).

3.7.4 Localized corrosion

For corrosion in the initial oxidic phase of the repository, in the Japanese concept the loss due to corrosion is bounded by the conservative assumption that all oxygen in the buffer and backfill is consumed by pitting corrosion of the carbon steel, and that no oxygen from the tunnel reaches the canister surface. The total corrosion allowance allocated to this process is between 5-12 mm and was calculated based on extreme value statistical analysis, and hence it is more conservative than assuming uniform corrosion loss across the canister surface (NUMO, 2021).

Classical pitting corrosion of emplaced steel canisters is only considered to be feasible in the early oxic period. The extent of inhomogeneity in the corrosion of carbon steel was evaluated from the results of long-term field burial tests (JNC, 2000). From these tests, it has been highlighted (Johnson & King, 2003) that the pitting was initially characterized by high empirical pitting factors of ~100, however, once general corrosion had reached a depth of ~0.3 mm, pitting factors reduced to ~10. Consequently, a corrosion allowance of 10 mm has been estimated for pitting in the oxidic phase of the Swiss disposal concept (Johnson & King, 2003).

The presence of a passivating magnetite film introduces the risk of localized corrosion if breakdown of the film occurs, particularly in a high pH environment, such as a hydrated cementitious buffer. The propensity for pitting was examined extensively using electrochemical measurements for conditions relevant to the Belgian disposal concept (Kursten, Macdonald, Smart, & Gaggiano, 2016) and demonstrated that the pitting potential had a strong dependence on chloride concentration (between 0.01M and 1M), where the pitting potential was shifted in the active direction at higher chloride concentrations. A similar effect was observed at elevated temperatures, where increasing the temperature from 25°C to 85°C caused a shift in the pitting potential in the active direction. In the most aggressive conditions considered (1M chloride, 85°C), and taking account of statistical variations in pitting potential, the lowest potential at which pitting was observed was ~+200 mV vs. the corrosion potential.

EURAD (Deliverable n° 1.1) – Initial State-of-the-art of WP ConCorD
Dissemination level: Public
Date of issue of this report: 17/08/2022

Page 120

In the Japanese concept, pitting corrosion during the long-term anoxic phase is excluded due to the combination of near-neutral bentonite pore-water pH, a carbonate concentration of less than 0.5 mol L^{-1} and the absence of strong oxidizing species. However, as noted in the previous subsection, the non-uniformity of general corrosion is treated with a pitting factor of 3, which considerably increases the level of conservatism in the design. Moreover, treatment of the expected pitting corrosion during the oxidic phase by use of a combined mass balance and extreme value statistical analysis approach is also conservative, leading to an allowance of up to 12 mm (NUMO, 2021).

3.7.5   Radiation-assisted corrosion

As with the corrosion of copper, radiolysis can lead to the formation of oxidants such as nitric acid, during the unsaturated phase, and H_2O_2 in the saturated phase, that can lead to an acceleration of the corrosion rate during the period in which the waste form is still sufficiently radioactive. However, since the corrosion rate of carbon steel is greater than that of copper in repository conditions, due to the spontaneous corrosion of steel in anoxic porewater, the additional oxidation of steel by radiolysis products is small in comparison to the general corrosion loss by water oxidation.

In a series of year-long corrosion tests, Andra investigated the influence of gamma irradiation on the corrosion rate of carbon steel in humid air to simulate conditions arising in the unsaturated phase of a repository. Compared to unirradiated conditions a gamma dose rate of 80 Gy hr^{-1} was found to increase the corrosion rate, whereas no effect was observed for dose rates of 20 Gy hr^{-1}, hence no influence of radiation is expected at the overpack surface, as the design limits the external surface dose rate to less than 10 Gy hr^{-1} (Crusset, et al., 2017).

Gutierrez et al. (2018) consider the influence of radiolysis on corrosion of steel canisters for HLW and SNF to be negligible in the saturated phase, owing to the thickness of the canister walls (14 cm), which provide sufficient radiation shielding to attenuate the initial surface gamma dose to ~0.2 Gy hr^{-1}, which is significantly below the critical value expected to enhance corrosion (Marsh & Taylor, 1988). Corrosion testing in support of the Czech concept, considers surface dose rates around ten times greater, at around 0.3 Gy hr^{-1} (Popsikova, et al., 2017), but these are still assumed to be too low to significantly accelerate the corrosion process. Similarly, acceleration of corrosion by gamma radiation is eliminated in the Japanese concept by the use of an 80 mm shielding allowance, which is expected to attenuate the surface dose rate to significantly below the threshold of ~3 Gy hr^{-1}, which is considered to influence corrosion under relevant conditions (NUMO, 2021). Under conditions relevant to the Belgian Supercontainer concept (i.e., young cement water containing thiosulphate, sulphide and chloride at 25 °C and 80 °C), dose rates of up to 25 Gy hr^{-1} had no significant effect on the anaerobic corrosion rate of carbon steel, with rates as low as 0.03 µm yr^{-1} measured by hydrogen gas evolution (Kursten, Macdonald, Smart, & Gaggiano, 2016).

3.7.6   Microbiologically influenced corrosion

As with copper-bentonite systems, the high bentonite density is expected to reduce microbial activity to the extent where sulphate reduction is negligible. Equally, within a cementitious buffer the high pH of the porewater is also expected to restrict microbiological activity to negligibly low levels such that sulphate reduction is only considered in the far-field (NUMO, 2021) (Nagra, 2002) (Kursten, Macdonald, Smart, & Gaggiano, 2016). Consequently, for an intact buffer, the influence of MIC is only attributable to sulphate reduction in the far-field, leading to a sulphate flux through the buffer to the canister surface. This process is the same as that for a copper-based system, since the flux is determined largely by the microbial activity and the properties of the buffer material (e.g., pH, thickness etc.).

Since the anaerobic corrosion rate of carbon steel is greater than that of copper in repository conditions, as discussed in the previous subsection, steel corrosion losses due to a sulphide flux tend to be less significant compared to general anaerobic corrosion arising from water oxidation. As an example, in an Opalinus clay environment, Nagra (Nagra, 2002) consider the extent of corrosion that could occur due

EURAD (Deliverable n° 1.1) – Initial State-of-the-art of WP ConCorD
Dissemination level: Public
Date of issue of this report: 17/08/2022

Page 121

to a sulphide flux to the container surface, due to microbiological sulphate reduction from outside the buffer, to lead to ~0.02 mm of corrosion loss over a period of 10^3 years, whereas, the estimated anaerobic corrosion rate due to water reduction over this period is 1 mm (Johnson & King, 2003).

3.7.7 Environmental-assisted cracking

SCC at a weld has been evaluated and deemed unlikely based on a range of reported studies (JNC, 2000). Nagra (Nagra, 2002) also consider SCC of welded steel containers to be unlikely owing to the anticipated pH of the bentonite porewater (~7.3), which is outside the range at which SCC of steel in HCO_3^-/CO_3^{-2} occurs (i.e., around pH 10-11 or around pH 6) (Johnson & King, 2003). Furthermore, if a crack was able to initiate, its growth is expected to stifle in a repository environment, owing to the absence of cyclic loading (Nagra, 2002).

Cracking of carbon steel by SCC and hydrogen embrittlement is excluded by reasoned argument in the Japanese concept. This is achieved by consideration of the chemical environment, the material properties (e.g., strength of steel) and the expected stress levels. In particular, the use of heat treatments, both on the bulk material and for welds, is expected to largely eliminate tensile residual stresses or reduce them to levels where they are insignificant from an environmental-assisted cracking perspective (NUMO, 2021).

The susceptibility of both plain and welded carbon steel to SCC in high pH (13.6) porewater was investigated for conditions relevant to the Belgian Supercontainer concept. Slow strain rate testing was performed at 140°C in the presence of sulphide concentrations up to 15.6 mM. During testing, the fracture properties of plain carbon steel in the test solution were comparable to that in argon, indicating no susceptibility to SCC. In comparison, welded specimens exhibited a slight reduction in ductility but not to the extent that would constitute a susceptibility to SCC and this was supported by fractographic analysis of the fracture surfaces, which exhibited ductile fracture features. Hence it was concluded that carbon steel is immune to SCC in the conditions tested (Kursten B., 2017).

The risk of hydrogen embrittlement of carbon steel containers was reviewed in the context of the Swiss concept by Turnbull (Turnbull, 2009). This assessment concluded that the risk of hydrogen embrittlement and cracking of the carbon steel canisters was minimal.

3.7.8 Weld corrosion

In the Japanese concept, the risk of weld corrosion is accounted for by allowing an additional 3 mm corrosion allowance for welded regions, to account for the possibility of undetected welding defects of up to 3 mm in depth. Preferential weld corrosion is also considered and is mitigated by the use of Ni doping of the weld material.

3.7.9 Prediction of canister lifetimes and implications for PA

Steel canisters are designed with conservative lifetimes of 1,000 to 10,000 years, which is considerably shorter than for copper canisters owing to continuous corrosion during anoxic conditions of the order of <0.1 μm yr^{-1}, for cementitious alkaline conditions, or 1-2 μm yr^{-1} , for carbon steel in bentonite (Nagra, 2002) (Kursten B., 2017) (NUMO, 2021). However, due to the level of conservativism adopted, it is expected that actual canister lifetimes will far exceed the design life. For example, in the Japanese concept, the overpack is expected to last in excess of 17,000 years, which is far beyond the design life. Table 3-5 summarises the approaches taken for dealing with the corrosion of iron-based canisters in PAs by various WMOs, according to the various possible corrosion mechanisms for steel. It should be noted that the planned experimental work in the ConCorD project should provide information that can be used to support the assessment of radiation-induced corrosion effects and microbial corrosion.

EURAD (Deliverable n° 1.1) – Initial State-of-the-art of WP ConCorD
Dissemination level: Public
Date of issue of this report: 17/08/2022

Page 122

Mode of corrosion	France	Belgium	Switzerland	Japan	United Kingdom	Czech republic
Anaerobic general corrosion	Empirical corrosion rate		Empirical corrosion rate and pitting factor		Empirical corrosion rate	
Radiolysis-induced corrosion	Limit dose rate to 10 Gy hr^{-1}.	No effect for dose rate of 25 Gy hr^{-1}.	Design requirement (<1 Gy hr^{-1})	Limit dose rate to 3 Gy hr^{-1}		
Localised corrosion		Reasoned argument based on passivity of surface film	Depth-dependent pitting factor	Mass balance and extreme value statistical analysis		
SCC	Specify resistant material	Exclude by reasoned argument				
MIC			Corrosion allowance based on mass transport	Excluded by reasoned argument – negligible rate		

Table 3-5: Comparison of approaches currently taken to account for various different types of corrosion in performance assessments for <u>iron-based</u> canisters by international waste management organisations (blank cells reflect an absence of information within the public domain).

3.8   Summary

The role of Task 6 within ConCorD will be to use modelling to support future performance assessments by developing tools to support the prediction of canister lifetimes with respect to degradation by corrosion. Inputs to modelling will be taken from experimental work generated from other Tasks within ConCorD as well as from existing data taken from the wider literature, and will focus on producing tools to be applied at the laboratory scale (e.g. supporting the interpretation of laboratory results through improved mechanistic understanding) and at the repository scale. It is the aim that by applying coupled models that address the influence of several phenomena simultaneously, new, deeper insights can be made into the dominant factors that need to be considered within canister performance assessment.

EURAD (Deliverable n° 1.1) – Initial State-of-the-art of WP ConCorD
Dissemination level: Public
Date of issue of this report: **17/08/2022**

Page 123

References

Adams, J., Cowgill, M., Moskowitz, P., Rokhvarger, A.E., 2000, Effect of radiation on spinel ceramics for permanent containers for nuclear waste transportation and storage. BNL Report BNL-67518, Brookhaven National Laboratory, Upton NY.

Ahmad, Z., 2006. Principles of Corrosion Engineering and Corrosion Control. Butterworth-Heinemann, p. 672

Ahn, T.M., Soo, P. 1995. Corrosion of Low-Carbon Cast Steel in Concentrated Synthetic Groundwater at 80 to 150°C. Waste Management 15: 471–76.

Alkhimov, A.P., Kosarev, V.F., Klinkov, S.V., Sova, A.A., 2012. Effect of a conical separation region on cold gas-dynamic spraying. Journal of Applied Mechanics and Technical Physics 53: 948-953.

Alkhimov, A.P., Kosarev, V.F., Klinkov, S.V., Sova, A.A., Trubacheev, G.V. 2012. Conical separation zone formation at impingement of supersonic jet on obstacle under cold spraying. Thermophysics and Aeromechanics 19: 225-232.

Allard, Th, Balan, E., Calas, G., Fourdrin, C., Morichon, E., Sorieul, S. 2012. Radiation-Induced Defects in Clay Minerals: A Review. Nucl. Instrum. Methods Phys. Res. B 277: 112–20.

Allard, Th, Calas, G. 2009. Radiation Effects on Clay Mineral Properties. Appl. Clay Sci. 43: 143-49.

Andersson, C.-G., et al. 2004. SKB TR-04-23 - Status report, canister fabrication. SKB, p. 96.

Andersson, J. 1999. Data and data uncertainties. Compilation of data and data uncertainties for radionuclide transport calculations. SKB Technical Report TR-99-09. Stockholm: Swedish Nuclear Fuel and Waste Management Co.

Andra 2005. Dossier 2005 Argile - Phenomenological evolution of a gelogical repository.

Anon., 1980, Comparison of the various alternative shielding methods and evaluation of their practicability. KfK 3000, Nuclear Research Centre, Karlsruhe.

Appelo, C. A. J. 2013. A review of porosity and diffusion in bentonite. Working Report 2013-29, Posiva Oy, Finland.

Arcos, D., Hernán, P., de la Cruz, B., Herbert, H.-J., Savage, D., Smart, N.R., Villar, M.V., Van Loon L.R. 2005. NF-PRO: Understanding and physical and numerical modelling of the key processes in the near field and their coupling for different host rocks and repository strategies, EDZ development and evolution. RTDC-2 Synthesis report, EC integrated project NF-PRO Deliverable D-No:2.6.4.

Arthur, R., Zhou, W. 2005. Reactive-transport model of buffer cementation. SKI Report 2005:59, Swedish Nuclear Power Inspectorate, Stockholm, Sweden.

ASTM. 2005. Standard Guide for Examination and Evaluation of Pitting Corrosion. ASTM G 46 94, American Society for Testing and Materials.

ASTM. 2010. Standard Guide for Applying Statistics to Analysis of Corrosion Data. ASTM G 16 95, American Society for Testing and Materials.

Atkinson, A., Everitt, N.M., Guppy, R.M. 1988. Evolution of pH in a radwaste repository: Internal reactions between concrete constituents. UKAEA Report AERE-R12939.

Aurubis, 2022. Finland Oy - Download Center, datasheets 2022, available/ link: Download Center - Aurubis Finland Oy).

Aziz, P. M., 1956. Application of the Statistical Theory of Extreme Values to the Analysis of Maximum Pit Depth Data for Aluminium. Corrosion 12: 37.

EURAD (Deliverable n° 1.1) – Initial State-of-the-art of WP ConCorD
Dissemination level: Public
Date of issue of this report: 17/08/2022

Page 124

Bagnoud, A., et al. 2016. A minimalistic microbial food web in an excavated deep subsurface clay rock. FEMS microbiology ecology 92: fiv138. https://doi.org/10.1093/femsec/fiv138

Bamoulid, L., et al. 2008. An efficient protection of stainless steel against corrosion: Combination of a conversion layer and titanium dioxide deposit. Surf. Coat. Technol. 202: 5020-5026.

Baroux, C., Martin, C. 2016. Summary Report of the preliminary feasibility study for ceramic HLW overpacks. Andra Report CG.RP.ASCM.13.0023.

Beattie, T.M., Williams, S.J. 2012. An overview of near-field evolution research in support of the UK geological disposal programme. Mineralogical Magazine 76: 2995-3001.

Beese-Vasbender, P.F., Nayak, S., Erbe, A., Stratmann, M., Mayrhofer, K.J.J. 2015. Electrochemical characterization of direct electron uptake in electrical microbially influenced corrosion of iron by the lithoautotrophic SRB Desulfopila corrodens strain IS4. Electrochim. Acta 167: 321-329.

Belmokhtar, M., Delage, P., Ghabezloo, S., Conil, N. 2017. Thermal volume changes and creep in the Callovo-Oxfordian claystone. Rock Mechanics and Rock Engineering 50: 2297-2309.

Belous, V.A. et al. 2013. Development of ion-plasma technology of deposition of the nanostructure bactericidal coatings on orthopaedic implantats and fixative devices. Production of pilot samples for verification of their use in clinic. Science and Innovation 9: 46-60. ISSN 1815-2066.

Belous, V.A., Lunyov, V.M., Kuprin, A.S., Bortnitskaya, M.A. 2018. Structure and properties of TiOx and TiNxOy coatings formed in vacuum arc plasma fluxes. Probl. At. Sci. Technol. 118: 297-299.

Ben Lagha, S., Crusset, D., Mabille, I., Tran, M., Bernard, M.C., Sutter, E. 2007. Corrosion of iron: A study for radioactive waste canisters. J. Nucl. Mater. 362: 485-492.

Bengtsson, A. et al. 2017. Technical report NAB 16-15FEBEX-DP: Microbiological report. Nagra, Wettingen, Switzerland.

Bengtsson, A., Blom, A., Hallbeck, B., Heed, C., Johansson, L., Stalén, J., Pedersen, K., 2017. Microbial sulphide-producing activity in water saturated MX-80, Asha and Calcigel bentonite at wet densities from 1 500 to 2000 kg m−3. SKB TR-16-09, SKB, Sweden.

Bengtsson, A., Blom, A., Taborowski, T., Schippers, A., Edlund, J., Kalinowski, B., Pedersen, K., 2017. FEBEX-DP: Microbiological Report. NAB 16-015, Nagra, Switzerland.

Bengtsson, A., Pedersen, K. 2017. Microbial sulphide-producing activity in water saturated Wyoming MX-80, Asha and Calcigel bentonites at wet densities from 1500 to 2000kgm−3. Appl. Clay Sci. 137: 203-212.

Bengtsson, A., Pedersen, K. 2017. Microbial sulphide-producing activity in water saturated Wyoming MX-80, Asha and Calcigel bentonites at wet densities from 1500 to 2000 kg m−3. Appl. Clay Sci. 137: 203-212.

Bessho, K., Oki, Y., Akimune, N., Matsumura, H., Masumoto, K., Sekimoto, S., Osada, N., Kinoshita, N., Monjushiro, H., Shibata, S. 2015. Corrosion of copper in water and colloid formation under intense radiation field. J. Radioanal. Nucl. Chem. 303: 1117-1121.

Bienek, H., Finkbeiner, R., Wick, W. 1984. Container closure means for storage of radioactive material. US Patent 4,437,578, March-1984.

Biesinger M. C. 2017. Advanced analysis of copper X-ray photoelectron spectra. Surf. Interface Anal. 49: 1325-1334.

Biesinger, M. C.; Lau, L. W. M.; Gerson, A. R.; Smart, R. S. C., Resolving surface chemical states in XPS analysis of first row transition metals, oxides and hydroxides: Sc, Ti, V, Cu and Zn. Appl. Surf. Sci. 2010, 257, 887-898.

EURAD (Deliverable n° 1.1) – Initial State-of-the-art of WP ConCorD
Dissemination level: Public
Date of issue of this report: 17/08/2022

Page 125

Bildstein, O., Trotignon, L., Perronnet, M., Jullien, M. 2006. Modelling iron–clay interactions in deep geological disposal conditions. Phys. Chem. Earth 31: 618–625.

Birgersson, M., Karnland, O. 2009. Ion equilibrium between montmorillonite interlayer space and an external solution – Consequences for diffusional transport. Geochim. Cosmochim. Acta 73: 1908–1923.

Björkbacka, Å., Hosseinpour, S., Johnson, M., Leygraf, C., Jonsson., M. 2013. Radiation induced corrosion of copper for spent fuel storage. Radiat. Phys. Chem. 92: 80-86.

Björkbacka, Å., Hosseinpour, S., Leygraf, C., Jonsson, M. 2012. Radiation induced corrosion of copper in anoxic aqueous solution. Electrochem. Solid-State Lett. 15: C5-C7.

Bjorkbacka, Å., Hosseinpour, S., Leygraf, C., Jonsson, M. 2012. Radiation Induced Corrosion of Copper in Anoxic Aqueous Solution. Electrochem. Solid-State Lett. 15: C5-C6.

Björkbacka, Å., Johnson, C.M., Leygraf, C., Jonsson, M. 2016. Role of the oxide layer in radiation-induced corrosion of copper in anoxic water. J. Phys. Chem. C 120: 11450-11455.

Björkbacka, Å., Johnson, C.M., Leygraf, C., Jonsson, M. 2016. Role of the oxide layer in radiation-induced corrosion of copper ion anoxic water. J. Phys. Chem. C 120: 11450-11455.

Björkbacka, Å., Johnson, C.M., Leygraf, C., Jonsson, M. 2017. Radiation induced corrosion of copper in humid air and argon atmospheres. J. Electrochem. Soc. 164: C201-C206.

Björkbacka, Å., Yang, M., Gasparrini, C., Leygraf, C., Jonsson M. 2015. Kinetics and mechanisms of reactions between H_2O_2 and copper and copper oxides. Dalton Trans. DOI: 10.1039/c5dt02024g.

Boyle, C.H., Meguid, S.A., 2015. Mechanical performance of integrally bonded copper coatings for the long-term disposal of used nuclear fuel. Nucl. Eng. Des. 293: 403-412.

Brachet, J., Le Saux, M., Le Flem, M., Urvoy, S., et al. 2015. Ongoing studies at CEA on chromium coated zirconium based nuclear fuel claddings for enhanced accident tolerant LWRs fuel. In Proceedings of the Top Fuel, Zurich, Switzerland, 13–19 September 2015, pp. 13-19.

Braithwaite, J.W., Magnani, N.J.,Munford, J.W. 1980. Titanium alloy corrosion in nuclear waste environments. NACE CONF-800305, p. SAND-79-2023C.

Brandberg, F., Skagius, K. 1991. Porosity, sorption, and diffusivity data compiled for the SKB 91 study. TR 91-16, SKB, Sweden.

Brehm, W.F. 1990. Corrosion of Ferrous Materials in a Basaltic Environment, in Workshop on corrosion of nuclear fuel waste containers, AECL-10121, 227-233.

Brennenstuhl, A.M., McBride, A., Ramamurthy, S., Davidson, R. 2002. The effects of microstructural and environmental factors on underdeposit corrosion of oxygen-free phosphorous-doped copper. Report 06819-REP-01200-10079-R00, Ontario Power Generation, Nuclear Waste Management.

Bresle, S.Å., Arrhenius, B. 1983. Studies in pitting corrosion on archaeological bronzes. Copper. SKB TR 83-05. Svensk Kärnbränslehantering AB.

Briggs, S., Lilja, C., King, F. 2020. Probabilistic model for pitting of copper canisters. Mater. Corros. 72: 308-316.

Briggs, S., McKelvie, J., Keech, P., Sleep, B., Krol, M. 2017. Transient modelling of sulphide diffusion under conditions typical of a deep geological repository. Corros. Eng. Sci. Technol. 52: 200-203.

Brown, A.R., Boothman, C., Pimblott, S.M., Lloyd, J.R. 2015. The Impact of Gamma Radiation on Sediment Microbial Processes. Appl. Environ. Microbiol. 81: 4014-4025.

Burzan, N. 2021. Energetics and Dynamics of Copper-coordinated Complexes Using Force Fields and Density Functional Theory, Thesis for: Master of Science, March 2016. DOI:10.13140/RG.2.1.3036.3282. EPFL, Lausanne.

EURAD (Deliverable n° 1.1) – Initial State-of-the-art of WP ConCorD
Dissemination level: Public
Date of issue of this report: 17/08/2022

Page 126

Burzan, N., 2021. Growth and viability of microorganisms in bentonite and their potential activity in deep geological repository environments, PhD Thesis, École Polytechnique Fédérale de Lausanne EPFL, Lausanne.

Carlson, L., Karnland, O., Olsson, S., Rance, A., Smart, N. 2006. Experimental studies on the interactions between anaerobically corroding iron and bentonite. Posiva Working Report 2006-06. Posiva.

Carlsson, T., Muurinen, A. 2008. A Practical and Theoretical Basis for Performing Redox-measurements in compacted Bentonite _ A Literature Survey. Posiva Working Report 2008-51. Posiva, Eurajoki, Finland.

Carpen, L., Rajala, P., Bomberg, M. 2018. Corrosion of Copper in Anoxic Ground Water in the Presence of SRB. Corros. Sci. Technol.-Korea 17: 147-153.

Cedeno-Vente, M.L. et al. 2021. Application of a transmission line model to evaluate the influence of structural defects on the corrosion behaviorbehaviour of arc-PVD CrN coatings. Ceram. Int. 47: 20885-20899.

Cen, S., Lv, X., Xu, B., Xu, Y. 2018. The Effect of Gradient Bias Design on Electrochemistry and Tribology BehaviorBehaviours of PVD CrN Film in a Simulative Marine Environment. Materials 11: 1753-16.

Černá, K., Bartak, D.S., 2019. State of art – attachment I to the Work report 2019, Project Limiting Factors for survivability and proliferation of microorganisms significant for corrosion of deep geological repository barrier systems (BioBen) Project number: TAČR TK02010169.

Černá, K., Černoušek, T., Polívka, P., Ševců, A., Steinová, J. 2015. MIND Deliverable 2.15: Survival of microorganisms in bentonite subjected to different levels of irradiation and pressure. https://www.mind15.eu/deliverables/

Červinka, R., Vašíček, R., a kolektiv 2018. Kompletní charakterizace bentonitu. BCV 2017, SÚRAO TZ 419/2019.

Chapon, V., Piette, L., Vesvres, M.-H., Coppin, F., Marrec, C.L., Christen, R., Theodorakopoulos, N., Février, L., Levchuk, S., Martin-Garin, A., Berthomieu, C., Sergeant, C. 2012. Microbial diversity in contaminated soils along the T22 trench of the Chernobyl experimental platform. Appl. Geochem. 27: 1375-1383.

Chatterjee, M. et al. 2021. Proteomic study of Desulfovibrio ferrophilus IS5 reveals overexpressed extracellular multi-heme cytochrome associated with severe microbiologically influenced corrosion. Sci. Rep. 11: 15458.

Cheptsov V.S., Vorobyova, E.A., Gorlenko, M.V., Manucharova, N.A., Pavlov, A.K., Lomasov, V.N. 2018. Effect of gamma radiation on viability of a soil microbial community under conditions of Mars. Paleontol. J. 52: 1217-1223.

Chikkamath, S., Manjanna, J., Kabadagi, A., Patil, D., Tripathi, V.S., Kar, A.S., Tomar, B.S. 2021. Gamma (^{60}Co) Irradiation and Thermal Effect on Redox BehaviorBehaviour of Interlayer Iron in Montmorillonite. Appl. Clay Sci. 200: 105893. doi: 10.1016/j.clay.2020.105893.

Clark, D.E., Sutton, W.H. 1996. Microwave Processing of Materials. Ann. Rev. Mater. Sci. 26: 299-331.

Cloet, V., Pekala, M., Smith, P., Wersin, P., Diomidis, N. 2017. An evaluation of sulphide fluxes in the near field of a HLW repository. Technical Report 17-04, Nagra, Switzerland

COMSOL, 2020. COMSOL Multiphysics® v. 5.6. COMSOL AB, Sweden.

Corbel, C., Féron, D., Roy, M., Maurel, F., Wasselin-Trupin, V., Hickel, B. 2003. Effect of irradiation on long term alteration of oxides and metals in aqueous solutions. In: Féron, D., Macdonald, D.D. (eds). Prediction of long-term corrosion behaviour in nuclear waste systems: proceedings of an international

EURAD (Deliverable n° 1.1) – Initial State-of-the-art of WP ConCorD
Dissemination level: Public
Date of issue of this report: 17/08/2022

Page 127

workshop, November, Cadarache, France. London: Maney Pub. European Federation of Corrosion Publications 36: 484–502.

Costello, J.A. 1974. Cathodic depolarization by sulfate-reducing bacteria. S. Afr. J. Sci. 70: 202-204.

Cottis, R. A. 2010. Neural Network Methods for Corrosion Data Reduction, Chapter 2.40 in Shreir's Corrosion. 4th. Edited by M.J. Graham, R. Lindsay, S.B. Lyon, J.A. Richardson, J.D. Scantlebury and F.H. Stott R.A. Cottis. Vol. 2. Elsevier.

Couture, R.A. 1985. Steam rapidly reduces the swelling capacity of bentonite. Nature 318: 50-52.

Crusset, D. et al. 2017. Corrosion of carbon steel components in the French high-level waste program: evolution of disposal concept and selection of materials. Corros. Eng. Sci. Technol. 52: 17-24.

Crusset, D., Deydier,V., Necib, S., Gras, J.-M., Combrade, P., Féron, D., Burger, E. 2017. Corrosion of Carbon Steel Components in the French High-Level Waste Programme: Evolution of Disposal Concept and Selection of Materials. Corros. Eng. Sci. Technol. 52: 17–24. doi: 10.1080/1478422X.2017.1344416.

Čuba, V., Silber, R., Múčka, V., Pospíšil, M., Neufuss, S., Bárta, J., Vokál, A. 2011. Radiolytic Formation of Ferrous and Ferric Ions in Carbon Steel – Deaerated Water System. Radiat. Phys. Chem. 80: 440–45. doi: 10.1016/j.radphyschem.2010.09.012.

Cuevas, J., Villar, M., Fernández, A., Gomez, P., Martín, P. 1997. Pore waters extracted from compacted bentonite subjected to simultaneous heating and hydration. Appl. Geochem. 12: 473-481.

Dadachova, E., Casadevall, A. 2008. Ionizing radiation: how fungi cope, adapt, and exploit with the help of melanin. Curr. Opin. Microbiol. 11: 525-531.

Daly, M.J. 2009. A new perspective on radiation resistance based on *Deinococcus radiodurans*. Nat. Rev. Microbiol. 7: 237-245.

Daly, M.J. et al. 2007. Protein Oxidation Implicated as the Primary Determinant of Bacterial Radioresistance. PLOS Biology 5: e92.

Dante, J.F., Kelly, R.G. 1993. The Evolution of the Adsorbed Solution Layer during Atmospheric Corrosion and Its Effects on the Corrosion Rate of Copper. J. Electrochem. Soc. 140: 1890.

Daub, K., Van Nieuwenhove, R., Nordin, H. 2015. Investigation of the impact of coatings on corrosion and hydrogen uptake of Zircaloy-4. J. Nucl. Mater. 467: 260-270.

Daub, K., Zhang, X., Noël, J.J., Wren, J.C. 2010. Effects of γ-Radiation versus H_2O_2 on Carbon Steel Corrosion. Electrochim. Acta 55: 2767–2776. doi: 10.1016/j.electacta.2009.12.028.

Daub, K., Zhang, X., Noël, J.J., Wren, J.C. 2019. Gamma Radiation-Induced Carbon Steel Corrosion. ECS Trans. 33:15–24. doi: 10.1149/1.3557748.

Daub, K., Zhang, X., Noël, J.J., Wren, J.C.. 2011. Gamma-Radiation-Induced Corrosion of Carbon Steel in Neutral and Mildly Basic Water at 150°C. Corros. Sci. 53: 11–16. doi: 10.1016/j.corsci.2010.09.048.

de Chialvo, M.R., Salvarezza, R.C., Vasquez, M.D., Arvia, A.J. 1985. Kinetics of passivation and pitting corrosion of polycrystalline copper in borate buffer solutions containing sodium chloride. Electrochim. Acta 30: 1501-1511.

De Windt L., Miron G.D., Fabian M., Goethals, J., Wittebroodt C. 2020. First results on the thermodynamic databases and reactive transport models for steel-cement interfaces at high temperature. Final version of deliverable D2.8 of the HORIZON 2020 project EURAD. EC Grant agreement no: 847593.

Debruyn, W. 1988. Corrosion of Container Materials under Clay Repository Conditions. Proceedings of a workshop on corrosion of nuclear fuel waste containers 148: 148–162.

Deck, C.P., Khalifa, H.E., Shapovalov, K.S. 2018. SiC-SiC Composite Cladding Development for Accident Tolerant Fuel. Trans. Am. Nucl. Soc. 118: 1305-1308.

Deissmann G., Ait Mouheb, N., Martin, C., Turrero, M.J., Torres, E., Kursten, B., Weetjens, E., Jacques, D., Cuevas, J., Samper, J., Montenegro, L., Leivo, M., Somervuori, M., Carpen, L. 2021. Experiments and numerical model studies on interfaces. Final version as of 12.05.2021 of deliverable D2.5 of the HORIZON 2020 project EURAD. EC Grant agreement no: 847593.

Diler, E. et al. 2021. Potential influence of microorganisms on the corrosion of carbon steel in the French high- and intermediate-level long-lived radioactive waste disposal context. Mater. Corros. 72: 218-234.

Diomidis N., Johnson, L.H. 2014. Materials options and corrosion-related considerations in the design of spent fuel and high-level waste disposal canisters for a deep geological repository in opalinus clay. JOM. 66:461–470.

Diomidis, N., Cloet, V., Leupin, O., Marschall, P., Poller, A., Stein, M., 2016. Production, consumption and transport of gases in deep geological repositories according to the Swiss disposal concept. Nagra Technical Report NTB 16-03.

Dixon, D.A. 2019. Review of the T-H-M-C Properties of MX-80 Bentonite. Technical report NWMO-TR 2019-07, Nuclear Waste Management Organization, Toronto, Ontario, Canada.

Drogowska, M., Brossard, L., Ménard, H. 1992. Copper dissolution in $NaHCO_3$ and $NaHCO_3$ + NaCl aqueous solutions at pH 8. J. Electrochem. Soc. 139: 39-47.

Duro, L., Bruno, J., Grivé, M., Montoya, V., Kienzler, B., Altmaier, M., Buckau, G. 2014. Redox processes in the safety case of deep geological repositories of radioactive wastes. Contribution of the European RECOSY Collaborative Project. Appl. Geochem. 49: 206-217.

Ekeroth, E., Roth, O., Jonsson, M. 2006. The relative impact of radiolysis products in radiation induced oxidative dissolution of UO_2. J. Nucl. Mater. 355: 38-46.

El Hajj, H., Abdelouas, A., El Mendili, Y., Karakurt, G., Grambow, B., Martin, C. 2013. Corrosion of carbon steel under sequential aerobic-anaerobic environmental conditions. Corros. Sci. 76: 432-440.

El Mendili, Y., Abdelouas, A., Karakurt, G., Ait Chaou, A., Essehli, R., Bardeau, J.-F., Grenèche, J.-M., 2015. The effect of temperature on carbon steel corrosion under geological conditions. Appl. Geochem. 52: 76-85.

Eldredge, G.G. 1957. Analysis of Corrosion Pitting by Extreme Value Statistics and its Application to Oil Well Tubing Caliper Surveys. Corrosion 13: 67.

Enning, D. et al. 2012. Marine sulfate-reducing bacteria cause serious corrosion of iron under electroconductive biogenic mineral crust. Environ. Microbiol. 14: 1772-1787.

Enning, D., Garrelfs, J. 2014. Corrosion of Iron by Sulphate-Reducing Bacteria: New Views of an Old Problem. Appl. Environ. Microbiol. 80: 1226-1236.

Esbelin, J., Santos, T., Hébraud, M. 2018. Desiccation: An environmental and food industry stress that bacteria commonly face. Food Microbiol. 69: 82-88.

Escobar, I S, E Silva, C Silva, and A Ubal. 1999. Study of the effect of sulphide ions on the corrosion resistance of copper for use in containers for high-level waste. Proceedings of 4th International Conference Copper 99 – Cobre 99. Vol. I. Warrendale, PA. Minerals, Metals, and Materials Society: 371–386.

Fénart, M., Lameille, J. M., Le Flem, M., Le Tutour, P., & Féron, D. 2021. Influence of irradiation on water-saturated corrosion of carbon steels at 80ºC. Mater. Corros. 72: 255-267.

Fernández, A.M, Alonso, U. 2021. Revision of existing data for the selection of Cu ad Fe-corrosion products. Milestone MS.264: Concord Project.

EURAD (Deliverable n° 1.1) – Initial State-of-the-art of WP ConCorD
Dissemination level: Public
Date of issue of this report: 17/08/2022

Page 129

Fernández, A.M, Baeyens, B., Bradbury, M. and Rivas, P. 2004. Analysis of the porewater chemical composition of a Spanish compacted bentonite used in an engineered barrier. Phys. Chem. Earth 29: 105-119.

Fernández, A.M. 2019. Gas and water sampling from the FEBEX in situ test. Nagra Working Reports. NAB 16-13, 155 pp. NAGRA Technical Report.

Fernández, A.M. 2019. Geochemical outcomes of the dismantling of the engineered barrier emplacement (EB) experiment at Mont Terri (Switzerland). Informes Técnicos CIEMAT. 1469, 133. CIEMAT, 22/12/2019. ISSN 1135-9420.

Fernández, A.M., Marco, J.F., Nieto, P., León, F.J., Robredo, L.M., Clavero, M.A., Cardona, A., Fernández, S., Svensson, D., Sellin, P. 2022. Characterization of Bentonites from the in situ ABM5 Heater Experiment at Äspö Hard Rock Laboratory, Sweden. Minerals 12: 471. https://doi.org/10.3390/min12040471.

Fernández, A.M., Villar, M.V. 2010. Geochemical behaviour of a bentonite barrier: results up to 8 years of thermo-hydraulic treatment in the laboratory. Appl. Geochem. 25: 809-824.

Fernández, A.M.; Sánchez-Ledesma, D.M.; Melón, A.; Robredo, L.M.; Rey, J.J.; Labajo, M.; Clavero, M.A.; Fernández, S.; González, A.E. 2018. Thermo-hydro-chemical (THC) behaviour of a Spanish Bentonite after dismantling Heater#1 and Heater#2 of the FEBEX in situ test at the Grimsel Test Site. Nagra Working Reports. NAB 16-25, 583 pp. NAGRA, 2018.

Fernandez, R., Jodoin, B. 2018. Cold Spray Aluminum–Alumina Cermet Coatings: Effect of Alumina Content, J. Therm. Spray Technol., 27, 603-623.

Feron, D., Crusset, D. 2014. Microbial induced corrosion in French concept of nuclear waste underground disposal. Corros. Eng. Sci. Technol. 49: 540-547.

Finsterle, S., Muller, R.A., Baltzer, R., Payer, P., Rector, J.W. 2019. Thermal Evolution near Heat-Generating Nuclear Waste Canisters Disposed in Horizontal Drillholes. Energies 12: 596.

Fredrickson, J.K. et al. 1997. Pore-size constraints on the activity and survival of subsurface bacteria in a late cretaceous shale-sandstone sequence, northwestern New Mexico. Geomicrobiol. J. 14: 183-202.

Gens, A.; Sánchez, M.; Guimarães, L.; Alonso, A.A.; Loret, A.; Olivella, S.; Villar, M.V.; Huertas, F.A. 2009. Full-scale in situ heating test for high-level nuclear waste disposal: Observations, analysis and interpretation. Géotechnique 59: 377–399.

Gimmi, T., Alt-Epping, P. 2018. Simulating Donnan equilibria based on the Nernst-Planck equation. Geochim. Cosmochim. Acta 232: 1–13.

Gournis, D., Mantaka-Marketou, A.E., Karakassides, M.A., Petridis, D. 2000. Effect of γ-Irradiation on Clays and Organoclays: A Mössbauer and XRD Study. Phys. Chem. Miner. 27: 514–21. doi: 10.1007/s002690000089.

Gray, W. J. 1987. Effects of Radiation on the Oxidation Potential of Salt Brine. MRS Proceedings 112: 405. doi: 10.1557/PROC-112-405.

Greffe, V.R.G., Michiels, J. 2020. Desiccation-induced cell damage in bacteria and the relevance for inoculant production. Appl. Microbiol. Biot. 104: 3757-3770.

Grousset, S., et al. 2020. Biocorrosion detection by sulphur isotopic fractionation measurements. Corros. Sci. 165: 108386.

Gu, B.X., Wang, L.M., Minc, L.D., Ewing, R.C. 2001. Temperature Effects on the Radiation Stability and Ion Exchange Capacity of Smectites. J. Nucl. Mater. 297: 345–54. doi: 10.1016/S0022-3115(01)00631-6.

Guinan, M.W. 2001. Radiation effects in spent nuclear fuel canisters. Swedish Nuclear Fuel and Waste Management Co, SKB Technical Report TR-01-32.

EURAD (Deliverable n° 1.1) – Initial State-of-the-art of WP ConCorD
Dissemination level: Public
Date of issue of this report: 17/08/2022

Page 130

Gumbel, E.J. 1958. Statistics of Extremes. Columbia University Press.

Gunasegaram, D.R., Ventaraman, M.S., Cole, I.S. 2014. Towards Multiscale Modelling of Localised Corrosion. Int. Mater. Rev. 59: 84-114.

Gutiérrez, M.M., Caruso, S., Diomidis, N. 2018. Effects of materials and design on the criticality and shielding assessment of canister concepts for the disposal of spent nuclear fuel. Appl. Radiat. Isot. 139: 201-208.

Hadi, J., Wersin, P., Serneels, V., Greneche, J.M. 2019. Eighteen years of steel-bentonite interaction in the FEBEX "in situ" test at the Grimsel Test Site in Switzerland. Clays Clay Miner. 67: 111–131.

Hall, D.S., et al. 2021. An evaluation of corrosion processes affecting copper-coated nuclear waste containers in a deep geological repository. Prog. Mater. Sci. 118: 100766.

Hall, D.S., Keech, P.G. 2017. An Overview of the Canadian Corrosion Program for the Long-term Management of Nuclear Waste. Corros. Eng. Sci. Technol. 52: 2-5.

Hallberg, R.O., Engvall, A.G., Wadston, T. 1984. Corrosion of copper lightning conductor plates. Br. Corros. J. 19: 85-88.

Hammond, G., Lichtner, P., Mills, R. 2014. Evaluating the performance of parallel subsurface simulators: An illustrative example with PFLOTRAN. Water Resour. Res. 50: 208–228.

Haynes, H.M., Pearce, C.I., Boothman, C., Lloyd, J.R. 2018. Response of bentonite microbial communities to stresses relevant to geodisposal of radioactive waste. Chem. Geol. 501: 58-67.

Heuser, M., Weber, C., Stanjek, H., Chen, H., Jordan, G., Schmahl, W.W., Natzeck, C. 2014. The Interaction between Bentonite and Water Vapor. I: Examination of Physical and Chemical Properties. Clays and Clay Miner. 62: 188–202. doi: 10.1346/CCMN.2014.0620303.

Hoch, A., Turnbull, A., Smart, N.R. 2018. Literature Review of AGR-relevant Corrosion Modelling and Simulation. NDA Report 207338/001, NDA.

Hoch, A.R., Smart, N.R., Wilson, J.D., Reddy, B. 2010. A Survey of Reactive Metal Corrosion Data for Use in the SMOGG Gas Generation Model. Serco Report SA/ENV-0895, issue 2.

Holdsworth, S.R. 2018. Alternative coating Materials as Corrosion Barriers for SF and HLW Disposal Canisters. NAGRA report NAB18-19.

Holdsworth, S.R., 2013. Ceramic Material Solutions for Nuclear Waste Disposal Canisters. NAGRA report NAB12-45.

Holdsworth, S.R., 2014. Feasibility evaluation study of candidate canister solutions for the disposal of spent nuclear fuel and high-level waste-A status review. NAGRA report NAB14-90.

Holmboe, M., Jonsson, M., Wold, S. 2012. Influence of γ-Radiation on the Reactivity of Montmorillonite towards H_2O_2. Radiat. Phys. Chem. 81:190–94. doi: 10.1016/j.radphyschem.2011.10.009.

Hou, Y., Aldrich, C. Lepkova, K., Machuca, L.L., Kinsella, B. 2016. Monitoring of Carbon Steel Corrosion by Use of Electrochemical Noise and Recurrence Quantification Analysis. Corros. Sci. 112: 63-72.

Huertas, F. et al. 2005. Full-Scale Engineered Barriers Experiment for a Deep Geological Repository for High-Level Waste in Crystalline Host Rock – Phase II. Euratom EUR 21922.

Huertas, F., Fariña, P., Farias, J., García-Siñeriz, J.L., Villar, A.M., Fernández, A.M., Martín, P.L., Elorza, F.J., Gens, A., Sánchez, M., Lloret, A., Samper, J., Martínez, M.A. 2006. FEBEX Project. Full-scale engineered barriers experiment for a deep geological repository for high level radioactive waste in crystalline host rock. Updated Final Report 1994-2004. Technical Publication ENRESA 5-0/2006: 590. Madrid.

Hunter, F., Bate, F., Heath, T., Hoch, A. 2007. Geochemical Investigation of Iron Transport into Bentonite as Steel Corrodes. SKB Report TR-07-09.

EURAD (Deliverable n° 1.1) – Initial State-of-the-art of WP ConCorD
Dissemination level: Public
Date of issue of this report: 17/08/2022

Page 131

Hutchison, E.A., Miller, D.A., Angert, E.R., Eichenberger, P., Driks, A. 2014. Sporulation in Bacteria: Beyond the Standard Model. Microbiol. Spectr. 2: doi: 10.1128/microbiolspec.TBS-0013-2012.

IAEA, 2006. Development of Specifications for Radioactive Waste Packages. Technical report TECDOC-1515. 2006. International Atomic Energy Agency, Austria. ISBN 92–0–109206–7 ISSN 1011–4289.

Ibrahim, B., Zagidulin, D., Behazin, M., Ramamurthy, S., Wren, J.C., Shoesmith., D.W. 2018. The corrosion of copper in irradiated and unirradiated humid air. Corros. Sci. 141: 53-62.

Ibrahim, B., Zagidulin, D., Behazin, M., Ramamurthy, S., Wren, J.C., Shoesmith, D.W. 2018. The corrosion of copper in irradiated and unirradiated humid air. Corros. Sci. 141: 53-62.

Idiart, A., Coene, E. 2019. Modelling diffusion through compacted bentonite in the BHA vault. R-19-10, SKB, Sweden.

Idiart, A., Coene, E., Bagaria F., Román-Ross G., Birgersson, M. 2019. Reactive transport modelling considering transport in interlayer water. New model, sensitivity analyses and results from the Integrated Sulphide Project inter-model comparison exercise. TR-18-07, SKB, Sweden.

Itälä, A. 2009. Chemical Evolution of Bentonite Buffer in a Final Repository of Spent Nuclear Fuel During the Thermal Phase. VTT Publications 721: 78.

Jacobs, S., Edwards, O. 2000. Sulphide scale catalysis of copper corrosion. Water Res. 34: 2798-2808.

Jakupi, P. et al. 2015. Characterization of commercially cold sprayed copper coatings and determination of the effects of impacting copper powder velocities. J. Nucl. Mater. 466: 1-11.

Jalique, D.R. et al. 2016. Culturability and diversity of microorganisms recovered from an eight-years old highly compacted, saturated MX-80 Wyoming bentonite plug. Appl. Clay Sci. 126: 245-250.

Jenni, A., Wersin, P., Thoene, T., Baeyens, Ferrari, A., Gimmi, T., Mäder , U., Marschall, P. 2019. Bentonite backfill performance in a high-level waste repository: A geochemical perspective. Nagra Technical Report 19-03.

Jia, R., Unsal, T., Xu, D.K., Lekbach, Y., Gu, T.Y. 2019. Microbiologically influenced corrosion and current mitigation strategies: A state of the art review. Int. Biodeterior. Biodegrad. 137: 42-58.

Jiménez-Come, M.J., Turias, I.J. Ruiz-Aguilar, J.J, Trujillo, F.J. 2015. Characterization of Pitting Corrosion of Stainless Steel Using Artificial Neural Networks. Mater.Corros. 66: 1084-1091.

Jiménez-Come, M.J., Turias, I.J., Ruiz-Aguilar, J.J. 2016. A Two-Stage Model Based on Artificial Neural Networks to Determine Pitting Corrosion Status of 316L Stainless Steel. Corros. Rev. 34: 113-125.

JNC 2000. H12: Project to establish the scientific and technical basis for HLW disposal in Japan, Supporting report 2 - Repository Design and Engineering Technology. Technical report JNC TN1410 2000-003. Japan Nuclear Cycle Development Institute, Ibaraki, Japan.

Johansson, A.J., Lilja, C., Sjögren, L., Gordon, A., Hallbeck, L., Johansson, L. 2017. Insights from post-test examination of three packages from the MiniCan test series of copper-cast iron canisters for geological disposal of spent nuclear fuel: impact of the presence and density of bentonite clay. Corros. Eng. Sci. Technol. 52: 54-60.

Johnson, L.H., King, F. 2003. Canister Options for the Disposal of Spent Fuel. Technical report 02-11, National Cooperative for the Disposal of Radioactive Waste, Wettingen, Switzerland.

Johnson, L.H., King, F. 2008. The effect of the evolution of environmental conditions on the corrosion evolutionary path in a repository for spent fuel and high-level waste in Opalinus Clay. J. Nucl. Mater. 379: 9–15.

Johnson, L.H., LeNeveu, D.M., King, F., Shoesmith, D.W., Kolar, M., Oscarson, D.W., Sunder, S., Onofrei, C., Crosthwaite, J.L. 1996. The disposal of Canada's nuclear fuel waste: a study of postclosure

safety of in-room emplacement of used CANDU fuel in copper containers in permeable plutonic rock. Volume 2: vault model. Atomic Energy of Canada Limited Report, AECL-11494-2, COG-96-552-2.

Jolivet, E., L'Haridon, S., Corre, E., Forterre, P., Prieur, D. 2003. Thermococcus gammatolerans sp. nov., a hyperthermophilic archaeon from a deep-sea hydrothermal vent that resists ionizing radiation. Int. J. Syst. Evol. Microbiol. 53: 847-851.

Jonsson, M. 2012. Radiation Effects on Materials Used in Geological Repositories for Spent Nuclear Fuel. International Scholarly Research Notices 2012: 1-13. doi: 10.5402/2012/639520.

Joyce, S., Applegate, D., Appleyard, P., Gordon, A., Heath, T., Hunter, F., Hoek, J., Jackson, P., Swan, D., Woollard, H. 2015. Groundwater Flow and Reactive Transport Modelling in ConnectFlow. SKB Report R-14-19.

Jung, K.-W., Lim, S., Bahn, Y.-S. 2017. Microbial radiation-resistance mechanisms. J. Microbiol. 55: 499-507.

Kalfayan, G. 2019. PhD-Thesis. Procédé d''assemblage par chauffage micro-ondes à température modérée d''un matériau céramique alumino-silicaté pour conteneur de déchets radioactifs. École nationale supérieure des Mines de Saint-Etienne.

Kania, A., Szindler, M.M., Szindler, M. 2021. Structure and corrosion behaviorbehaviour of TiO2 thin films deposited by ALD on a biomedical magnesium alloy. Coatings 11: 70-84.

Kass J., 1990. Evaluation of copper, aluminum bronze, and copper-nickel container material for the Yucca Mountain Project. In: Shoesmith, D.W. (ed). Corrosion of nuclear fuel containers: proceedings of a workshop. AECL-10121, Atomic Energy of Canada Limited: 87–108.

Kaufhold, S., Baille, W., Schanz, T., Dohrmann, R. 2015. About differences of swelling pressure — dry density relations of compacted bentonites. Appl. Clay Sci. 107: 52-61.

Kawana, A., Ichimura, H., Iwata, Y., Ono, S. 1996. Development of PVD ceramic coatings for valve seats. Surf. Coat. Technol. 86-87: 212-117.

Keech, P.G. et al. 2014. Design and development of copper coatings for long term storage of used nuclear fuel. Corros. Eng. Sci. Technol. 49: 425-430.

Keech, P.G., Behazin, M., Binns, J.W., Briggs, S. 2020. An update on the copper corrosion program for the long-term management of used nuclear fuel in Canada. Mater. Corros. 72: 25-31.

Kerber, A., Knorr, J. 2013. SiC encapsulation of high-level waste for long-term immobilization. atw 58: 8-13.

Khadom, A.A. 2016. Comparison of Mathematical and Artificial Neural Network Models for Inhibition of Fuel Oil Ash Under High Temperature Corrosion. Corros. Eng. Sci. Techn. 51: 278-284.

Kiczka, M., Pekala, M., Maanoja, S., Muuri, E., Wersin, P. 2021. Modelling of solute transport and microbial activity in diffusion cells simulating a bentonite barrier of a spent nuclear fuel repository. Appl. Clay Sci. 211: 106193.

King, F. 2005. Evolution of environmental conditions in a deep geological repository in the sedimentary rock of the Michigan Basin, Ontario. Ontario Power Generation Nuclear Waste Management Division Report 06819-REP-01300-10102-R00.

King, F. 2006. Review and gap analysis of the corrosion of copper containers under unsaturated conditions', Ontario Power Generation, Nuclear Waste Management Division Report 06819-REP-01300-10124-R00.

King, F. 2007. Overview of a carbon steel container corrosion model for a deep geological repository in sedimentary rock', Nuclear Waste Management Organization Report NWMO TR-2007-01.

EURAD (Deliverable n° 1.1) – Initial State-of-the-art of WP ConCorD
Dissemination level: Public
Date of issue of this report: 17/08/2022

Page 133

King, F. 2008. Corrosion of carbon steel under anaerobic conditions in a repository for SF and HLW in Opalinus Clay', Nagra Technical Report 08-12, Nagra, Wettingen, Switzerland.

King, F. 2008. Mixed-Potential Modelling of the Corrosion of Copper in the Presence of Sulphide. Working Report 2007-63, Posiva Oy, Finland.

King, F. 2009. Microbiologically influenced corrosion of nuclear waste containers. Corrosion, 65, 233–251.

King, F. 2013. A review of the properties of pyrite and the implications for corrosion of the copper canister. TR-13-19, SKB, Sweden.

King, F. 2013. Container materials for the storage and disposal of nuclear waste. Corrosion 69, 986e1011.

King, F. 2014. Durability of High Level Waste and Spent Fuel Disposal Containers-an overview of the combined effect of chemical and mechanical degradation mechanisms. Appendix B. 6-Corrosion of Nickel Alloys. AMEC Nuclear UK Limited (AMEC).

King, F. 2014. Predicting the Lifetimes of Nuclear Waste Containers. J. Mater. 66: 526-537.

King, F. 2017.Nuclear waste canister materials: corrosion behaviour and long-term performance in geological repository systems. Chapter in: Geological Repository Systems for Safe Disposal of Spent Nuclear Fuels and Radioactive Waste. Eds. Apted, M.J., Ahn, J. Elsevier Ltd: 365-408.

King, F. 2020. Canister Materials for the Disposal of Nuclear Waste. In: Comprehensive Nuclear Materials. 2nd Edition. Elsevier.

King, F. 2021. Review of the effects of γ-radiation on the corrosion behaviour of copper used-fuel containers. Nuclear Waste Management Organization Technical Report, NWMO-TR-2021-22. https://www.nwmo.ca/en/Reports.

King, F., Kolar, M. 2000. The copper container corrosion model used in AECL's second case study. 06819-REP-01200-10041-R00. Ontario Power Generation, Nuclear Waste Management Division.

King, F., Ahonen, C., Taxen, C., Vuorinen, U., Werme, L. 2001. Copper corrosion under expected conditions in a deep geologic repository. SKB Technical Report TR-01-23, Stockholm.

King, F., Ahonen, L., Taxén, C., Vuorinen, U., Werme, L., 2001: Copper corrosion under expected conditions in a deep geologic repository'. SKB report no. TR 01-23, Swedish Nuclear Fuel and Waste Management Company Report, 2001, http://www.skb.se and Posiva Oy report no. POSIVA 2002-01, 2002, http://www.posiva.fi.

King, F., Behazin, M. 2021. A Review of the Effect of Irradiation on the Corrosion of Copper-Coated Used Fuel Containers. Corros. Mater. Degrad. 2: 678-707.

King, F., Chen, J., Qin, Z., Shoesmith, D., Lilja, C. 2017. Sulphide-transport control of the corrosion of copper canisters. Corros. Eng. Sci. Technol. 52: 210-216.

King, F., Hall, D.S., Keech, P.G. 2017. Nature of the near-field environment in a deep geological repository and the implications for the corrosion behaviour of the container. Corros. Eng. Sci. Technol. 52: 25-30.

King, F., Kolar, M. 2006. Consequences of microbial activity for corrosion of copper used fuel containers–analyses using the CCM-MIC. OPG 06819-REP-1300-10120-R00. Toronto, Canada: Ontario Power Generation.

King, F., Kolar, M. 2018. Lifetime Predictions for Nuclear Waste Disposal Containers. Corrosion 75: 309–323.

King, F., Kolar, M. 2019. Copper Sulphide Model (CSM). Model improvements, sensitivity analyses, and results from the Integrated Sulphide Project inter-model comparison exercise. TR-18-08, SKB, Sweden.

EURAD (Deliverable n° 1.1) – Initial State-of-the-art of WP ConCorD
Dissemination level: Public
Date of issue of this report: 17/08/2022

Page 134

King, F., Kolar, M., Maak, P. 2008. Reactive-transport model for the prediction of the uniform corrosion behaviour of copper used fuel containers. J. Nucl. Mater. 379: 133-141.

King, F., Kolář, M., Puigdomenech, I., Pitkänen, P., Lilja, C. 2021. Modelling microbial sulphate reduction and the consequences for corrosion of copper canisters. Mater. Corros. 72: 339-347.

King, F., Kolar, M., Vähänen, M., & Lilja, C. 2011. Modelling long term corrosion behaviour of copper canisters in KBS-3 repository. Corros. Eng. Sci. Technol. 46: 217-222.

King, F., LeNeveu, D. 1991. Prediction of the lifetimes of copper nuclear waste containers. Proceedings of the Topical Meeting on Nuclear Waste Packaging, Focus '91. Las Vegas: La Grange Park: American Nuclear Society: 253-261.

King, F., Lilja, C. 2014. Localised corrosion of copper canisters. Corros. Eng. Sci. Technol. 49: 420-424.

King, F., Lilja, C., Pedersen, K., Pitkänen, P., Vähänen, M. 2010. An Update of the State-of-the-Art Report on the Corrosion of Copper Under Expected Conditions in a Deep Geologic Repository. Swedish Nuclear Fuel and Waste Management Co. Report, Technical Report TR-10-67 and Posiva Oy Report, POSIVA 2011-01.

King, F., Lilja, C., Pedersen, K., Pitkänen, P., Vähänen, M. 2010. An update of the state-of-the-art report on the corrosion of copper under expected conditions in a deep geologic repository. Technical Report TR-10-67, Svensk Kärnbränslehantering AB, Stockholm.

King, F., Litke, C.D. 1987. The corrosion of copper in synthetic groundwater at 150°C. Part I. The results of short-term electrochemical tests. Technical Record TR-428, Atomic Energy of Canada Limited.

King, F., Litke, C.D., George, K.J. 1989. The corrosion of copper in synthetic groundwater at 150ºC. Part II. The characteization of surface films; TR-464; Atomic Energy of Canada Limited.

King, F., Litke, C.D., Quinn, M.J., LeNeveu, D.M. 1995. The measurement and prediction of the corrosion potential of copper in chloride solutions as a function of oxygen concentration and mass-transfer coefficient. Corros. Sci. 37: 833-851.

King, F., Litke, C.D., Ryan, S.R. 1992. A Mechanistic Study Of The Uniform Corrosion Of Copper In Compacted Na-Montmorillonite/Sand Mixtures. Corros. Sci. 33: 1979-1995.

King, F., Newman, R. 2010. Stress corrosion cracking of copper canisters. SKB-TR-10-04, Svensk Kärnbränslehantering AB, Stockholm.

King, F., Padovani, C. 2011. Review of the corrosion performance of selected canister materials for disposal of UK HLW and/or spent fuel. Corros. Eng. Sci. Technol. 46: 82-90.

King, F., Sanderson, D., Watson, S. 2016. Durability of High-Level Waste and Spent Fuel Disposal Containers – an overview of the combined effect of chemical and mechanical degradation mechanisms. AMEC Report 17697/TR/03.

King, F., Watson, S., Wilson, J., Mackenzie, J. 2011. Corrosion of Candidate HLW/Spent Fuel Container Materials in Generic Environments – Operational Aspects. Quintessa.

Knorr, J., Lippmann, W., Reinecke, A-M., Wolf, R., Kerber, A. & Wolter, A. 2008. SiC encapsulation of (V)HTR components and waste by laser beam joining of ceramics. Nucl. Eng. Des. 238: 3129-3135.

Koivuluoto, H., Vuoristo, P. 2010. Structural analysis of cold-sprayed nickel-based metallic and metallic ceramic coatings. J. Therm. Spray Technol. 19: 975-989.

Kojima, Y., Hioki, T., Tsujikawa, S. 1995. Simulations of the state of carbon steel n years after disposal with n years of corrosion product on its surface in a bentonite environment. Materials Research Society Symposium Proceedings 353: 711-718.

Konovalova, V. 2021. The Effect of Temperature on the Corrosion Rate of Iron-Carbon Alloys. Materials Today: Proceedings 38: 1326–29. doi: 10.1016/j.matpr.2020.08.094.

EURAD (Deliverable n° 1.1) – Initial State-of-the-art of WP ConCorD
Dissemination level: Public
Date of issue of this report: 17/08/2022

Page 135

Kottemann, M., Kish, A., Iloanusi, C., Bjork, S., DiRuggiero, J. 2005. Physiological responses of the halophilic archaeon Halobacterium sp. strain NRC1 to desiccation and gamma irradiation. Extremophiles 9: 219-227.

Kowaka, M. 1994. Introduction to Life Prediction of Industrial Plant Materials. Application of the Extreme Value Statistical Method for Corrosion Analysis. Allerton Press.

Kumari, A., Das, S.K., Srivastava, P.K. 2016. Modelling Fireside Corrosion Rate in a Coal Fired Boiler Using Adaptive Neural Network Formalism. Port. Electrochim. Acta 34: 23-38.

Kumpalainen, S., Kiviranta, L., Korkeakoski, P. 2016. Long-term effects of an iron heater and Äspö groundwater on smectite clays: Chemical and hydromechanical results from the in situ alternative buffer material (ABM) test package 2. Clay Miner. 51: 129–144.

Kursten B., MacDonald, D.D., Smart, N.R., Gaggiano, R. 2017. Corrosion Issues of Carbon Steel Radioactive Waste Packages Exposed to Cementitious Materials with Respect to the Belgian Sipercontainer Concept. Corros. Eng. Sci. Technol. 52: 11-16.

Kursten, B., Druyts, F. 2008. Methodology to make a robust estimation of the carbon steel overpack lifetime with respect to the Belgian Supercontainer design. J. Nucl. Mater. 379: 91-96.

Kursten, B., Macdonald, D.D., Smart, N.R., Gaggiano, R. 2016. Corrosion issues of carbon steel radioactive waste packages exposed to cementitious materials with respect to the Belgian supercontainer concept. Corros. Eng. Sci. Technol. 52: 11-16.

Kursten, B., Smailos, E., Azkarate, I., Werme, L., Smart, N.R., Santarini, G. 2003. COBECOMA State-of-the-Art Document on the Corrosion Behaviour of Container Materials. EUROPEAN COMMISSION 5th EURATOM FRAMEWORK PROGRAMME 1998-2002.

Kwong, G.M. 2011. Status of Corrosion Studies for Copper Used Fuel Containers Under Low Salinity Conditions. NWMO TR-2011-14. Nuclear Waste Management Organization.

Lainé, M., Balan, E., Allard, T., Paineau, E., Jeunesse, P., Mostafavi, M., Robert, J.L., Le Caër, S. 2017. Reaction Mechanisms in Swelling Clays under Ionizing Radiation: Influence of the Water Amount and of the Nature of the Clay Mineral. RSC Advances 7:526–34. doi: 10.1039/C6RA24861F.

Landolt, D., Davenport A., Payer A., Shoesmitth D. 2009. A review of materials and corrosion issues regarding canisters for disposal of spent fuel and high-level waste in Opalinus clay. NAGRA Technical Report 09-02.

Lapuerta, S., Bérerd, N., Moncoffre, N., Millard-Pinard, N., Jaffrézic, H., Crusset, D., Féron. D. 2008. The Influence of Relative Humidity on Iron Corrosion under Proton Irradiation. J. Nucl. Mater. 375: 80–85. doi: 10.1016/j.jnucmat.2007.10.011.

Larker, H. 1980. Method of containing spent nuclear fuel or high-level nuclear fuel waste. Patent US4209420, United States.

Laycock, P.J., Cottis R.A., Scarf, P.A. 1990. Extrapolation of Extreme Pit Depths in Space and Time. J. Electrochem. Soc. 137: 65.

Lee, M.S, et al. 2011. Application of Cold Spray Technique to the underground disposal copper canister and its corrosion properties, Nucl. Eng. Technol. 43: 557-566.

Lee, S., Staehle, R.W. 1997. Adsorption of water on copper, nickel and iron. Corrosion 53: 33-42.

Lee, Y.T.R., Ashrafizadeh, H., Fisher, G., McDonald, A. 2017. Effect of type of reinforcing particles on the deposition efficiency and wear resistance of low-pressure cold-sprayed metal matrix composite coatings. Surf. Coat. Technol. 324: 190-200.

Legoux, J.G. 2014. Development of cold spray coating for nuclear waste storage container application, EUCOSS 2014, Paris, May 26th.

EURAD (Deliverable n° 1.1) – Initial State-of-the-art of WP ConCorD
Dissemination level: Public
Date of issue of this report: 17/08/2022

Page 136

Leupin, O., Smith, P., Savage, D., Johnson, L., Marschall, P., Schneider, J., Senger, R. 2016. High-level waste repository-induced effects. Nagra Technical Report NTB 14-13.

Li, M., Zinkle, S.J. 2012. Physical and mechanical properties of copper and copper alloys. In Comprehensive Nuclear Materials, Vol. 4 (Elsevier, Amsterdam), Ch. 4.20, pp. 667-690.

Li, X., Zhang, D., Liu, Z., Li, Z., Du, C., Dong, C. 2015. Materials science: Share Corrosion Data. Nature 527: 441-442.

Liang, D. et al. 2021. Extracellular electron exchange capabilities of Desulfovibrio ferrophilus and Desulfopila corrodens. Environ. Sci. Tech. 55: 16195-16203.

Litke, C.D., King, F. 1987. Atomic Energy of Canada Limited Technical Record, TR-428. Ontario: AECL Research, Chalk River.

Litke, C.D., Ryan, S.R., King, F. 1992. TA mechanistic study of the uniform corrosion of copper in compacted clay-sand soil. AECL-10397, COG-91-304, Atomic Energy of Canada Ltd.

Little, B.J., Hinks, J., Blackwood, D.J. 2020. Microbially influenced corrosion: Towards an interdisciplinary perspective on mechanisms. Int. Biodeterior. Biodegrad. 154: 105062.

Liu, C., Wang, J., Zhang, Z., Han, E-H. 2017. Studies on Corrosion Behaviour of Low Carbon Steel Canister with and without γ-Irradiation in China's HLW Disposal Repository. Corros. Eng. Sci. Technol. 52: 136–40. doi: 10.1080/1478422X.2017.1348762.

Lloyd, A.C., Schuler, R.J., Noël, J.J., Shoesmith, D.W., King, F. 2004. The Influence of Environmental Conditions and Passive Film Properties on the MIC of Engineered Barriers in the Yucca Mountain Repository, in Scientific Basis for Nuclear Waste Management XXVIII. J.M. Hanchar, S. Stroes-Gascoyne, L. Browning (eds). Mater. Res. Soc. Symp. Proc. 824: 3-9.

Lobach, K., Kupriiyanova, Y., Kolodiy, I., Sayenko, S., Shkuropatenko, V., Voyevodin, V., Zykova, A., Bykov, A., Chunyayev, O., Tovazhnyanskyy, L. 2018. Optimisation of Properties of Silicon Carbide Ceramics with the Use of Different Additives. Funct. Mater. 25: 496-504.

Lobach, K.V. et al. 2020. Corrosion stability of SiC-based ceramics in hydrothermal conditions. Mater. Sci. 55: 672-682.

Lopez-Fernandez, M., Cherkouk, A., Vilchez-Vargas, R., Jauregui, R., Pieper, D., Boon, N., Sanchez-Castro, I., Merroun, M.L. 2015. Bacterial Diversity in Bentonites, Engineered Barrier for Deep Geological Disposal of Radioactive Wastes. Microb. Ecol. 70: 922–935.

Lousada, C.M., I.L. Soroka, Y. Yagodzinskyy, N.V. Tarakina, O. Todoshchenko, H. Hänninen, P.A. Korzhavyi, and M. Jonsson. 2016. Gamma radiation induces hydrogen absorption by copper in water. Scientific Reports 6, Article number 24234.

Lundgren, K. 2004. Final disposal of fuel - electron radiation outside copper canister. Technical Report SKB-TR-04-06. Swedish Nuclear Fuel and Waste Management Co., Stockholm, Sweden.

Lv, M.Y., Du, M. 2018. A review: microbiologically influenced corrosion and the effect of cathodic polarization on typical bacteria. Rev. Environ. Sci. Biotechnol. 17: 431-446.

Maak, P., King, F. 2006. A Model for Predicting Stress Corrosion Cracking of Copper Containers in A Deep Geologic Repository. MRS Online proceedings Library 932: 291.

Maanoja, S. et al. 2020. Compacted bentonite as a source of substrates for sulfate-reducing microorganisms in a simulated excavation-damaged zone of a spent nuclear fuel repository. Appl. Clay Sci. 196, 105746.

Maanoja, S. et al. 2021. The effect of compaction and microbial activity on the quantity and release rate of water-soluble organic matter from bentonites. Appl. Clay Sci. 211: 106192.

EURAD (Deliverable n° 1.1) – Initial State-of-the-art of WP ConCorD
Dissemination level: Public
Date of issue of this report: 17/08/2022

Page 137

Mabbutt, S., Picton, P., Shaw, P., Black, S. 2012. Review of Artificial Neural Networks (ANN) Applied to Corrosion Monitoring. J. Phys.: Conf. Ser. 364: 012114.

Mareci, D., Suditu, G.D., Trincă, L.C., Curteanu, S. 2016. Prediction of Corrosion Resistance of Some Dental Metallic Materials Applying Artificial Neural Networks. Mater. Corros. 67: 1213-1219.

Marsh, G.P., Taylor, K.J. 1988. An Assessment of Carbon Steel Containers for Radioactive Waste Disposal. Corros. Sci. 28: 289–320. doi: 10.1016/0010-938X(88)90111-4.

Marshall, M.H.M., McKelvie, J.R., Simpson, A.J., Simpson, M.J. 2015. Characterization of natural organic matter in bentonite clays for potential use in deep geological repositories for used nuclear fuel. Appl. Geochem. 54: 43-53.

Marty, N.C.M., Fritz, B., Clément, A., Michau, N. 2010. Modelling the long-term alteration of the engineered bentonite barrier in an underground radioactive waste repository. Appl. Clay Sci. 47: 82–90.

Masurat, P., Eriksson, S., Pedersen, K. 2010. Microbial sulphide production in compacted Wyoming bentonite MX-80 under in situ conditions relevant to a repository for high-level radioactive waste. Appl. Clay Sci. 47: 58-64.

Matschiavelli, N. et al. 2019. The Year-Long Development of Microorganisms in Uncompacted Bavarian Bentonite Slurries at 30 and 60 °C. Environ. Sci. Tech. 53: 10514-10524.

Matts, O. et al. 2019. Influence of Cold Spray Nozzle Displacement Strategy on Microstructure and Mechanical Properties of Cu/SiC Composites Coating. Key Eng. Mater. 813: 110-115.

Mattson, E. 1980. Aluminium oxide as the encapsulation material for unreprocessed nuclear fuel waste-evaluation from the viewpoint of corrosion, Swedish Corrosion Institute, Final Report KBS 80-15.

McMurry, J., Dixon, D.A., Garroni, J.D., Ikeda, B.M., Stroes-Gascoyne, S., Baumgartner, P., Melnyk, T.W. 2003. Evolution of a Canadian Deep Geologic Repository: Base Scenario. Ontario Power Generation Nuclear Waste Management Division Report No 06819-REP-01200-100.

McNamara, N.P., Black, H.I.J., Beresford, N.A., Parekh, N.R. 2003. Effects of acute gamma irradiation on chemical, physical and biological properties of soils. Appl. Soil Ecol. 24: 117-132.

Mendoza, A. 2017. Gas generation and migration in clay media as a result of anaerobic steel corrosion. Technical report No. 187/2017. SURAO, Prague.

Miller, W., Alexander, R., Chapman, N., McKinley, M., Smellie, J. 1994. Natural analogue studies in the geological disposal of radioactive wastes. Nagra Technical Report NTB-93-03. Wettington, Sweden

Milošev, I., Navinšek, B. 1993. Corrosion properties of selected Cr-based hard and protective coatings. Surf. Coat. Technol. 60: 545-548.

Milošev, I., Strehblow, H.H., Navinšek, B. 1997. Comparison of TiN, ZrN and CrN hard nitride coatings: electrochemical and thermal oxidation. Thin Solid Films 303: 246-254.

Minhas, B., Dino, S., Zuo, Y., Qian, H., Zhao, X. 2021. Improvement of Corrosion Resistance of TiO2 Layers in Strong Acidic Solutions by Anodizing and Thermal Oxidation Treatment. Materials 14: 1188-13.

Mironenko, N.V., Alekhina, I.A., Zhdanova, N.N., Bulat, S.A. 2000. Intraspecific variation in gamma-radiation resistance and genomic structure in the filamentous fungus Alternaria alternata: A case study of strains inhabiting chernobyl reactor no. 4. Ecotoxicology & Environmental Safety 45: 177-187.

Morris, J.E., Winpenny, D.B. 2012. The atmospheric corrosion of ductile cast iron, AMEC 17391-TR-003.

Müller, H.R., Garitte, B., Vogt, T., Köhler, S., Sakaki, T., Weber, H., Spillman, T., Hertrich, M., Becker, J.K., Giroud, N., Cloet, V., Diomidis, N., Vietor, T., 2017. Implementation of the full-scale emplacement (FE) experiment at the Mont Terri rock laboratory. Swiss J. Geosci. 110: 287-306.

EURAD (Deliverable n° 1.1) – Initial State-of-the-art of WP ConCorD
Dissemination level: Public
Date of issue of this report: 17/08/2022

Page 138

Muyzer, G., Stams, A.J. 2008. The ecology and biotechnology of sulphate-reducing bacteria. Nat. Rev. Microbiol. 6: 441-454.

Nagra. 2002. Demonstration of disposal feasibility for spent fuel, vitrified high-level waste and long-lived intermediate-level waste (Entsorgungsnachweis). Nagra Technical Report Number 02-05.

Nardi, A., Idiart, A., Trinchero, P., de Vries, L. M., Molinero, J., 2014. Interface COMSOL-PHREEQC (iCP), an efficient numerical framework for the solution of coupled multiphysics and geochemistry. Comput. Geosci. 69: 10–21.

Necib, S., Diomidis, N., Keech, P., Nakayama, M. 2017. Corrosion of carbon steel in clay environments relevant to radioactive waste geological disposals, Mont Terri rock laboratory (Switzerland). Swiss J. Geosci. 110: 329-342.

Necib, S., Linard, Y., Crusset, D., Michau, N., Daumas, S., Burger, E., Romaine, A., Schlegel, M.L. 2016. Corrosion at the carbon steel-clay borehole water and gas interfaces at 85°C under anoxic and acidic transient conditions. Corros. Sci. 111: 242-258.

Negron, A., Ramos, S., Blumenfeld, A.L., Pacheco, G., Fripiat, J.J. 2002. On the Structural Stability of Montmorillonite Submitted to Heavy γ-Irradiation. Clays and Clay Miner. 50: 35–37. doi: 10.1346/000986002761002649.

Nelson, J.L., Westerman, R.E., Gerber, F.S. 1983. Irradiation-Corrosion Evaluation of Metals for Nuclear Waste Package Applications in Grande Ronde Basalt Groundwater. MRS Proceedings 26: 121. doi: 10.1557/PROC-26-121.

Nesic, S. 2007. Key issue related to modelling of internal corrosion of oil and gas pipelines – A review. Corros. Sci. 49: 4308-4338.

Nguyen, T.S., Selvadurai, A.P.S., Armand, G. 2005. Modelling the FEBEX THM experiment using a state surface approach. Int. J. Rock Mech. Min. Sci. 42: 639–651.

NWMO 2016. Implementing Adaptive Phased Management 2016 to 2020. Nuclear Waste Management Organization Report.

Ochs, M., Talerico, C. 2004. SR-Can. Data and uncertainty assessment. Migration parameters for the bentonite buffer in the KBS-3 concept. SKB TR-04-18, SKB, Sweden.

Ogawa, K., et al. 2008. Characterization of low pressure cold-sprayed aluminium coatings, J. Therm. Spray Technol. 17: 728-735.

Ojovan, M.I., Lee, W.E., Kalmykov, S.N. 2019. Nuclear Waste Disposal in An Introduction to Nuclear Waste Immobilisation, pp. 415–432. Elsevier, Amsterdam.

Osgerby, S., Fry, A.T. 2007. The Use of Neural Networks in Understanding and Predicting Oxidation and Corrosion Behaviour in Advanced Energy Conversion Systems. Mater. High Temp. 24: 259-263.

Otte, J.M., Blackwell, N., Soos, V., Rughöft, S., Maisch, M., Kappler, A., Kleindienst, S., Schmidt, C. 2018. Sterilization impacts on marine sediment - Are we able to inactivate microorganisms in environmental samples? EMS Microbiol. Ecol. 94: fiy189. https://doi.org/10.1093/femsec/fiy189

Padovani, C. et al. 2017. The corrosion behaviour of candidate container materials for the disposal of high-level waste and spent fuel–a summary of the state of the art and opportunities for synergies in future R&D. Corros. Eng. Sci. Technol. 52: 227-231.

Padovani, C., King, F., Lilja, C., Féron, D., Necib, S., Crusset, D., Deydier, V., Diomidis, N., Gaggiano, R., Ahn, T., Keech, P.G., Macdonald, D.D., Asano, H., Smart, N., Hall, D.S., Hänninen, H., Engelberg, D., Noël, J.J., Shoesmith, D.W. 2017. The Corrosion Behaviour of Candidate Container Materials for the Disposal of High-Level Waste and Spent Fuel – a Summary of the State of the Art and Opportunities for Synergies in Future R&D. Corr. Eng. Sci. Tech. 52: 227–31. doi: 10.1080/1478422X.2017.1356973.

EURAD (Deliverable n° 1.1) – Initial State-of-the-art of WP ConCorD
Dissemination level: Public
Date of issue of this report: 17/08/2022

Page 139

Padovani, C., Pletser, D., Jurkschat, K., Dugdale, S., Brunt, D., Faulkner, R., Was, G., Johansson, A.J. 2019. Assessment of microstructural changes in copper due to gamma radiation damage. Swedish Nuclear Fuel and Waste Management Co Technical Report, SKB TR-19-12.

Parkhurst, D.L., Appelo, C.A.J. 2013. Description of input and examples for PHREEQC version 3 – A computer program for speciation, batch-reaction, one-dimensional transport, and inverse geochemical calculations. Techniques and Methods 6–A43, U.S. Geological Survey, Denver, Colorado.

Patel, R., Punshon, C., Nicolas, J., Bastid, P., Zhou, R., Schneider, C., Bagshaw, N., Howse, D. 2012. Canister design concepts for disposal of spent fuel and high level waste, Nagra Technical Report, NTB 12-06.

Payer, J.H., Finsterle, S., Apps, J.A., Muller, R.H. 2019. Corrosion Performance of Engineered Barrier System in Deep Horizontal Drillholes. Energies 12: 1491.

Pedersen, K. 2010. Analysis of copper corrosion in compacted bentonite clay as a function of clay density and growth conditions for sulfate-reducing bacteria. J. Appl. Microbiol. 108: 1094-1104.

Pedersen, K. 2017. MIND deliverable 2.4: Bacterial activity in compacted bentonites. https://mind15.eu/deliverables/

Pedersen, K., Motamedi, M., Karnland, O., Sandén, T. 2000. Mixing and sulphate-reducing activity of bacteria in swelling, compacted bentonite clay under high-level radioactive waste repository conditions. J. Appl. Microbiol. 89: 1038-1047.

Phillips, R.W., Wiegel, J., Berry, C.J., Fliermans, C., Peacock, A.D., White, D.C., Shimkets, L.J. 2002. Kineococcus radiotolerans sp. nov., a radiationresistant, Gram-positive bacterium. Int. J. Syst. Evol. Microbiol. 52: 933-938.

Pignatelli, I., Bourdelle, F., Bartier, D., Mosser-Ruck, R., Truche, L., Mugnaioli, E., Michau, N. 2014. Iron-clay interactions: Detailed study of the mineralogical transformation of claysone with emphasis on the formation of iron-rich T-O phyllosilicates in a step-by-step cooling experiment from 90 °C to 40 °C. Chem. Geol. 387: 1-11.

Pignatelli, I., Mugnaioli, E., Hybler, J., Mosser-Ruck, R., Cathelineau, M., Michau, N. 2013. A multi-technique characterization of cronstedtite synthesized by iron-clay interaction in a step-by-step cooling procedure. Clays and Clay Miner. 61: 277-289.

Pinnel, M.R., Tompkins, H.G., Heath, D.E. 1979. Oxidation of copper in controlled clean air and standard laboratory air at 50°C to 150°C. Appl. Surf. Sci. 2: 558-577.

Popsikova, L., Dobrev, D., Kouril, M., Stoulil, J., Novikova, D., Kotnour, P., Matal, O. 2017. Czech national programe and disposal canister concept. Corros. Eng. Sci. Technol. 52: 6-10.

Posiva, Oy. 2007. Expected evolution of a spent nuclear fuel repository at Olkiluoto. Posiva Report 2006-05.

Posiva, Oy. 2013. Safety Case for the Disposal of Spent Nuclear Fuel at Oikiluoto - Models and Data for the Repository System 2012. Eurajoki: Posiva Oy.

Posiva. 2021. Canister evolution. Posiva Oy Working Report, WR-2021-06.

Pourbaix, M. 1974. Atlas of Electrochemical Equilibria in Aqueous Solutions. NACE International.

Pusch, R., Karnland, O., Lajudie, A., Decarreau, A. 1992. MX 80 Clay Exposed to High Temperatures and Gamma Radiation. SKB Technical Report 93–03(93–03).

Pusch, R., Yong, R.N. 2006. Microstructure of Smectite Clays and Engineering Performance. Taylor & Francis.

Qin, Z., Daljeet, R., Ai, M., Farhangi, N., Noël, J.J., Ramamurthy, S., Shoesmith, D., King, F., Keech, P. 2017. The active/passive conditions for copper corrosion under nuclear waste repository environment. Corros. Eng. Sci. Technol. 52: 45-49.

Rajala, P. et al. 2015. Microbially induced corrosion of carbon steel in deep groundwater environment. Front. Microbiol. 6: 647.

Rebata-Landa, V., Santamarina, J.C. 2006. Mechanical limits to microbial activity in deep sediments. Geochem. Geophys. Geosystems 7, doi:10.1029/2006GC001355.

Reed D.T., Van Konynenburg R.A. 1991. Effect of ionizing radiation on moist air systems. In: Abrajano T.A., Johnson, L.H. (eds). Materials Research Society Symposium Proceedings 212: 317–325.

Reed, D.T., Swayambunathan, V., Tani, B.S., Van Konynenburg, R.A. 1989. Corrosion product identification and relative rates of corrosion of candidate metals in an irradiated air steam environment. Proc. Mat. Res. Soc. Symp. 176: 517-524.

Refait, P., Grolleau, A.-M., Jeannin, M., Francois, E., Sabot, R. 2016. Localized corrosion of carbon steel in marine media: Galvanic coupling and heterogeneity of the corrosion product layer. Corros. Sci. 111: 583-595.

Rockhvarger, A.E., Khizh, A.B. 1998. Large size, thick-walled ceramic containers. NUCON SYSTEMS INC, Patent WO9844834.

Rockhvarger, A.E., Khizh, A.B. 1999. Process for the preparation of thick-walled ceramic products. ROKON SYSTEMS INC., Patent US5911941A.

Rockhvarger, A.E., Khizh, A.B. 2000. Processus and apparatus for joining thick-walled ceramic parts. Patent US6054700.

Romaine, A., Jeannin, M., Sabot, R., Necib, S., Refait, P. 2015. Corrosion processes of carbon steel in argillite: Galvanic effects associated with the heterogeneity of the corrosion product layer. Electrochim. Acta 182: 1019-1028.

Romanoff, M. 1957. Underground Corrosion. NIST Technical Series National Bureau of Standards Circular 579.

Romanoff, M. 1989. Underground corrosion. Houston: NACE International.

Roy, S.K., Sircar, S.C. 1981. A critical appraisal of the logarithmic rate law in thin-film formation during oxidation of copper and its alloys. Oxidation of Metals 15: 9-20.

Rutqvist, J., Tsang,C-F. 2008. Review of SKB´s Work on Coupled THM Processes Within SR-Can: external review contribution in support of SKI´s and SSI´s review of SR-Can. SKI Report 2008:08.

RWM 2016. Geological Disposal-Waste Evolution Status Report, NDA Report DSSC/451/01. Radioactive Waste Management.

Safi, I. 2017. PhD Thesis. Radiation Effects on KBS-3 Barriers. KTH, School of Chemical Science and Engineering (CHE), Stockholm, Sweden.

Saheb, M., Marsal, F., Matthiesen, H., Neff, D., Dillmann, P., Pellegrini, D. 2011. Fluctuation of redox conditions in radioactive waste disposal cell: characterisation of corrosion layers formed on archaeological analogues. Corros. Eng. Sci. Technol. 46: 199-204.

Sánchez, M., Gens, A., Olivella, S. 2012. THM analysis of a large-scale heating test incorporating material fabric changes. Int. J. Numer. Anal. Meth. Geomech. 36: 391–421.

Sato, N. 1976. Stochastic Process of Chloride Pit Generation in Passive Stainless Steel. J. Electrochem. Soc. 123: 1197.

Schanz, T. 2016. Transient boundary conditions in the frame of THM processes at nuclear waste repositories. E-UNSAT 2016. E3S Web of Conferences 9, 03001.

EURAD (Deliverable n° 1.1) – Initial State-of-the-art of WP ConCorD
Dissemination level: Public
Date of issue of this report: 17/08/2022

Page 141

Schlegel, M.L., Necib, S., Daumas, S., Blanc, C., Foy, E., Trcera, N., Romaine, A. 2016. Microstructural characterization of carbon steel corrosion in clay borehole water under anoxic and transient acidic conditions. Corros. Sci. 109: 126-144.

Schlegel, M.L., Necib, S., Daumas, S., Labat, M., Blanc, C., Foy, E., Linard, Y. 2018. Corrosion at the carbon steel-clay borehole water interface under anoxic alkaline and fluctuating temperature conditions. Corros. Sci. 136: 70-90.

Schutz, R.W. 1996. Ruthenium enhanced titanium alloys: Minor ruthenium additions produce cost effective corrosion resistant commercial titanium alloys. Platinum Metals Review 40: 54–61.

Scully, J.R., Edwards, M. 2013. Review of the NWMO Copper Corrosion Allowance. Toronto: NWMO TR-2013-04.

Sharland, S.M. 1987. A Review of the Theoretical Modelling of Crevice and Pitting Corrosion. Corros. Sci. 27: 289-323.

Sharma A. et. al. 2017. Across the tree of life, radiation resistance is governed by antioxidant Mn2+, gauged by paramagnetic resonance. PNAS 114, E9253-E9260. https://doi.org/10.1073/pnas.1713608114

Sherar, B.W.A., Keech, P.G., Shoesmith, D.W. 2011. Carbon steel corrosion under anaerobic-aerobic cycling conditions in near-neutral pH saline solutions – Part 1: Long term corrosion behaviour. Corros. Sci. 53: 3636-3642.

Sherar, B.W.A., Keech, P.G., Shoesmith, D.W. 2011b. Carbon steel corrosion under anaerobic-aerobic cycling conditions in near-neutral pH saline solutions – Part 2: Corrosion mechanism. Corros. Sci. 53: 3643-3650.

Shi, J., Wang, J., Macdonald, D.D. 2015. Prediction of Primary Water Stress Corrosion Crack Growth Rates in Alloy 600 Using Artificial Neural Networks. Corros. Sci. 92: 217-227.

Shibata, T. 1996. Statistical and Stochastic Approaches to Localized Corrosion. Corrosion 52: 813.

Shindleholtz, E., Risteen, B.E., Kelly, R.G. 2014. Effect of relative humidity on corrosion of carbon steel under sea salt aerosol proxies I. NaCl. J. Electrochem. Soc. 161: C450-C459.

Shoesmith, D.W. 2006. Assessing the corrosion performance of high-level nuclear waste containers. Corrosion 62: 703-722.

Shoesmith, D.W., King, F. 1999. The effects of gamma radiation on the corrosion of candidate materials for the fabrication of nuclear waste packages. AECL-11999, Atomic Energy of Canada Limited.

Shrestha, R. et al. 2021. Anaerobic microbial corrosion of carbon steel under conditions relevant for deep geological repository of nuclear waste. Sci. Total Environ. 800: 149539.

Shuryak, I. et al. 2017. Microbial cells can cooperate to resist high level chronic ionizing radiation. PloS one 12: e0189261. https://doi.org/10.1371/journal.pone.0189261

Silva, O., Coene, E., Molinero, J., Laviña M., Idiart, A. 2019. Gas release from the BHK vault – Multiphase flow modelling of the near-field. Report for the safety evaluation SE-SFL. R-19-06, SKB, Sweden.

Simanjuntak, S., Cavanaugh, M.K.; Gandel, D.S., Easton, M.A., Gibson, M.A., Birbilis, N. 2015. The Influence of Iron, Manganese, and Zirconium on the Corrosion of Magnesium: An Artificial Neural Network Approach. Corrosion 71: 199-208.

Simpson J.P. 1984. Experiments on container materials for Swiss high-level waste disposal projects. Part II. Nagra Technical Report 84-01. National Cooperative for the Disposal of Radioactive Waste, Switzerland.

EURAD (Deliverable n° 1.1) – Initial State-of-the-art of WP ConCorD
Dissemination level: Public
Date of issue of this report: 17/08/2022
Page 142

SKB 2006. Buffer and backfill process report for the safety assessment SR-Can. SKB Technical Report TR-06-18: 201.

SKB 2006b. Long-term safety for KBS-3 repositories at Forsmark and Laxemar - a first evaluation. Main report of the SR-Can project, SKB Technical Report TR-06-09. Swedish Nuclear Fuel and Waste Management Company, Stockholm, Sweden.

SKB 2010. Corrosion calculations report for the safety assessment SR-Site. SKB TR-10-66, Svensk Kärnbränslehantering AB, Stockholm, Sweden.

SKB 2010a. Fuel and canister process report for the safety assessment SR-Site. Updated 2015-06. SKB Technical Report TR-10-46, Stockholm: SKB.

SKB 2010b. Corrosion calculations report for the Safety Assessment SR-site. SKB Technical report TR-10-66, SKB.

SKB 2010c. Design, production and initial state of the buffer. Stockholm: Svensk Kärnbränslehantering AB.

SKB 2011. Long-term safety for the final repository for spent nuclear fuel at Forsmark, Main report of the SR-Site project, Volume 2. Svensk Kärnbränslehantering AB, Stockholm.

SKB. 2019. Supplementary information on canister integrity issues. Swedish Nuclear Fuel and Waste Management Co, SKB Report TR-19-15.

SKB. 2010. Fuel and canister process report for the safety assessment SR-Site. Swedish Nuclear Fuel and Waste Management Co, SKB Report TR-10-46.

Smailos, E., Schwarzkopf, W., Koester, R., Fiehn, B., Halm, G. 1991. Corrosion Testing of Selected Packaging Materials for Disposal of High-Level Waste Glass in Rock-Salt Formations. Report EUR-13672. Commission of the European Communities, Luxembourg.

Smailos, E., Schwarzkopf, W., Storch, R. 1992. Corrosion studies on packaging materials for high-level waste disposal in a rock-salt repository. In Proc. of the 12th Scandinavian Corrosion Congress and Eurocorr 92: 327-338.

Small, J.S., Thompson, O.R. 2010. Development of a spatial and temporal evolution of pH in cementitious backfill of a geological repository. Nexia Solutions Report (07) 8869, Issue 3.

Smart, N., Rance, A., Reddy, B., Lydmark, S., Pedersen, K., Lilja, C. 2011. Further studies of in situ corrosion testing of miniature copper-cast iron nuclear waste containers. Corr. Eng. Sci. Tech. 46: 142-147.

Smart, N.R. 2009. Corrosion behavior of carbon steel radioactive waste packages: A summary review of Swedish and U.K. Research. Corrosion 65: 195–212.

Smart, N.R. et al. 2017. The anaerobic corrosion of carbon steel in compacted bentonite exposed to natural Opalinus Clay porewater containing native microbial populations. Corros. Eng. Sci. Technol. 52: 101-112.

Smart, N.R., Blackwood, D.J., Werme, L. 2001. The anaerobic corrosion of carbon steel and cast iron in artificial groundwaters. Technical Report SKB-TR-01-22, Swedish Nuclear Fuel and Waste Management Co., Stockholm, Sweden.

Smart, N.R., Blackwood, D.J., Werme, L. 2002a. Anaerobic corrosion of carbon steel and cast iron in artificial groundwaters: Part 1 – Electrochemical aspects. Corrosion 58: 547-559.

Smart, N.R., Blackwood, D.J., Werme, L. 2002b. Anaerobic corrosion of carbon steel and cast iron in artificial groundwaters: Part 2 – Gas generation. Corrosion 58: 627-637.

EURAD (Deliverable n° 1.1) – Initial State-of-the-art of WP ConCorD
Dissemination level: Public
Date of issue of this report: 17/08/2022

Page 143

Smart, N.R., Blackwood, D.J., Werme, L.O. 2001. The anaerobic corrosion of carbon steel and cast iron in artificial groundwaters, SKB Technical Report TR-99-06. Swedish Nuclear Fuel and Waste Mangement Co., Stockholm.

Smart, N.R., Hoch, A.R. 2010. A Survey of Steel and Zircaloy Corrosion Data for Use in the SMOGG Gas Generation Model. Serco Assurance Report SA/ENV 0841 issue 3.

Smart, N.R., Rance, A.P. 2005. Effect of radiation on anaerobic corrosion of iron (No. SKB-TR--05-05). Swedish Nuclear Fuel and Waste Management Co.

Smart, N.R., Rance, A.P., Werme, L.O. 2008. The Effect of Radiation on the Anaerobic Corrosion of Steel. J. Nucl. Mater. 379: 97-104. doi: 10.1016/j.jnucmat.2008.06.007.

Smart, N.R., Rance, A.P., Werme, L.O. 2004. Anaerobic corrosion of steel in bentonite. Materials Research Society Symposium Proceedings 807: 441-449.

Smith, J.M., Qin, Z., Wren, J.C., Shoesmith, D.W. 2006. The influence of peroxidation on the corrosion of copper nuclear waste canister in aqueous anoxic sulphide solutions. MRS Online Proceedings Library 985: 811.

Sorieul, S., Allard, T., Wang, L.M., Grambin-Lapeyre, C., Lian, J., Calas, G., Ewing, R.C. 2008. Radiation-Stability of Smectite. Environ. Sci. Technol. 42: 8407–8411. doi: 10.1021/es800766b.

Soroka, I., Chae, N., Jonsson, M. 2021. On the mechanism of γ-radiation-induced corrosion of copper in water. Corros. Sci. 182: 109279.

Soroka, I., Chae, N., Jonsson, M. 2021. On the mechanism of γ-radiation-induced corrosion of copper in water. Corros. Sci. 182: 109279.

Sova, A., Doubenskaia, M., Grigoriev, S., Okunkova, A., Smurov, I. 2013. Parameters of the Gas-Powder Supersonic Jet in Cold Spraying Using a Mask. J. Therm. Spray Technol. 22: 551-556.

Sova, A., Klinkov, S., Kosarev, V., Ryashin, N., Smurov, I. 2013. Preliminary study on deposition of aluminium and copper powders by cold spray micronozzle using helium. Surf. Coat. Technol. 220: 98-101.

Sova, A., Okunkova, A., Grigoryev, S., Smurov, I. 2013. Velocity of the particles accelerated by a cold spray micronozzle: Experimental measurements and numerical simulation. J. Therm. Spray Technol. 22: 75-80.

Stroes-Gascoyne, S. 2010. Microbial occurrence in bentonite-based buffer, backfill and sealing materials from large-scale experiments at AECL's Underground Research Laboratory. Appl. Clay Sci. 47: 36-42.

Stroes-Gascoyne, S., Hamon, C.J., Dixon, D.A., Kohle, C.L., Maak, P. 2007. The Effects of Dry Density and Porewater Salinity on the Physical and Microbiological Characteristics of Compacted 100% Bentonite. MRS Online Proceedings Library, 985: 1302. https://doi.org/10.1557/PROC-985-0985-NN13-02.

Stroes-Gascoyne, S., Hamon, C.J., Maak, P. 2011. Limits to the use of highly compacted bentonite as a deterrent for microbiologically influenced corrosion in a nuclear fuel waste repository. Phys. Chem. Earth, Parts A/B/C 36: 1630-1638.

Stroes-Gascoyne, S., Hamon, C.J., Maak, P., Russell, S. 2010. The effects of the physical properties of highly compacted smectitic clay (bentonite) on the culturability of indigenous microorganisms. Appl. Clay Sci. 47: 155-162.

Stroes-Gascoyne, S., Hamon, C.J., Vilks, P., Gierszewski, P. 2002. Microbial, redox, and organic characteristics of compacted clay-based buffer after 6.5 years of burial at AECL''s Underground Research Laboratory. Appl. Geochem. 17: 1287-1303.

EURAD (Deliverable n° 1.1) – Initial State-of-the-art of WP ConCorD
Dissemination level: Public
Date of issue of this report: 17/08/2022

Page 144

Stroes-Gascoyne, S., Lucht, L.M., Borsa, J., Delaney, T.L., Haveman, S.A., Hamon, C.J. 1995. Radiation Resistance of the Natural Microbial Population in Buffer Materials. MRS Online Proceedings Library Archive 353: 345–352. https://doi.org/10.1557/PROC-353-345.

Sudharshan Phani, P., Vishnukanthan, V., Sundararajan, G. 2007. Effect of heat treatment on properties of cold sprayed nanocrystalline copper alumina coatings. Acta Mater. 55: 4741-4751.

Svemar, C., Johannesson, L-E., Grahm, Svensson, D. 2016. Opening and retrieval of outer section of Prototype Repository at Äspö Hard Rock Laboratory. Svensk Kärnbränslehantering AB, Stockholm.

Svensk Kärnbränslehantering AB, 2006. Buffer and backfill process report for the safety assessment SR-Can. Technical Report TR-06-18. Swedish Nuclear Fuel and Waste Management Co, Stockholm, Sweden.

Svensson, D., Sandén, T., Olsson, S., Dueck, A., Eriksson, S., Jägerwall, S., Hansen, S. 2011. Alternative buffer material Status of the ongoing laboratory investigation of reference materials and test package 1. SKB TR-11-06: 146. Svensk Kärnbränslehantering AB: Stockholm, Sweden.

Swanton, S.W., Baston, G.M.N., Smart, N.R. 2015. Rates of steel corrosion and carbon-14 release from irradiated steels – state of the art review (D.2.1): 160. Carbon-14 Source Term (CAST Project).

Takase, H. 2004. Discussion on PA model development for bentonite barriers affected by chemical interaction with concrete: do we have enough evidence to support bentonite stability?. In: International Workshop on Bentonite-Cement Interaction in Repository Environments, Tokyo, Japan, NUMO-TR 04-05, A3-172 – A3-177; Posiva Report 2004-25: 192.

Tang, A.M., Cui, Y.J. 2007. Controlling suction by vapour equilibrium technique at different temperatures, application to the determination of the water retention properties of MX80 clay. Can. Geotech. J. 42: 287–296.

Taniguchi, N. 2003. Effect of magnetite as a corrosion product on the corrosion of carbon steel overpack. In: Prediction of Long-Term Corrosion Behaviour in Nuclear Waste Systems. European Federation of Corrosion Publication No. 36 :424– 438.

Taxén, C. 2003. Atmospheric corrosion of copper 450 metres underground. Results from three years exposure in the Äspö HRL. MRS Online Proceedings Library volume 807: 612–617.

Tay, B.K., Zhao, Z.W., Chua, D.H.C. 2006. Review of metal oxide films deposited by filtered cathodic vacuum arc technique. Mater. Sci. Eng.:R.:Rep. 52: 1-48.

Taylor, K.J., Smart, N.R., Porter, F.M. 2002. The Propagation of Localised Corrosion of Carbon Steel in Cementitious Environments. AEA Technology Report AEAT/ERRA-0309.

Terlain, A., Desgranges, C., Gauvain, D., Feron, D., Galtayries, A., Marcus, P. 2001. Oxidation of materials for nuclear waste containers under long term conditions, Corrosion/2001, Paper 01119. NACE International, 2001: Houston, TX.

Theodorakopoulos, N., Février, L., Barakat, M., Ortet, P., Christen, R., Piette, L., Levchuk, S., Beaugelin-Seiller, K., Sergeant, C., Berthomieu, C., Chapon, V. 2017. Soil prokaryotic communities in Chernobyl waste disposal trench T22 are modulated by organic matter and radionuclide contamination. EMS Microbiol. Ecol. 93: fix079. https://doi.org/10.1093/femsec/fix079.

Tournassat, C., Steefel, C.I., Bourg, I.C., Bergaya, F. 2015. Natural and Engineered Clay Barriers. Develop. Clay Sci. 6: 432.

Triantou, K.I., Pantelis, D.I., Guipont, V., Jeandin, M. 2015. Microstructure and tribological behaviorbehaviour of copper and composite copper+alumina cold sprayed coatings for various alumina contents. Wear 336-337: 96-107.

EURAD (Deliverable n° 1.1) – Initial State-of-the-art of WP ConCorD
Dissemination level: Public
Date of issue of this report: 17/08/2022

Page 145

Trinchero, P., Molinero, J., Román-Ross, G., Berglund, S., Selroos, J.O. 2014. FASTREACT–An efficient numerical framework for the solution of reactive transport problems. Appl. Geochem. 49: 159-167.

Truche, L., Berger, G., Destrigneville, C., Guillaume, D., Giffaut E. 2010. Kinetics of pyrite to pyrrhotite reduction by hydrogen in calcite buffered solutions between 90 and 180 °C: Implications for nuclear waste storage. Geochim. Cosmochim. Acta 74: 2894-2914.

Truche, L., Berger, G., Destrigneville, C., Pages, A., Guillaume, D., Giffaut E., Jacquot, E. 2009. Experimental reduction of aqueous sulphate by hadrogen under hydrothermal conditions: Implication for the nuclear waste storage. Geochim. Cosmochim. Acta 73: 4824-4835.

Turnbull, A. 1982. Review of the Electrochemical Conditions in Cracks with Particular Reference to Corrosion Fatigue of Structural Steels in Sea Water. Rev. Coat. Corros. 5: 43-171.

Turnbull, A. 1993. Review of Modelling of Pit Propagation Kinetics. Br. Corros. J. 24: 297.

Turnbull, A. 2001. Modelling of the Chemistry and Electrochemistry in Cracks – A Review. Corrosion 57: 175-189.

Turnbull, A., 2009. A Review of the Possible Effects of Hydrogen on Lifetime of Carbon Steel Nuclear Waste Canisters. Technical Report 09-04, Nagra, Wettingen, Switzerland.

Vachon, M.A. et al. 2021. Fifteen shades of clay: distinct microbial community profiles obtained from bentonite samples by cultivation and direct nucleic acid extraction. Sci. Rep. 11: 22349.

Van Gerwen, S.J.C., Rombouts, F M., Van´t Riet, K., Zwietering, M.H. 1999. A Data analysis of the irradiation parameter D10 for bacteria and spores under various conditions. J. Food Prot. 62: 1024-1032.

Van Loon, L.R., Glaus, M.A., Müller, W. 2007. Anion exclusion effects in compacted bentonites: towards a better understanding of anion diffusion. Appl. Geochem. 22: 2536–2552.

Vandenborre, J., Crumière, F., Blain, G., Essehli, R., Humbert, B., Fattahi, M. 2013. Alpha Localized Radiolysis and Corrosion Mechanisms at the Iron/Water Interface: Role of Molecular Species. J. Nucl. Mater. 433:124–31. doi: 10.1016/j.jnucmat.2012.09.034.

Venzlaff, H. et al. 2013. Accelerated cathodic reaction in microbial corrosion of iron due to direct electron uptake by sulfate-reducing bacteria. Corros. Sci. 66: 88-96.

Villar, M.V., Armand, G., Conil, N., de Lesquen, Ch., Herold, Ph., Simo, E., Mayor, J.C., Dizier, A., Li, X., Chen, G., Leupin, O., Niskanen, M., Bailey, M., Thompson, S., Svensson, D., Sellin, P., Hausmannova, L. 2020. D7.1 HITEC. Initial State-of-the-Art on THM behaviour of i) Buffer clay materials and of ii) Host clay materials. Deliverable D7.1 HITEC. EURAD Project, Horizon 2020 No 847593: 214.

Villar, M.V., Fernández, A.M., Romero, E, Dueck, A., Cuevas, J., Plötze, M., Kaufhold, S., Dohrmann, R., Iglesias, R., Sakaki, T., Voltolini, M., Zheng, L., Kawamoto, K., Kober, F., 2017. FEBEX-DP: Post-mortem THM/THC Report. Analysis of Results. Nagra Working Report NAB 16-017: 147.

Villar, M.V., Lloret, A. 2008. Influence of dry density and water content on the swelling of a compacted bentonite. Appl. Clay Sci. 39: 38-49.

Wang, Y., Normand, B., Mary, N., Yu, M., Liao, H. 2014. Microstructure and corrosion behaviour of cold sprayed SiCp/Al 5056 composite coatings. Surf. Coat. Technol. 251: 264-275.

Wanga, L. et al. 2020. Pressure-less joining of SiCf/SiC composites by 2O3–Al2O3–SiO2 glass: Microstructure and properties. Ceram. Int. 46: 27046–27056.

Weetjens, E., Marivoet, J., Govaerts, J. 2012. Conceptual model description of the reference case, External Report SCK•CEN-ER-215. Niras / Ondraf.

EURAD (Deliverable n° 1.1) – Initial State-of-the-art of WP ConCorD
Dissemination level: Public
Date of issue of this report: 17/08/2022

Page 146

Wei, T. et al. 2019. Microstructure, corrosion resistance and oxidation behaviour of Cr-coatings on Zircaloy-4 prepared by vacuum arc plasma deposition. Corros. Sci. 158: 108077.

Wersin, P., Alt-Epping, P., Pitkänen, P., Román-Ross, G. 2014. Sulphide Fluxes and Concentrations in the Spent Nuclear Fuel Repository at Olkiluoto. Posiva 2014-01, Posiva Oy, Finland.

Wersin, P., Hadi, J., Jenni, A., Svensson, D., Grenèche, J.-M., Sellin, P., Leupin, O.X. 2021. Interaction of Corroding Iron with Eight Bentonites in the Alternative Buffer Materials Field Experiment (ABM2). Minerals 11: 907.

Wersin, P., Kiczka, M., Rosch, D. 2014. Safety case for the disposal of spent nuclear fuel at Olkiluoto. Radionuclide solubility limits and migration parameters for the canister and buffer. Posiva 2012-39, Posiva Oy, Finland.

Wersin, P., Kober, F. 2017. FEBEX-DP. Metal Corrosion and Iron-Bentonite Interaction Studies. Nagra Working Report NAB 16-016.

Wersin, P., Spahiu, K., Bruno, J. 1994. Kinetic modelling of bentonite-canister interaction. Long-term predictions of copper canister corrosion under oxic and anoxic conditions. Stockholm: Swedish Nuclear Fuel and Waste Management Co.

Wersin, P., Spahiu, K., Bruno, J. 1994. Time evolution of dissolved oxygen and redox conditions in a HLW repository. TR 94-02, SKB, Sweden.

Westerman, R.E., Nelson, J.L., Pitman, S.G., Kuhn, W.L., Basham, S.J., Moak, D.P. 1983. Evaluation of Iron-Base Materials for Waste Package Containers in a Salt Repository. MRS Proceedings 26: 427. doi: 10.1557/PROC-26-427.

Westerman, R.E., Pitman, S.G., Nelson, J.L. 1982. General Corrosion, Irradiation-Corrosion and Environmental-Mechanical Evaluation of Nuclear-Waste-Package Structural-Barrier Materials. Progress report PNL-4364, Office of Nuclear Waste Isolation, Pacific Northwest Laboratory, Washington.

Wieland, E., Hummel, W. 2015. Formation and stability of 14C-cointaining organic compounds in alkaline iron-water systems: preliminary assessment based on a literature survey and thermodynamic modelling. Mineral. Mag. 79: 1275-1286.

Wilfinger, K. 1994. Ceramic Package Fabrication for YMP Nuclear Waste Disposal. Lawrence Livermore National Laboratory, Report UCRL-ID-118660, California, US.

Wilson, J., Savage, D., Bond, A., Watson, S., Pusch, R., Bennett, D. 2011. Bentonite. A Review of key properties, processes and issues for consideration in the UK context. Quintesa report QRS-1378ZG-1 : 137.

Winsley, R.J., Smart, N.R., Rance, A.P., Fennell, P.A.H., Reddy, B., Kursten, B. 2011. Further Studies on the Effect of Irradiation on the Corrosion of Carbon Steel in Alkaline Media. Corros. Eng. Sci. Technol. 46:111–16. doi: 10.1179/1743278210Y.0000000010.

Wolfaardt, G.M., Korber, D.R. 2012. Near-filed microbiological considerations relevent to a deep geological repository for used nuclear fuel - Stae of science review. Toronto: Nuclear Waste Management Organisation.

Wötting, G., Martin, W. 2007. Large sized, complex shaped sintered silicon carbide components with excellent mechanical properties. Proceedings of the 10th ECerS Conference, Baden-Baden: 1067-1070.

Xiong, Y. et al. 2021. Lead/lead-alloy as a corrosion-resistant outer layer packaging material for high level nuclear waste disposal. Nucl. Eng. Des. 380: 111294.

Xu, Y., Sun, D., Zeng, Z., Lv, H. 2019. Temperature dependence of apparent thermal conductivity of compacted bentonites as buffer material for high-level radioactive waste repository. Appl. Clay Sci. 174: 10-14.

EURAD (Deliverable n° 1.1) – Initial State-of-the-art of WP ConCorD
Dissemination level: Public
Date of issue of this report: 17/08/2022

Page 147

Yang, Q., Toijer, E., Olsson, P. 2019. Analysis of radiation damage in the KBS-3 canister materials. Swedish Nuclear Fuel and Waste Management Co Technical Report, SKB TR-19-14.

Yin, S. et al. 2017. Advanced diamond-reinforced metal matrix composites via cold spray: properties and deposition mechanism. Compos. B. Eng. 113: 44-54.

Yunker, W.H. 1990. Corrosion behavior of copper-base materials in a gamma-irradiated environment. Westinghouse Hanford Company Report, WHC-EP-0188.

Yunker, W.H., Glass, R.S. 1987. Long-term corrosion behaviour of copper-base materials in a gamma-irradiated environment. Mater. Res. Soc. Symp. Proc. 84: 579-590.

Zhang, H., Datta, A.K. 2003. Microwave Power Absorption in Single - and Multiple - Item Foods. Food Bioprod. Process. 81: 257–265.

Zhang, Q., Zheng, M., Huang, Y., Kunte, H. J., Wang, X., Liu, Y., Zheng, C. 2019. Long term corrosion estimation of carbon steel, titanium and its alloy in backfill material of compacted bentonite for nuclear waste repository. Sci Rep 9: 3195. doi.org/10.1038/s41598-019-39751-9.

Zheng, L., Rutqvist, J., Birkholzer, J.T., Liu, H.H. 2015. On the impact of temperatures up to 200°C in clay repositories with bentonite engineer barrier systems: A study with coupled thermal, hydrological, chemical, and mechanical modeling. Eng. Geol. 197: 278–295.

Zheng, L., Xu, H., Ruqvist, J.; Reagan, M.; Birkholzer, J.; Villar, M.V.; Fernández, A.M. 2020. The hydration of bentonite buffer material revealed by modeling analysis of a long-term in situ test. Appl. Clay Sci. 185: 105360.

Zheng, L.; Samper, J.; Montenegro, L.; Fernández, A.M. 2011. A coupled THMC model of a heating and hydration laboratory experiment in unsaturated compacted FEBEX bentonite. J. Hydrol. 386: 80–94.

Zymelka, D. 2013. PhD Thesis. Suivi par méthode optique du frittage micro-ondes d''oxydes céramiques. École Nationale Supérieure des Mines de Saint-Etienne.

EURAD (Deliverable n° 1.1) – Initial State-of-the-art of WP ConCorD
Dissemination level: Public
Date of issue of this report: 17/08/2022

Page 148